Rydberg Spectroscopy of Calcium Monofluoride and Calcium Monochloride

by
Nicole Harris
B.S., University of Tampa (1988)

Submitted to the Department of Chemistry in Partial
Fulfillment of the Requirements for the Degree of

DOCTOR OF PHILOSOPHY IN CHEMISTRY

at the

MASSACHUSETTS INSTITUTE OF TECHNOLOGY

September 1995

Signature of Author _____
Department of Chemistry
May 28, 1995

Certified by _____
Robert W. Field
Thesis Supervisor

Accepted by _____
Dietmar Seyferth, Chairman
Departmental Committee on
Graduate Students

This doctoral thesis has been examined by a Committee of the Department of Chemistry as follows:

Professor Robert Silbey _____
                                                                    Chairman

Professor Robert W. Field _____
                                                              Thesis Supervisor

Professor Sylvia T. Ceyer _____

2

Rydberg Spectroscopy of Calcium Monofluoride and Calcium Monochloride

by Nicole Harris

Abstract

CaF and CaCl are well described as a three body system consisting of two closed shell atomic ions (Ca^{2+} and F^- or Cl^-) and a single nonbonding electron, although CaCl is more difficult to study due to the early onset of predissociation. Previously, all spectroscopy on CaF has involved only the valence and core-penetrating Rydberg states ($\ell < 3$). The spectroscopy on CaCl has involved valence and low energy core-penetrating Rydberg states only. These states can be modeled as Ca^+ ion states perturbed by a point charge (the F^- or Cl^-). We have expanded the data available on the core-penetrating states of CaF to include n*=13, 14, 17 and 18 (the highest previously observed Rydberg state of CaF was n*=9.98). We have expanded the data available on the core-penetrating states of CaCl to include n*= 3-4 and n*=16-18 (the highest previously observed Rydberg state of CaCl was n*=3.05). Some spectra in the high-n* region (n*=20-30) has also been recorded for both CaCl and CaF.

We have observed another set of states which can be detected by using the $C^2\Pi$ state as the intermediate state in a double resonance experiment. These are the core-nonpenetrating series ($\ell > 2$). These states are special because they are not effected by collisions with the CaF^+ core. The Rydberg electron in a nonpenetrating orbital only interacts with the core through long range forces due to the multipole moments of the core. Thus the pattern of levels within an f (or g) complex is determined by the multipole moments of the CaF^+ core. Measurements of these splitting patterns provides the best way of characterizing the longest-range interaction of the ion-core with the outside world.

The n*=14 f complex in CaF presented in this thesis is the first example of a core-nonpenetrating f complex observed and assigned for a highly polar molecule. The complete analysis of these states will eventually allow us to answer the question, what happens to the

energy levels of a hydrogen atom when the point monopole is replaced a large point dipole?

The methods used to detect and assign the core-nonpenetrating states of CaF and the n*=13-18 core-penetrating states of CaF and CaCl are discussed in this thesis. Predissociation of CaCl is briefly discussed. The current theories available to explain the f (and g) states of CaF are also mentioned.

Thesis Supervisor: Dr. Robert W. Field
Title: Professor of Chemistry

Dedication

Dedicated to the memory of my husband and best friend,
Christopher Douglas Schneider
November 21, 1962 - March 28, 1995

"The best manner of avenging ourselves is by not resembling him who has injured us."

- Jane Porter

Acknowledgments

There have been many people who have offered help, inspiration, encouragement and support while I was working on my thesis. I am sure that I will forget to mention some of your names. I thank all of you who had a part in helping me complete this project.

There are certain special people who must be acknowledged individually.

Our dog Thea is the most beautiful, gentle, well behaved black lab I have ever met. My husband did an excellent job training her. She has been a great companion. She has taken me for hikes, bike rides and even skiing. I have to thank her for getting me out of the house for exercise so I could return and concentrate on my work.

Chris Gittins deserves recognition for building a truly great machine which enabled us to collect most of the data that is presented in this thesis.

George Adamson deserves special recognition for listening to my complaints and being one of the few people who understood what I was talking about. He kept me sane at times when I was very confused about the way certain people behave.

Zygmunt Jakubek has impressed me in many different ways. First by his amazing strength, also by his determination and finally by his remarkable knowledge. If I had a question, I could always ask Zygmunt and he would do his best to explain it. I learned a lot from him. I will miss being able to call him and ask questions. I also enjoyed his wife, Beata, and his daughter, Ania. I hope they are happy in Japan.

Jim Murphy and John Berg were great people to work with. They were both very nice people and very easy to work with. They were truly team players. I am very thankful that I was assigned to the project they were working on.

Foss Hill was another person who was a member of the group when I first joined. He was the first MIT chemistry grad student that I met. His love for science was great.

I will remember Bob Field for his enthusiasm. It was almost frightening at times to take him results that I knew he would be excited about (just kidding). Anyone who knows him can relate. His enthusiasm made me feel my project was important and worthwhile which certainly helped my motivation. I appreciate Bob's kindness and understanding toward me while I was at MIT.

Peter Giunta, Bob secretary, has gone out of his way to help me many times. I really appreciate all his help.

Other members of the Field group that I have enjoyed knowing are Kevin Cunningham, Stephani Solina, Hui Ma, Amy Miller, Jon O'Brien, and Bhavani Rajaram.

Christian Jungen has been extremely useful in helping us understand the theoretical side of the CaF project. I enjoyed working with him in France and I hope I will get another opportunity to visit Orsay.

One of the first people I met at MIT, Rob Martello, is still a good friend and always cheered me up with his great sense of humor. I will miss our lunches at the Chinese restaurant. Rob introduced me to another person, Mike McCandless, who was an important person in my life for three years. I will always have good memories of the time we spent together. I am glad to have met nice friends like them while I was at MIT.

My aunts and uncles have provided support and encouragement while I was at MIT. I thank them for helping me in many different ways.

My sister, Cathy Harris has showed support, encouragement and concern during my time at M.I.T. I enjoy having a sister to discuss family matters and memories from childhood with.

My mother and my step-father, Bill and Irmgard Pawlowski have been there though out my time at MIT to provided emotional and financial support.

My father, Lewis Harris, kept me happy and energized by taking me on ski trips in the winter. Those chances to get out of Boston and away from MIT certainly helped my attitude and motivation. It was really fun learning to ski together. Someday maybe he will even be able to beat me in a ski race.

My grandmother, Maria Lipowsky, has always been a source of inspiration. I am very impressed that she could survive such enormous hardship and never give up. She is one of the kindest, most generous people I have ever met. She has always provided support and encouragement. She always wants copies of all my papers even though she can't read English (she is German) and does not have a scientific background.

My friends in Vermont, Matt and Kim Robertson, Rob and Linda Beers, Jeff Hopkins, Kyle McEwen and all the others who I did not name have been very kind recently. They are doing there best to keep me busy and make sure I am not lonely. I really appreciate their concern and consideration.

I have to thank Roger and Bambi Rivera for giving me a place to stay during my visits to Boston. I really appreciated having a place to stay where I felt welcome.

My mother-in-law and father-in-law, Uwe and Carol Schneider have been wonderful. They have been so kind and supportive. Even though Chris and I did not even get to celebrate our first anniversary they make me feel like I am truly part of the family.

I need to thank my brother-in-law, Uwe Schneider, and his girlfriend, Carla Mason, for taking me rock climbing and frightening so bad that I forgot all my troubles temporarily. I actually liked it after the first day and would even be willing to try it again. After realizing what I had done, I felt really good for a few days and now I have some stories to tell and I even have some pictures.

Finally and most importantly, I thank my husband Chris. He was kind, loving, gentle and honest and the least judgmental person I have ever known. He is the only person I have ever met who I could tell absolutely anything and not worry what he would think. He was truly a special person. He was supportive yet never applied any pressure. I know he was very proud of the work I was doing. I wish he could be here to see me finish. I would gladly give it up this degree to have him back. His death has made it extremely difficult to finish my thesis and I realize if he were still alive it would have been better.

Table of Contents

Chapter 1
Introduction

The alkaline earth monohalides, in particular CaF, have been the subject of numerous theoretical and experimental studies[1-9]. This is in part due to their simple structure. CaF is well described as a three body system consisting of two closed shell atomic ions (Ca^{2+} and F^-) and a single nonbonding electron. Previously, all spectroscopy on CaF has involved only the valence and core-penetrating Rydberg states ($\ell < 3$)[1-4]. These states can be modeled as Ca^+ ion states perturbed by a point charge (the F^-)[5,6]. We have expanded the data available on the core-penetrating states to include $n^*=13$, 14, 17 and 18 (the highest previously observed Rydberg state of CaF was $n^*=9.98$). These new states can be used to test the limits of the scaling relations developed for the Rydberg states below $n^*=10$.

Only core-penetrating states were detected previously because all the spectra were recorded out of the $A^2\Pi$ state or the $X^2\Sigma^+$ state (see Chapter 3)[1-4]. We now know that there is another set of states which can be detected by using the $C^2\Pi$ state as the intermediate state in a double resonance experiment. These are the core-nonpenetrating series ($\ell > 2$). These states are special because they are not effected by collisions with the CaF^+ core. The Rydberg electron in a nonpenetrating orbital only interacts with the core through long range forces due to the multipole moments of the core. Thus the pattern of levels within an f (or g) complex is determined by the multipole moments of the CaF^+ core. Measurements of these splitting patterns provides the best way of characterizing the longest-range interaction of the ion-core with the outside world.

These nonpenetrating states, which have not been observed previously, were first detected in the $n^*=7$ region. A direct comparison of spectra recorded out of the $A^2\Pi$ state in the $n^*=13$ and 14 regions and spectra in the $n^*=13$ and 14 regions recorded out of the $C^2\Pi$ state proved that these new states were not higher vibrational levels of the core-penetrating states detected previously. The complete analysis of these states will eventually allow us to answer the question, what happens to the energy levels of a hydrogen atom when the point monopole is replaced a large point dipole?

The core non-penetrating states of molecules such as NO, N_2, H_2, and He_2 have been observed[10-16] and are well characterized,

however these molecules have a zero or very small dipole moment and cannot be used as a prototype to understand the f-complex observed in CaF or in any highly polar molecule. This new type of highly polar core-nonpenetrating states require new methods of detection, analysis, and assignment.

The methods used to detect and assign the core-nonpenetrating states of CaF and the theories which could explain these states are the main topics of this thesis. The core-penetrating states of CaF observed in the $n*=13$, 14, 17 and 18 regions and the CaCl spectra recorded in the $n*=16$, 17, and 18 regions are also included. The high-$n*$ spectra of CaF and CaCl used to determine the ionization potential of CaCl and refine the ionization potential of CaF are mentioned briefly.

Chapter 2 describes the experimental methods used to record the spectra presented in this thesis. Both fluorescence based and ion based detection schemes were used to record the spectra in this thesis.

Chapter 3 contains a description of the core-penetrating series. Each of the core-penetrating series of CaF and CaCl can be traced back to a "valence"-state precursor. This is the lowest state in that series. The properties of each series can be understood based on this lowest state of the series. Scaling laws determine how the properties of a particular Rydberg series evolve with $n*$. A unique property of Rydberg states is that an infinite number of states and the associated ionization continuum can be described with a limited number of parameters using scaling relations.

The predissociation of the CaCl molecule is discussed only briefly in Chapter 3 because the quantity and quality of the CaCl spectra recorded did not allow any of the scaling relations for the predissociation rates to be tested.

Chapter 4 describes theoretical models that are currently available to explain the core-nonpenetrating states of CaF. The model traditionally used to describe this kind of state does not describe the observed states of CaF. CaF^+ has a electric dipole moment which is much larger than that of any molecule for which a complete f-complex has been observed. This f-complex (and fragments of a g-complex) is very important because it can be used to test the current theoretical models. If those models fail to describe these state completely, a new model must be developed. Once a model is developed to describe the core-nonpenetrating states of CaF, it can be used to describe the core-nonpenetrating states of other molecules such as BaF, CaCl, ArH, KrH and possibly even molecules like HCl.

Chapter 5 contains tables of all the transitions that were detected in the experiments described in Chapter 2. All observed transitions were included along with their relative intensities and assignments for many of them. The unassigned transitions were also included because they may become useful as the study of these molecules continues.

Chapter 6 describes the methods used to assign the spectra. These methods are original to this work and will be generally applicable to the study of molecular Rydberg spectra. A discussion of each n*-region and the preliminary multichannel quantum defect theory (MQDT) fits are also included in this chapter.

Chapter 7 is the conclusion. Suggestions for new experiments which would complement the spectra presented in this thesis and those recorded previously are also included in this chapter.

References

[1] J. E. Murphy, J. M. Berg, N. A. Harris, and R. W. Field, Phys. Rev. Lett. **65**, 1861 (1990).

[2] J. E. Murphy, Ph.D. thesis, Massachusetts Institute of Technology, 1992.

[3] N. A. Harris and R. W. Field, J. Chem. Phys. **98**, 2642 (1993).

[4] J. M. Berg, J. E. Murphy, N. A. Harris, and R. W. Field, Phys. Rev. A **48**, 3012 (1993).

[5] S. F. Rice, H. Martin, and R. W. Field, J. Chem. Phys. **82**, 5023 (1985).

[6] N. A. Harris and Ch. Jungen, Phys. Rev. Lett., **70**, 2549-2552 (1993).

[7] T. Torring, W. Ernst and J Kandler, J. Chem. Phys. **90**, 4927 (1989).

[8] P. Bernath, Ph.D. Thesis, Massachusetts Institute of Technology, 1980.

[9] P. Bundgen, B. Engels, and S. D. Peyerimhoff, Chem. Phys. Lett. **176**, 407 (1991).

[10] K. P. Huber, Ch. Jungen, K. Joshino, K. Ito and G. Stark, J. Chem. Phys., **100**, 7957 (1994).

[11] P. Arrowsmith, W. J. Jones and R. P Tuckett, J. Mol. Spec. **86**, 216 (1981).

[12] G. Herzberg and Ch. Jungen, J. Chem. Phys. **84**, 1181 (1986).

[13] E. Miecher, Can. J. Phys. **54**, 2074 (1976).

[14] Ch. Jungen and E. Miecher, Can. J. Phys. **47**, 1769 (1969).

[15] G. Herzberg and Ch. Jungen, J. Chem. Phys. **77**, 5876 (1982).

[16] E. E. Eyler and F. M. Pipkin, Phys. Rev. A **27**, 2462 (1983).

Chapter 2
Experimental Section

The spectra presented in this thesis were recorded with two different detection schemes. Each detection scheme was used with a different method of molecule production. The first detection scheme to be discussed, fluorescence detection, was used previously to record intermediate-n* CaF Rydberg states[1-3]. The molecules for this method were produced in a high temperature oven.

The second detection method, ion-detection, had not been used previously to record CaF or CaCl Rydberg spectra and proved an extremely valuable method for observing Rydberg states above n*=13 (for CaF) and n*= 16 (for CaCl). The molecules for this method were produced by laser ablation of calcium metal in a high vacuum chamber.

Part 2.1 - Fluorescence

All of the Rydberg states of the CaF molecule observed previously have been detected using fluorescence-based detection schemes[2]. The first Rydberg states of CaF were observed by Murphy[1,2] and Berg et al[3] using the fluorescence dip detection scheme (described in Part 2.1.2). The signal-to-noise for this method quickly proved to be inferior to the direct UV fluorescence method described in Part 2.1.1.

CaF Rydberg spectra can be recorded using direct fluorescence, but the CaCl molecule has a low dissociation limit[4], 32,898 cm^{-1}, which makes the observation of direct UV fluorescence from levels which lie above 41,300 cm^{-1} difficult. For CaCl, the fluorescence dip scheme can be used to observe Rydberg spectra in the intermediate-n* region.

For both fluorescence-based techniques, gaseous calcium monofluoride was produced from crystalline calcium difluoride in a high temperature oven. The temperature of the oven was approximately 1400 °C [3]. The pressure was maintained at about 200 mTorr by a constant flow of Argon which was used as a carrier gas. CaCl was produced by using calcium dichloride instead of calcium difluoride. Since $CaCl_2$ melts at a lower temperature, the oven was maintained at approximately 800 °C. The temperature used for the CaF experiment caused the CaCl to vaporize too quickly, so the oven had to maintained at a temperature closer to the $CaCl_2$ melting point.

Part 2.1.1 - Direct UV Fluorescence

Direct UV fluorescence is a two-laser technique (see Figure 2.1). The first laser, the PUMP, is tuned to a single rovibronic level in the intermediate state. The PUMP laser frequency is then fixed and the PROBE laser frequency is scanned. When the PROBE laser is resonant with a Rydberg transition, a positive signal is observed. We used a solar blind photomultiplier (Hamamatsu model R166) behind a broad band UV interference filter (Andover) to detect the UV fluorescence. Four experiments were done using this technique, with three different laser configurations. They are discussed separately below. In most cases, the PUMP laser pulse energy was too high to allow the PUMPing of a single rovibronic transition so the power was reduced with a neutral density filter. The approximate pulse energy used is in parentheses next to the typical output of the PUMP laser. In each case the pulsed dye lasers described were pumped by the same Spectra Physics DCR2A Nd:YAG laser.

Direct UV fluorescence detection was used to record CaF Rydberg spectra in the 36,000-40,000 cm^{-1} energy region with the $A^2\Pi_{3/2}$ (v=0) state as the intermediate state. That work is discussed in the paper included as Appendix 1. The PUMP laser for that experiment was a Lambda Physik 3002E (linewidth $\approx$ 0.05 cm^{-1}) which was calibrated (to ±0.01 cm^{-1}) using fluorescence from an iodine cell. The PROBE laser was a Spectra Physics PDL-1 pulsed dye laser (linewidth $\approx$ 0.03 cm^{-1}) which was calibrated (to ±0.01 cm^{-1}) using absorption from a tellurium cell (T= 500 ºC). Typical pulse energies were 500 µJ for the PROBE and 5 mJ (about 100 µJ entering the oven) for the PUMP.

In the n*=7 region, with the $C^2\Pi_{3/2}$ (v=0) state as the intermediate state, Rydberg spectra of CaF were recorded in the 44700 - 44820 cm^{-1} energy region. In that experiment, a doubled Spectra Physics PDL-1 pulsed dye laser (linewidth $\approx$ 0.03 cm^{-1}) was used as the PUMP. It was calibrated (to ±0.01 cm^{-1}) using fluorescence from an iodine cell. The PROBE was the Lambda Physik 3002E dye laser (linewidth $\approx$ 0.05 cm^{-1}) which was also calibrated (to ±0.01 cm^{-1}) using fluorescence from an iodine cell. Typical pulse energies were 500 µJ (about 100 µJ entering the oven) for the PUMP and 5 mJ for the PROBE.

Direct UV fluorescence from one CaCl Rydberg state at about 41,300 cm^{-1} was observed using the $B^2\Sigma$ (v=0) state as the intermediate state. The PUMP laser used for that experiment was a Spectra Physics Pulsed Dye Amplifier pumped by a Spectra Physics

DCR2A Nd:YAG laser and a Coherent 699-21 dye laser (linewidth $\approx$ 0.003 cm^{-1}). It was calibrated (to ±0.001 cm^{-1}) using fluorescence from an iodine cell. The PROBE was a doubled Lambda Physik 3002E dye laser [linewidth $\approx$ 0.10 cm^{-1} (no intracavity etalon was used)]. Typical pulsed energies were 500 μJ for the PUMP and about 5 mJ for the PROBE. The Lambda Physik 3002E dye laser was calibrated (to ±0.1 cm^{-1}) with uranium and neon spectra from a Uranium optogalvanic lamp (PHOTRON) and an etalon. Due to severe predissociation, no additional vibronic states were observed above 41,300 cm^{-1} using this technique. Vibronic states were observed above this energy using the fluorescence dip scheme, which is described below. Figure 2.3 shows a result of using the two different techniques in the 44,400 cm^{-1} energy region. It is clear that signal appears using fluorescence dip detection that does not appear when using direct fluorescence. This is direct evidence for predissociation.

Seven additional vibronic states were observed using direct UV fluorescence detection in CaCl in the 37000-39000 cm^{-1} energy region. The B$^2\Sigma$ (v=0) state was also used as the intermediate state in that experiment. The PUMP laser was a Lambda Physik 3002E (linewidth $\approx$ 0.05 cm^{-1}) which was calibrated (to ±0.01 cm^{-1}) using fluorescence from an iodine cell. The PROBE laser was a Spectra Physics PDL-1 pulsed dye laser (linewidth $\approx$ 0.03 cm^{-1}), which was calibrated (to ±0.01 cm^{-1}) using absorption in a tellurium cell (T= 500 ºC). Typical pulse energies were 5 mJ (about 100 μJ entering the oven) for the PUMP and 1 mJ for the PROBE. The scans recorded in this region were only survey scans and not carefully calibrated (only a few of the observed transitions were calibrated).

Part 2.1.2 Fluorescence Dip

The crucial difference between the fluorescence dip and direct UV fluorescence scheme is the wavelength of fluorescence that is monitored. In the fluorescence dip scheme the B-X fluorescence is monitored instead of the Rydberg→X fluorescence, see Figure 2.2. When the PROBE is resonant with a Rydberg transition we observe a dip in the intensity of the B-X fluorescence. We used this technique to detect predissociated states of CaCl in the n*$\approx$5 region, since no direct fluorescence was observed above 41,300 cm^{-1} (about 11,000 cm^{-1} above the dissociation limit). The signal to noise was poor due to laser fluctuations and fluctuations in the amount of CaCl that was produced by the oven. The signal-to-noise was better for a similar technique, SEP (Stimulated Emission Pumping)[5], which employs a

dual-beam null scheme and has been used on permanent gases, such as acetylene. The signal-to-noise decreases for SEP when a non-permanent gas, such as HCO, is used[6]. It should be possible to improve the signal to noise by using some type of normalization scheme. A different oven would have to be built in order to use any kind of dual-beam null scheme. Normalization would not eliminate another problem associated with this technique: positive signal from the PROBE laser. The PROBE laser excites transitions from the ground state which fluoresce through the intermediate state and thereby produce a positive signal which interferes with the observation of dips in the intensity of the B-X fluorescence (see figure 2.4).

The PUMP laser used for this experiment was a Spectra Physics Pulsed Dye Amplifier (PDA) pumped by a Spectra Physics DCR2A Nd:YAG laser and a Coherent 699-21 cw dye laser (linewidth $\approx$ 0.003 cm^{-1}). Typical pulse energies from the PDA were $500\mu J$. The PROBE was a doubled Lambda Physik 3002E pulsed dye laser [linewidth $\approx$ 0.10 cm^{-1} (no intracavity etalon was used)] pumped by the same Spectra Physics Nd:YAG laser. The typical pulse energy after doubling was about 1 mJ. The 3002E dye laser was not wavelength calibrated for the initial survey scans recorded. The correction of the wavelength dial on the dye laser was known approximately[1-3]. The grating readings were adjusted by that estimated offset and should be accurate to about ± 5 cm^{-1}. Fluorescence from an iodine cell was used as a calibration source (to ± 0.001 cm^{-1}) for the 699-21 cw dye laser. The experiment worked best when both lasers were focused to about the size of the window going into the oven (approximately 2 cm).

Although one can observe predissociated states of CaCl using this fluorescence dip method, non-fluorescence based techniques are likely to work better. One such technique might involve probing one of the products of the dissociation, the calcium atoms. That method will be discussed in Chapter 7, Part 3.

2.2 Ion detection

Ion detection was used to detect Rydberg states of CaCl and CaF. Those experiments and the apparatus are described in detail by Gittins[7] and will only be briefly discussed here.

2.2.1 REMPI

Resonance enhanced multiphoton ionization (REMPI) was used to record CaCl Rydberg spectra in the 36700-38200 cm^{-1} energy region (see Figure 2.5). The $A^2\Pi_{3/2}$ (v=0) state was used as the intermediate state in that experiment. The PROBE laser was a Lumonics HyperDYE 550 dye laser (linewidth $\approx$ 0.1 cm^{-1}) and the PUMP was a Lumonics HyperDYE 300 dye laser (linewidth $\approx$ 0.1 cm^{-1}). Typical pulse energies used were 200 μJ for the PROBE and 250 μJ for the PUMP. Both lasers were pumped by a Spectra Physics DCR1A Nd:YAG laser. Iodine fluorescence was used to calibrate the PUMP laser (to ±0.02 cm^{-1}). Neon spectra from a uranium optogalvanic lamp (PHOTRON) was used to calibrate the PROBE laser to ±0.1 cm^{-1}.

2.2.2 Autoionization

Ion detection was used to detect autoionizing Rydberg states of CaCl and CaF above the v=0 ionization potential. This technique allowed the observation of v=1 Rydberg states from n*=13 (for CaF) and n*=16 (for CaCl) up to n*$\approx$ 40. Some v=2 and v=3 states were also detected. One v=4 state was detected (with the $C^2\Pi_{3/2}$ (v=0) state as the intermediate state).

CaF was produced in a supersonic jet by laser ablation of calcium metal. The calcium metal reacted with the fluoroform (5%) that was added to the carrier gas (helium) to produce gaseous CaF. CaCl was produced the same way but chloroform (5% in He carrier gas) was used instead of fluoroform gas.

As in the direct fluorescence experiment, the PUMP laser is used to select a particular rovibronic level in the intermediate state. The PROBE laser is then scanned. After the PROBE laser has excited a transition to a v>0 Rydberg level, the excited state autoionizes and ions are detected with a time-of-flight mass spectrometer. Mass detection was used so the signal from the $Ca^{35}Cl$ and $Ca^{37}Cl$ isotopomers could be separated and recorded simultaneously. That greatly simplified the absolute vibrational assignments of the CaCl spectra and allowed us to estimate the vibrational constant, ω_e, of the $CaCl^+$ ion. It had been difficult to determine the $CaCl^+$ vibrational constant from the fluorescence data. CaF does not have any naturally abundant isotopomers so the vibrational assignments are considerably more difficult for CaF.

The PUMP laser in the autoionization detected experiment, was a Lumonics HyperDYE 550 dye laser (linewidth $\approx$ 0.1 cm^{-1}) and the PROBE was a doubled Lumonics HyperDYE 300 dye laser (linewidth $\approx$ 0.15 cm^{-1}). Both lasers were pumped by a Spectra Physics DCR1A Nd:YAG laser. Iodine fluorescence was used to calibrate both lasers (to $\pm$0.02 cm^{-1}). Typical pulse energies used were 2 μJ for the PROBE and 250 μJ for the PUMP. All of the CaCl spectra were recorded using the $A^2\Pi_{3/2}$ (v=0) state as the intermediate state. CaF spectra were recorded using both the $A^2\Pi_{3/2}$ (v=0) and the $C^2\Pi_{3/2}$ (v=0) states as intermediate states.

References

[1] J. E. Murphy, J. M. Berg, N. A. Harris, and R. W. Field, Phys. Rev. Lett. **65**, 1861 (1990).

[2] J. M. Berg, J. E. Murphy, N. A. Harris, and R. W. Field, Phys. Rev. A **48**, 3012 (1993).

[3] J. E. Murphy, Ph.D. thesis, Massachusetts Institute of Technology, 1992.

[4] K. P. Huber and G. Herzberg, *Constants of Diatomic Molecules* (Van Nostand, New York, 1979).

[5] C. E. Hamilton, J. L. Kinsey, and R. W. Field, Annu. Rev. Phys. Chem. **37**, 493 (1986).

[6] G. W. Adamson, Ph.D. thesis, Massachusetts Institute of Technology, 1994.

[7] C. M. Gittins, Ph.D. thesis, Massachusetts Institute of Technology, 1995.

Figure Captions

Figure 2.1   A schematic diagram of the direct fluorescence method used to detect both CaF and CaCl spectra.

Figure 2.2   A schematic diagram of the fluorescence dip method used to detect CaCl spectra.

Figure 2.3   This figure shows a predissociated state in CaCl that was detected using the fluorescence dip method that did appear when direct fluorescence detection was used.

Figure 2.4   This figure shows the spurious positive signal that interfered with the observation of dips in the CaCl fluorescence dip detected experiment.   The spurious signal is due to excitation of the $C^2\Pi$ (v=3) state by the PROBE laser.

Figure 2.5   A schematic diagram of the REMPI method used to record CaCl spectra.

Figure 2.6   A schematic diagram of how autoionization was used to detect both CaCl and CaF spectra.

Figure 2.7   a) In this region, autoionization spectra were recorded using the $A^2\Pi_{3/2}(v=0)$ state of CaF as the intermediate state. b)   In this region autoionization spectra were recorded using both the $A^2\Pi_{3/2}(v=0)$ and the $C^2\Pi_{3/2}(v=0)$ states as intermediate states. c) In this region, direct UV fluorescence was detected using the $C^2\Pi_{3/2}(v=0)$ state as the intermediate state.   d) In this region, direct UV fluorescence was detected using the $A^2\Pi_{3/2}(v=0)$ state as the intermediate   state.

Figure 2.8   a) In this region, autoionization spectra were recorded using the $A^2\Pi_{3/2}(v=0)$ state of CaCl as the intermediate state.   b) In this region the fluorescence dip scheme was used to detect transitions with the $B^2\Sigma$ (v=0) state as the intermediate state.   c) In this region, direct UV fluorescence was detected using the $B^2\Sigma(v=0)$ state as the intermediate state.   d) In this region, REMPI and direct UV fluorescence spectra were recorded using the $A^2\Pi_{3/2}(v=0)$ and $B^2\Sigma(v=0)$ states respectively as intermediate states.

Figure 2.1 Direct Fluorescence
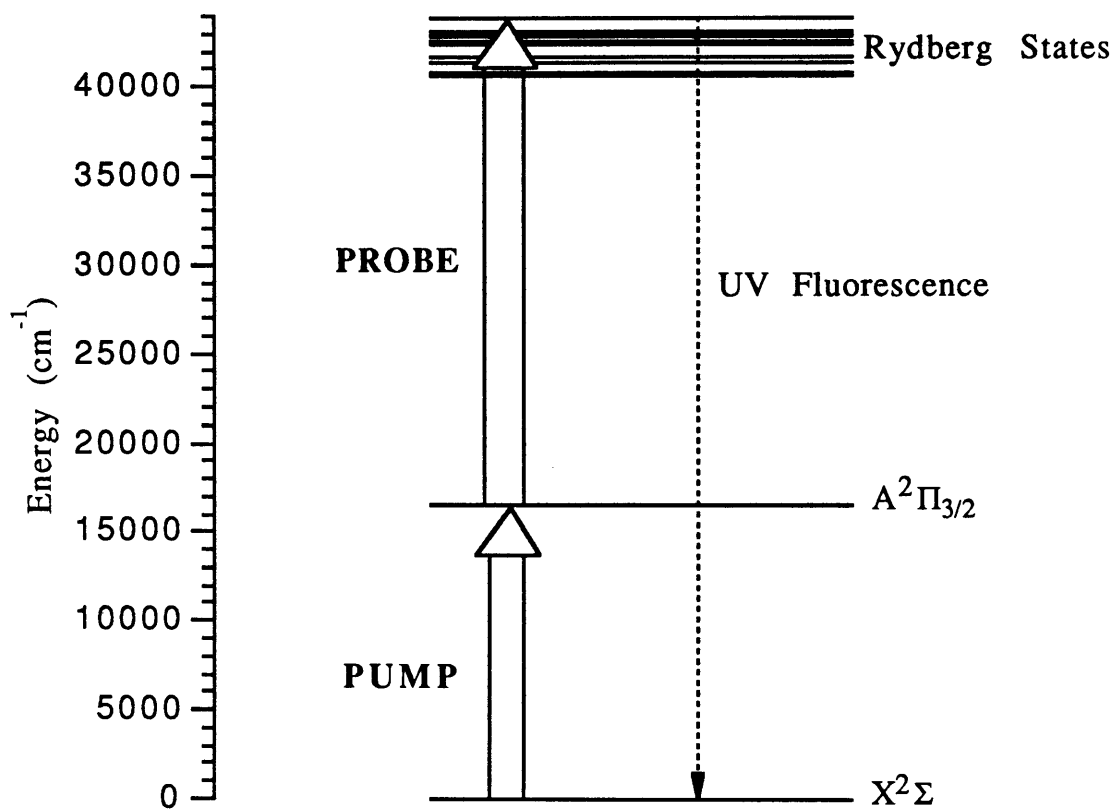
Figure 2.2 Fluorescence Dip
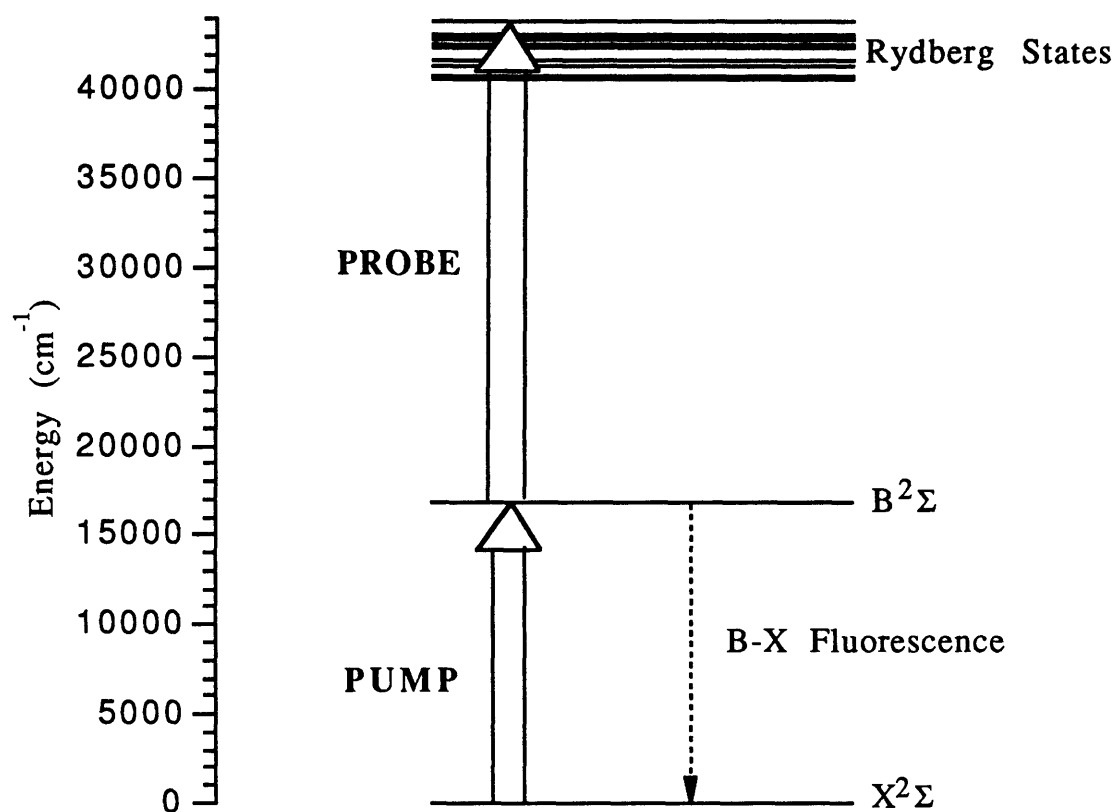
Figure 2.3 Direct Fluorescence vs. Fluorescence Dip for CaCl

$B^2\Sigma$, $R_1(24)$ PUMP

16,863.451 cm^{-1}

Fluorescence Dip

Direct Fluorescence

27545   27550   27555   27560   27565   27570   27575

PROBE Energy (cm^{-1})

Intensity
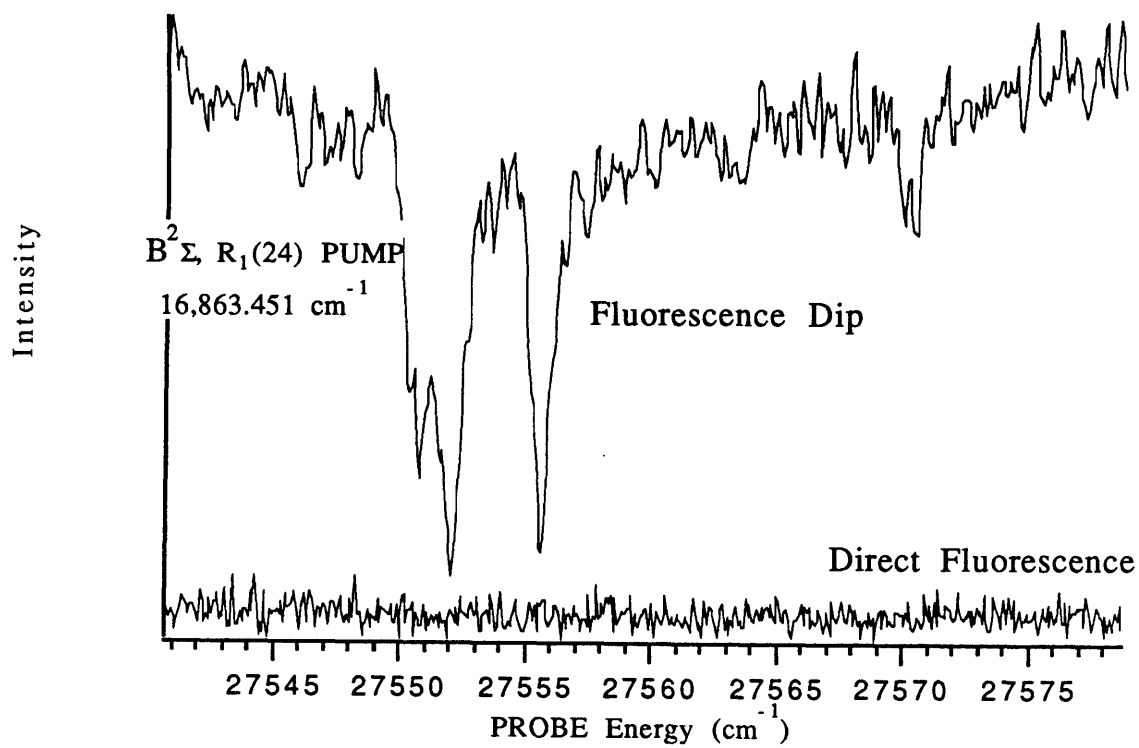
Figure 2.4 Positive signal due to excitation of the $C^2\Pi$ (v=3) state by the PROBE laser

Spurious positive signal due to PROBE laser

Fluorescence Dip

PROBE Energy (cm^{-1})

27545   27550   27555   27560   27565   27570   27575
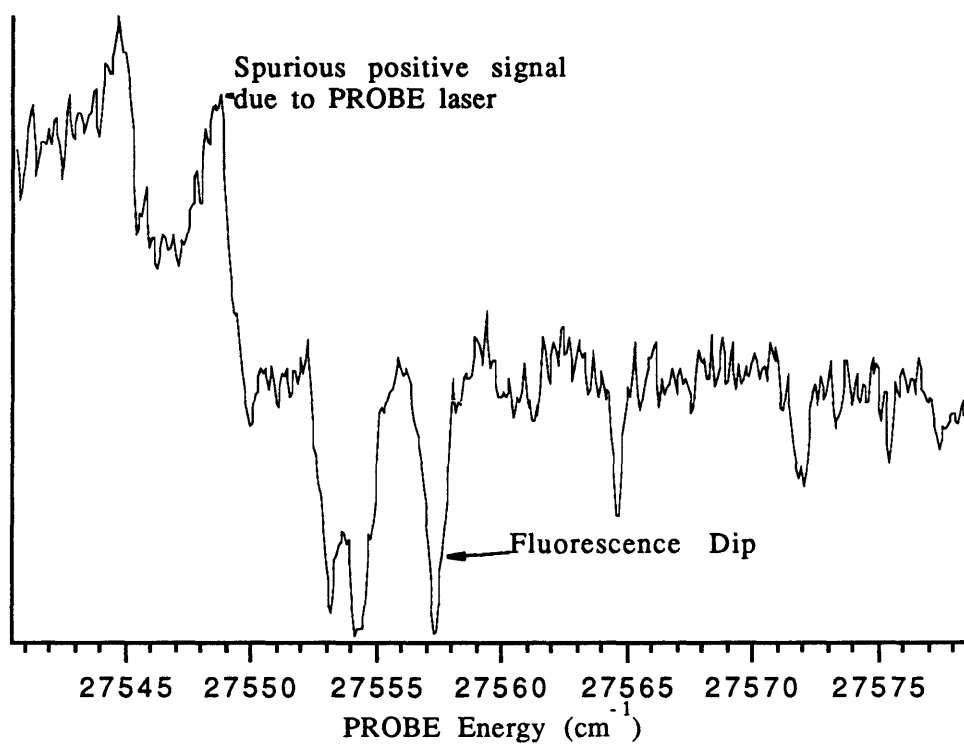
Figure 2.5 REMPI

Figure 2.6 Autoionization
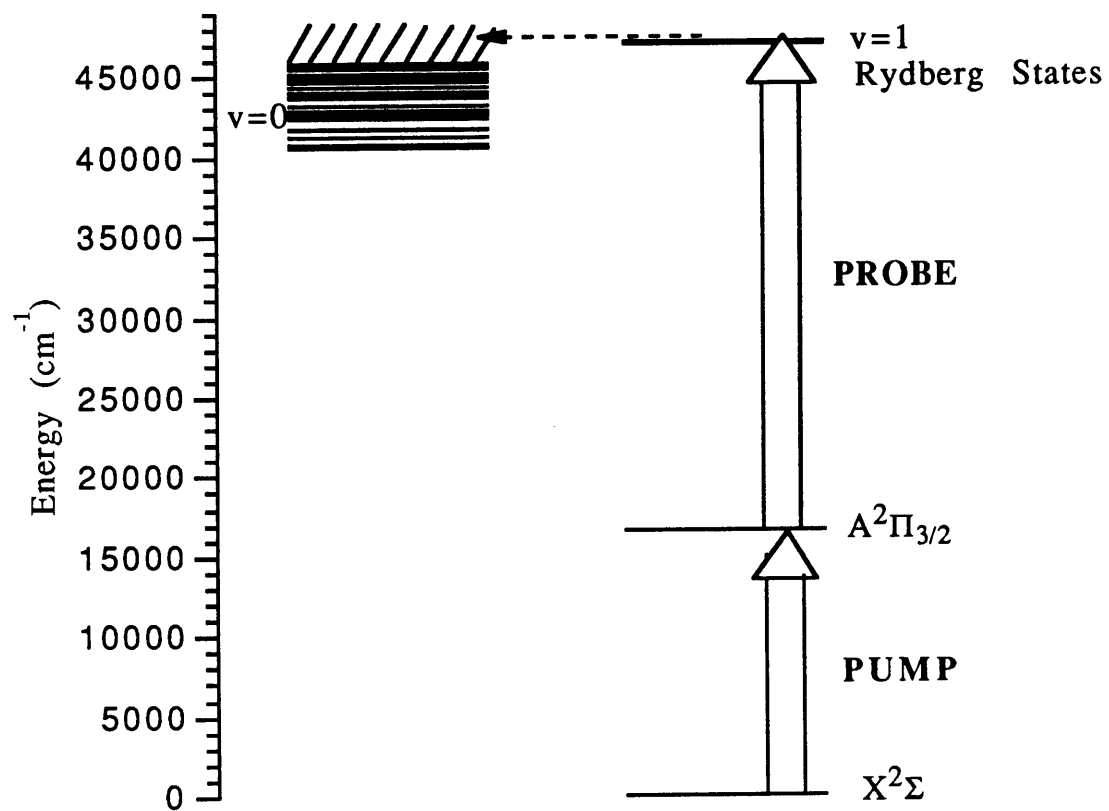
Figure 2.7 CaF
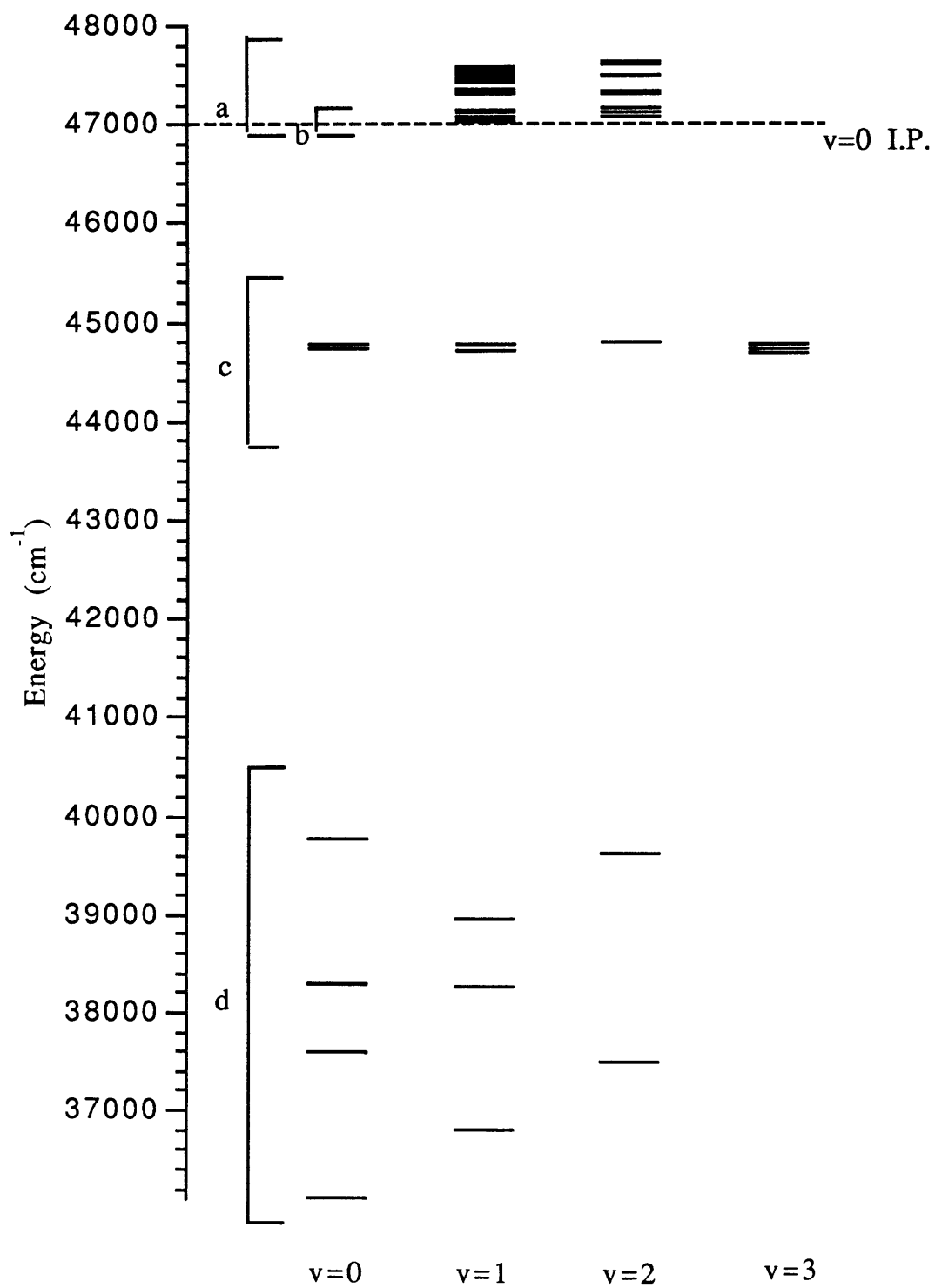
Figure 2.8 CaCl
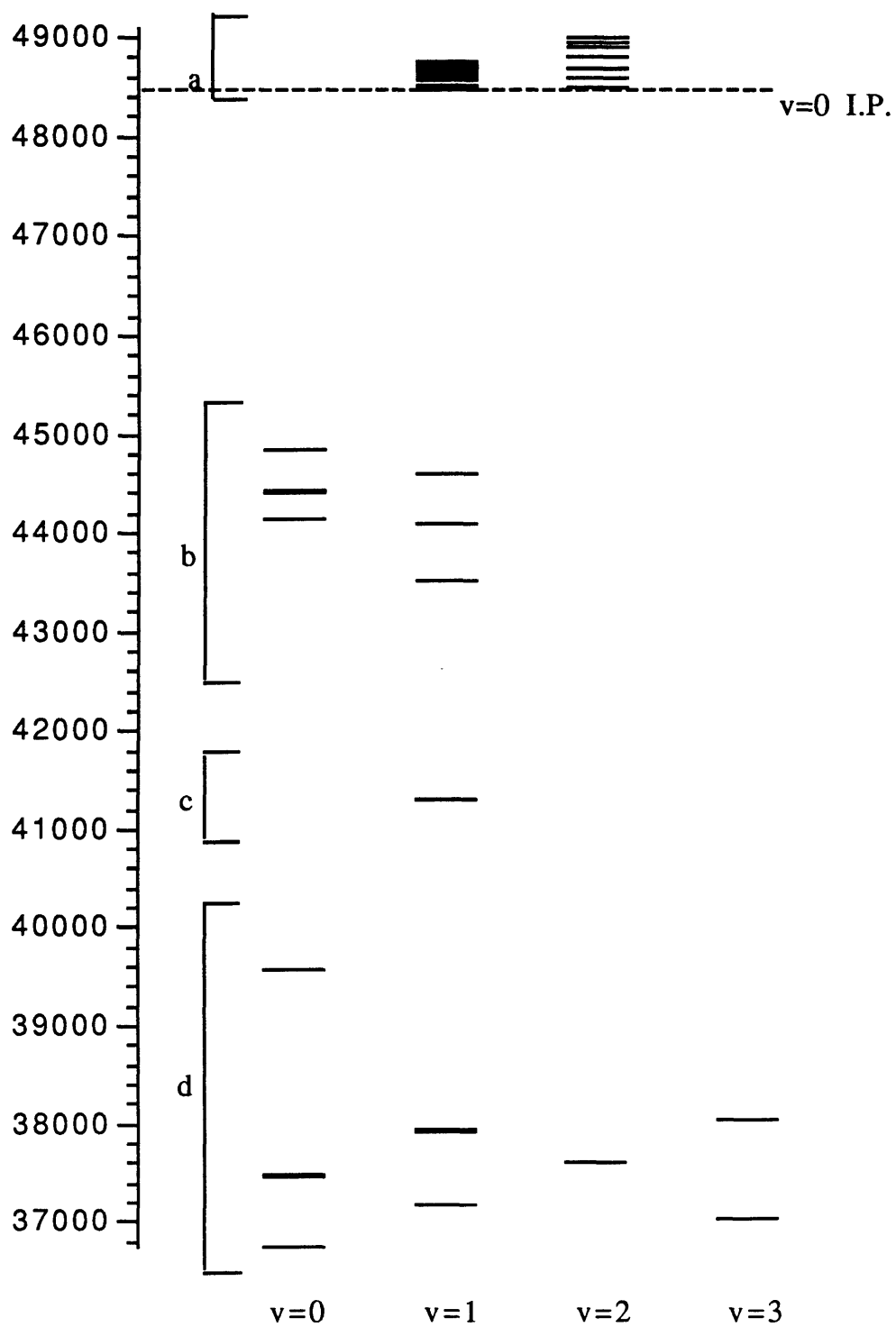
Chapter 3
The Core Penetrating States: "Valence"-state Precursors, Scaling, and Predissociation

Part 3.1 CaF

Part 3.1.1 Core-penetrating vs. Core-nonpenetrating

The calcium fluoride electronic states can be grouped into two general categories, core-penetrating and core-nonpenetrating states. Each group of states has a unique set of characteristics which enables them to provide information about the interaction of the nonbonding Rydberg electron with the CaF^+ cation. The core-penetrating states have amplitude in region I (see Figure 3.1) and derive a significant part of their quantum defect (scattering phase shift) from short range interactions. These states sample the core (regions I and II) and provide information about the bonding between the atomic ions, and interactions of the electron with the Ca^{2+} and F^- ions. The core-nonpenetrating states (those with $\ell > 2$) are held out of the core by the centrifugal barrier ($\ell(\ell +1)/r^2$). They have negligible amplitude in region II. The core-nonpenetrating states derive their quantum defects from long-range interactions with the core and therefore provide information about the multipole moments of the molecular cation. These states will be discussed further in Chapter 4.

Part 3.1.3 "Valence"-state Precursors

Each of the core-penetrating Rydberg series can be extrapolated back to a "valence"-state precursor. This is the lowest energy state that belongs to a Rydberg series. These states are well represented by a ligand-field atomic-ion-in-molecule model[1]. In that model the CaF states are described as Ca^+ atomic-ion states perturbed by a point charge, the F^-, which causes the atomic Ca^+ $n\ell\lambda$ states to mix and thereby destroys ℓ. Each precursor state of CaF is represented as a linear combination of Ca^+ $n\ell\lambda$ atomic-ion states.

In the "valence" -state precursor, the unpaired electron occupies an orbital which consists only of the intracore loops of the Rydberg orbital. Each Rydberg orbital within a series is built upon these intracore loops (the nodes line up inside the core) which express the complex interactions of the nonbonding electron with the molecular ion-core. The quantum defect is a measure of these complex interactions and therefore is expected to be nearly constant

(it is only weakly energy dependent[2]) within a series. There are small deviations in the quantum defect for the n*-lowest states, but in each case the Rydberg series connects smoothly to its "valence"-state precursor and the deviations can be explained based on the expected polarization of the orbitals (in the core region)[3]. The "valence"-state precursors for each of the six core penetrating Rydberg series are labeled in Figures 3.2 and 3.3. Table 3.1 contains each of the "valence"-state precursors with its nominal Ca^+ $n\ell$ character and the n*-label for its series (the series label is just the n*(mod 1) for the series). The states are referred to by this label in the sense that the 9.55 $^2\Sigma^+$ state is a member of the 0.55 $^2\Sigma^+$ series and the 8.98 $^2\Pi$ state is a member of the 0.98 $^2\Pi$ series.

Table 3.1 "Valence"-state precursors with their dominant ℓ character and n* and the n* label for its series

	T_0 (cm^{-1})	n*	Nominal Ca^+ $n\ell$	n*-label for series
X $^2\Sigma^+$	0.00	1.53	4 s	0.55
A $^2\Pi$	16,529.69	1.90	4 p	0.98
B $^2\Sigma^+$	18,841.31	1.97	3 d	0.88
B' $^2\Delta$	21,543.89	2.08	3 d	0.14
C $^2\Pi$	30,215.95	2.56	3 d	0.36
F' $^2\Sigma^+$	36,125.98	3.18	4 p	0.19

Part 3.1.2 Scaling

The core penetrating states have been arranged into six Rydberg series with the familiar Rydberg equation[4-6].

$$E_{IP} - E_{n*} = \frac{R}{n*^2}, \quad n* = n - \mu. \quad (3.1)$$

E_{n*} is the rotationless term value of each Rydberg state, n* is the effective principal quantum number, μ is the quantum defect mentioned above, R is the Rydberg constant (which is equal to 109,737 cm^{-1}), and $E_{I.P.}$ is the ionization potential (46998 ± 5 cm^{-1})[4-6]. After vibrational assignments were made, the ionization potential was determined by Murphy assuming a constant quantum defect. As the energy of the states used to calculate the I.P. increase, the accuracy of the calculated ionization potential increase. The

value of 46998 ± 5 cm^{-1} determined by Murphy et al. for the v=0 ionization potential has proven to be sufficiently accurate to assign the v=1 states in the n* = 13-18 region observed by autoionization. A slightly more accurate value of the v=1 ionization potential [which is $E_{I.P.}$(v=0) + $\Delta G_{1/2}$(for CaF$^+$), $\Delta G_{1/2}$= G(1) - G(0)] of 47,687.5 ± 0.5 cm^{-1} has been determined from the v=1 states in the n*=27-32 region.

Equation 3.1 represents one of most important scaling relations used to arrange the states into series. Knowledge of the scaling relations of molecular constants such as the spin-orbit constant (A_{SO}) for $^2\Pi$ and $^2\Delta$ states and spin-rotation constant (γ) for $^2\Sigma^+$ states, were also a great help to Murphy et. al. in grouping the states into series and confirming the series assignment[5,6]. The spin-orbit constant is expected to scale as n*$^{-3}$. The origin of this scaling is in the r^{-3} dependence of the spin-orbit operator[6]. Figure 3.4 shows the scaling for A_{SO}. The spin-rotation constant,

$$\gamma = \frac{2AB\, \ell(\ell +1)}{E_\Pi - E_\Sigma} , \qquad (3.2)$$

is expected to be constant within a series because both the numerator and denominator scale as n*$^{-3}$.[5,6] Figure 3.5 shows the scaling behavior of γ. This scaling relation is likely to break down at very high n* where the energy difference becomes small and rapid ℓ-uncoupling occurs. This scaling relation assumes that the rotational constant, B, will be constant as n* increases. Figures 3.6 and 3.7 show that this assumption is not valid (this effect will become more important at high-n*).

The variations of the rotational and vibrational constants as n* decreases are more of a trend rather than a true scaling relation. However insight into the bonding of the calcium fluoride molecule, the direction of the polarization of the orbitals of the "valence"-state precursors, and the shape of the inner lobes of the Rydberg orbitals is provided by studying these trends. Figures 3.6 and 3.7 show how the rotational constants increase as n* increases and become nearly constant at about n*=4. This trend is observed for the vibrational constants as well (Figures 3.8 and 3.9)

CaF is ionically bound, thus when the Rydberg orbital collapses at low-n* into the core region, the Rydberg electron partially shields the Ca^{2+} ion from the F$^-$ ion and thereby weakens the ionic bond. This weakening of the ionic bond causes a decrease in the rotational

and vibrational constants. This weakening of the ionic bond causes a decrease in the rotational and vibrational constants at low n*.

Two states stand out as opposite extremes in this trend, the $C^2\Pi$ state and the F' $^2\Sigma^+$ state. Ligand field theory predicts that the open-shell orbital in the $A^2\Pi$ state will be polarized away from the ligand and that in the $C^2\Pi$ state it will be polarized toward the ligand. Due to the direction of its orbital polarization, the $C^2\Pi$ state is expected to have higher electron density between (e.g. shielding) the two ions than any of the other electronic states of CaF. This increased electron density between the ions causes the $C^2\Pi$ state to have the smallest rotational and vibrational constants of all known states of CaF. Figures 3.7 and 3.9 illustrate this. The F' $^2\Sigma^+$ state is similar to the $C^2\Pi$ state in that it is polarized toward the F⁻, however Figures 3.6 and 3.8 show that it does not have small rotational and vibrational constants, but instead has the largest of all the observed CaF rotational and vibrational constants in this energy region. The F' $^2\Sigma^+$ orbital is pushed so high in energy due to repulsion by the F⁻ that the corresponding orbital is essentially pushed entirely out of the core region and therefore the F' $^2\Sigma^+$ has the largest rotational and vibrational constants of all of the "valence"-state precursors.[3]

Part 3.1.3 Comparison of the $A^2\Pi$ and $C^2\Pi$ States ("Valence"-State Precursors) as Intermediate (PUMP) States in Double Resonance Experiments

In the experiments presented in this thesis both the $C^2\Pi$ and $A^2\Pi$ "valence"-state precursors have been used as intermediate states in optical-optical double resonance experiments. Although these two states both have p and d character according to ligand field theory[1], we found that we are able to access a complementary set of states with the $C^2\Pi$ state as the intermediate state instead of the $A^2\Pi$ state. The A $^2\Pi$ state has 60%/40% p/d Ca⁺ character. Based on atomic ($\Delta \ell = \pm 1$) and molecular ($\Delta \Lambda = 0, \pm 1$) selection rules, we should be able to access sΣ, pΣ, dΣ, fΣ, pΠ, dΠ, fΠ, dΔ, and fΔ through the $A^2\Pi$ state. However, Murphy et al, who used the $A^2\Pi$ state for most of his experiments observed only the core-penetrating states in his spectra[4-6]. He did observe weak fragments of what he thought might be an f-complex, however, those states were never conclusively assigned.[7] States that were strong in Murphy's spectra

were weak or did not appear in the spectra recorded out of the $C^2\Pi$ state in the n*=7 region, with the exception of the 5.55 $^2\Sigma^+$(v=2) state. Although the spectra were difficult to assign, it was clear that a new set of states could be observed out of the $C^2\Pi$ state. This new set of states had to be the core-nonpenetrating states. The spectra recorded in the n*=13 and 14 regions confirmed that the core-nonpenetrating states are observed out of the $C^2\Pi$ state and the core-penetrating states are observed out of the $A^2\Pi$ state. This would seem to suggest that the $A^2\Pi$ state is more "p-like" and the $C^2\Pi$ state is more "d-like". If this were the case, the pΠ series should be strong in the $C^2\Pi$ state PUMP spectra, it is not. Simple atomic selection rules are not enough to explain the difference in the intensity patterns of the two sets of spectra.

The polarization of the orbitals in the $A^2\Pi$ and $C^2\Pi$ states[1] could provide a simple, possibly naive, explanation for the difference in the intensity patterns of the spectra. The orbitals of the core-penetrating states are centered on the Ca^{2+} core and will overlap well with the orbital of the $A^2\Pi$ state which is polarized away from the F^-. The orbitals of the core-nonpenetrating states should be centered closer to the center of mass of the molecule, so they probably overlap better with the orbitals of the $C^2\Pi$ state which is polarized toward the F^- (has the most electron density between the two ions). Figures 3.10 and 3.11 summarize which of the states appear in the spectra when the $A^2\Pi$ state is used as the intermediate state and the complementary group of states that appear when the $C^2\Pi$ state is used as the intermediate.

It would seem as CaF is the perfect molecule for studying core-nonpenetrating Rydberg states, since these states show up so easily and selectively from the $C^2\Pi$ intermediate state. Although it is convenient that we have a way to observe these states, the fact that $C^2\Pi$ state is reverse polarized adds a degree of difficulty to assigning the spectra recorded from this state that does not exist for spectra recorded out of the $A^2\Pi$ state. Tables 3.2 and 3.3 show vibrational overlap integrals of the Rydberg $\leftarrow$ A $^2\Pi$ transition and the Rydberg $\leftarrow$ C $^2\Pi$ transition. Murphy observed v=0-3 Rydberg states out of the $A^2\Pi$ state[6]. According to the vibrational overlap integrals we should be able to observe v=0-6 out of the $C^2\Pi$ state. The fact the we could observe v=0-6 Rydberg states makes the spectra considerably more difficult to assign (especially for the core-nonpenetrating states since we do not know the vibrational dependence of the splittings in the f

33

and g complexes). Recording autoionization detected spectra simplifies the spectra slightly because v=0 is not observed. v=4 is the highest vibrational level assigned so far in the autoionization detected spectra.

Table 3.2 Vibrational overlap integrals of the Rydberg ← $A^2\Pi$ transition. Both $A^2\Pi$ and Rydberg state potential curves were calculated using the RKR method.

Rydberg v'	$A^2\Pi$ v"	<v'lv">
0	0	0.796
1	0	0.544
2	0	0.251
3	0	0.089
0	1	-0.530
1	1	0.427
2	1	0.603
3	1	0.379

Table 3.3 Vibrational overlap integrals of the Rydberg ← $C^2\Pi$ transition. Both $C^2\Pi$ and Rydberg state potential curves were calculated using the RKR method.

Rydberg v'	$C^2\Pi$ v"	<v'lv">
0	0	0.347
1	0	0.504
2	0	0.519
3	0	0.436
4	0	0.318
5	0	0.208
6	0	0.124
7	0	0.069
0	1	-0.499
1	1	-0.385
2	1	-0.479
3	1	0.257
4	1	0.407
5	1	0.411

6	1	0.334
7	1	0.234

Part 3.2 CaCl

Part 3.2.1 Predissociation

The electronic structure of CaCl is expected to be similar to that of CaF, but there is one important difference. This is that the dissociation limit is only 32,990 cm^{-1} [8], which is lies 15,500 cm^{-1} (n*= 2.7)*below* the ionization potential (48,489 cm^{-1})[9], whereas the dissociation limit of CaF is 44,200 cm^{-1} [8], only 2,800 cm^{-1} (n*= 6.3) below its ionization potential (46,998 cm^{-1})[4-6]. This low dissociation limit of CaCl has both good and bad consequences. The disadvantage is that the intermediate-n* states (n*=4-10), that provide the foundation for understanding the higher n* states, are predissociated, thus making them difficult to observe. The good side is that unique insights into the mechanism of the $Ca^{2+}Cl^-$ ($X^1\Sigma$) + e$^-$ ⇨ $Ca^o(^1S)$+ $Cl^o(^2P)$ dissociative recombination reaction could be provided by studying accurate measurements of linewidths vs. n*, ℓ, λ, v, and N.

The dissociation of the $CaCl^+$ ion core is surprising because it requires two electron-transfer steps. In the first step, the Rydberg must enter the spatial region of the 4sσ orbital on the Ca^{2+}. Second, while the Rydberg electron is near the Ca^{2+}, an F$^-$ 2pπ or 2pσ electron must transfer to the Ca 4sσ. The rates, Γ, of such two-e$^-$ dissociative processes[10-12] are determined by the product of an interelectronic $1/r_{12}$ matrix element and a vibrational overlap factor

$$\Gamma \propto |<Ca^o4s, Ca^o4s|\frac{1}{r_{12}}|CaCl\ n^*\ell\lambda, Cl^-3p\sigma\ or\ 3p\pi> \times <v_{n^*\ell\lambda}|\varepsilon_{Ca,Cl}>|^2 . \quad (3.3)$$

The vibrational dependence of the predissociation rate of a particular Rydberg state could provide information about where the Ca^o + Cl^o curve crosses the $Ca^{2+}Cl^-$ Rydberg curves (see Figure 3.12). If some vibrational levels are more strongly predissociated, this might suggest the path that the Ca^o + Cl^o curve takes through the $Ca^{2+}Cl^-$ Rydberg curves. For example, if the v=0 level is strongly predissociated but the v=1 level is relatively free of predissociation this could suggest the repulsive curve passes directly though the

minimum of the Rydberg curve. The vibrational integral also depends on n^* because the intersection of the repulsive $Ca^{o+} + Cl^o$ and bound $Ca^{2+}Cl^-$ potential curves moves from near R_e at low n^* to shorter internuclear distances as n^* increases.

The electronic integral is nonzero only for $\lambda=0(\Sigma)$ or $1(\Pi)$ Rydberg states and should scale according to the $\sim n^{*-3/2}$ dependent amplitude of the CaCl $n^*\ell\lambda$ orbital inside the $Ca^o 4s$ atomic orbital (largest for low-ℓ, very small for nonpenetrating series). It should be larger for $^2\Sigma$ than $^2\Pi$ Rydberg states due to the larger overlap of the $Cl^o 3p\sigma$ with the $Ca^o 4s$ than that of the $Cl^o 3p\pi$ (the Rydberg e^- must be in a π orbital for the two-e^- $1/r_{12}$ matrix element between $Ca^o 4s$ and $Cl^o 3p\pi$ to be nonzero) with the $Ca^o 4s$.

The $\lambda>1$ states can only be predissociated by mixing with states that are predissociated, thus we expect the $^2\Delta$ states will be free of predissociation at low n^* and low N. As N (and n^*) increases the $^2\Delta$ should display an N^2-dependent predissociation rate.

The amount and quality of spectra currently available does not allow these scaling relations for predissociation rates to be tested. The spectra available could be more completely analyzed if spectra in the critical n^*=4-10 region were recorded and analyzed. Chapter 7 describes an experiment which might provide this important information. Currently, only spectra in the $n^*<$ 5 (fluorescence) and n^*=16-40 (v=1 autoionization) regions have been recorded.

Part 3.2.2   "Valence"-state Precursors

The Rydberg spectra that have been recorded in the n^* < 5 region can be arranged into six Rydberg series and assigned a "valence"-state precursor as was done for CaF. Molecular constants have not been measured for the states in the n^*=3-5 region, so scaling relations cannot be used to confirm assignments. The six series along with their "valence"-state precursors are presented in Figure 3.13. A comparison of the energy and n^* values for the lowest CaF and CaCl electronic states presented in Figure 3.14 shows that the electronic structures of these two molecules are similar but not identical.

References

1 S. F. Rice, H. Martin, and R. W. Field, J. Chem. Phys. 82, 5023 (1985).

2 C. H. Greene and Ch. Jungen, Adv. At. Mol. Phys. **21**, 51 (1985).

3 N. A. Harris and R. W. Field, J. Chem. Phys. **98**, 2642 (1993).

4 J. E. Murphy, J. M. Berg, N. A. Harris, and R. W. Field, Phys. Rev. Lett. **65**, 1861 (1990).

5 J. M. Berg, J. E. Murphy, N. A. Harris, and R. W. Field, Phys. Rev. A **48**, 3012 (1993).

6 J. E. Murphy, Ph.D. thesis, Massachusetts Institute of Technology, 1992.

7 J. E. Murphy, private communication.

8 K. P. Huber and G. Herzberg, *Constants of Diatomic Molecules* (Van Nostand, New York, 1979).

9 N. A. Harris, C. M. Gittins, and R. W. Field, to be published.

10 A. Giusti, J. Phys. B: Atom. Molec. Phys. **13**, 3867 (1980).

11 W. A. Chupka, J. Chem. Phys. **98**, 4520 (1993).

12 A. Fujii and N. Morita, J. Chem. Phys. **98**, 4581 (1993).

Figure Captions

Figure 3.1 - This is a schematic representation of the different regions of the core. Region I is the Ca^{2+} ion, Region II is the entire area inside the ellipse, which is the molecular core. Region III is outside the core, and is the spectral region where the core-nonpenetrating states have all of their amplitude.

Figure 3.2 - n* vs. n*(mod 1) for CaF. This figure shows how the "valence"-state precursors connect to the three Σ-series.

Figure 3.3- n* vs. n*(mod 1) for CaF. This figure shows how the "valence"-state precursors connect to the two Π and one Δ series. The n*= 3.11 $^2\Delta$ state is predicted because this state has not yet been observed.

Figure 3.4 - Spin-rotation constant vs. n* for CaF. This figure shows how γ displays the expected n^{*0} scaling relationship. The deviations from the expected scaling behavior are due to the energy reordering at low-n* and can be qualitatively accounted for.

Figure 3.5 - A_{SO} x n^{*3} vs. n* for CaF. This figure shows the n*-scaling of the spin-orbit constant. The deviations at low-n* are due to

reverse polarization effects. The 3.11 $^2\Delta$ state has not yet been observed. The value of the spin-orbit constant for the 3.11 $^2\Delta$ state is predicted by extrapolation from the other states in the 0.11 Δ-series.

Figure 3.6 - B vs. n* for CaF. This figure shows how the rotational constant of the Σ-states increases as n* increases. B^+ is the rotational constant of the CaF^+ ion. The deviations above n*=5 are due to the onset of ℓ-uncoupling.

Figure 3.7 - B vs. n* for CaF. This figure shows how the rotational constants of the Π and Δ states increase as n* increases. The B^+ value is the rotational constant of the CaF^+ ion in v=0. The deviations above n*=5 are due to the onset of ℓ-uncoupling. The spin-orbit constant for the 3.11 $^2\Delta$ state was predicted from the other states in the 0.11 Δ-series.

Figure 3.8 - $\Delta G_{1/2}$ vs. n* for CaF. This figure shows how the vibrational constant of the Σ-states increases as n* increases. $\Delta G^+_{1/2}$ is the vibrational interval of the CaF^+ ion.

Figure 3.9 - $\Delta G_{1/2}$ vs. n* for CaF. This figure shows how the vibrational constants of the Π-and Δ-states increase as n* increases. The $\Delta G^+_{1/2}$ value is the vibrational interval of the CaF^+ ion. The vibrational constant for the 3.11 $^2\Delta$ state was predicted from the other states in the 0.11 Δ-series.

Figure 3.10 - This figure shows spectra in the n*=13 region recorded from both the $A^2\Pi$ and $C^2\Pi$ states of CaF. This figure displays that the intensity pattern in not the same for spectra recorded out of the different intermediate states.

Figure 3.11 - This figure shows spectra in the n*=14 region recorded from both the $A^2\Pi$ and $C^2\Pi$ states of CaF. The figure displays that the intensity pattern is not the same for spectra recorded out of the two different intermediate states.

Figure 3.12 - This figure shows a schematic diagram of the potential curves of CaCl.

Figure 3.13 - n* vs. n*-n*(mod 1) for CaCl. This figure shows the "valence"-state precursors for all six series in CaCl.

Figure 3.14 - This figure shows the energy and n* values of the lowest states of CaF and CaCl. The ground state is not on the plot so the energy scale of the graph could be expanded. The n* values for the ground states are 1.53 and 1.50 for CaF and CaCl, respectively.

Figure   3.1
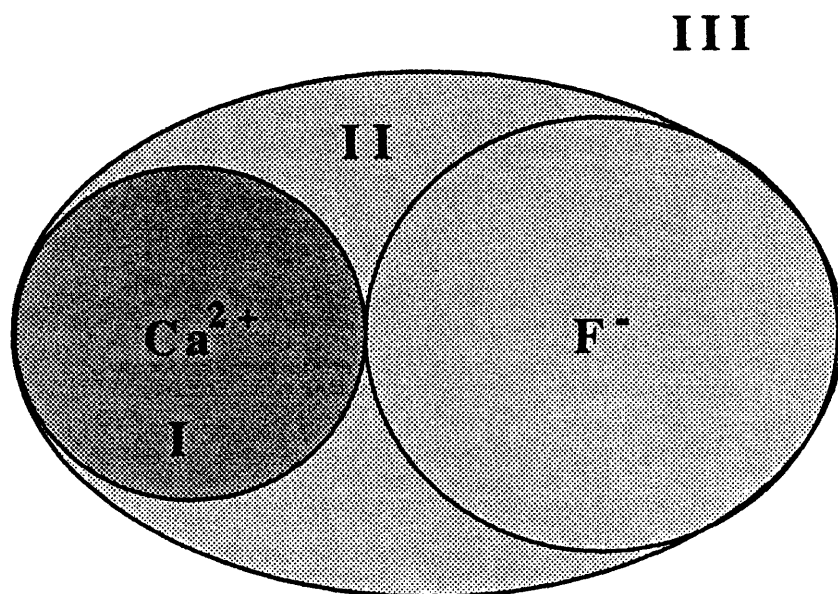
Figure 3.2
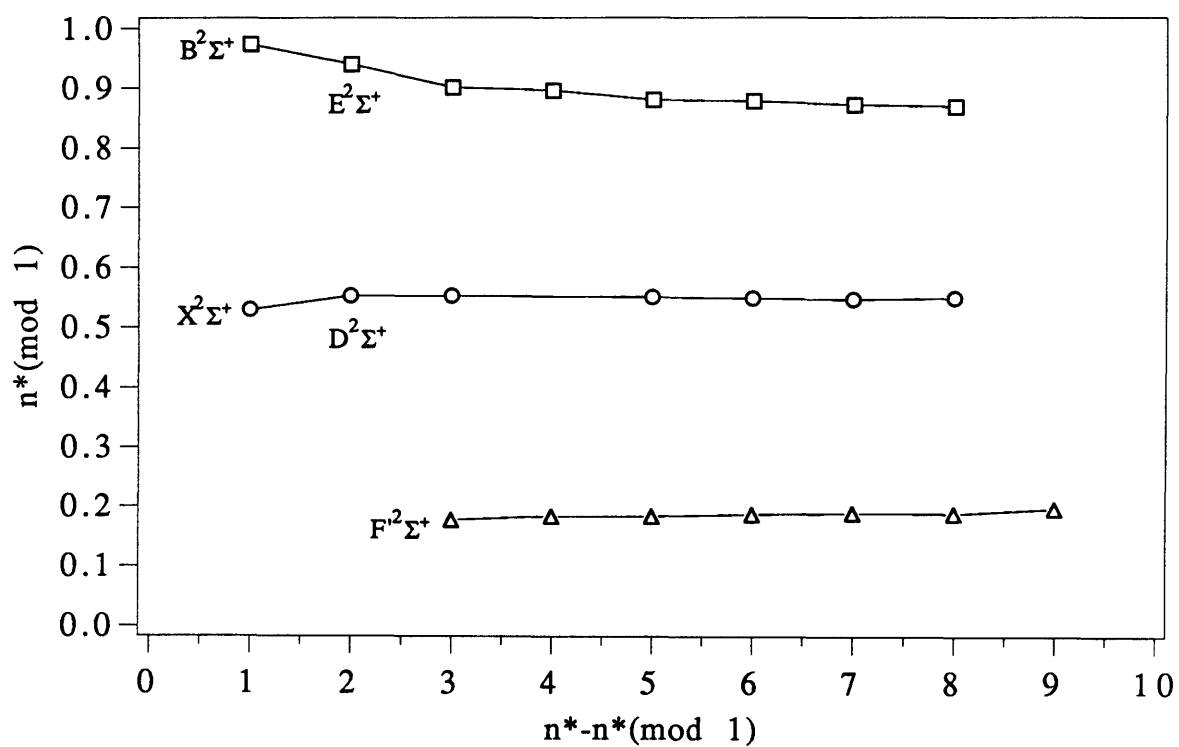
Figure 3.3
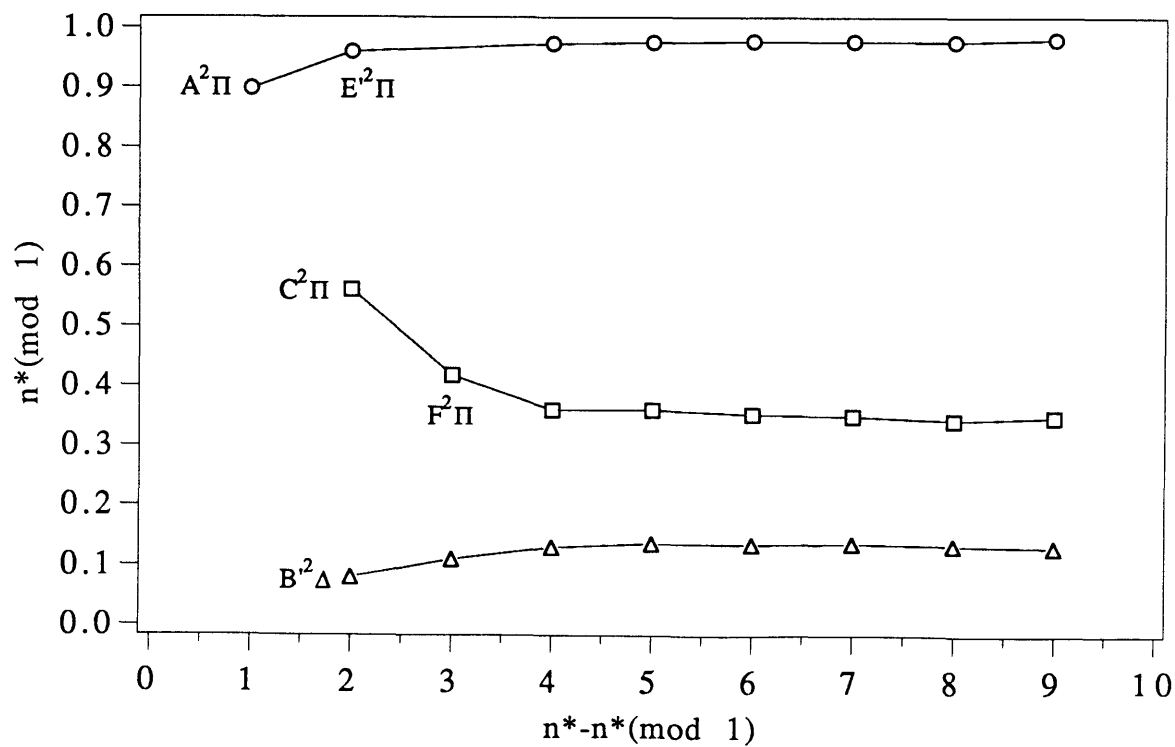
Figure 3.4
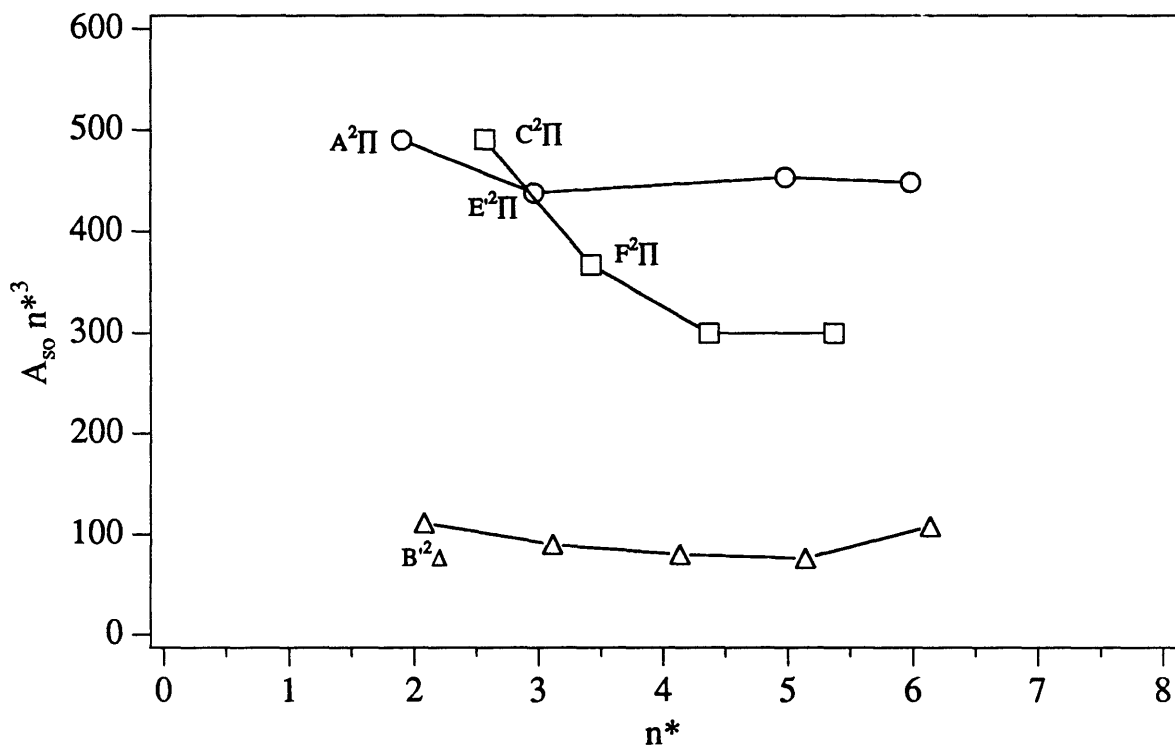
Figure 3.5
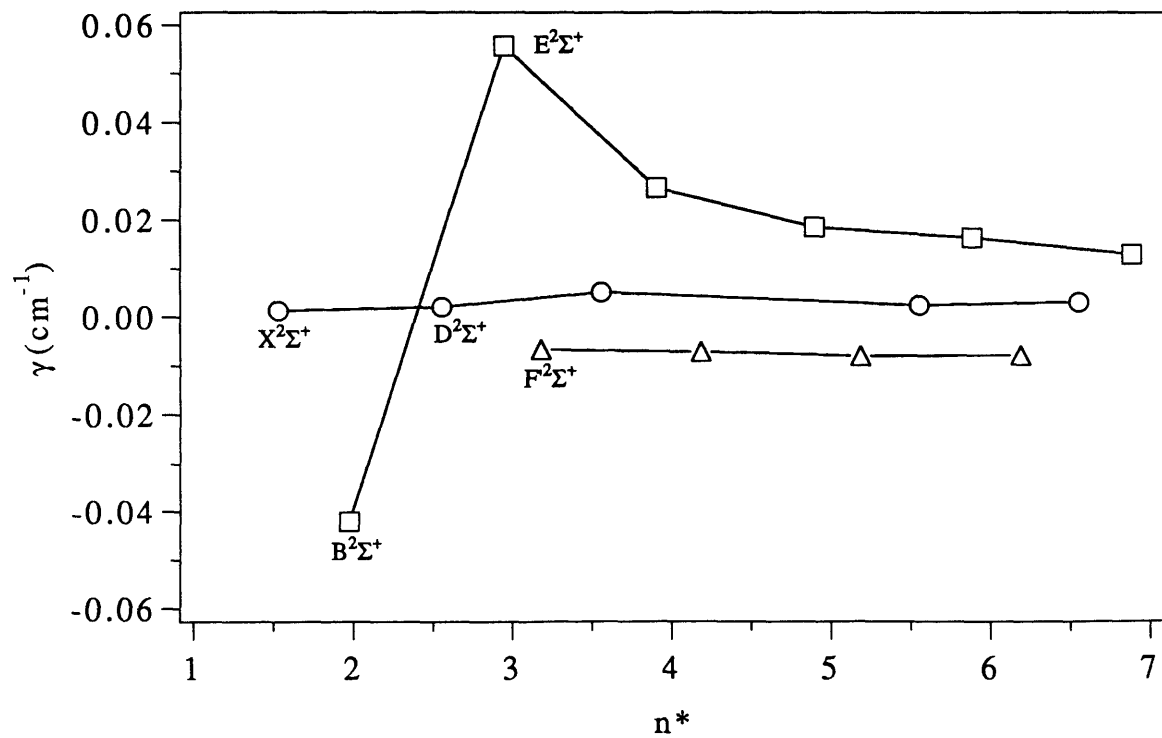
Figure 3.6
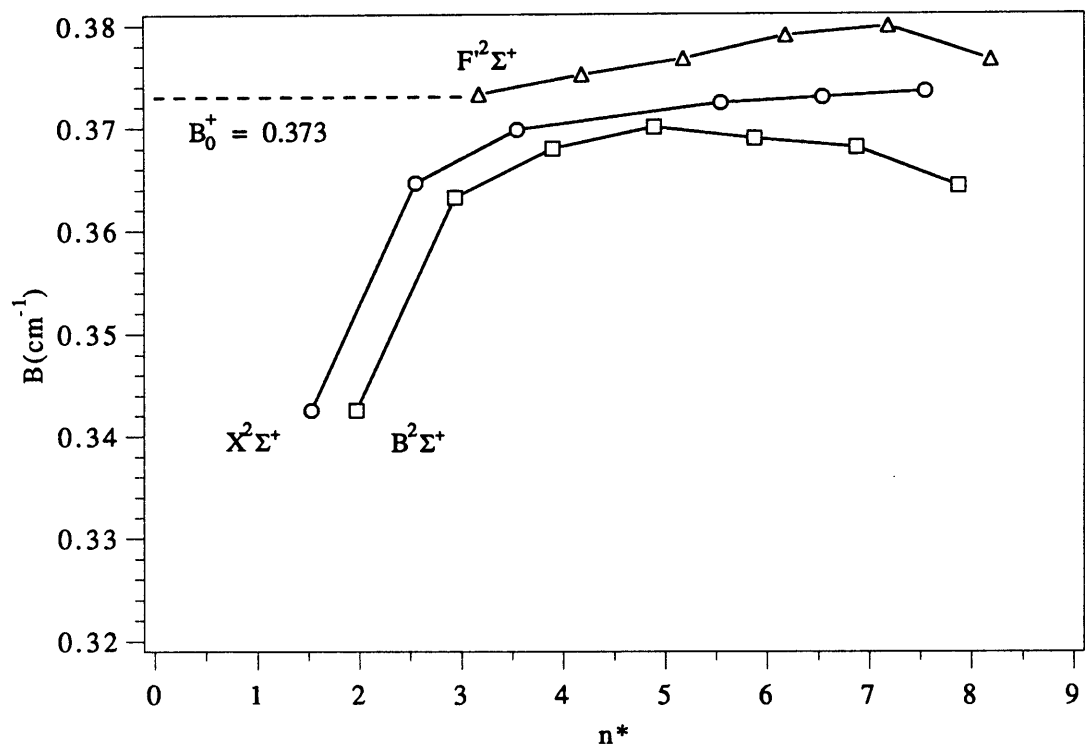
Figure 3.7
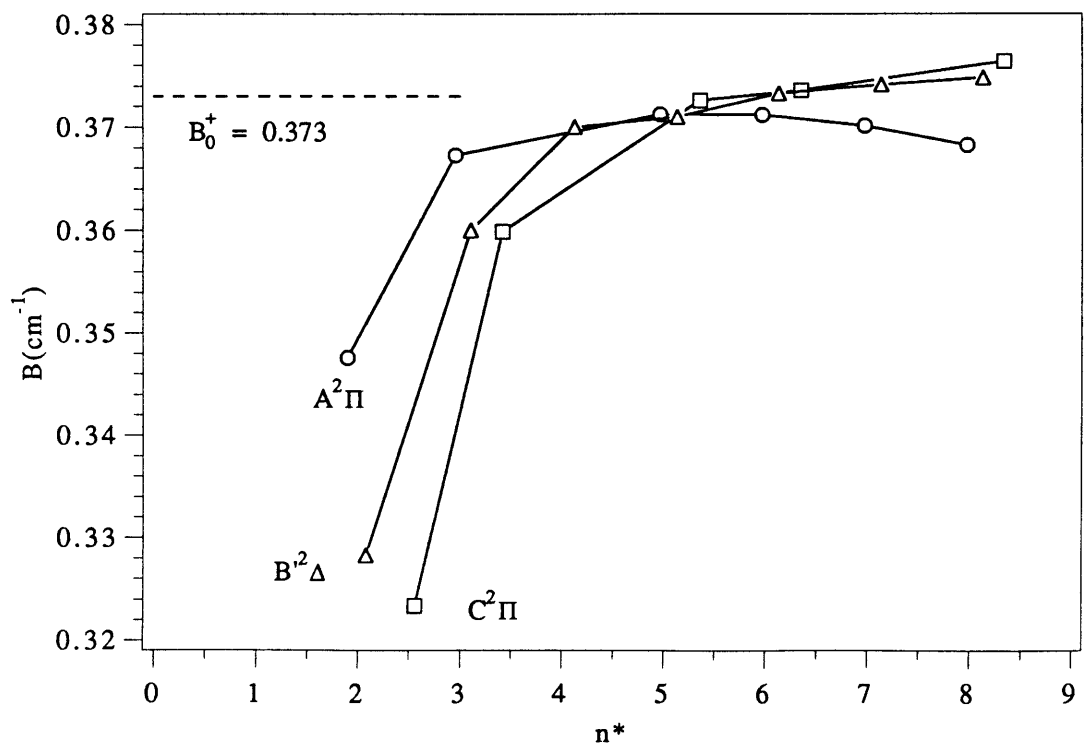
Figure 3.8
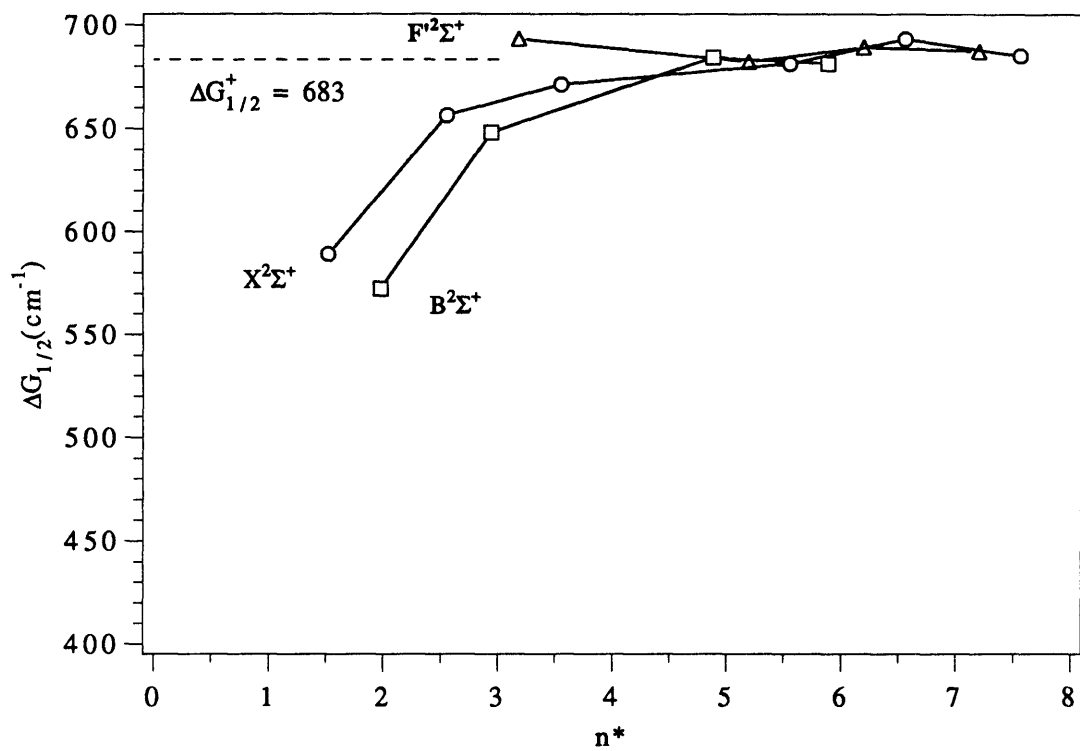
Figure 3.9

Figure 3.10 n*=13 for CaF

$\mathcal{L} = +1$, v=2 $\mathcal{L} = -1$, v=2

$\mathcal{L} = 0$, v=2 $\mathcal{L} = -2$, v=2

$\mathcal{L} = -2$

$\mathcal{L} = -1$ $\mathcal{L} = -3$

$R_{21}(6.5)$
J=7.5 e

$C^2\Pi$ State PUMP

$A^2\Pi$ State PUMP

$Q_2(6.5)$
J=6.5 e

$R_{21}(5.5)$
J=6.5 e

$C^2\Pi$ State PUMP

$A^2\Pi$ State PUMP

$Q_2(5.5)$
J=5.5 e

$R_{21}(4.5)$
J=5.5 e

$Q_{14.14\Delta}$ $C^2\Pi$ State PUMP

$R_{14.14\Delta}$

$P_{14.14\Delta}$ $A^2\Pi$ State PUMP

$Q_2(4.5)$
J=4.5 e

$R_{21}(3.5)$
J=4.5 e

$C^2\Pi$ State PUMP

760   780   800   820   840

$\nu_{PROBE} - 15000\ cm^{-1}$ ($C^2\Pi$ state)
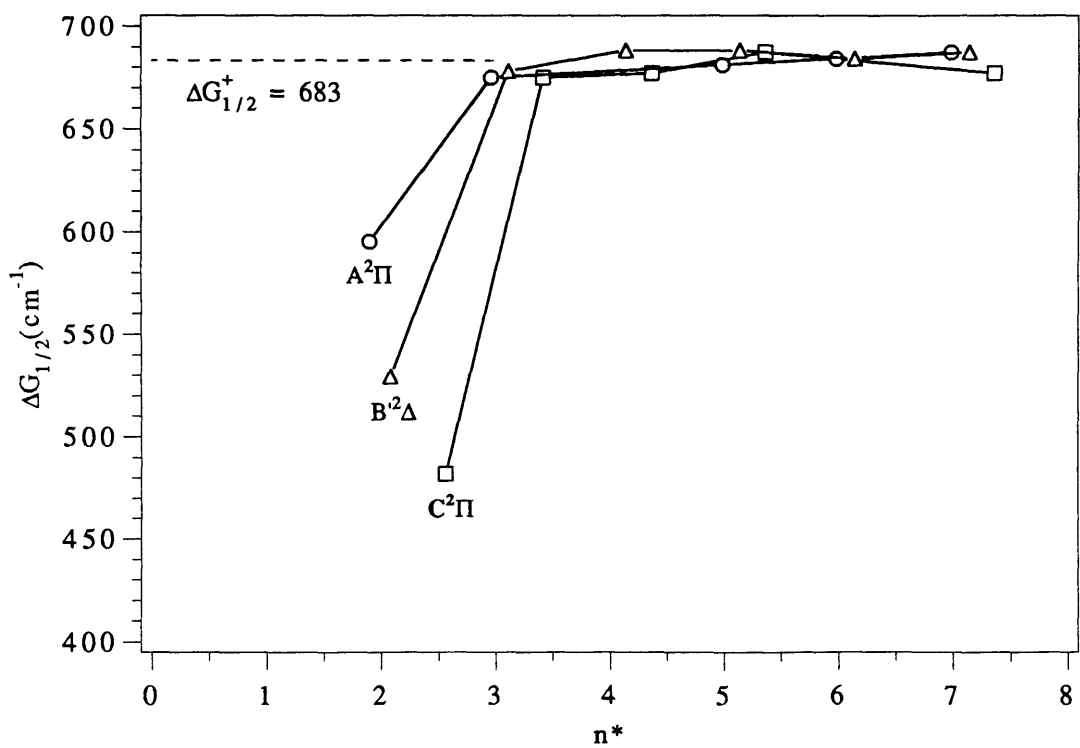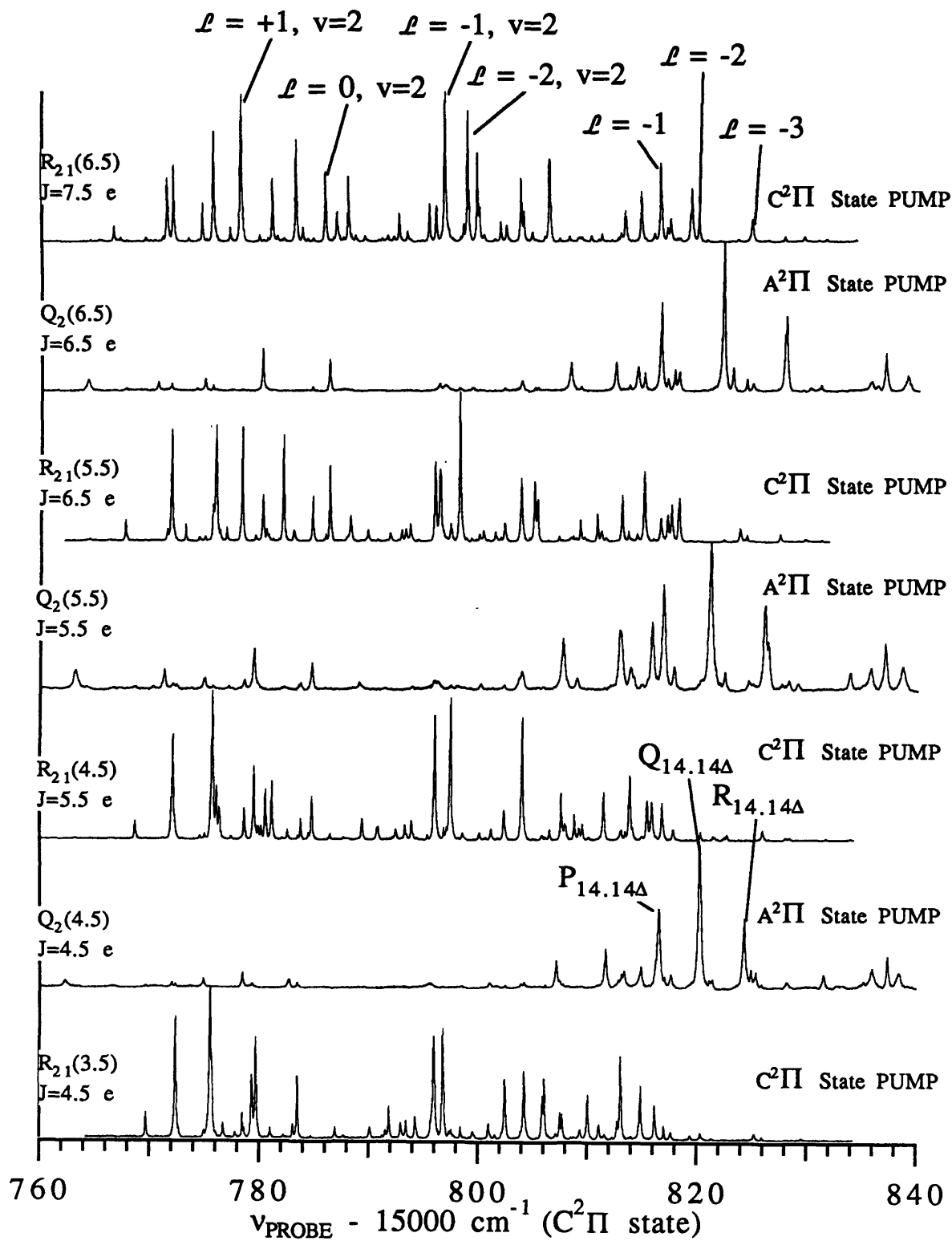
Figure 3.11 n*=14 for CaF

Figure 3.12

CaCl $^+$

All n* > 3
Rydberg states

^2P + ^1S_o ➔ $^2\Pi$, $^2\Sigma$
Dissociation Limit

C $^2\Pi$

B $^2\Sigma^+$

A $^2\Pi$

X $^2\Sigma^+$

Energy (cm^{-1})

Internuclear Distance (a.u.)

Figure 3.13

Figure 3.14

Figure 3.14

Energy level diagram:

Energy (cm^{-1}), axis from 16000 to 38000.

CaF:
- $-n^* = 3.42-$ F$^2\Pi$
- F$'^2\Sigma^+ - n^* = 3.18-$
- $-n^* = 3.11-{}^2\Delta$(predicted)
- E$^2\Pi - n^* = 2.96-$
- $-n^* = 2.92-$ E$^2\Sigma^+$
- C$^2\Pi$ and D$^2\Sigma^+$ — $n^* = 2.55$
- $-n^* = 2.08-$ B$'^2\Delta$
- $-n^* = 1.97-$ B$^2\Sigma^+$
- $-n^* = 1.90-$ A$^2\Pi$

CaCl:
- $n^* = 3.16\,{}^2\Pi$
- $n^* = 3.15\,{}^2\Sigma^+$
- G$^2\Delta - n^* = 3.05-$
- $-n^* = 2.93-$ F$^2\Pi$
- $-n^* = 2.78-$ E$^2\Sigma^+$
- $-n^* = 2.51-$ D$^2\Sigma^+$
- $-n^* = 2.23-$ C$^2\Pi$
- $-n^* = 2.03-$ B$'^2\Delta$(predicted)
- $-n^* = 1.86-$ B$^2\Sigma^+$
- $-n^* = 1.84-$ A$^2\Pi$

CaF

CaCl
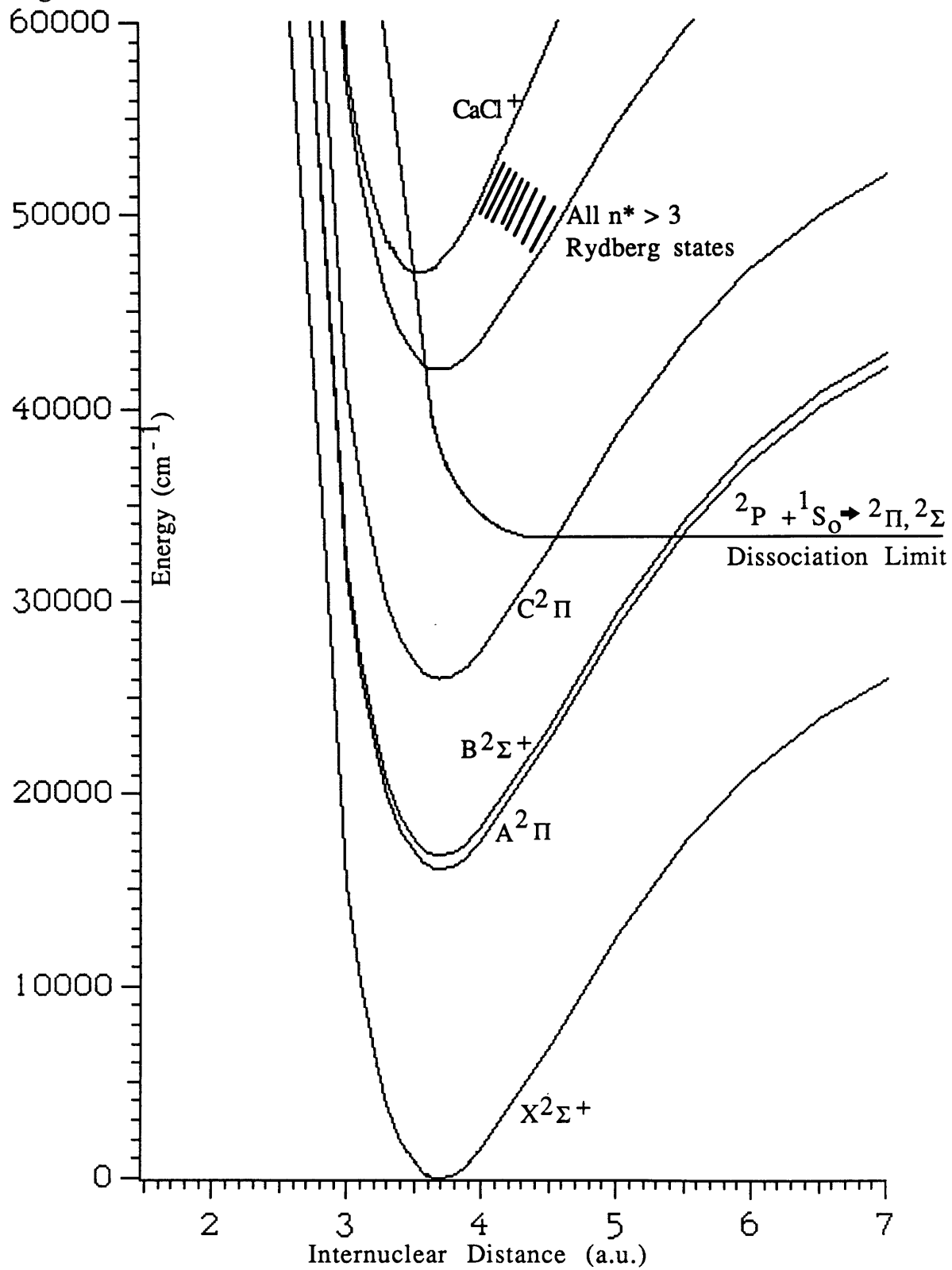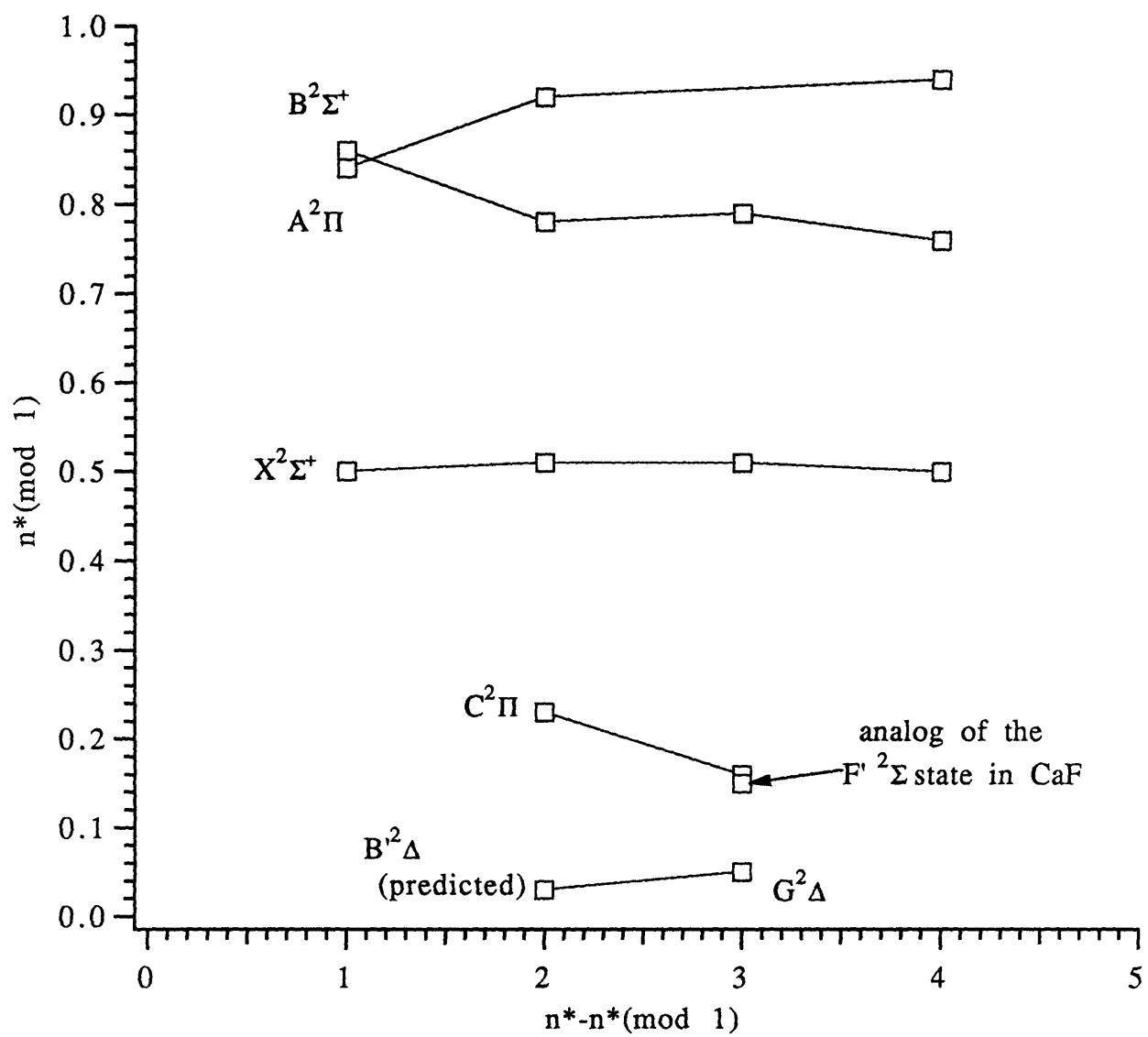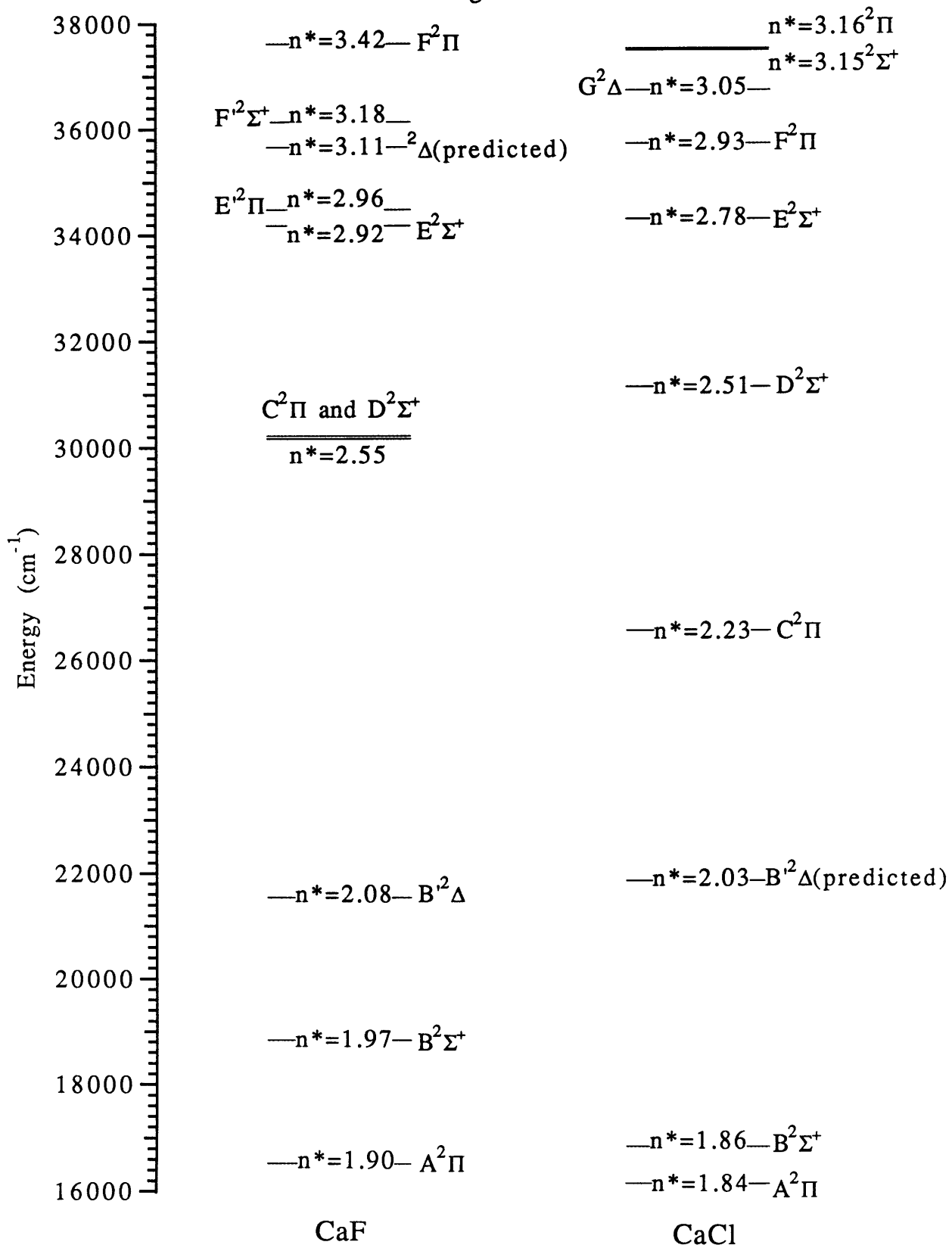
Chapter 4
Theories Which Describe Core-Nonpenetrating States and Comparison of Observations to Theories

Part 4.1 CaF

The core-nonpenetrating states of a number of systems have been recorded and analyzed. These systems include N_2, NO, He_2, and H_2.[1-7] The ion cores of most of these molecules have no dipole moment, NO^+ has a small dipole moment. The CaF^+ cation has a huge dipole moment, about 10 Debye.[8] The long range force model traditionally used to describe molecules such as H_2 and NO does not adequately describe the f complex that has been recorded at n*=14 (v=1) in CaF. Two other theoretical models exist which could describe these states more accurately. Each of these three models are discussed breifly below and a comparison of each model with the experimental results is presented in Table 4.1 and Figure 4.1.

Table 4.1 Comparison of the Predictions of the Splittings for the $\ell=3$ States for the Three Different Models for n*=14 (v=1)

Λ	[a]Experimental Results (n*=14 f complex)	Long Range Force Model	[b]Watson	Jungen and Harris
Σ	14.12	14.00	14.10	14.186
Π	14.021	13.99	14.07	14.091
Δ	14.004	13.97	14.00	13.966
Φ	13.934	13.90	13.88	

[a]These quantum defects are from preliminary MQDT fits and may be revised when the fits are complete.

[b]The effects of polarization which could improve the agreement were not consided when these values were calculated.

Part 4.1.1 Long Range Force Model

Traditionally the long range force model has been used to determine the quadrupole moments of the ion core from the splittings in a core-nonpenetrating complex such as the f-complexes in NO[5] and the 4d-complex in H_2[7].

In this model it is assumed that the quantum defect of the core-nonpenetrating states is due only to long range forces such the quadrupole moment and the polarizability. The equation that describes the splittings due is the quadrupole moment of the ion core is:

$$\mu_{n\ell\lambda} = Q_{20} \frac{2[\ell(\ell + 1) - 3\lambda^2]}{(2\ell + 3)(2\ell + 1)(2\ell - 1)\ell(\ell + 1)} \qquad \text{Eq. 4.1}$$

where Q_{20} is the quadrupole moment and $\mu_{n\ell\lambda}$ is the quantum defect.

This model works well for states that have a zero or a very small dipole moment. Watson[9] recognized the importance of the effects of a large molecular core dipole. First order effects of a dipole moment are zero, however he pointed out that second-order energetic effects of the dipole can be important in such systems.

Part 4.1.2 Watson's Point Dipole Model

Watson calculated the energy correction due to the second order dipole using the simple model of a hydrogen atom with a point dipole moment. The core dipole moment, Q_{10}, mixes only the angular part of the $n\ell\lambda$ wavefunctions of $\ell\pm1$. Watson calculated the second-order correction to be:

$$\mu_{n\ell\lambda} = -Q_{10}^2 \frac{2[\ell(\ell + 1) - 3\lambda^2]}{(2\ell + 3)(2\ell + 1)(2\ell - 1)\ell(\ell + 1)} \qquad \text{Eq. 4.2}$$

Part 4.1.3 μ^2 - Q, Origin-Independent Model

The energy correction from Watson's model and the long range force model have the same form. This is convient because both models can be combined to omit the question of how to choose your origin of coordinates when calculating the multipole moments of the ion core (see Eq. 4.3). The choice of origin is very important when calculating the dipole moment of a highly polar molecule. The origin is usually chosen at the center of mass.

$$\mu_{n\ell\lambda} = -(Q_{10}^2 - Q_{20}) \frac{2[\ell(\ell + 1) - 3\lambda^2]}{(2\ell + 3)(2\ell + 1)(2\ell - 1)\ell(\ell + 1)} \qquad \text{Eq. 4.3}$$

This model *should* be better than either of the models described above, however, Watson's model does not include higher order multipole moments which could be important and may change his results and make the combination of the two models invalid.

Part 4.1.3 Atomic-Ion-in Molecule Quantum Defect Theory (Jungen and Harris)

The paper[10] which describes this model in detail is included in Appendix 2. This model is different from the others in at least three different ways. One, it can used to calculate both the core-penetrating and the core-nonpenetrating states of CaF. Two, it was designed specifically for the CaF molecule. Three, elliptical coordinates are used in the calculation which eliminates the concern of multipole moments.

The energy levels calculated for the f states of CaF using this model do not agree well with the observed levels. This is surprising because it seems to be the most physically intuitive model and it does not have the same type of approximations (concerning the multipole moments) as the other models. The effects of polarizability and the volume of the F⁻ have not been included in this model yet, perhaps that will improve the agreement.

Part 4.1.4 Conclusion

None of the currently available theoretical models agree well with the observed levels. Clearly this problem needs more work. The model that is most likely to work well will probably be one like the Harris and Jungen[10] model which calculates the f states with elliptical coordinates.

References

[1] K. P. Huber, Ch. Jungen, K. Joshino, K. Ito and G. Stark, J. Chem. Phys., **100**, 7957 (1994).

[2] P. Arrowsmith, W. J. Jones and R. P Tuckett, J. Mol. Spec. **86**, 216 (1981).

[3] G. Herzberg and Ch. Jungen, J. Chem. Phys. **84**, 1181 (1986).

[4] E. Miecher, Can. J. Phys. **54**, 2074 (1976).

[5] Ch. Jungen and E. Miecher, Can. J. Phys. **47**, 1769 (1969).

[6] G. Herzberg and Ch. Jungen, J. Chem. Phys. **77**, 5876 (1982).

7 E. E. Eyler and F. M. Pipkin, Phys. Rev. A **27**, 2462 (1983).

8 Zygmunt Jakubek, private communication.

9 J. K. G. Watson, Mol. Phys. 81 (2), 277 (1994).

10 N. A. Harris and Ch. Jungen, Phys. Rev. Lett. 70 (17), 2549 (1993).

Figure 4.1   Graphical Comparison of Observed States and Theoretical
Predictions for n*=14 f-Complex of CaF
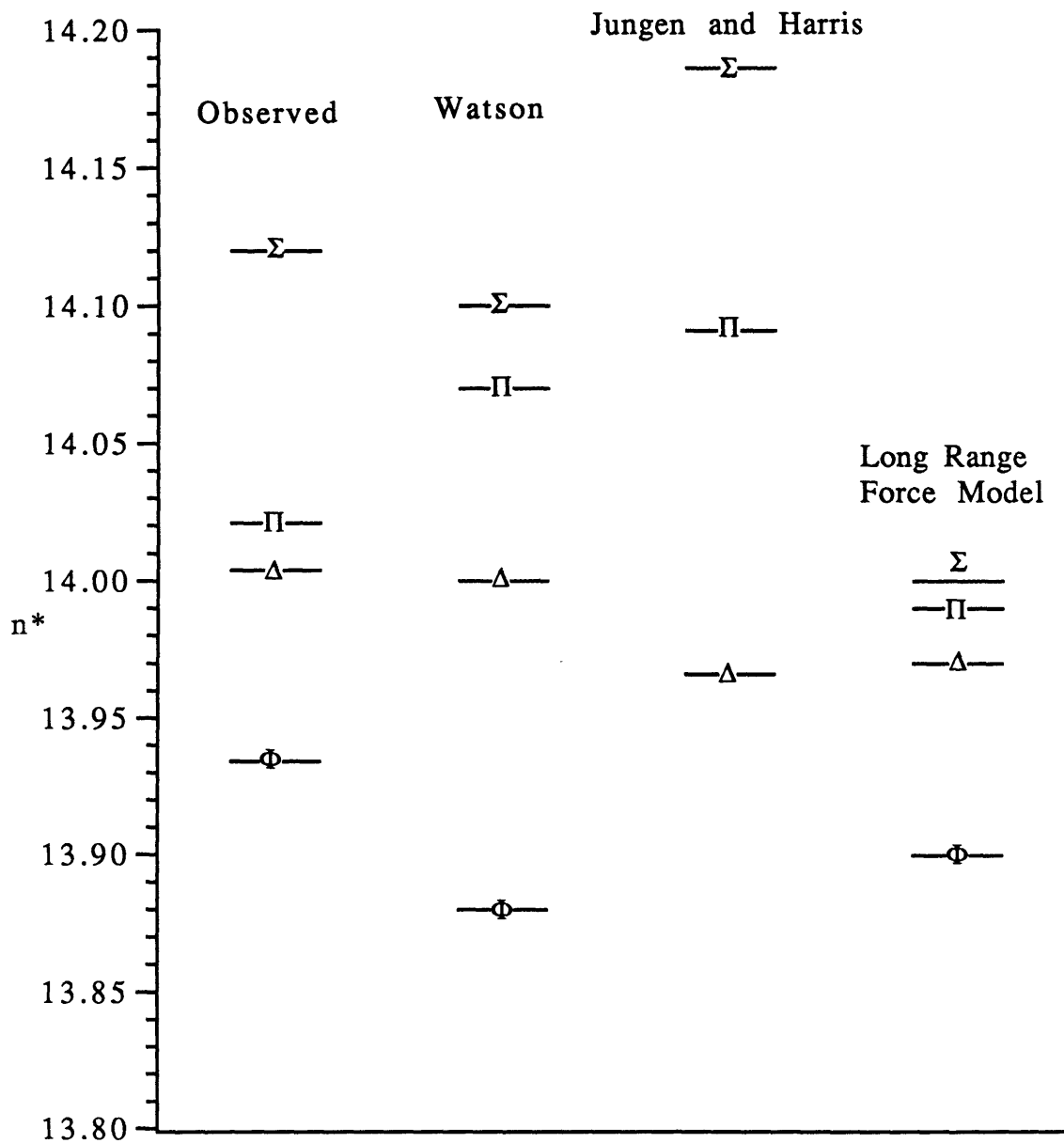
Chapter 5
Experimental Results

This chapter contains tables of the transitions observed in each type of experiment described in Chapter 2 except the CaF direct fluorescence experiments in the 36,000-40,000 cm^{-1} energy range. The results of those experiments are presented in the paper[1] in Appendix 1.

Term Value in the tables below is the total energy from $X^2\Sigma(v=0)$, v=0, J=1/2, F_1 which is the PROBE Energy plus the Term Value for the upper level of the PUMP transitions listed in the tables below.

Since only the relative intensity within one scan is meaningful, all intensities are listed as a fraction of that for the strongest line for each PUMP transition. For example, the strongest line within a PUMP band will be listed with an intensity of 1.0, and a line half as strong is listed as 0.50. In the n*=7 region, spectra from a single PUMP transition were recorded in 10 cm^{-1} pieces and the amount of CaF produced by the oven fluctuated over time, so the intensities are only qualitative, not quantitative measures of transition strengths. Also, since we were detecting cascade fluorescence to the ground state with a fixed gate width on the boxcar, it can not be assumed that the intensity is a direct measure of the Rydberg-$C^2\Pi$ transition strength.

Unlike the fluorescence-detected spectra, which were recorded in pieces, much of the autoionization data was recorded as a continuous scan for a particular PUMP transition. The production of CaF was more constant in the ablation source than in the oven. The relative intensities are more meaningful for those spectra. The intensities depend on both autoionization rate and the transition strength from the intermediate state.

n*-values are not meant to be exact. They are approximate values which are used as labels to group the states into Rydberg series. See Chapter 3 for a description of the six core-penetrating series. Since the high ℓ ($\ell > 2$) states had not been previously observed and arranged into series, they are not assigned an n* value. Instead they are assigned ℓ, Λ, and $\mathcal{L}$ values. Assigning Λ to ℓ >2 states should not imply that Λ is a good quantum number (it is useful for bookkeeping purposes).

"Extra lines" can result from PUMPing blended lines which produce transitions that are not related to the intended PUMP transition. This is one source of unassignable transitions. One way

to identify "real" transitions is to PUMP the same level using two different rotational transitions, for example, the $R_{21}(4.5)$ and the $Q_2(5.5)$ PUMP transitions both terminate at the J=5.5, N=6, e-parity level in the $A^2\Pi_{3/2}$ state, see Figure 5.1. The transitions that appear in the PROBE spectra recorded via both the $R_{21}(4.5)$ and $Q_2(5.5)$ PUMP transitions are "real" transitions. The problem of PUMPing blended lines is worse for the $C\ ^2\Pi$ state than the $A^2\Pi$ state because the rotational constant for the $C\ ^2\Pi$ state is smaller than it is for the $A^2\Pi$ state.

The presence of unexpected transitions, such as those to $\ell > 3$ and v >3 states, is the primary source of transitions that are difficult to assign, especially when only a few transitions terminating in a particular Rydberg state are observed. In the n*=7 region (Section 2.1), many of the unassigned transitions mostly likely originate from unexpected high v or high ℓ transitions. The fact that we do not know the vibrational dependence of rotation-vibration constants for the core-nonpenetrating states adds an additional degree of difficulty to assigning the states in this region.

The unassigned term curves in Figure 6.7 (the reduced term value plot for the n*=7 region) are numbered, such as term1, term2, etc. (Only terms which could be assigned with a reasonable degree of certainty were assigned an ℓ, Λ, and $\mathcal{L}$ values). A note in the Λ and n* section of the tables identifies transitions that belong to these unassigned terms. The unassigned term curves in the n*=17 and n*=18 region are also given term1, term2, etc. labels. All other unassigned transitions will have only a term value and intensity listed in the tables below.

In the cases where transitions to two different Rydberg rovibronic levels are not resolved (for example a P and an R transition from two different states happen to occur at the same energy), the term value and transition intensity is repeated and the word "blended" is written in the comment section.

In the high n* region for both CaF and CaCl the ionization potential used to identify a particular high-n* series is listed at the bottom of Tables 2.3.1-2.3.3 and Table 3.3.1 which contain those series.

There were numerous perturbations in all n* regions. In the n*=13 and n*=14 region, the assignments in the tables are written as if the term curves cross (although the term curves in Figures 6.20-6.23 and Figures 6.28- 6.31 of Chapter 6 do not cross). In the n*=7, n*=17 and n*=18 regions, the assignments are simply follow the

label of the term curves in Figures 6.25-6.27 of Chapter 6 because the perturbations in those regions were not analyzed.

Part 1 - CaF Fluorescence Spectra

The spectra presented in Part 1 were recorded using the $C^2\Pi_{3/2}$ state as the intermediate state. The fluorescence based detection scheme described in Chapter 2, Section 1.1 was used to detect the transitions listed in Tables 1.2 to 1.13.

Table 1.1 - $C^2\Pi_{3/2}$ (0,0) State PUMP Lines[2]

PUMP line	PUMP Energy (cm^{-1})	Term Value (cm^{-1})
$Q_2(5.5)$	30227.348	30241.727
$Q_2(6.5)$	30226.806	30245.979
$Q_2(7.5)$	30226.233	30250.884
$Q_2(8.5)$	30225.628	30256.442
$Q_2(9.5)$	30224.993	30262.654
$Q_2(10.5)$	30224.326	30269.518
$Q_2(11.5)$	30223.627	30277.035
$Q_2(12.5)$	30222.897	30285.205
$Q_2(13.5)$	30222.135	30294.027
$P_2(8.5)$	30220.070	30250.884
$P_2(10.5)$	30217.461	30262.653
$P_2(13.5)$	30213.313	30285.205

Table 1.2 - Direct Fluorescence Spectra Observed in the n*=7 Region.

PUMP line - $A^2\Pi$-$X^2\Sigma$ (0,0) $Q_2(5.5)$ J=5.5, N=6, e-parity

Term Value(cm^{-1})	Intensity	v'	J'	N'	Λ and n*	comment
44705.89	0.17					
44715.32	0.83		4.5	5	term18	
44721.57	0.31		4.5	5	term17	
44725.43	0.71		6.5	7	term18	
44728.74	0.09					
44731.03	0.12					
44731.89	0.05					
44732.82	0.15		6.5	7	term17	

Term Value(cm⁻¹)	Intensity	v'	J'	N'	Λ and n*
44733.49	0.15		4.5	5	term16
44733.96	0.15				
44735.10	0.49		4.5	4	term15
44739.92	0.85		4.5	5	term14
44740.54	0.23				
44741.50	0.25				
44742.14	1.0		6.5	6	term15
44743.11	0.28	0	4.5	4	f $^2\Delta$ (ℓ=+1)
44744.26	0.11				
44744.57	0.10				
44745.92	0.14				
44746.08	0.15		6.5	7	term16
44746.65	0.75	0	4.5	5	f $^2\Delta$ (ℓ=0)
44747.55	0.25				
44748.20	0.23				
44748.97	0.14		6.5		
44749.16	0.12		5.5		
44749.68	0.55		6.5	7	term14
44750.90	0.74	0	6.5	6	f $^2\Delta$ (ℓ=+1)
44755.94	0.25	0	6.5	7	f $^2\Delta$ (ℓ=0)

Table 1.3 - Direct Fluorescence Spectra Observed in the n*=7 Region.

PUMP line - A$^2\Pi$-X$^2\Sigma$ (0,0) Q$_2$(6.5)   J=6.5, N=7, e-parity

Term Value(cm⁻¹)	Intensity	v'	J'	N'	Λ and n*	comment
44713.0	0.06		7.5	8	term19	
44719.97	0.25		5.5	6	term18	
44726.77	0.04		5.5	6	term17	
44731.76	0.66		7.5	8	term18	
44734.90	0.08					
44738.25	0.40		5.5	5	term15	
44739.66	0.08		7.5	8	term17	
44744.31	0.51		5.5	6	term18	
44746.72	0.72	0	5.5	5	f $^2\Delta$ (ℓ=+1)	
44746.77	0.59		7.5	7	term15	
44749.19	0.06					
44750.90	0.34	0	5.5	6	f $^2\Delta$ (ℓ=0)	
44751.79	0.08					
44752.41	0.08					
44753.51	0.08		7.5	8	term16	
44753.65	0.09					

44755.75	0.47		7.5	8	term14	
44755.91	0.45	0	7.5	7	$f\,^2\Delta\,(\ell=+1)$	
44756.10	0.17					
44758.56	0.08					
44760.20	0.06					
44761.61	0.21	0	7.5	8	$f\,^2\Delta\,(\ell=0)$	
44763.94	0.17					
44765.36	0.13					
44765.85	0.06		5.5	6	term9	
44769.66	0.08		7.5	8	term11	
44770.83	0.11		7.5	8	term10	
44780.96	0.11					
44785.80	0.04					
44786.32	0.04					
44789.02	0.33		5.5	5	term7	
44790.95	0.06					
44791.81	0.28		5.5	5	term6	
44793.12	0.04					
44794.30	0.04					
44794.72	0.04					
44795.88	0.10		7.5	7	term8	
44796.36	0.07					
44797.40	0.07					
44799.55	0.51		7.5	7	term6	
44799.84	0.40		5.5	6	term5	blended
44799.84	0.40		7.5	7	term7	blended
44802.20	0.26		5.5	5	term4	
44804.98	0.06		7.5			
44805.92	0.10		5.5	5	term3	
44807.69	0.11					
44809.53	0.14					
44812.05	0.31		7.5	8	term5	
44812.59	0.81	2	5.5	5	$5.55\,^2\Sigma$	
44815.11	0.57					
44816.27	0.17		7.5	7	term4	
44820.96	0.10		7.5	7	term3	
44822.33	1.0	2	7.5	7	$5.55\,^2\Sigma$	
44823.88	0.04					
44824.37	0.07					
44825.89	0.07		7.5			
44826.47	0.10					
44826.89	0.06					

44827.60	0.17		7.5			
44832.26	0.56		5.5	6	term1	

Table 1.4 - Direct Fluorescence Spectra Observed in the n*=7 Region.

PUMP line - $A^2\Pi$-$X^2\Sigma$ (0,0) Q_2(7.5)   J=7.5, N=8, e-parity

Term Value(cm⁻¹)	Intensity	v'	J'	N'	Λ and n*	comment
44714.21	0.11		8.5	9	term21	
44715.45	0.03					
44717.24	0.01					
44717.41	0.02					
44718.42	0.02		8.5	9	term20	
44719.51	0.02					
44721.94	0.01		8.5	9	term19	
44725.20	0.06					
44725.40	0.18		6.5	7	term18	
44732.81	0.13		6.5	7	term17	
44736.58	0.03					
44738.86	0.71		8.5	9	term18	
44739.72	0.06					
44741.24	0.08					
44741.56	0.07		6.5			
44742.17	0.61		6.5	6	term15	
44743.16	0.03		6.5			
44746.10	0.10		6.5	7	term16	
44746.22	0.04					
44747.34	0.07		8.5	9	term17	
44748.71	0.06					
44749.64	0.37		6.5	7	term14	
44750.93	0.20	0	6.5	6	f $^2\Delta$ (ℓ=+1)	
44751.61	0.11					
44751.95	0.43		8.5	8	term15	
44752.91	0.07					
44754.83	0.08					
44755.85	0.71	0	6.5	7	f $^2\Delta$ (ℓ=0)	
44757.91	0.03					
44758.54	0.06					
44758.38	0.08					
44758.82	0.06					
44760.11	0.10					
44760.34	0.11					
44760.53	0.08					

44761.00	0.13				
44761.52	1.0	0	8.5	8	f $^2\Delta$ (ℓ=+1)
44761.93	0.16		8.5	9	term16
44762.45	0.64		8.5	9	term14
44762.89	0.13				
44763.67	0.11				
44764.22	0.08				
44765.07	0.14		8.5		
44765.67	0.07				
44766.50	0.01		8.5		
44768.00	0.33	0	8.5	9	f $^2\Delta$ (ℓ=0)
44769.49	0.01				
44770.42	0.08		6.5	7	term9
44772.11	0.02				
44776.86	0.23		8.5	9	term10
44777.86	0.06				
44779.92	0.04				
44780.29	0.03				
44784.74	0.06		8.5		
44785.21	0.06				
44785.83	0.08				
44787.54	0.03				
44789.62	0.14				
44790.28	0.06		6.5	6	term8
44790.84	0.04				
44791.14	0.13				
44793.68	0.08				
44793.95	0.44		6.5	6	term7
44794.38	0.11				
44795.32	0.40		6.5	6	term6
44801.26	0.04				
44802.30	0.24		8.5	8	term8
44804.13	0.07				
44804.71	0.71		8.5	8	term6
44805.13	0.10				
44805.44	0.70		6.5	7	term5
44806.50	0.46		8.5	8	term7
44808.68	0.17		6.5	6	term4
44809.69	0.04				
44809.88	0.04				
44812.55	0.04				
44813.10	0.16		6.5	6	term3

Term Value	Intensity	v'	J'	N'	Λ and n*	comment
44815.35	0.06					
44817.00	0.28	2	6.5	6	5.55 $^2\Sigma$	
44819.33	0.26		8.5	9	term5	
44820.02	0.06					
44820.83	0.31					
44824.61	0.08		8.5	8	term4	
44828.22	0.74	2	8.5	8	5.55 $^2\Sigma$	
44829.49	0.06		8.5	8	term3	
44831.36	0.06					
44831.88	0.07					
44834.25	0.11		8.5			
44836.05	0.07		8.5			
44836.90	0.27		6.5	7	term1	

Table 1.5 - Direct Fluorescence Spectra Observed in the n*=7 Region.

PUMP line - A$^2\Pi$-X$^2\Sigma$ (0,0) Q$_2$(8.5)   J=8.5, N=9, e-parity

Term Value(cm^{-1})	Intensity	v'	J'	N'	Λ and n*	comment
44722.24	0.54		9.5	10	term21	
44724.54	0.21					
44725.17	0.09					
44728.07	0.15		9.5	10	term20	
44730.82	0.24					
44731.68	1.0		7.5	8	term18	
44731.85	0.30		9.5	10	term19	
44739.64	0.36		7.5	8	term17	
44746.77	0.51		7.5	7	term15	
44746.85	0.54		9.5	10	term18	
44753.56	0.15		7.5	8	term16	
44755.69	0.64		7.5	8	term14	
44755.84	0.24		9.5	10	term17	blended
44755.84	0.24		7.5	7	term7	blended
44757.72	0.21					
44757.90	0.76		9.5	9	term15	
44761.57	0.36	0	7.5	8	f $^2\Delta$ (ℓ=0)	
44767.77	0.51	0	9.5	9	f $^2\Delta$ (ℓ=+1)	
44769.99	0.33		9.5	10	term14	
44770.96	0.06		9.5	10	term16	
44775.08	0.21	0	9.5	10	f $^2\Delta$ (ℓ=0)	
44775.70	0.09		7.5	8	term9	
44776.58	0.15					

44784.03	0.09			9.5	10	term10
44795.87	0.05			7.5	7	term8
44798.34	0.07					
44799.59	0.18			7.5	7	term6
44799.81	0.35			7.5	7	term7
44805.00	0.03			7.5		
44808.58	0.05					
44809.24	0.41			9.5	9	term8
44810.78	0.33			9.5	9	term6
44811.98	0.40			7.5	8	term5
44813.94	0.35			9.5	9	term7
44816.22	0.14			7.5	7	term4
44820.89	0.25			7.5	7	term3
44822.47	0.56	2		7.5	7	5.55 $^2\Sigma$
44823.80	0.10					
44825.89	0.12			7.5		
44827.42	0.18			9.5	10	term5
44827.60	0.13			7.5		
44833.80	0.05			9.5	9	term4
44834.85	0.78	2		9.5	9	5.55 $^2\Sigma$
44838.57	0.05			9.5	9	term3
44840.27	0.05					
44842.29	0.20			7.5	8	term1

Table 1.6 - Direct Fluorescence Spectra Observed in the n*=7 Region.

PUMP line - $A^2\Pi$-$X^2\Sigma$ (0,0) $Q_2(9.5)$ J=9.5, N=10, e-parity

Term Value(cm^{-1})	Intensity	v'	J'	N'	Λ and n*	comment
44726.38	0.03					
44728.31	0.18		10.5	11	term22	
44731.13	0.16		10.5	11	term21	
44732.28	0.07					
44733.63	0.03					
44735.23	0.02					
44736.46	0.02					
44737.48	0.08					
44738.41	0.05		10.5	11	term20	
44738.85	0.25		8.5	9	term18	
44742.57	0.05		10.5	11	term19	
44747.32	0.07		8.5	9	term17	
44752.06	0.24		8.5	8	term15	
44755.67	0.26		10.5	11	term18	

44758.38	0.02					
44759.88	0.02					
44761.27	0.03					
44761.47	0.08	0	8.5	8	f $^2\Delta$ $(\ell=+1)$	
44761.88	0.08		8.5	9	term16	
44762.43	0.32		8.5	9	term14	
44763.93	0.05					
44764.15	0.08		8.5			
44764.53	0.37		10.5	10	term15	
44765.07	0.06		10.5	11	term17	
44765.83	0.05					
44766.45	0.05		8.5			
44767.90	0.24	0	8.5	9	f $^2\Delta$ $(\ell=0)$	
44768.29	0.04					
44768.89	0.03					
44769.49	0.02		8.5			
44770.56	0.04					
44771.83	0.02					
44773.94	0.03					
44774.73	0.16	0	10.5	10	f $^2\Delta$ $(\ell=+1)$	
44775.98	0.04					
44776.17	0.03					
44776.86	0.04					
44777.17	0.03					
44778.00	0.05					
44778.24	0.14		10.5	11	term14	
44782.02	0.09		8.5	9	term9	
44782.95	0.14	0	10.5	11	f $^2\Delta$ $(\ell=0)$	
44783.77	0.04					
44784.69	0.03		10.5			blended
44784.69	0.03		8.5			blended
44786.28	0.03		10.5			
44788.25	0.04					
44790.47	0.05		10.5	11	term11	
44792.08	0.15		10.5	11	term10	
44802.30	0.06		8.5	8	term8	
44804.41	0.04					
44804.64	0.24		8.5	8	term6	
44806.46	0.34		8.5	8	term7	
44811.96	0.06					
44813.27	0.06					
44816.27	0.50		10.5	10	term8	

Term Value(cm^{-1})	Intensity	v'	J'	N'	Λ and n*	comment
44818.61	0.24		10.5	10	term6	
44819.35	0.46		8.5	9	term5	
44822.22	0.40		10.5	10	term7	
44824.62	0.06		8.5	8	term4	
44828.22	0.90	2	8.5	8	5.55 $^2\Sigma$	
44829.54	0.24		8.5	8	term3	
44832.75	0.04					
44834.28	0.12		8.5			blended
44834.28	0.12		10.5			blended
44836.20	0.12		10.5	11	term5	
44842.25	1.0	2	10.5	10	5.55 $^2\Sigma$	
44843.47	0.02					
44843.75	0.02		10.5	10	term4	
44846.43	0.04					
44848.27	0.10		10.5	10	term3	
44848.55	0.26		8.5	9	term1	

Table 1.7 - Direct Fluorescence Spectra Observed in the n*=7 Region.

PUMP line - A$^2\Pi$-X$^2\Sigma$ (0,0) Q$_2$(10.5)   J=10.5, N=11, e-parity

Term Value(cm^{-1})	Intensity	v'	J'	N'	Λ and n*	comment
44738.24	0.24		11.5	12	term22	
44741.12	0.25		11.5	12	term21	
44745.05	0.10					
44746.80	0.44		9.5	10	term18	
44749.32	0.10		11.5	12	term20	
44754.12	0.06		11.5	12	term19	
44755.75	0.18		9.5	10	term17	
44757.94	0.32		9.5	9	term15	
44765.26	0.29		11.5	12	term18	
44767.47	0.06					
44767.79	0.14	0	9.5	9	f $^2\Delta$ ($\mathcal{l}$=+1)	
44769.99	0.39		9.5	10	term14	
44770.97	0.11		9.5	10	term16	
44771.78	0.38		11.5	11	term15	
44775.06	0.27		11.5	12	term17	
44775.06	0.27	0	9.5	10	f $^2\Delta$ ($\mathcal{l}$=0)	
44782.13	0.20	0	11.5	11	f $^2\Delta$ ($\mathcal{l}$=+1)	
44782.89	0.14					
44787.29	0.32		11.5	12	term14	
44788.93	0.21		9.5	10	term9	

Term Value(cm⁻¹)	Intensity	v'	J'	N'	Λ and n*	comment
44791.44	0.46	0	11.5	12	f $^2\Delta$ (ℓ=0)	
44791.84	0.13					
44793.69	0.15					
44795.63	0.07					
44798.58	0.20		11.5	12	term11	
44800.95	0.24		11.5	12	term10	
44809.27	0.22		9.5	9	term8	
44810.80	0.14		9.5	9	term6	
44813.74	0.15					
44813.92	0.44		9.5	9	term7	
44823.70	0.58		11.5	11	term8	
44827.37	0.56		9.5	10	term5	
44827.49	0.14		11.5	11	term6	
44831.32	0.29		11.5	11	term7	
44833.69	0.04					
44833.84	0.08		9.5	9	term4	
44834.89	0.90	2	9.5	9	5.55 $^2\Sigma$	
44838.58	0.21		9.5	9	term3	
44842.70	0.22		9.5			
44845.59	0.07					
44845.83	0.42		11.5	12	term5	
44850.36	1.0	2	11.5	11	5.55 $^2\Sigma$	
44854.69	0.06		11.5	11	term4	
44854.99	0.06					
44855.28	0.04					
44855.65	0.27		9.5	10	term1	
44858.38	0.11					

Table 1.8 - Direct Fluorescence Spectra Observed in the n*=7 Region.

PUMP line - A$^2\Pi$-X$^2\Sigma$ (0,0)   Q$_2$(11.5)   J=11.5,   N=12,   e-parity

Term Value(cm⁻¹)	Intensity	v'	J'	N'	Λ and n*	comment
44740.78	0.15					
44741.55	0.09					
44742.54	0.15					
44748.67	0.49		12.5	13	term22	
44749.99	0.21					
44752.12	0.38		12.5	13	term21	
44753.51	0.13					
44755.65	0.68		10.5	11	term18	
44760.96	0.13		12.5	13	term20	
44764.59	0.45		10.5	10	term15	

44765.09	0.36		10.5	11	term17
44766.50	0.19		12.5	13	term19
44774.72	0.15	0	10.5	10	$f\,^2\Delta\,(\ell=+1)$
44775.66	0.56		12.5	13	term18
44778.23	0.94		10.5	11	term14
44779.80	0.87		12.5	12	term15
44780.81	0.23		10.5	11	term16
44782.90	0.43	0	10.5	10	$f\,^2\Delta\,(\ell=0)$
44784.73	0.06				
44786.00	0.09		12.5	13	term17
44786.26	0.06				
44788.70	0.04				
44790.50	0.11				
44790.77	0.64	0	12.5	12	$f\,^2\Delta\,(\ell=+1)$
44792.10	0.04				
44794.52	0.03				
44796.38	0.26		10.5	11	term9
44797.05	0.41		12.5	13	term14
44800.51	0.30	0	12.5	13	$f\,^2\Delta\,(\ell=0)$
44801.87	0.19				
44802.76	0.06		12.5	13	term16
44803.24	0.01				
44807.48	0.53		12.5	13	term11
44809.91	0.05				
44810.55	0.68		12.5	13	term10
44816.32	0.47		10.5	10	term8
44818.58	0.07		10.5	10	term6
44822.14	0.87		10.5	10	term7
44828.33	0.06				
44829.16	0.07				
44831.84	0.77		12.5	12	term8
44836.23	0.77		10.5	11	term5
44837.36	0.07		12.5	12	term6
44841.10	0.68		12.5	12	term7
44842.21	0.75	2	10.5	10	5.55 $^2\Sigma$
44843.67	0.07				
44843.81	0.07		10.5	10	term4
44844.78	0.06				
44848.26	0.38		10.5	10	term3
44850.29	0.04				
44851.95	0.23				
44856.22	0.49		12.5	13	term5

Term Value(cm⁻¹)	Intensity	v'	J'	N'	Λ and n*	comment
44857.32	0.07					
44859.17	1.0	2	12.5	12	5.55 $^2\Sigma$	
44863.55	0.45		10.5	11	term1	
44866.19	0.04		12.5	12	term4	

Table 1.9 - Direct Fluorescence Spectra Observed in the n*=7 Region.

PUMP line - $A^2\Pi$-$X^2\Sigma$ (0,0) $Q_2(12.5)$ J=12.5, N=13, e-parity

Term Value(cm⁻¹)	Intensity	v'	J'	N'	Λ and n*	comment
44749.36	0.44					
44750.03	0.35					
44754.12	0.41					
44754.56	0.06					
44759.62	0.59					
44759.93	0.50		13.5	14	term22	
44762.89	0.26					
44764.10	0.38		13.5	14	term21	
44765.26	1.0		11.5	12	term18	
44771.84	0.82		11.5	11	term15	
44773.32	0.26		13.5	14	term20	
44775.16	0.41		11.5	12	term17	
44779.60	0.15		13.5	14	term19	
44782.13	0.08	0	11.5	11	$f\,^2\Delta\,(\ell=+1)$	
44782.93	0.03					
44784.79	0.02					
44786.92	0.20		13.5	14	term18	
44787.29	0.26		11.5	12	term14	
44788.52	0.29		13.5	13	term15	
44791.44	0.20	0	11.5	12	$f\,^2\Delta\,(\ell=0)$	blended
44791.44	0.20		11.5	12	term16	blended
44797.63	0.08		13.5	14	term17	
44798.63	0.08					
44799.58	0.29	0	13.5	13	$f\,^2\Delta\,(\ell=+1)$	
44800.98	0.06					
44804.72	0.59		11.5	12	term16	
44807.64	0.76		13.5	14	term14	
44809.30	0.06					
44809.96	0.85					
44810.22	0.32	0	13.5	14	$f\,^2\Delta\,(\ell=0)$	
44811.23	0.76					

68

Table 1.10 - Direct Fluorescence Spectra Observed in the n*=7 Region.

PUMP line - $A^2\Pi$-$X^2\Sigma$ (0,0) Q_2(13.5)   J=13.5, N=14, e-parity

Term Value(cm⁻¹)	Intensity	v'	J'	N'	Λ and n*	comment
44758.85	0.29					
44759.87	0.25					
44760.89	0.40					
44766.47	0.15					
44771.45	0.44		14.5	15	term22	
44773.08	0.08					
44775.67	0.38		12.5	13	term18	
44776.83	0.15		14.5	15	term21	
44779.81	0.56		12.5	12	term15	
44786.05	0.31		12.5	13	term17	
44786.36	0.17		14.5	15	term20	
44790.78	0.38	0	12.5	12	$f\,^2\Delta\,(\ell=+1)$	
44793.47	0.31		14.5	15	term19	
44793.94	0.10					
44796.39	0.10					
44797.07	0.88		12.5	13	term14	
44797.90	1.0		14.5	14	term15	
44798.94	0.46		14.5	15	term18	
44800.51	0.42	0	12.5	13	$f\,^2\Delta\,(\ell=0)$	
44801.87	0.33					
44802.75	0.27		12.5	13	term16	
44803.24	0.03					
44803.40	0.05					
44803.89	0.13					
44807.48	0.26		12.5	13	term11	
44808.92	0.84	0	14.5	14	$f\,^2\Delta\,(\ell=+1)$	
44810.05	0.14		14.5	15	term17	
44810.58	0.06					
44813.80	0.60		12.5	13	term9	
44814.57	0.06					
44816.07	0.06					
44818.93	0.58		14.5	15	term14	
44819.80	0.06					
44820.35	0.02					
44820.56	0.10					
44821.77	0.24					
44827.56	0.18		14.5	15	term11	
44827.70	0.03					

Term Value (cm⁻¹)	Intensity	v'	J'	N'	Λ and n*
44831.84	0.11		12.5	12	term8
44832.00	0.13		14.5	15	term10
44836.18	0.02				
44836.31	0.03				
44837.37	0.03		12.5	12	term6
44841.13	0.34		12.5	12	term7
44843.37	0.06				
44844.53	0.03				
44845.29	0.03				
44845.88	0.03				
44850.42	0.32		14.5	14	term8
44856.24	0.35		12.5	13	term5
44859.25	0.42	2	12.5	12	5.55 $^2\Sigma$
44863.22	0.19		14.5	14	term7
44866.16	0.01		12.5	12	term4
44867.36	0.01				
44869.00	0.24		12.5	12	term3
44879.06	0.52	2	14.5	14	5.55 $^2\Sigma$
44879.31	0.16		14.5	15	term5
44880.64	0.21		12.5	13	term1

Table 1.11 - Direct Fluorescence Spectra Observed in the n*=7 Region.

PUMP line - $A^2\Pi$-$X^2\Sigma$ (0,0) P_2(8.5)   J=7.5, N=8, f-parity

Term Value(cm⁻¹)	Intensity	v'	J'	N'	Λ and n*	comment
44731.72	0.81		8.5	8	term18	
44739.66	0.31		8.5	8	term17	
44744.41	0.82		6.5	6	term14	
44746.76	0.79		6.5	7	term15	
44747.30	0.18					
44749.22	0.12					
44750.96	0.40	0	6.5	6	f $^2\Delta$ (ℓ=+1)	
44753.63	0.29		8.5	8	term16	
44755.64	0.62		8.5	8	term14	
44755.85	0.66	0	6.5	7	f $^2\Delta$ (ℓ=+1)	
44757.87	0.52		8.5	9	term15	
44761.63	0.69	0	8.5	8	f $^2\Delta$ (ℓ=+1)	
44767.71	0.44	0	8.5	9	f $^2\Delta$ (ℓ=+1)	
44770.82	0.31		8.5	8	term10	
44771.94	0.14					
44772.94	0.13					

Term Value	Intensity	v'	J'	N'	Λ and n*
44775.65	0.14		8.5	8	term9
44776.54	0.24				
44799.56	0.69		6.5	7	term6
44799.80	0.72		6.5	6	term5
44799.80	0.72		6.7	7	term7
44801.87	0.18				
44802.24	0.35				
44809.24	0.22		8.5	9	term8
44809.40	0.19				
44810.85	0.56		8.5	9	term6
44812.03	0.38		8.5	8	term5
44813.94	0.26		8.5	9	term7
44816.35	0.35		6.5	7	term4
44816.62	0.36				
44818.58	0.53				
44820.93	0.68		6.5	7	term3
44822.35	1.0	2	6.5	7	5.55 $^2\Sigma$
44825.58	0.13				
44825.86	0.38				
44827.51	0.62				
44834.84	0.48	2	8.5	9	5.55 $^2\Sigma$
44839.19	0.17				

Table 1.12 - Direct Fluorescence Spectra Observed in the n*=7 Region.

PUMP line - $A^2\Pi$-$X^2\Sigma$ (0,0) P_2(10.5)   J=9.5, N=10, f-parity

Term Value(cm⁻¹)	Intensity	v'	J'	N'	Λ and n*	comment
44726.97	0.10					
44728.08	0.20		10.5	10	term20	
44730.80	0.07					
44731.85	0.10		10.5	10	term19	
44732.24	0.07					
44739.64	0.15		8.5	8	term17	
44745.43	0.16					
44746.81	0.66		10.5	10	term18	
44753.34	0.13					
44755.66	0.35		8.5	8	term14	
44755.98	0.44					
44756.29	0.18					
44757.90	0.94		8.5	9	term15	
44759.49	0.12					
44761.67	0.26	0	8.5	8	f $^2\Delta$ ($\mathcal{L}$=+1)	

44765.24	0.19				
44766.60	0.15				
44767.74	0.78	0	8.5	9	f $^2\Delta\,(\ell=+1)$
44769.23	0.12				
44769.97	1.0		10.5	10	term14
44770.11	0.49				
44770.94	0.59		10.5	10	term16
44771.14	0.23				
44771.78	0.86		10.5	11	term15
44772.20	0.38				
44775.14	0.82	0	10.5	10	f $^2\Delta\,(\ell=+1)$
44775.65	0.21		8.5	8	term9
44782.13	0.34				
44782.93	0.31				
44783.06	0.26				
44784.01	0.20		10.5	10	term10
44787.03	0.12				
44788.07	0.09				
44788.90	0.15		10.5	10	term9
44791.96	0.37				
44798.03	0.06				
44800.28	0.05				
44801.87	0.06				
44806.29	0.05				
44809.25	0.15		8.5	9	term8
44810.85	0.06		8.5	9	term6
44812.04	0.17				
44813.94	0.11		8.5	9	term7
44822.71	0.05				
44823.69	0.09		10.5	11	term8
44825.85	0.05				
44827.40	0.16		10.5	10	term5
44831.34	0.07		10.5	11	term7
44834.84	0.31	2	8.5	9	5.55 $^2\Sigma$
44838.59	0.15		8.5	9	term3
44842.75	0.10				
44850.33	0.10	2	10.5	11	5.55 $^2\Sigma$

Table 1.13 - Direct Fluorescence Spectra Observed in the n*=7 Region.

PUMP line - $A^2\Pi$-$X^2\Sigma$ (0,0) P_2(13.5)   J=12.5, N=13, f-parity

Term Value(cm^{-1})	Intensity	v'	J'	N'	Λ and n*	comment
44748.59	0.28		13.5	13	term22	
44749.94	0.20					
44752.14	0.14		13.5	13	term21	
44753.57	0.11					
44755.58	0.06		11.5	11	term18	
44756.91	0.09					
44759.93	0.07					
44760.92	0.17		13.5	13	term20	
44765.08	0.08		11.5	11	term17	
44766.51	0.18		13.5	13	term19	
44771.01	0.08					
44775.67	0.83		13.5	13	term18	
44778.21	0.69					
44779.73	0.93		11.5	12	term15	
44780.39	0.11					
44782.94	0.23					
44784.72	0.10					
44785.99	0.20		13.5	13	term17	
44786.28	0.08					
44790.79	0.62	0	11.5	12	f $^2\Delta$ ($\mathcal{L}$=+1)	
44793.18	0.13					
44793.46	0.12					
44793.94	0.09					
44796.44	0.38		11.5	11	term9	
44797.08	0.89		13.5	13	term14	
44797.87	0.74		13.5	14	term15	
44798.95	0.11					
44800.40	0.66	0	13.5	13	f $^2\Delta$ ($\mathcal{L}$=+1)	
44800.60	0.11					
44801.89	0.49					
44802.74	0.29		13.5	13	term16	
44803.91	0.04					
44805.17	0.05					
44807.50	0.34		13.5	13	term11	
44808.91	0.30	0	13.5	14	f $^2\Delta$ ($\mathcal{L}$=+1)	
44810.57	0.16		13.5	13	term10	
44813.83	0.26		13.5	13	term9	

44814.94	0.04					
44820.74	0.15					
44831.71	0.10					
44836.20	0.11		11.5	11		term5
44841.13	0.30		11.5	12		term7
44850.38	0.25		13.5	14		term8
44856.23	0.26		13.5	13		term5
44856.86	0.05					
44859.19	1.0	2	11.5	12	5.55	$^2\Sigma$
44863.25	0.21		13.5	14		term7
44864.99	0.05					
44866.20	0.05		11.5	12		term4
44866.99	0.10					
44869.05	0.58		11.5	12		term3

Part 2 - CaF Autoionization Data

Part 2.1 - CaF Autoionization Data - A $^2\Pi$ State Intermediate

The data presented in Part 2.1 were recorded using the $A^2\Pi_{3/2}$ (v=0) state as the intermediate state. The ion based detection scheme described in Chapter 2, Section 3 was used to detect the transitions listed in Tables 2.2.1 to 2.2.30. CaF^+ ions resulted from autoionization of the v>0 Rydberg states above the v=0 ionization potential.

Table 2.1.1 - $A^2\Pi_{3/2}$ (v=0) State PUMP Lines[3]

PUMP line	PUMP Energy (cm^{-1})	Term Value (cm^{-1})
Q_2(1.5)	16564.059	16566.112
Q_2(2.5)	16563.745	16566.852
Q_2(3.5)	16563.438	16570.284
Q_2(4.5)	16563.162	16573.432
Q_2(5.5)	16562.896	16577.275
Q_2(6.5)	16562.641	16581.814
Q_2(7.5)	16562.399	16587.05
P_2(5.5)	16559.064	16573.443
P_2(6.5)	16558.108	16577.281
P_2(7.5)	16557.163	16581.814
P_2(8.5)	16556.234	16587.048
P_2(9.5)	16555.321	16592.282
P_2(10.5)	16554.410	16599.602
P_2(11.5)	16553.524	16606.932
P_2(12.5)	16552.638	16614.946

Table 2.1.2 - Autoionization Spectra Observed in the n*=13 Region.
PUMP line - $A^2\Pi$-$X^2\Sigma$ (0,0) Q_2(1.5) J=1.5, N=2, e-parity

Term Value(cm^{-1})	Intensity	v'	J'	N'	Λ and n*	comment
46989.32	0.04	1	0.5	0	12.55 $^2\Sigma$	
46991.48	0.06	1	2.5	2	12.55 $^2\Sigma$	
47005.80	0.03					
47006.54	0.12	2	0.5	1	8.98 $^2\Pi$	

47007.88	0.14	2	2.5	2	8.98 $^2\Pi$
47010.09	0.14	2	2.5	3	8.98 $^2\Pi$
47035.83	0.20	1	0.5	1	12.98 $^2\Pi$
47037.13	0.22	1	2.5	2	12.98 $^2\Pi$
47039.32	0.11	1	2.5	3	12.98 $^2\Pi$
47045.47	0.06				
47047.50	0.08				
47048.63	0.12				
47049.19	1.0	1	2.5	2	13.14 $^2\Delta$
47050.70	0.08				
47051.48	0.38	1	2.5	3	13.14 $^2\Delta$
47054.56	0.06	1	2.5	2	f $^2\Sigma$ (ℓ=-3)
47057.31	0.08				
47058.01	0.14				
47060.73	0.15				
47069.66	0.15	1	0.5	1	13.36 $^2\Pi$
47070.64	0.18	2	0.5	0	9.19 $^2\Sigma$
47071.41	0.12	1	2.5	2	13.36 $^2\Pi$
47073.04	0.08	2	2.5	2	9.19 $^2\Sigma$
47073.44	0.06	1	2.5	3	13.36 $^2\Pi$
47087.87	0.10	1	0.5	0	13.55 $^2\Sigma$
47090.08	0.12	1	2.5	2	13.55 $^2\Sigma$

Table 2.1.3 - Autoionization Spectra Observed in the n*=13 Region. **PUMP line** - $A^2\Pi$-$X^2\Sigma$ (0,0) Q_2(2.5) J=2.5, N=3, e-parity

Term Value(cm^{-1})	Intensity	v'	J'	N'	Λ and n*	comment
46990.03	0.05	1	1.5	1	12.55 $^2\Sigma$	
46991.55	0.03					
46993.75	0.07	1	3.5	3	12.55 $^2\Sigma$	
47005.82	0.03					
47006.55	0.08	2	1.5	1	8.98 $^2\Pi$	
47007.86	0.08	2	1.5	3	8.98 $^2\Pi$	
47008.01	0.08					
47010.10	0.23	2	3.5	3	8.98 $^2\Pi$	
47013.01	0.19	2	3.5	4	8.98 $^2\Pi$	
47035.75	0.04	1	1.5	1	12.98 $^2\Pi$	
47037.24	0.04	1	1.5	2	12.98 $^2\Pi$	
47038.67	0.02					

Term Value(cm⁻¹)	Intensity	v'	J'	N'	Λ and n*	comment
47039.18	0.14					
47042.08	0.10	1	3.5	4	12.98 $^2\Pi$	
47045.10	0.02					
47047.70	0.04					
47049.20	0.33	1	1.5	2	13.14 $^2\Delta$	
47051.47	1.0	1	3.5	3	13.14 $^2\Delta$	
47052.75	0.04	3	3.5	3	7.36 $^2\Pi$	
47053.02	0.04	1	3.5	4	f $^2\Pi$ (ℓ=-2)	
47054.32	0.14					
47054.54	0.33	1	3.5	4	13.14 $^2\Delta$	
47058.91	0.06					
47059.23	0.04	1	3.5	3	f $^2\Sigma$ (ℓ=-3)	
47059.55	0.04					
47063.34	0.08					
47069.71	0.06	2	1.5	1	13.36 $^2\Pi$	
47071.19	0.06	1	1.5	2	13.36 $^2\Pi$	
47071.41	0.17	2	1.5	1	9.19 $^2\Sigma$	
47074.03	0.06	1	3.5	3	13.36 $^2\Pi$	
47075.47	0.06	2	3.5	3	9.19 $^2\Sigma$	
47076.51	0.04	1	3.5	4	13.36 $^2\Pi$	
47088.60	0.02	1	1.5	1	14.55 $^2\Sigma$	
47092.38	0.06	1	3.5	3	14.55 $^2\Sigma$	

Table 2.1.4 - Autoionization Spectra Observed in the n*=13 Region.
PUMP line - $A^2\Pi$-$X^2\Sigma$ (0,0) Q_2(3.5)   J=3.5, N=4, e-parity

Term Value(cm⁻¹)	Intensity	v'	J'	N'	Λ and n*	comment
46991.50	0.05	1	2.5	2	12.55 $^2\Sigma$	
46996.76	0.07	1	4.5	4	12.55 $^2\Sigma$	
47007.93	0.07	2	2.5	2	8.98 $^2\Pi$	
47010.10	0.10	2	2.5	3	8.98 $^2\Pi$	
47013.01	0.18	2	4.5	4	8.98 $^2\Pi$	
47016.62	0.15	2	4.5	5	8.98 $^2\Pi$	
47017.76	0.01	2	4.5	5	f $^2\Delta$ (ℓ=0)	
47030.24	0.04	1	4.5	4	12.88 $^2\Sigma$	
47037.12	0.04	1	2.5	2	12.98 $^2\Pi$	
47039.29	0.05	1	2.5	3	12.98 $^2\Pi$	
47039.70	0.04					
47041.80	0.22	1	4.5	4	12.98 $^2\Pi$	

47045.54	0.16	1	4.5	5	12.98 $^2\Pi$	
47047.50	0.04					
47049.17	0.15	1	2.5	2	13.14 $^2\Delta$	
47050.62	0.10					
47051.48	0.61	1	2.5	3	13.14 $^2\Delta$	
47052.63	0.04	3	2.5	3	7.36 $^2\Pi$	
47054.53	1.0	1	4.5	4	13.14 $^2\Delta$	
47055.73	0.03	3	4.5	4	7.36 $^2\Pi$	
47057.46	0.12	2	4.5	5	f $^2\Pi$ (ℓ=-2)	
47058.50	0.45	1	4.5	5	13.14 $^2\Delta$	
47059.56	0.01					
47060.73	0.03					
47062.56	0.04					
47064.30	0.06	1	4.5	5	f $^2\Sigma$ (ℓ=-3)	
47067.50	0.09					
47071.42	0.09	1	2.5	2	13.36 $^2\Pi$	
47073.02	0.18	2	2.5	2	9.19 $^2\Sigma$	
47073.47	0.10	1	2.5	3	13.36 $^2\Pi$	
47077.40	0.13	1	4.5	4	13.36 $^2\Pi$	
47078.75	0.09	2	4.5	4	9.19 $^2\Sigma$	
47080.35	0.07	1	4.5	5	13.36 $^2\Pi$	
47090.08	0.03	1	2.5	2	13.55 $^2\Sigma$	
47095.36	0.07	1	4.5	4	13.55 $^2\Sigma$	

Table 2.1.5 - Autoionization Spectra Observed in the n*=13 Region. **PUMP line** - $A^2\Pi$-$X^2\Sigma$ (0,0) Q_2(4.5) J=4.5, N=5, e-parity

Term Value(cm^{-1})	Intensity	v'	J'	N'	Λ and n*	comment
46993.76	0.01	1	3.5	3	12.55 $^2\Sigma$	
46700.48	0.04	1	5.5	5	12.55 $^2\Sigma$	
47010.11	0.03	2	3.5	3	8.98 $^2\Pi$	
47010.45	0.03					
47011.82	0.01					
47013.01	0.06	2	3.5	4	8.98 $^2\Pi$	
47016.57	0.10	2	5.5	5	8.98 $^2\Pi$	
47017.43	0.03	2	5.5	5	f $^2\Delta$ (ℓ=+1)	
47020.79	0.06	2	5.5	6	f $^2\Delta$ (ℓ=0)	
47021.55	0.04					
47033.69	0.03					
47034.86	0.01					

47036.63	0.01				
47039.17	0.03	1	3.5	3	12.98 $^2\Pi$
47040.60	0.01				
47042.06	0.01	1	3.5	4	12.98 $^2\Pi$
47042.36	0.03				
47044.26	0.01				
47045.28	0.17	1	5.5	5	12.98 $^2\Pi$
47049.80	0.26	1	5.5	6	12.98 $^2\Pi$
47050.96	0.04				
47051.25	0.09				
47051.50	0.10	1	3.5	3	13.14 $^2\Delta$
47053.04	0.13	1	3.5	4	f $^2\Pi$ $(\ell=-2)$
47054.40	0.19				
47054.63	0.51	1	3.5	4	13.14 $^2\Delta$
47055.18	0.06				
47055.75	0.09	3	3.5	4	7.36 $^2\Pi$
47058.34	1.0	1	5.5	5	13.14 $^2\Delta$
47058.91	0.06				
47059.26	0.06	1	3.5	3	f $^2\Sigma$ $(\ell=-3)$
47059.35	0.06				
47062.43	0.46	1	5.5	6	13.14 $^2\Delta$
47063.09	0.11				
47063.50	0.10				
47064.01	0.01	1	5.5	6	f $^2\Pi$ $(\ell=-2)$
47066.32	0.04				
47069.67	0.09	1	5.5	5	f $^2\Sigma$ $(\ell=-3)$
47073.33	0.04				
47074.07	0.11	1	3.5	3	13.36 $^2\Pi$
47075.50	0.20	2	3.5	3	9.19 $^2\Sigma$
47076.55	0.09	1	3.5	4	13.36 $^2\Pi$
47081.60	0.14	1	5.5	5	13.36 $^2\Pi$
47082.96	0.03	2	5.5	5	9.19 $^2\Sigma$
47084.98	0.07	1	5.5	6	13.36 $^2\Sigma$
47092.34	0.01	1	3.5	3	13.55 $^2\Sigma$
47097.25	0.01				
47099.16	0.07	1	5.5	5	13.55 $^2\Sigma$

Table 2.1.6 - Autoionization Spectra Observed in the n*=13 Region.
PUMP line - $A^2\Pi$-$X^2\Sigma$ (0,0) $Q_2(5.5)$ J=5.5, N=6, e-parity

Term Value(cm^{-1})	Intensity	v'	J'	N'	Λ and n*	comment
46996.73	0.03	1	4.5	4	12.55 $^2\Sigma$	
47004.93	0.13	1	6.5	6	12.55 $^2\Sigma$	
47013.00	0.13	2	4.5	4	8.98 $^2\Pi$	
47013.76	0.03					
47014.07	0.03					
47016.64	0.07	2	4.5	5	8.98 $^2\Pi$	
47018.82	0.02					
47020.26	0.07	2	6.5	6	f $^2\Delta$ (ℓ=+1)	
47021.14	0.27	2	6.5	6	8.98 $^2\Pi$	
47025.37	0.05	2	6.5	7	f $^2\Delta$ (ℓ=0)	
47026.43	0.17	2	6.5	7	8.98 $^2\Pi$	
47030.72	0.05					
47037.69	0.05					
47041.81	0.03	1	4.5	4	12.98 $^2\Pi$	
47043.97	0.02					
47045.56	0.12	1	4.5	5	12.98 $^2\Pi$	
47049.39	0.33	1	6.5	6	12.98 $^2\Pi$	
47050.62	0.07					
47054.61	0.38	1	6.5	7	12.98 $^2\Pi$	blended
47054.61	0.38	1	4.5	4	13.14 $^2\Delta$	blended
47055.53	0.15					
47055.77	0.08	3	4.5	4	7.36 $^2\Pi$	
47057.49	0.47	2	4.5	5	f $^2\Pi$ (ℓ=-2)	
47058.52	0.72	1	4.5	5	13.14 $^2\Delta$	
47059.48	0.15	3	4.5	5	7.36 $^2\Pi$	
47062.82	1.0	1	6.5	6	13.14 $^2\Delta$	
47064.10	0.11	3	6.5	7	7.36 $^2\Pi$	
47066.28	0.07					
47067.77	0.57	1	6.5	7	13.14 $^2\Delta$	
47068.09	0.32	1	6.5	6	13.19 $^2\Sigma$	
47069.95	0.07					
47070.76	0.05					
47075.53	0.08	1	6.5	6	f $^2\Sigma$ (ℓ=-3)	
47077.42	0.13	1	4.5	4	13.36 $^2\Pi$	
47078.75	0.30	2	4.5	4	9.19 $^2\Sigma$	

Term Value(cm^{-1})	Intensity	v'	J'	N'	Λ and n*	comment
47080.34	0.15	1	4.5	5	13.36 $^2\Pi$	
47086.44	0.13	1	6.5	6	13.36 $^2\Pi$	
47088.00	0.05	2	6.5	6	9.19 $^2\Sigma$	
47090.28	0.07	1	6.5	7	13.36 $^2\Pi$	
47095.37	0.02	1	4.5	4	13.55 $^2\Sigma$	
47103.59	0.10	1	6.5	6	13.55 $^2\Sigma$	

Table 2.1.7 - Autoionization Spectra Observed in the n*=13 Region.
PUMP line - A$^2\Pi$-X$^2\Sigma$ (0,0) Q$_2$(6.5)   J=6.5, N=7, e-parity

Term Value(cm^{-1})	Intensity	v'	J'	N'	Λ and n*	comment
46700.35	0.01	1	5.5	5	12.55 $^2\Sigma$	
47010.19	0.07	1	7.5	7	12.55 $^2\Sigma$	
47016.55	0.06	2	5.5	5	8.98 $^2\Pi$	
47017.78	0.04					
47020.07	0.01					
47020.82	0.08	2	5.5	6	f $^2\Delta$ (ℓ=0)	
47021.55	0.03	2	5.5	6	8.98 $^2\Pi$	
47026.09	0.28	2	7.5	7	8.98 $^2\Pi$	
47030.60	0.03	2	7.5	8	f $^2\Delta$ (ℓ=0)	
47032.17	0.21	2	7.5	8	8.98 $^2\Pi$	
47042.21	0.06					
47042.75	0.04	1	7.5	7	12.88 $^2\Sigma$	
47044.07	0.02					
47045.25	0.02	1	5.5	5	12.98 $^2\Pi$	
47048.16	0.02					
47049.76	0.07	1	5.5	6	12.98 $^2\Pi$	
47050.96	0.02					
47051.22	0.02					
47054.25	0.18	1	7.5	7	12.98 $^2\Pi$	
47055.16	0.03					
47058.36	0.18	1	5.5	5	13.14 $^2\Delta$	
47059.61	0.03	3	5.5	5	7.36 $^2\Pi$	
47060.35	0.15	1	7.5	8	12.98 $^2\Pi$	
47060.99	0.12					
47062.50	0.60	1	5.5	6	13.14 $^2\Delta$	
47063.10	0.07					
47063.73	0.14	3	5.5	6	7.36 $^2\Pi$	
47064.13	0.12	1	5.5	6	f $^2\Pi$ (ℓ=-2)	
47066.38	0.01					

Term Value(cm^{-1})	Intensity	v'	J'	N'	Λ and n*	comment
47068.17	1.0	1	7.5	7	13.14 $^2\Delta$	
47069.05	0.17	3	7.5	7	7.36 $^2\Pi$	
47069.58	0.01					
47070.27	0.08					
47070.83	0.05					
47073.90	0.50	1	7.5	8	13.14 $^2\Delta$	
47075.41	0.01					
47076.06	0.03					
47077.05	0.04					
47081.60	0.06	1	5.5	5	13.36 $^2\Pi$	
47082.23	0.03	1	7.5	7	f $^2\Sigma$ (ℓ=-3)	
47082.94	0.25	2	5.5	5	9.19 $^2\Sigma$	
47084.98	0.11	1	5.5	6	13.36 $^2\Pi$	
47092.23	0.12	1	7.5	7	13.36 $^2\Pi$	
47093.89	0.04	2	7.5	7	9.19 $^2\Sigma$	
47096.47	0.07	1	7.5	8	13.36 $^2\Pi$	
47099.12	0.01	1	5.5	5	13.55 $^2\Sigma$	

Table 2.1.8 - Autoionization Spectra Observed in the n*=13 Region. PUMP line - $A^2\Pi$-$X^2\Sigma$ (0,0) P$_2$(5.5) J=4.5, N=5, f-parity

Term Value(cm^{-1})	Intensity	v'	J'	N'	Λ and n*	comment
46996.81	0.11	1	3.5	4	12.55 $^2\Sigma$	
46705.05	0.04	1	5.5	6	12.55 $^2\Sigma$	
47010.21	0.11	2	3.5	3	8.98 $^2\Pi$	
47010.41	0.08					
47013.00	0.19	2	3.5	4	8.98 $^2\Pi$	
47013.72	0.03					
47016.73	0.25	2	5.5	5	8.98 $^2\Pi$	
47017.74	0.04	2	5.5	5	f $^2\Delta$ (ℓ=0)	
47020.30	0.09	2	5.5	6	f $^2\Delta$ (ℓ=+1)	
47021.18	0.23	2	5.5	6	8.98 $^2\Pi$	
47030.40	0.05					
47030.80	0.04					
47037.59	0.04					
47038.01	0.04					
47039.30	0.09	1	3.5	3	12.98 $^2\Pi$	
47041.86	0.05	1	3.5	4	12.98 $^2\Pi$	
47044.05	0.04					
47044.98	0.01					

Term Value(cm^{-1})	Intensity	v'	J'	N'	Λ and n*	comment
47045.63	0.41	1	5.5	5	12.98 $^2\Pi$	
47047.54	0.11	1	3.5	4	f $^2\Pi$ (ℓ=-1)	
47049.45	0.27	1	5.5	6	12.98 $^2\Pi$	
47051.53	0.16	1	3.5	2	13.14 $^2\Delta$	
47052.74	0.08	3	3.5	3	7.36 $^2\Pi$	
47054.57	1.0	1	3.5	4	13.14 $^2\Delta$	
47055.86	0.11	1	5.5	6	f $^2\Pi$ (ℓ=-1)	blended
47055.86	0.11	3	3.5	4	7.36 $^2\Pi$	blended
47057.54	0.75	1	5.5	5	f $^2\Pi$ (ℓ=-2)	
47058.62	0.90	1	5.5	5	13.14 $^2\Delta$	
47059.48	0.11	3	5.5	5	7.36 $^2\Pi$	
47061.97	0.04	3	5.5	6	7.36 $^2\Pi$	
47062.87	0.68	1	5.5	6	13.14 $^2\Delta$	
47063.25	0.09					
47064.34	0.14	1	3.5	4	f $^2\Sigma$ (ℓ=-3)	
47066.34	0.08					
47067.58	0.05					
47068.18	0.09	1	5.5	6	13.19 $^2\Sigma$	
47070.82	0.01					
47073.49	0.15	1	3.5	3	13.36 $^2\Pi$	
47075.55	0.05	1	5.5	6	f $^2\Sigma$ (ℓ=-3)	
47076.46	0.01					
47077.30	0.12	1	3.5	4	13.36 $^2\Pi$	
47077.51	0.12					
47078.81	0.42	2	3.5	4	9.19 $^2\Sigma$	
47080.37	0.12	1	5.5	5	13.36 $^2\Pi$	
47086.50	0.08	1	5.5	6	13.36 $^2\Pi$	
47095.39	0.11	1	3.5	4	13.55 $^2\Sigma$	
47103.60	0.03	1	5.5	6	13.55 $^2\Sigma$	

Table 2.1.9 - Autoionization Spectra Observed in the n*=13 Region. PUMP line - A$^2\Pi$-X$^2\Sigma$ (0,0) P$_2$(6.5)   J=5.5, N=6, f-parity

Term Value(cm^{-1})	Intensity	v'	J'	N'	Λ and n*	comment
47000.54	0.09	1	4.5	5	12.55 $^2\Sigma$	
47010.23	0.03	1	6.5	7	12.55 $^2\Sigma$	
47013.09	0.08	2	4.5	4	8.98 $^2\Pi$	
47013.64	0.04					
47014.10	0.01					

47016.53	0.13	2	4.5	5	8.98 $^2\Pi$
47017.79	0.02				
47020.87	0.23	2	6.5	6	f $^2\Delta$ ($\mathscr{l}$=0)
47021.57	0.15	2	6.5	6	8.98 $^2\Pi$
47024.20	0.01	2	6.5	7	f $^2\Delta$ ($\mathscr{l}$=+1)
47026.12	0.32	2	6.5	7	8.98 $^2\Pi$
47033.81	0.06				
47034.89	0.02				
47037.60	0.01				
47039.65	0.01				
47042.10	0.08	1	4.5	4	12.98 $^2\Pi$
47042.74	0.02	1	6.5	7	12.88 $^2\Sigma$
47045.32	0.03	1	4.5	5	12.98 $^2\Pi$
47048.23	0.02				
47049.81	0.40	1	6.5	6	12.98 $^2\Pi$
47050.96	0.09				
47051.24	0.17	1	4.5	5	f $^2\Pi$ ($\mathscr{l}$=-1)
47053.03	0.09	1	4.5	4	f $^2\Pi$ ($\mathscr{l}$=-2)
47054.30	0.30	1	6.5	7	12.98 $^2\Pi$
47054.60	0.22	1	4.5	4	13.14 $^2\Delta$
47055.17	0.03	3	4.5	5	7.39 $^2\Pi$
47055.83	0.09	3	4.5	5	7.36 $^2\Pi$
47057.52	0.05	1	4.5	4	f $^2\Pi$ ($\mathscr{l}$=-2)
47058.40	1.0	1	4.5	5	13.14 $^2\Delta$
47059.61	0.17	1	4.5	5	7.36 $^2\Pi$
47060.99	0.05	1	6.5	7	f $^2\Pi$ ($\mathscr{l}$=-1)
47061.68	0.04				
47062.47	0.85	1	6.5	6	13.14 $^2\Delta$
47063.10	0.32	1	4.5	5	13.19 $^2\Sigma$
47063.46	0.16				
47063.68	0.28	3	6.5	6	7.36 $^2\Pi$
47064.10	0.18	1	6.5	6	f $^2\Pi$ ($\mathscr{l}$=-2)
47066.36	0.07				
47068.15	0.57	1	6.5	7	13.14 $^2\Delta$
47069.68	0.13	1	4.5	5	f $^2\Sigma$ ($\mathscr{l}$=-3)
47070.29	0.02	3	6.5	7	7.36 $^2\Pi$
47070.87	0.04				
47073.30	0.03				
47073.79	0.10	1	6.5	7	13.19 $^2\Sigma$

Term Value(cm^{-1})	Intensity	v'	J'	N'	Λ and n*	comment
47076.13	0.06					
47076.53	0.15	1	4.5	4	13.36 $^2\Pi$	
47081.65	0.16	1	4.5	5	13.36 $^2\Pi$	
47082.26	0.03	1	6.5	7	f $^2\Sigma$ (ℓ=-3)	
47082.93	0.36	2	4.5	5	9.19 $^2\Sigma$	
47084.92	0.15	1	6.5	6	13.36 $^2\Pi$	
47092.27	0.13	1	6.5	7	13.36 $^2\Pi$	
47099.11	0.09	1	4.5	5	13.55 $^2\Sigma$	
47108.87	0.02	1	6.5	7	13.55 $^2\Sigma$	

Table 2.1.10 - Autoionization Spectra Observed in the n*=13 Region.

PUMP line - A$^2\Pi$-X$^2\Sigma$ (0,0) P$_2$(7.5) J=6.5, N=7, f-parity

Term Value(cm^{-1})	Intensity	v'	J'	N'	Λ and n*	comment
47005.01	0.09	1	5.5	6	12.55 $^2\Sigma$	
47016.18	0.04	1	7.5	8	12.55 $^2\Sigma$	
47016.72	0.08	2	5.5	5	8.98 $^2\Pi$	
47017.39	0.03					
47020.31	0.04	2	5.5	6	f $^2\Delta$ (ℓ=+1)	
47021.17	0.09	2	5.5	6	8.98 $^2\Pi$	
47025.40	0.05	2	7.5	7	f $^2\Delta$ (ℓ=0)	
47026.45	0.13	2	7.5	7	8.98 $^2\Pi$	
47031.83	0.26	2	7.5	8	8.98 $^2\Pi$	
47037.63	0.03					
47045.57	0.03	1	5.5	5	12.98 $^2\Pi$	
47047.99	0.03					
47048.28	0.03	1	7.5	8	12.88 $^2\Sigma$	
47049.46	0.02	1	5.5	6	12.98 $^2\Pi$	
47053.21	0.02					
47054.77	0.34	1	7.5	7	12.98 $^2\Pi$	
47055.58	0.14	1	5.5	6	f $^2\Pi$ (ℓ=-1)	
47057.13	0.09					
47057.54	0.10	1	5.5	5	f $^2\Pi$ (ℓ=-2)	
47058.62	0.15	1	5.5	5	13.14 $^2\Delta$	
47059.56	0.11					
47059.86	0.21	1	7.5	8	12.98 $^2\Pi$	
47062.00	0.05	3	5.5	6	7.36 $^2\Pi$	
47062.92	0.74	1	5.5	6	13.14 $^2\Delta$	

Term Value	Intensity	v'	J'	N'	Λ and n*
47064.19	0.17	3	5.5	6	7.36 $^2\Pi$
47066.42	0.03				
47067.88	1.0	1	7.5	7	13.14 $^2\Delta$
47068.15	0.39	1	5.5	6	13.19 $^2\Sigma$
47068.95	0.05	3	7.5	7	7.36 $^2\Pi$
47070.07	0.14				
47070.86	0.06	1	7.5	7	f $^2\Pi$ (ℓ=-2)
47074.29	0.42	1	7.5	7	13.14 $^2\Delta$
47075.58	0.05	1	5.5	6	f $^2\Sigma$ (ℓ=-3)
47076.08	0.03				
47078.56	0.03	3	7.5	8	7.36 $^2\Pi$
47079.99	0.11	1	7.5	8	13.19 $^2\Sigma$
47080.36	0.11	1	5.5	5	13.36 $^2\Pi$
47086.30	0.05				
47086.48	0.12	1	5.5	6	13.36 $^2\Pi$
47087.11	0.05				
47088.06	0.26	2	5.5	6	9.19 $^2\Sigma$
47089.87	0.05	1	7.5	8	f $^2\Sigma$ (ℓ=-3)
47090.32	0.11	1	7.5	7	13.36 $^2\Pi$
47098.78	0.06	1	7.5	8	13.36 $^2\Pi$
47103.66	0.06	1	5.5	6	13.55 $^2\Pi$

Table 2.1.11 - Autoionization Spectra Observed in the n*=13 Region.

PUMP line - $A^2\Pi$-$X^2\Sigma$ (0,0) P_2(8.5)   J=7.5, N=8, f-parity

Term Value(cm^{-1})	Intensity	v'	J'	N'	Λ and n*	comment
47003.18	0.03					
47010.26	0.06	1	6.5	7	12.55 $^2\Sigma$	
47017.79	0.02					
47020.87	0.08	2	6.5	6	f $^2\Delta$ (ℓ=0)	
47021.56	0.02	2	6.5	6	8.98 $^2\Pi$	
47022.89	0.03	1	8.5	9	12.55 $^2\Sigma$	
47024.22	0.02	2	6.5	7	f $^2\Delta$ (ℓ=+1)	
47026.13	0.04	2	6.5	7	8.98 $^2\Pi$	
47030.62	0.02	2	8.5	8	f $^2\Delta$ (ℓ=0)	
47030.24	0.19	2	8.5	8	8.98 $^2\Pi$	
47038.27	0.17	2	8.5	9	8.98 $^2\Pi$	
47042.25	0.02					
47044.07	0.01					

47049.82	0.02	1	6.5	6	12.98 $^2\Pi$
47054.33	0.05	1	8.5	9	12.88 $^2\Sigma$
47060.36	0.30	1	8.5	8	12.98 $^2\Pi$
47060.98	0.13	1	6.5	7	f $^2\Pi$ (ℓ=-1)
47062.47	0.43	1	6.5	6	13.14 $^2\Delta$
47063.46	0.02				
47063.65	0.07	3	6.5	6	7.36 $^2\Pi$
47064.12	0.13	1	6.5	6	f $^2\Pi$ (ℓ=-2)
47066.15	0.19	1	8.5	9	12.98 $^2\Pi$
47068.22	0.67	1	6.5	7	13.14 $^2\Delta$
47069.10	0.30	3	6.5	7	7.36 $^2\Pi$
47069.61	0.01				
47070.31	0.06	3	6.5	7	7.36 $^2\Pi$
47070.90	0.02				
47073.95	1.0	1	8.5	8	13.14 $^2\Delta$
47074.93	0.11	3	8.5	8	7.36 $^2\Pi$
47076.11	0.04				
47077.06	0.05				
47078.24	0.03	1	8.5	8	f $^2\Pi$ (ℓ=-2)
47081.17	0.34	1	8.5	9	13.14 $^2\Delta$
47082.08	0.07				
47082.18	0.08	1	6.5	7	f $^2\Sigma$ (ℓ=-3)
47085.00	0.13	1	6.5	6	13.36 $^2\Pi$
47086.77	0.07	1	8.5	9	13.19 $^2\Sigma$
47092.24	0.13	1	6.5	7	13.36 $^2\Pi$
47093.92	0.29	2	6.5	7	9.19 $^2\Sigma$
47096.44	0.07	1	8.5	8	13.36 $^2\Pi$
47098.14	0.03	1	8.5	9	f $^2\Sigma$ (ℓ=-3)
47105.54	0.04	1	8.5	9	g $^2\Sigma$ (ℓ=-4)
47106.52	0.03	1	8.5	9	13.36 $^2\Pi$
47108.87	0.08	1	6.5	7	13.55 $^2\Sigma$
47121.66	0.03	1	8.5	9	13.55 $^2\Sigma$
47126.48	0.09				

Table 2.1.12 - Autoionization Spectra Observed in the n*=13 Region.

PUMP line - $A^2\Pi$-$X^2\Sigma$ (0,0) P$_2$(9.5)   J=8.5, N=9, f-parity

Term Value(cm^{-1})	Intensity	v'	J'	N'	Λ and n*	comment
47009.33	0.02					
47010.37	0.04					
47016.22	0.05	1	7.5	8	12.55 $^2\Sigma$	
47025.42	0.02	2	7.5	7	f $^2\Delta$ (ℓ=0)	
47026.48	0.07	2	7.5	7	8.98 $^2\Pi$	
47028.90	0.01	2	7.5	8	f $^2\Delta$ (ℓ=+1)	
47030.30	0.05	1	9.5	10	12.55 $^2\Sigma$	
47031.84	0.06	2	7.5	8	8.98 $^2\Pi$	
47036.61	0.01	2	9.5	9	f $^2\Delta$ (ℓ=0)	
47038.72	0.21	2	9.5	9	8.98 $^2\Pi$	
47045.42	0.35	2	9.5	10	8.98 $^2\Pi$	
47047.51	0.02					
47048.33	0.02	1	7.5	8	12.88 $^2\Sigma$	
47055.74	0.04					
47061.15	0.06	1	9.5	10	12.88 $^2\Sigma$	
47064.03	0.01					
47066.72	0.30	1	9.5	9	12.98 $^2\Pi$	
47067.23	0.19	1	7.5	8	f $^2\Pi$ (ℓ=-1)	
47067.88	0.30	1	7.5	7	13.14 $^2\Delta$	
47068.97	0.06	3	7.5	7	7.36 $^2\Pi$	
47070.74	0.15	1	7.5	7	f $^2\Pi$ (ℓ=-2)	
47073.16	0.19	1	9.5	10	12.98 $^2\Pi$	
47074.30	0.76	1	7.5	8	13.14 $^2\Delta$	
47075.42	0.26	3	7.5	8	7.36 $^2\Pi$	
47076.98	0.01					
47078.56	0.06	3	7.5	8	7.36 $^2\Pi$	
47079.92	0.30	1	7.5	8	13.19 $^2\Sigma$	
47080.68	1.0	1	9.5	9	13.14 $^2\Delta$	
47081.62	0.22					
47082.10	0.06	1	9.5	10	f $^2\Pi$ (ℓ=-1)	
47084.91	0.02					
47086.21	0.12	1	9.5	9	f $^2\Pi$ (ℓ=-2)	
47088.88	0.27	1	9.5	10	13.14 $^2\Delta$	
47089.84	0.09	1	7.5	8	f $^2\Sigma$ (ℓ=-3)	

88

47090.38	0.15	1	7.5	7	13.36 $^2\Pi$	blended
47090.38	0.15	3	9.5	10	7.36 $^2\Pi$	blended
47093.61	0.04	1	9.5	10	g $^2\Pi$ ($\ell=-2$)	
47094.53	0.05	1	9.5	10	13.19 $^2\Sigma$	
47096.73	0.04					
47098.82	0.14	1	8.5	9	13.36 $^2\Pi$	
47100.73	0.22	2	7.5	8	9.19 $^2\Sigma$	
47103.36	0.09	1	9.5	9	13.36 $^2\Pi$	
47113.89	0.11	1	9.5	10	13.36 $^2\Pi$	
47114.49	0.01					
47114.88	0.07	1	7.5	8	13.55 $^2\Sigma$	
47117.56	0.01					
47129.24	0.02	1	9.5	10	13.55 $^2\Sigma$	
47132.32	0.04					
47137.27	0.19					

Table 2.1.13 - Autoionization Spectra Observed in the n*=13 Region.

PUMP line - $A^2\Pi$-$X^2\Sigma$ (0,0) P_2(10.5)   J=9.5, N=10, f-parity

Term Value(cm^{-1})	Intensity	v'	J'	N'	Λ and n*	comment
47017.70	0.06					
47018.26	0.04					
47022.96	0.07	1	8.9	9	12.55 $^2\Sigma$	
47027.94	0.01					
47030.63	0.03	2	8.5	8	f $^2\Delta$ ($\ell=0$)	
47032.24	0.11	2	8.5	8	8.98 $^2\Pi$	
47034.51	0.03	2	8.5	9	f $^2\Delta$ ($\ell=+1$)	
47038.28	0.06	2	8.5	9	8.98 $^2\Pi$	
47038.62	0.04	1	10.5	11	12.55 $^2\Sigma$	
47043.43	0.01	2	10.5	10	f $^2\Delta$ ($\ell=0$)	
47045.99	0.33	2	10.5	10	8.98 $^2\Pi$	
47046.72	0.01					
47053.28	0.38	2	10.5	11	8.98 $^2\Pi$	
47054.48	0.04					
47056.71	0.02					
47060.31	0.02	1	8.5	8	12.98 $^2\Pi$	
47064.17	0.01					
47066.09	0.02	1	8.5	9	12.98 $^2\Pi$	
47068.68	0.07	1	10.5	11	12.88 $^2\Sigma$	

47072.07	0.01				
47072.89	0.01				
47073.76	0.55	1	10.5	10	12.98 $^2\Pi$
47073.95	0.35	1	8.5	8	13.14 $^2\Delta$
47074.29	0.28	1	8.5	9	f $^2\Pi$ (ℓ=-1)
47074.94	0.19	3	8.5	8	7.36 $^2\Pi$
47078.26	0.19	1	8.5	8	f $^2\Pi$ (ℓ=-2)
47080.89	0.34	1	10.5	11	12.98 $^2\Pi$
47081.21	1.0	1	8.5	9	13.14 $^2\Delta$
47082.14	0.04				
47082.46	0.39	3	8.5	9	7.36 $^2\Pi$
47084.99	0.03				
47086.72	0.27	1	8.5	9	13.19 $^2\Sigma$
47088.16	0.84	1	10.5	10	13.14 $^2\Delta$
47089.12	0.43	3	10.5	10	7.36 $^2\Pi$
47090.77	0.06	1	10.5	11	f $^2\Pi$ (ℓ=-1)
47092.21	0.02				
47093.56	0.04				
47094.58	0.13	1	10.5	10	f $^2\Pi$ (ℓ=-2)
47096.44	0.20	1	8.5	8	13.36 $^2\Pi$
47097.31	0.38	1	10.5	11	13.14 $^2\Delta$
47098.13	0.06	1	8.5	9	f $^2\Sigma$ (ℓ=-3)
47099.42	0.08				
47102.26	0.08	1	10.5	11	13.19 $^2\Sigma$
47105.50	0.14	1	8.5	9	g $^2\Sigma$ (ℓ=-4)
47106.54	0.15	1	8.5	9	13.36 $^2\Pi$
47108.55	0.52	2	8.5	9	8.19 $^2\Sigma$
47111.00	0.13	1	10.5	10	13.36 $^2\Pi$
47117.09	0.02	1	10.5	11	f $^2\Sigma$ (ℓ=-3)
47121.61	0.07	1	8.5	9	13.55 $^2\Sigma$
47122.89	0.11	1	10.5	11	13.36 $^2\Pi$
47137.39	0.05	1	10.5	11	13.55 $^2\Sigma$
47138.85	0.05				
47143.16	0.22				

Table 2.1.14 - Autoionization Spectra Observed in the n*=13 Region.

PUMP line - $A^2\Pi$-$X^2\Sigma$ (0,0) P_2(11.5)   J=10.5, N=11, f-parity

Term Value(cm⁻¹)	Intensity	v'	J'	N'	Λ and n*	comment
47026.67	0.04					
47026.89	0.04					
47030.36	0.08	1	9.5	10	12.55 $^2\Sigma$	
47036.65	0.02	2	9.5	9	f $^2\Delta$ (ℓ=0)	
47038.76	0.07	2	9.5	9	8.98 $^2\Pi$	
47040.99	0.03	2	9.5	10	f $^2\Delta$ (ℓ=+1)	
47041.09	0.02					
47045.44	0.08	2	9.5	10	8.98 $^2\Pi$	
47047.55	0.06	1	11.5	12	12.55 $^2\Sigma$	
47051.05	0.02	2	11.5	11	f $^2\Delta$ (ℓ=0)	
47053.95	0.20	2	11.5	11	8.98 $^2\Pi$	
47060.18	0.04	1	9.5	10	12.88 $^2\Sigma$	
47061.89	0.03	2	11.5	12	8.98 $^2\Pi$	
47064.00	0.04					
47066.58	0.03					
47073.16	0.02	1	9.5	10	12.98 $^2\Pi$	
47076.87	0.08	1	11.5	12	12.88 $^2\Sigma$	
47080.68	0.35	1	9.5	9	13.14 $^2\Delta$	
47081.55	0.63	1	11.5	11	12.98 $^2\Pi$	
47082.14	0.27	1	9.5	10	f $^2\Pi$ (ℓ=-1)	
47086.20	0.11	1	9.5	9	f $^2\Pi$ (ℓ=-2)	
47088.89	1.0	1	9.5	10	13.14 $^2\Delta$	
47089.29	0.16	1	11.5	12	12.98 $^2\Pi$	
47090.45	0.19	3	9.5	10	7.36 $^2\Pi$	
47093.58	0.13	1	9.5	10	g $^2\Pi$ (ℓ=-2)	
47094.45	0.16	1	9.5	10	13.19 $^2\Sigma$	
47096.34	0.85	1	11.5	11	13.14 $^2\Delta$	
47097.32	0.48	3	11.5	11	7.36 $^2\Pi$	
47100.18	0.09	1	11.5	12	f $^2\Pi$ (ℓ=-1)	
47102.99	0.07					
47103.37	0.15	1	9.5	9	13.36 $^2\Pi$	
47103.62	0.20	1	11.5	11	f $^2\Pi$ (ℓ=-2)	
47104.59	0.33					
47106.45	0.29	1	11.5	12	13.14 $^2\Delta$	

Term Value(cm^{-1})	Intensity	v'	J'	N'	Λ and n*	comment
47107.25	0.09	1	9.5	10	f $^2\Sigma$ (ℓ=-3)	
47109.12	0.17					
47111.32	0.04	1	11.5	12	13.19 $^2\Sigma$	
47113.83	0.16	1	9.5	10	13.36 $^2\Pi$	
47115.79	0.28	1	9.5	10	g $^2\Sigma$ (ℓ=-4)	
47117.71	0.26	2	9.5	10	9.19 $^2\Sigma$	
47119.45	0.09	1	11.5	11	13.36 $^2\Pi$	
47126.55	0.01					
47127.73	0.01	1	11.5	12	f $^2\Sigma$ (ℓ=-3)	
47129.25	0.07	1	9.5	10	13.55 $^2\Sigma$	
47130.88	0.01					
47132.89	0.04	1	11.5	12	13.36 $^2\Pi$	
47146.25	0.06					
47146.54	0.06	1	11.5	12	13.55 $^2\Sigma$	
47149.88	0.15					
47152.22	0.03					
47155.88	0.06					
47158.67	0.21					

Table 2.1.15 - Autoionization Spectra Observed in the n*=14 Region.

PUMP line - A$^2\Pi$-X$^2\Sigma$ (0,0) Q$_2$(1.5) J=1.5, N=2, e-parity

Term Value(cm^{-1})	Intensity	v'	J'	N'	Λ and n*	comment
47117.36	0.39	2	0.5	1	9.36 $^2\Pi$	
47118.76	0.43					
47118.84	0.39	2	2.5	2	9.36 $^2\Pi$	
47120.97	0.21	2	2.5	3	9.36 $^2\Pi$	
47125.62	0.19	1	0.5	1	13.98 $^2\Pi$	
47125.99	0.06					
47126.90	0.45	1	2.5	2	13.98 $^2\Pi$	
47129.03	0.13	1	2.5	3	13.98 $^2\Pi$	
47132.48	0.01	1	2.5	2	f $^2\Pi$ (ℓ=-1)	
47135.48	0.01					
47133.98	0.11	1	0.5	0	14.19 $^2\Sigma$	
47035.85	0.10					
47135.98	0.13					
47138.39	1.0	1	2.5	2	14.14 $^2\Delta$	
47139.05	0.10	1	2.5	2	14.19 $^2\Sigma$	
47140.70	0.24	1	2.5	3	14.14 $^2\Delta$	

92

47143.10	0.06					
47143.89	0.26	1	2.5	2	f $^2\Sigma$ (ℓ=-3)	
47144.81	0.08					
47146.65	0.16					
47146.84	0.13					
47154.22	0.22	1	0.5	1	14.36 $^2\Pi$	
47156.07	0.08	1	2.5	2	14.36 $^2\Pi$	
47157.94	0.05	1	2.5	3	14.36 $^2\Pi$	
47163.36	0.22	2	0.5	0	9.55 $^2\Sigma$	
47165.58	0.34	2	2.5	2	9.55 $^2\Sigma$	

Table 2.1.16 - Autoionization Spectra Observed in the n*=14 Region.

PUMP line - A$^2\Pi$-X$^2\Sigma$ (0,0) Q$_2$(2.5)   J=2.5, N=3, e-parity

Term Value(cm^{-1})	Intensity	v'	J'	N'	Λ and n*	comment
47110.32	0.05	3	3.5	3	7.55 $^2\Sigma$	
47117.37	0.22	2	1.5	1	9.36 $^2\Pi$	
47118.70	0.28	2	1.5	2	9.36 $^2\Pi$	
47118.83	0.24					
47121.09	0.44	2	3.5	3	9.36 $^2\Pi$	
47123.92	0.30	2	3.5	4	9.36 $^2\Pi$	
47125.58	0.14	1	1.5	1	13.98 $^2\Pi$	
47126.07	0.08	1	3.5	4	f $^2\Delta$ (ℓ=0)	
47126.97	0.11	1	1.5	2	13.98 $^2\Pi$	
47128.86	0.56	1	3.5	3	13.98 $^2\Pi$	
47129.85	0.03	1	3.5	4	13.98 $^2\Pi$	
47131.78	0.36					
47134.09	0.06	1	3.5	3	f $^2\Pi$ (ℓ=-1)	
47135.88	0.08					
47136.22	0.09	1	1.5	1	14.19 $^2\Sigma$	
47138.36	0.43	1	1.5	2	14.14 $^2\Delta$	
47139.78	0.16					
47140.50		1	1.5	1	f $^2\Sigma$ (ℓ=-3)	
47140.71	1.0	1	3.5	3	14.14 $^2\Delta$	
47142.47	0.22	1	3.5	3	14.19 $^2\Sigma$	
47143.88	0.36	1	3.5	4	14.14 $^2\Delta$	
47144.88	0.16					
47147.52	0.16	1	3.5	3	f $^2\Sigma$ (ℓ=-3)	

47150.33	0.13				
47154.28	0.14	1	1.5	1	14.36 $^2\Pi$
47155.70	0.13	1	1.5	2	14.36 $^2\Pi$
47158.71	0.06	1	3.5	3	14.36 $^2\Pi$
47161.08	0.06	1	3.5	4	14.36 $^2\Pi$
47164.12	0.11	2	1.5	1	9.55 $^2\Sigma$
47167.87	0.21	2	3.5	3	9.55 $^2\Sigma$
47173.55	0.06				

Table 2.1.17 - Autoionization Spectra Observed in the n*=14 Region.

PUMP line - $A^2\Pi$-$X^2\Sigma$ (0,0) $Q_2(3.5)$ J=3.5, N=4, e-parity

Term Value(cm⁻¹)	Intensity	v'	J'	N'	Λ and n*	comment
47113.26	0.05	3	4.5	4	7.55 $^2\Sigma$	
47118.86	0.31	2	2.5	2	9.36 $^2\Pi$	
47120.97	0.24	2	2.5	3	9.36 $^2\Pi$	
47121.73	0.08	1	4.5	4	13.88 $^2\Sigma$	
47124.10	0.42	2	4.5	4	9.36 $^2\Pi$	
47126.88	0.10	1	2.5	2	13.98 $^2\Pi$	
47127.63	0.29	2	4.5	5	9.36 $^2\Pi$	
47128.10	0.10	1	4.5	5	f $^2\Delta$ (ℓ=0)	
47129.01	0.09	1	2.5	3	13.98 $^2\Pi$	
47131.55	0.56	1	4.5	4	13.98 $^2\Pi$	
47132.43	0.03	1	2.5	2	f $^2\Pi$ (ℓ=-1)	
47135.22	0.40	1	4.5	5	13.98 $^2\Pi$	
47136.70	0.10					
47138.36	0.14	1	2.5	2	14.14 $^2\Delta$	
47139.04	0.19	1	2.5	2	14.19 $^2\Sigma$	
47140.67	0.68	1	2.5	3	14.14 $^2\Delta$	
47143.71	1.0	1	4.5	4	14.14 $^2\Delta$	
47143.90	0.32	1	2.5	2	f $^2\Sigma$ (ℓ=-3)	
47146.25	0.35	1	4.5	4	14.19 $^2\Sigma$	
47146.72	0.29	1	4.5	5	f $^2\Pi$ (ℓ=-2)	
47147.91	0.34	1	4.5	5	14.14 $^2\Delta$	
47151.75	0.08					
47152.11	0.13	1	4.5	4	f $^2\Sigma$ (ℓ=-3)	
47152.74	0.03					
47156.08	0.18	1	2.5	2	14.36 $^2\Pi$	
47157.98	0.14	1	2.5	3	14.36 $^2\Pi$	
47162.27	0.03	1	4.5	4	14.36 $^2\Pi$	
47164.93	0.08	1	4.5	5	14.36 $^2\Pi$	
47165.60	0.13	2	2.5	2	9.55 $^2\Sigma$	
47169.92	0.06					
47170.83	0.24	2	4.5	4	9.55 $^2\Sigma$	

Table 2.1.18 - Autoionization Spectra Observed in the n*=14 Region.

PUMP line - $A^2\Pi - X^2\Sigma$ (0,0) Q_2(4.5)   J=4.5, N=5, e-parity

Term Value(cm^{-1})	Intensity	v'	J'	N'	Λ and n*	comment
47116.92	0.05	3	5.5	5	7.55 $^2\Sigma$	
47121.08	0.26	2	3.5	3	9.36 $^2\Pi$	
47123.94	0.31	2	3.5	4	9.36 $^2\Pi$	
47125.23	0.09	1	5.5	5	13.88 $^2\Sigma$	
47127.85	0.37	2	5.5	5	9.36 $^2\Pi$	
47128.88	0.09	1	3.5	3	13.98 $^2\Pi$	
47130.77	0.05	1	5.5	6	f $^2\Delta$ (ℓ=0)	
47131.82	0.10	1	3.5	4	13.98 $^2\Pi$	
47132.08	0.34	2	5.5	6	9.36 $^2\Pi$	
47134.92	0.37	1	5.5	5	13.98 $^2\Pi$	
47139.40	0.39	1	5.5	6	13.98 $^2\Pi$	
47140.44	0.19	1	5.5	5	f $^2\Pi$ (ℓ=-1)	
47140.75	0.13	1	3.5	3	14.14 $^2\Delta$	
47142.22	0.13	1	3.5	4	f $^2\Pi$ (ℓ=-2)	
47142.88	0.13					
47143.88	0.61	1	3.5	4	14.14 $^2\Delta$	
47147.63	1.0	1	5.5	5	14.14 $^2\Delta$	
47150.57	0.40	1	5.5	5	14.19 $^2\Sigma$	
47151.76	0.31	1	5.5	6	14.14 $^2\Delta$	
47153.14	0.11	1	5.5	6	f $^2\Pi$ (ℓ=-2)	
47155.43	0.03					
47157.33	0.11	1	5.5	5	f $^2\Sigma$ (ℓ=-3)	
47158.74	0.19	1	3.5	3	14.36 $^2\Pi$	
47161.03	0.10	1	3.5	4	14.36 $^2\Pi$	
47166.65	0.05	1	5.5	5	14.36 $^2\Pi$	
47167.88	0.16	2	3.5	3	9.55 $^2\Sigma$	
47169.58	0.06	1	5.5	6	14.36 $^2\Pi$	
47173.06	0.06					
47174.61	0.37	2	5.5	5	9.55 $^2\Sigma$	

Table 2.1.19 - Autoionization Spectra Observed in the n*=14 Region.

PUMP line - $A^2\Pi$-$X^2\Sigma$ (0,0) $Q_2(5.5)$ J=5.5, N=6, e-parity

Term Value(cm^{-1})	Intensity	v'	J'	N'	Λ and n*	comment
47113.24	0.05	3	4.5	4	7.55 $^2\Sigma$	
47115.40	0.05					
47121.32	0.06	3	6.5	6	7.55 $^2\Sigma$	
47124.09	0.28	2	4.5	4	9.36 $^2\Pi$	
47126.06	0.05					
47127.65	0.30	2	4.5	5	9.36 $^2\Pi$	
47129.19	0.11	1	6.5	6	13.88 $^2\Sigma$	
47129.35	0.11					
47131.55	0.06	1	4.5	4	13.98 $^2\Pi$	
47132.03	0.27					
47132.45	0.30	2	6.5	6	9.36 $^2\Pi$	
47134.22	0.09	1	6.5	7	f $^2\Delta$ (ℓ=0)	
47134.39	0.06					
47135.23	0.09	1	4.5	5	13.98 $^2\Pi$	
47137.29	0.41	2	6.5	7	9.36 $^2\Pi$	
47139.01	0.54	1	6.5	6	13.98 $^2\Pi$	
47143.80	0.32	1	4.5	4	14.14 $^2\Delta$	
47144.26	0.66	1	6.5	7	13.98 $^2\Pi$	
47145.09	0.25	1	6.5	6	f $^2\Pi$ (ℓ=-1)	
47146.30	0.23	1	4.5	4	14.19 $^2\Sigma$	
47146.76	0.58	1	4.5	5	f $^2\Pi$ (ℓ=-2)	
47147.95	0.62	1	4.5	5	14.14 $^2\Delta$	
47149.23	0.17					
47152.22	1.0	1	6.5	6	14.14 $^2\Delta$	
47152.22	1.0	1	4.5	4	f $^2\Sigma$ (ℓ=-3)	
47154.21	0.28					
47155.31	0.44	1	6.5	6	14.19 $^2\Sigma$	
47157.21	0.40	1	6.5	7	14.14 $^2\Delta$	
47159.40	0.05	1	6.5	7	f $^2\Pi$ (ℓ=-2)	
47160.62	0.06					
47162.27	0.30	1	4.5	4	14.36 $^2\Pi$	
47163.35	0.08	1	6.5	6	f $^2\Sigma$ (ℓ=-3)	
47164.93	0.22	1	4.5	5	14.36 $^2\Pi$	
47170.85	0.14	2	4.5	4	9.55 $^2\Sigma$	

47171.78	0.08	1	6.5	6	14.36 $^2\Pi$	
47174.87	0.13	1	6.5	7	14.36 $^2\Pi$	
47176.80	0.08					
47179.09	0.43	2	6.5	6	9.55 $^2\Sigma$	

Table 2.1.20 - Autoionization Spectra Observed in the n*=14 Region.

PUMP line - $A^2\Pi$-$X^2\Sigma$ (0,0) Q_2(6.5)   J=6.5, N=7, e-parity

Term Value(cm^{-1})	Intensity	v'	J'	N'	Λ and n*	comment
47126.42	0.08	3	7.5	7	7.55 $^2\Sigma$	
4127.83	0.43	2	5.5	5	9.36 $^2\Pi$	
47132.09	0.34	2	5.5	6	9.36 $^2\Pi$	
47132.33	0.19	1	5.5	5	f $^2\Delta$ (ℓ=+1)	
47134.00	0.14	1	7.5	7	13.88 $^2\Sigma$	
47134.89	0.05	1	5.5	5	13.98 $^2\Pi$	
47137.41	0.63	2	7.5	7	9.36 $^2\Pi$	
47138.44	0.08	1	7.5	8	f $^2\Delta$ (ℓ=0)	
47139.40	0.14	1	5.5	6	13.98 $^2\Pi$	
47140.00	0.05	7	7.5	7	f $^2\Delta$ (ℓ=+1)	
47143.23	0.47	2	7.5	8	9.36 $^2\Pi$	
47143.83	0.56	1	7.5	7	13.98 $^2\Pi$	
47147.67	0.22	1	5.5	5	14.14 $^2\Delta$	
47149.83	0.55	1	7.5	8	13.98 $^2\Pi$	
47150.59	0.45	1	5.5	5	14.19 $^2\Sigma$	blended
47150.59	0.45	1	7.5	7	f $^2\Pi$ (ℓ=-1)	blended
47151.76	0.74	1	5.5	6	14.14 $^2\Delta$	
47153.16	0.22	1	5.5	6	f $^2\Pi$ (ℓ=-2)	
47155.42	0.05					
47157.59	1.0	1	7.5	7	14.14 $^2\Delta$	
47160.73	0.35	1	7.5	7	14.19 $^2\Sigma$	
47163.39	0.42	1	7.5	8	14.14 $^2\Delta$	
47166.65	0.34	1	5.5	5	14.36 $^2\Pi$	
47169.52	0.18	1	5.5	6	14.36 $^2\Pi$	
47170.21	0.06	1	7.5	7	f $^2\Sigma$ (ℓ=-3)	
47174.59	0.08	2	5.5	5	9.55 $^2\Sigma$	
47178.06	0.05	1	7.5	7	14.36 $^2\Pi$	
47181.06	0.06	1	7.5	8	14.36 $^2\Pi$	
47184.33	0.22	2	7.5	7	9.55 $^2\Sigma$	

Table 2.1.21 - Autoionization Spectra Observed in the n*=14 Region.

PUMP line - $A^2\Pi$ -$X^2\Sigma$ (0,0) P_2(5.5)   J=4.5, N=5, f-parity

Term Value(cm^{-1})	Intensity	v'	J'	N'	Λ and n*	comment
47120.99	0.46	2	5.5	3	9.36 $^2\Pi$	
47121.63	0.11	1	3.5	4	13.88 $^2\Sigma$	
47121.81	0.09					
47124.08	0.38	2	3.5	4	9.36 $^2\Pi$	
47127.67	0.52	2	5.5	5	9.36 $^2\Pi$	
47129.08	0.23	1	3.5	3	13.98 $^2\Pi$	
47129.64	0.15					
47131.55	0.10	1	3.5	4	13.98 $^2\Pi$	
47132.05	0.27					
47132.44	0.35	2	5.5	6	9.36 $^2\Pi$	
47135.29	1.0	1	5.5	5	13.98 $^2\Pi$	
47136.74	0.11	1	3.5	4	f $^2\Pi$ (ℓ=-1)	
47139.06	0.65	1	5.5	6	13.98 $^2\Pi$	
47140.74	0.15	1	3.5	3	14.14 $^2\Delta$	
47143.76	0.77	1	3.5	4	14.14 $^2\Delta$	
47145.07	0.11	1	5.5	6	f $^2\Pi$ (ℓ=-1)	
47146.29	0.75	1	3.5	4	14.19 $^2\Sigma$	
47146.55	0.27					
47146.76	0.63	1	5.5	5	f $^2\Pi$ (ℓ=-2)	
47148.01	0.98	1	5.5	5	14.14 $^2\Delta$	
47148.49	0.08					
47151.82	0.29					
47152.21	0.69	1	5.5	6	14.14 $^2\Delta$	blended
47152.21	0.69	1	3.5	4	f $^2\Sigma$ (ℓ=-3)	blended
47154.53	0.04					
47155.36	0.23	1	5.5	6	14.19 $^2\Sigma$	
47157.98	0.29	1	5.5	5	14.36 $^2\Pi$	
47161.75	0.15					
47162.29	0.35	1	3.5	4	14.36 $^2\Pi$	
47163.33	0.08	1	5.5	6	f $^2\Sigma$ (ℓ=-3)	
47164.96	0.21	1	5.5	5	14.36 $^2\Pi$	
47170.88	0.52	2	3.5	4	9.55 $^2\Sigma$	
44173.06	0.23	1	3.5	4	14.55 $^2\Sigma$	
47179.15	0.21	2	5.5	6	9.55 $^2\Sigma$	

Table 2.1.22 - Autoionization Spectra Observed in the n*=14 Region.

PUMP line - A$^2\Pi$-X$^2\Sigma$ (0,0)   P$_2$(6.5)   J=5.5,   N=6,   f-parity

Term Value(cm^{-1})	Intensity	v'	J'	N'	Λ and n*	comment
47123.98	0.47	2	4.5	4	9.36 $^2\Pi$	
47125.18	0.09	1	4.5	5	13.88 $^2\Sigma$	
47126.50	0.06					
47127.82	0.45	2	4.5	5	9.36 $^2\Pi$	
47129.66	0.06					
47131.84	0.16	1	4.5	4	13.98 $^2\Pi$	
47132.15	0.50	2	6.5	6	9.36 $^2\Pi$	
47134.03	0.12	1	6.5	7	13.88 $^2\Sigma$	
47134.97	0.07	1	4.5	5	13.98 $^2\Pi$	
47137.43	0.50	2	6.5	7	9.36 $^2\Pi$	
47138.52	0.07					
47139.46	0.59	1	6.5	6	13.98 $^2\Pi$	
47140.46	0.18	1	4.5	5	f $^2\Pi$ (ℓ=-1)	
47142.21	0.09	1	4.5	4	f $^2\Pi$ (ℓ=-2)	
47143.89	0.43	1	4.5	4	14.14 $^2\Delta$	
47147.30	0.24					
47147.65	0.93	1	4.5	5	14.14 $^2\Delta$	
47150.56	0.60	1	4.5	5	14.19 $^2\Sigma$	blended
47150.56	0.60	1	6.5	7	f $^2\Pi$ (ℓ=-1)	blended
47151.77	1.0	1	6.5	6	14.14 $^2\Delta$	
47153.19	0.41	1	6.5	6	f $^2\Pi$ (ℓ=-2)	
47155.45	0.13					
47157.37	0.19	1	4.5	5	f $^2\Sigma$ (ℓ=-3)	
47157.63	0.35	1	6.5	7	14.14 $^2\Delta$	
47160.80	0.25	1	6.5	7	14.19 $^2\Sigma$	
47161.15	0.23	1	4.5	4	14.36 $^2\Pi$	
47161.53	0.09					
47161.75	0.07					
47166.68	0.34	1	4.5	5	14.36 $^2\Pi$	
47167.95	0.04					
47169.57	0.18	1	6.5	6	14.36 $^2\Pi$	
47170.29	0.04	1	6.5	7	f $^2\Sigma$ (ℓ=-3)	
47174.61	0.29	2	4.5	5	9.55 $^2\Sigma$	
47176.84	0.15	1	4.5	5	14.55 $^2\Sigma$	blended

Term Value(cm⁻¹)	Intensity	v'	J'	N'	Λ and n*	comment
47176.84	0.15	1	6.5	7	14.36 $^2\Pi$	blended
47180.41	0.05					
47184.41	0.12	2	6.5	7	9.55 $^2\Sigma$	

Table 2.1.23 - Autoionization Spectra Observed in the n*=14 Region.

PUMP line - A$^2\Pi$-X$^2\Sigma$ (0,0) P$_2$(7.5)   J=6.5,   N=7,   f-parity

Term Value(cm⁻¹)	Intensity	v'	J'	N'	Λ and n*	comment
47127.69	0.26	2	5.5	5	9.36 $^2\Pi$	
47129.22	0.09	1	5.5	6	13.88 $^2\Sigma$	
47132.01	0.17					
47132.41	0.17	2	5.5	6	9.36 $^2\Pi$	
47134.21	0.06					
47135.27	0.11	1	5.5	5	13.98 $^2\Pi$	
47135.74	0.07	1	5.5	6	f $^2\Delta$ (ℓ=+1)	
47137.33	0.49	2	7.5	7	9.36 $^2\Pi$	
47139.28	0.17	1	7.5	8	13.88 $^2\Sigma$	
47140.15	0.03					
47143.09	0.49	2	7.5	8	9.36 $^2\Pi$	
47144.31	0.79	1	7.5	7	13.98 $^2\Pi$	
47145.09	0.24	1	5.5	6	f $^2\Pi$ (ℓ=-1)	
47145.24	0.19	1	7.5	8	f $^2\Delta$ (ℓ=+1)	
47146.78	0.13	1	5.5	5	f $^2\Pi$ (ℓ=-2)	
47148.03	0.15	1	5.5	5	14.14 $^2\Delta$	
47149.46	0.38	1	7.5	8	13.98 $^2\Pi$	
47152.25	1.0	1	5.5	6	14.14 $^2\Delta$	
47155.33	0.60	1	5.5	6	14.19 $^2\Sigma$	
47156.23	0.87	1	7.5	7	14.14 $^2\Delta$	
47159.43	0.09	1	7.5	7	f $^2\Pi$ (ℓ=-2)	
47159.76	0.03					
47163.39	0.13	1	5.5	6	f $^2\Sigma$ (ℓ=-3)	
47163.75	0.28	1	7.5	8	14.14 $^2\Delta$	
47164.92	0.21	1	5.5	5	14.36 $^2\Pi$	
47166.90	0.09	1	7.5	8	14.19 $^2\Sigma$	
47171.85	0.39	1	5.5	6	14.36 $^2\Pi$	
47174.85	0.21	1	7.5	7	14.36 $^2\Pi$	
47177.89	0.04	1	7.5	8	f $^2\Sigma$ (ℓ=-3)	
47179.12	0.34	2	5.5	6	9.55 $^2\Sigma$	

| 47181.47 | 0.09 | 1 | 5.5 | 6 | 14.55 $^2\Sigma$ |

Table 2.1.24 - Autoionization Spectra Observed in the n*=14 Region.

PUMP line - $A^2\Pi$-$X^2\Sigma$ (0,0) P_2(8.5) J=7.5, N=8, f-parity

Term Value(cm^{-1})	Intensity	v'	J'	N'	Λ and n*	comment
47126.44	0.10	3	6.5	7	7.55 $^2\Sigma$	
47130.07	0.02					
47132.14	0.32	2	6.5	6	9.36 $^2\Pi$	
47134.01	0.07	1	6.5	7	13.88 $^2\Sigma$	
47137.44	0.20	2	6.5	7	9.36 $^2\Pi$	
47138.47	0.07					
47139.44	0.07	1	6.5	6	13.98 $^2\Pi$	
47140.00	0.10	1	6.5	7	f $^2\Delta$ (ℓ=+1)	
47143.23	0.40	2	8.5	8	9.36 $^2\Pi$	
47145.29	0.18					
47145.48	0.16	1	8.5	9	13.88 $^2\Sigma$	
47149.27	0.32	1	8.5	9	f $^2\Delta$ (ℓ=+1)	
47149.89	0.63	1	8.5	8	13.98 $^2\Pi$	
47150.62	0.22	1	6.5	7	f $^2\Pi$ (ℓ=-1)	
47151.54	0.25	2	8.5	9	9.36 $^2\Pi$	
47151.79	0.22	1	6.5	6	14.14 $^2\Delta$	
47153.18	0.06	1	6.5	6	f $^2\Pi$ (ℓ=-2)	
47155.77	0.22	1	8.5	9	13.98 $^2\Pi$	
47157.00	0.07					
47157.65	0.78	1	6.5	7	14.14 $^2\Delta$	
47160.77	0.44	1	6.5	7	14.19 $^2\Sigma$	
47163.38	1.0	1	8.5	8	14.14 $^2\Delta$	
47164.05	0.10	1	8.5	9	f $^2\Pi$ (ℓ=-1)	
47164.86	0.06					
47169.53	0.22	1	6.5	6	14.36 $^2\Pi$	
47170.22	0.12	1	6.5	7	f $^2\Sigma$ (ℓ=-3)	
47170.62	0.23	1	8.5	9	14.14 $^2\Delta$	
47173.42	0.07	1	8.5	9	14.19 $^2\Sigma$	
47176.87	0.09	1	6.5	7	g $^2\Sigma$ (ℓ=-4)	
47177.93	0.32	1	6.5	7	14.36 $^2\Pi$	
47181.09	0.10	1	8.5	8	14.36 $^2\Pi$	
47184.34	0.23	2	6.5	7	9.55 $^2\Sigma$	

47186.77	0.12	1	6.5	7	14.55 $^2\Sigma$
47190.06	0.04				

Table 2.1.25 - Autoionization Spectra Observed in the n*=14 Region.

PUMP line - $A^2\Pi$-$X^2\Sigma$ (0,0) P_2(9.5)   J=8.5, N=9, f-parity

Term Value(cm^{-1})	Intensity	v'	J'	N'	Λ and n*	comment
47129.14	0.08					
47132.30	0.15	3	7.5	8	7.55 $^2\Sigma$	
47137.32	0.40	2	7.5	7	9.36 $^2\Pi$	
47139.14	0.02					
47139.43	0.04					
47140.14	0.03					
47143.07	0.35	2	7.5	8	9.36 $^2\Pi$	
47143.48	0.10					
47144.33	0.08	1	7.5	7	13.98 $^2\Pi$	
47145.24	0.19	1	7.5	8	f $^2\Delta$ (ℓ=+1)	
47146.21	0.08	3	9.5	10	7.55 $^2\Sigma$	
47149.90	0.31	2	9.5	9	9.36 $^2\Pi$	
47152.19	0.23	1	9.5	10	13.88 $^2\Sigma$	
47156.00	0.50	1	9.5	10	f $^2\Delta$ (ℓ=+1)	
47156.17	0.86	1	9.5	9	13.98 $^2\Pi$	
47156.97	0.27	1	7.5	8	f $^2\Pi$ (ℓ=-1)	
47156.26	0.21	1	7.5	7	14.14 $^2\Delta$	
47158.80	0.35	2	9.5	10	9.36 $^2\Pi$	
47162.67	0.21					
47162.87	0.48	1	9.5	10	13.98 $^2\Pi$	
47163.78	0.94	1	7.5	8	14.14 $^2\Delta$	
47166.25	0.10					
47166.92	0.31	1	7.5	8	14.19 $^2\Sigma$	
47168.43	0.01					
47170.30	1.0	1	9.5	9	14.14 $^2\Delta$	
47170.69	0.11					
47171.81	0.07					
47171.95	0.11	1	9.5	10	f $^2\Pi$ (ℓ=-1)	
47174.89	0.19	1	7.5	7	14.36 $^2\Pi$	
47177.91	0.15	1	7.5	8	f $^2\Sigma$ (ℓ=-3)	
47178.25	0.21	1	9.5	10	14.14 $^2\Delta$	
47180.69	0.04					

47181.05	0.11	1	9.5	10	14.19 $^2\Sigma$	
47184.57	0.38	1	7.5	8	14.36 $^2\Pi$	
47185.98	0.10	1	7.5	8	f $^2\Sigma$ (ℓ=-4)	
47187.99	0.13	1	9.5	9	14.36 $^2\Pi$	
47190.41	0.27	2	7.5	8	9.55 $^2\Sigma$	
47192.64	0.10	1	7.5	8	14.55 $^2\Sigma$	
47196.02	0.06					

Table 2.1.26 - Autoionization Spectra Observed in the n*=14 Region.

PUMP line - $A^2\Pi$-$X^2\Sigma$ (0,0) P_2(10.5)   J=9.5, N=10, f-parity

Term Value(cm^{-1})	Intensity	v'	J'	N'	Λ and n*	comment
47137.47	0.06					
47138.86	0.05	3	8.5	9	7.55 $^2\Sigma$	
47143.25	0.32	2	8.5	8	9.36 $^2\Pi$	
47145.49	0.06	1	8.5	9	13.88 $^2\Sigma$	
47146.97	0.01					
47149.27	0.16	1	8.5	9	f $^2\Delta$ (ℓ=+1)	
47151.53	0.27	2	8.5	9	9.36 $^2\Pi$	
47154.25	0.04					
47155.76	0.03	1	8.5	9	13.98 $^2\Pi$	
47157.21	0.27	2	10.5	10	9.36 $^2\Pi$	
47157.57	0.04					
47157.78	0.14	1	10.5	10	g $^2\Phi$ (ℓ=+1)	
47159.57	0.26	1	10.5	11	13.88 $^2\Sigma$	
47163.05	0.59	1	10.5	10	13.98 $^2\Pi$	
47163.35	0.49	1	8.5	8	14.14 $^2\Delta$	
47164.08	0.26	1	8.5	9	f $^2\Pi$ (ℓ=-1)	
47166.89	0.51	2	10.5	11	9.36 $^2\Pi$	
47169.54	0.09					
47170.63	1.0	1	8.5	9	14.14 $^2\Delta$	blended
47170.63	1.0	1	10.5	11	13.98 $^2\Pi$	blended
47173.44	0.20	1	8.5	9	14.19 $^2\Sigma$	
47174.56	0.04					
47175.59	0.04					
47177.91	0.78	1	10.5	10	14.14 $^2\Delta$	
47180.63	0.13	1	10.5	11	f $^2\Pi$ (ℓ=-1)	
47181.06	0.17	1	8.5	8	14.36 $^2\Pi$	
47186.24	0.10	1	8.5	9	f $^2\Sigma$ (ℓ=-3)	

47186.59	0.13	1	10.5	11	14.14 $^2\Delta$
47189.18	0.06	1	10.5	11	14.19 $^2\Sigma$
47192.27	0.46	1	8.5	9	14.36 $^2\Pi$
47195.62	0.10	1	10.5	10	14.36 $^2\Pi$
47197.26	0.17	2	8.5	9	9.55 $^2\Sigma$
47198.27	0.03				
47199.24	0.06	1	8.5	9	14.55 $^2\Sigma$
47202.77	0.04				

Table 2.1.27 - Autoionization Spectra Observed in the n*=14 Region.
PUMP line - $A^2\Pi$-$X^2\Sigma$ (0,0) P_2(11.5)   J=10.5, N=11, f-parity.

Term Value(cm^{-1})	Intensity	v'	J'	N'	Λ and n*	comment
47146.23	0.10	3	9.5	10	7.55 $^2\Sigma$	
47146.49	0.08					
47149.89	0.35	2	9.5	9	9.36 $^2\Pi$	
47156.00	0.09	1	9.5	10	f $^2\Delta$ (ℓ=+1)	
47158.81	0.25	2	9.5	10	9.36 $^2\Pi$	
47162.88	0.04	1	9.5	10	13.98 $^2\Pi$	
47164.95	0.06	1	11.5	11	g $^2\Phi$ (ℓ=+1)	
47165.65	0.33	2	11.5	11	9.36 $^2\Pi$	
47167.65	0.14	1	11.5	11	13.88 $^2\Sigma$	
47170.33	0.16					
47170.85	0.37	1	11.5	11	13.98 $^2\Pi$	
47171.32	0.05	1	9.5	9	14.14 $^2\Delta$	
47171.60	0.05					
47171.98	0.29	1	9.5	10	f $^2\Pi$ (ℓ=-1)	
47173.46	0.02					
47175.74	0.67	2	11.5	12	9.36 $^2\Pi$	
47178.27	1.0	1	9.5	10	14.14 $^2\Delta$	
47179.42	0.14	1	11.5	12	13.98 $^2\Pi$	
47180.41	0.06					
47181.03	0.21	1	9.5	10	14.19 $^2\Sigma$	
47184.12	0.04					
47184.54	0.06					
47186.26	0.57	1	11.5	11	14.14 $^2\Delta$	
47187.99	0.21	1	9.5	9	14.36 $^2\Pi$	
47190.07	0.08	1	11.5	12	f $^2\Pi$ (ℓ=-1)	
47195.36	0.21	1	9.5	10	f $^2\Sigma$ (ℓ=-3)	

105

47195.68	0.14	1	11.5	12	14.14	$^2\Delta$
47198.35	0.06	1	11.5	12	14.19	$^2\Sigma$
47200.71	0.69	1	9.5	10	14.36	$^2\Pi$
47204.01	0.14	1	11.5	11	14.36	$^2\Pi$
47204.57	0.20	2	9.5	10	9.55	$^2\Sigma$
47206.58	0.08	1	9.5	10	14.55	$^2\Sigma$

Table 2.1.28 - Autoionization Spectra Observed in the n*=17 and n*=18 Region.

PUMP line - $A^2\Pi$-$X^2\Sigma$ (0,0) Q_2(1.5)   J=1.5, N=2, e-parity

Term Value(cm^{-1})	Intensity	v'	J'	N'	Λ and n*	comment
47294.00	0.08					
47300.61	1.0	2	2.5	2	10.14 $^2\Delta$	
47302.70	0.56	2	2.5	3	10.14 $^2\Delta$	
47306.65	0.15	1	0.5	1	16.98 $^2\Pi$	
47307.84	0.33	1	2.5	2	16.98 $^2\Pi$	
47309.86	0.13	1	2.5	3	16.98 $^2\Pi$	
47311.70	0.23					
47314.12	0.48	1	2.5	2	17.14 $^2\Delta$	
47315.70	0.33	1	2.5	2	17.19 $^2\Sigma$	
47316.36	0.15	1	2.5	3	17.14 $^2\Delta$	
47317.72	0.10					
47318.38	0.11					
47319.82	0.10					
47320.22	0.11					
47321.68	0.25	1	0.5	1	17.36 $^2\Pi$	
47323.11	0.06					
47324.50	0.04	1	2.5	2	17.36 $^2\Pi$	
47325.63	0.06	1	2.5	3	17.36 $^2\Pi$	
47329.52	0.08	1	0.5	0	17.55 $^2\Sigma$	
47331.78	0.06	1	2.5	2	17.55 $^2\Sigma$	
47340.30	0.06					
47342.23	0.35	2	0.5	1	10.36 $^2\Pi$	
47343.69	0.23	2	2.5	2	10.36 $^2\Pi$	
47344.22	0.17		0.5	1	term3	
47345.98	0.21	2	2.5	3	10.36 $^2\Pi$	
47347.86	0.15	1	0.5	1	17.98 $^2\Pi$	
47348.97	0.33	1	2.5	2	17.98 $^2\Pi$	
47350.94	0.15	1	2.5	3	17.98 $^2\Pi$	
47352.10	0.08					
47352.76	0.13					
47354.07	0.69	1	2.5	2	18.14 $^2\Delta$	
47355.40	0.06					
47356.31	0.21	1	2.5	3	18.14 $^2\Delta$	
47356.84	0.13					

Term Value(cm⁻¹)	Intensity					
47357.76	0.10					
47361.44	0.11	1	0.5	1	18.36 $^2\Pi$	
47366.78	0.06					

Table 2.1.29 - Autoionization Spectra Observed in the n*=17 and n*=18 Region.

PUMP line - $A^2\Pi$-$X^2\Sigma$ (0,0) Q_2(2.5)   J=2.5, N=3, e-parity

Term Value(cm⁻¹)	Intensity	v'	J'	N'	Λ and n*	comment
47295.33	0.04		3.5	3	term1	
47298.31	0.09					
47300.61	0.35	2	1.5	2	10.14 $^2\Delta$	
47302.80	1.0	2	3.5	3	10.14 $^2\Delta$	
47303.26	0.23					
47304.26	0.06					
47305.67	0.49	2	3.5	4	10.14 $^2\Delta$	
47306.95	0.14	1	1.5	1	16.98 $^2\Pi$	
47308.02	0.09	1	1.5	2	16.98 $^2\Pi$	
47309.75	0.22	1	3.5	3	16.98 $^2\Pi$	
47312.53	0.11	1	3.5	4	16.98 $^2\Pi$	
47313.70	0.22					
47313.84	0.20	1	1.5	2	17.14 $^2\Delta$	
47313.97	0.24					
47316.53	0.30	1	3.5	3	17.14 $^2\Delta$	
47317.33	0.10	1	3.5	3	17.19 $^2\Sigma$	a
47318.24	0.27	1	3.5	3	17.19 $^2\Sigma$	a
47319.52	0.19	1	3.5	4	17.14 $^2\Delta$	
47322.09	0.26	1	1.5	1	17.36 $^2\Pi$	
47323.30	0.14	1	1.5	2	17.36 $^2\Pi$	
47323.58	0.11					
47324.93	0.08					
47327.34	0.04	1	3.5	3	17.36 $^2\Pi$	
47328.84	0.10	1	3.5	4	17.36 $^2\Pi$	
47330.32	0.06	1	1.5	1	17.55 $^2\Sigma$	
47333.99	0.04	1	3.5	3	17.55 $^2\Sigma$	
47342.24	0.23	2	1.5	1	10.36 $^2\Pi$	
47343.71	0.22	2	1.5	2	10.36 $^2\Pi$	
47346.19	0.35	2	3.5	3	10.36 $^2\Pi$	
47347.90	0.08	1	1.5	1	17.98 $^2\Pi$	
47349.03	0.26	1	1.5	2	17.98 $^2\Pi$	

Term Value(cm⁻¹)	Intensity	v'	J'	N'	Λ and n*	comment
47350.81	0.39	1	3.5	3	17.98 $^2\Pi$	
47351.86	0.06					
47353.53	0.26	1	1.5	2	18.14 $^2\Delta$	blended
47353.53	0.26	1	3.5	4	17.98 $^2\Pi$	blended
47353.91	0.38					
47354.33	0.22	1	3.5	3	f $^2\Pi$ (ℓ=-1)	
47354.72	0.14					
47356.55	0.49	1	3.5	3	18.14 $^2\Delta$	
47359.46	0.20	1	3.5	4	18.14 $^2\Delta$	
47361.78	0.14	1	1.5	1	18.36 $^2\Pi$	
47362.99	0.11	1	1.5	2	18.36 $^2\Pi$	
47364.54	0.10					
47365.30	0.04					
47367.53	0.09					
47368.55	0.03	1	3.5	4	18.36 $^2\Pi$	

[a]This state is perturbed by an unassigned state.

Table 2.1.30 - Autoionization Spectra Observed in the n*=17 and n*=18 Region.

PUMP line - $A^2\Pi$-$X^2\Sigma$ (0,0) Q_2(3.5) J=3.5, N=4, e-parity

Term Value(cm⁻¹)	Intensity	v'	J'	N'	Λ and n*	comment
47300.04	0.11					
47300.62	0.19	2	2.5	2	10.14 $^2\Delta$	
47302.86	0.88	2	2.5	3	10.14 $^2\Delta$	
47303.60	0.10					
47305.78	1.0	2	4.5	4	10.14 $^2\Delta$	
47306.78	0.15					
47307.93	0.08	1	2.5	2	16.98 $^2\Pi$	
47309.41	0.83	1	4.5	5	10.14 $^2\Delta$	
47312.27	0.46	1	4.5	4	16.98 $^2\Pi$	
47314.15	0.10	1	2.5	2	17.14 $^2\Delta$	
47315.77	0.54	1	2.5	2	17.19 $^2\Sigma$	blended
47315.77	0.54	1	4.5	5	16.98 $^2\Pi$	blended
47316.34	0.48	1	2.5	3	17.14 $^2\Delta$	
47319.69	0.67	1	4.5	4	17.14 $^2\Delta$	
47320.99	0.75	1	4.5	4	17.19 $^2\Sigma$	a
47321.93	0.15	1	4.5	4	17.19 $^2\Sigma$	a
47323.66	0.23					
47324.43	0.46	1	2.5	2	17.36 $^2\Pi$	

Term Value(cm⁻¹)	Intensity	v'	J'	N'	Λ and n*	comment
47324.99	0.19					
47325.66	0.35	1	2.5	3	17.36 $^2\Pi$	
47328.03	0.06					
47328.62	0.15					
47331.82	0.06	1	2.5	2	17.55 $^2\Sigma$	
47332.81	0.11	1	4.5	5	17.36 $^2\Pi$	
47337.20	0.10	1	4.5	4	17.55 $^2\Sigma$	
47343.70	0.46	2	2.5	2	10.36 $^2\Pi$	
47345.96	0.36	2	2.5	3	10.36 $^2\Pi$	
47348.35	0.11		2.5	3	term3	
47348.94	0.48	1	2.5	2	17.98 $^2\Pi$	
47349.12	0.36	2	4.5	4	10.36 $^2\Pi$	
47350.49	0.08					
47350.96	0.06	1	2.5	3	17.98 $^2\Pi$	
47351.48	0.04					
47352.75	0.46	2	4.5	5	10.36 $^2\Pi$	
47353.35	0.42					
47354.07	0.15	1	2.5	2	18.14 $^2\Delta$	
47356.31	0.46	1	2.5	3	18.14 $^2\Delta$	
47356.64	0.50	1	4.5	5	17.98 $^2\Pi$	
47357.33	0.33	1	4.5	4	f $^2\Pi$ (ℓ=-1)	
47359.79	0.52	1	4.5	4	18.14 $^2\Delta$	
47362.05	0.15					
47362.53	0.08					
47363.48	0.27	1	4.5	5	18.14 $^2\Delta$	
47363.70	0.19	1	2.5	2	18.36 $^2\Pi$	
47364.18	0.21					
47365.39	0.16	1	2.5	3	18.36 $^2\Pi$	
47366.63	0.06					
47369.11	0.06					

[a]This state is perturbed by an unassigned state.

Table 2.1.31 - Autoionization Spectra Observed in the n*=17 and n*=18 Region.

PUMP line - $A^2\Pi$-$X^2\Sigma$ (0,0) Q_2(4.5)   J=4.5, N=5, e-parity

Term Value(cm⁻¹)	Intensity	v'	J'	N'	Λ and n*	comment
47298.31	0.09					
47302.82	0.25	2	3.5	3	10.14 $^2\Delta$	
47305.39	0.23					

47305.82	0.88	2	3.5	4	10.14 $^2\Delta$	
47309.41	1.0	2	5.5	5	10.14 $^2\Delta$	
47309.58	0.62	1	3.5	3	16.98 $^2\Pi$	
47309.75	0.34					
47312.33	0.09					
47313.84	0.69					
47315.58	0.40	1	5.5	5	16.98 $^2\Pi$	
47316.52	0.10	1	3.5	3	17.14 $^2\Delta$	
47317.34	0.07	1	3.5	3	17.19 $^2\Sigma$	a
47318.20	0.18	1	3.5	3	17.19 $^2\Sigma$	a
47319.49	0.47	1	3.5	4	17.14 $^2\Delta$	
47319.87	0.41	1	5.5	6	16.98 $^2\Pi$	
47320.38	0.22					
47323.68	0.62	1	5.5	5	17.14 $^2\Delta$	
47324.83	0.65	1	5.5	5	17.19 $^2\Sigma$	
47327.36	0.43	1	3.5	3	17.36 $^2\Pi$	
47327.96	0.20	1	5.5	6	17.14 $^2\Delta$	
47328.46	0.20					
47328.79	0.45	1	3.5	4	17.36 $^2\Pi$	
47333.00	0.12					
47333.24	0.07					
47337.61	0.13	1	5.5	6	17.36 $^2\Pi$	
47340.48	0.09	1	5.5	5	17.55 $^2\Sigma$	a
47341.29	0.10	1	5.5	5	17.55 $^2\Sigma$	a
47345.84	0.31					
47346.18	0.16	2	3.5	3	10.36 $^2\Pi$	
47348.98	0.34	2	3.5	4	10.36 $^2\Pi$	
47350.84	0.06	1	3.5	3	17.98 $^2\Pi$	
47351.47	0.25		3.5	4	term3	
47352.58	0.48	2	5.5	5	10.36 $^2\Pi$	
47353.49	0.09	1	3.5	4	17.98 $^2\Pi$	
47353.87	0.09		5.5	5	term2	
47356.58	0.45	1	5.5	5	17.98 $^2\Pi$	
47356.58	0.45	1	3.5	3	18.14 $^2\Delta$	
47357.19	0.46	2	5.5	6	10.36 $^2\Pi$	
47359.23	0.23					
47359.53	0.48	1	3.5	4	18.14 $^2\Delta$	
47360.64	0.52	1	5.5	6	17.98 $^2\Pi$	
47361.38	0.41	1	5.5	5	f $^2\Pi$ ($\mathcal{L}$=-1)	

Term Value(cm⁻¹)	Intensity	v'	J'	N'	Λ and n*	comment
47363.83	0.54	1	5.5	5	18.14 $^2\Delta$	
47365.78	0.13					
47367.12	0.38	1	3.5	3	18.36 $^2\Pi$	
47367.52	0.10					
47368.18	0.22	1	5.5	6	18.14 $^2\Delta$	
47368.55	0.23	1	3.5	4	18.36 $^2\Pi$	

[a]This state is perturbed by an unassigned state.

Table 2.1.32 - Autoionization Spectra Observed in the n*=17 and n*=18 Region.

PUMP line - $A^2\Pi$-$X^2\Sigma$ (0,0) Q_2(5.5) J=5.5, N=6, e-parity

Term Value(cm⁻¹)	Intensity	v'	J'	N'	Λ and n*	comment
47305.84	0.43	2	4.5	4	10.14 $^2\Delta$	
47309.52	0.96	2	4.5	5	10.14 $^2\Delta$	
47311.30	0.18		6.5	6	term1	
47312.36	0.10	1	4.5	4	16.98 $^2\Pi$	
47313.55	1.0					
47314.13	0.88	2	6.5	6	10.14 $^2\Delta$	
47315.87	0.08	1	4.5	5	16.98 $^2\Pi$	
47319.08	0.90					
47319.62	0.31	1	6.5	6	16.98 $^2\Pi$	blended
47319.62	0.31	1	4.5	4	17.14 $^2\Delta$	blended
47320.53	0.06					
47320.98	0.15	1	4.5	4	17.19 $^2\Sigma$	a
47321.95	0.06	1	4.5	4	17.19 $^2\Sigma$	a
47323.40	0.29	1	4.5	5	17.14 $^2\Delta$	
47324.55	0.35	1	6.5	7	16.98 $^2\Pi$	
47325.21	0.20					
47328.06	0.35					
47328.37	0.43	1	6.5	6	17.14 $^2\Delta$	
47329.38	0.37	1	6.5	6	17.19 $^2\Sigma$	
47331.65	0.55	1	4.5	4	17.36 $^2\Pi$	
47332.80	0.37	1	4.5	5	17.36 $^2\Pi$	
47333.12	0.33	1	6.5	7	17.14 $^2\Delta$	
47333.35	0.21					
47338.09	0.14					
47343.22	0.10	1	6.5	7	17.36 $^2\Pi$	
47345.73	0.12	1	6.5	6	17.55 $^2\Sigma$	
47348.91	0.25					

Term Value (cm⁻¹)	Intensity	v'	J'	N'	Λ and n*	comment
47349.09	0.20	2	4.5	4	10.36 $^2\Pi$	
47351.04	0.06					
47352.72	0.39	2	4.5	5	10.36 $^2\Pi$	
47355.10	0.31		4.5	5	term3	
47356.65	0.18	2	6.5	6	10.36 $^2\Pi$	blended
47356.65	0.18	1	4.5	5	17.98 $^2\Pi$	blended
47357.78	0.31		6.5	6	term2	
47359.78	0.14	1	4.5	4	18.14 $^2\Delta$	
47360.19	0.25	1	6.5	6	17.98 $^2\Pi$	
47360.74	0.16					
47362.12	0.16					
47362.52	0.53	2	6.5	7	10.36 $^2\Pi$	
47363.46	0.47	1	4.5	5	18.14 $^2\Delta$	
47364.27	0.08		6.5	7	term3	
47365.31	0.39	1	6.5	7	17.98 $^2\Pi$	
47366.18	0.45	1	6.5	6	f $^2\Pi$ ($\ell=-1$)	
47368.61	0.51	1	6.5	6	18.14 $^2\Delta$	
47369.77	0.14					
47371.26	0.43	1	4.5	4	18.36 $^2\Pi$	
47372.54	0.23	1	4.5	5	18.36 $^2\Pi$	
47373.05	0.11					
47373.65	0.06	1	6.5	7	18.14 $^2\Delta$	
47374.22	0.04					
47374.83	0.10					

aThis state is perturbed by an unassigned state.

Table 2.1.33 - Autoionization Spectra Observed in the n*=17 and n*=18 Region.

PUMP line - A$^2\Pi$-X$^2\Sigma$ (0,0) Q$_2$(6.5) J=6.5, N=7, e-parity

Term Value (cm⁻¹)	Intensity	v'	J'	N'	Λ and n*	comment
47306.61	0.08					
47309.44	0.36	2	5.5	4	10.14 $^2\Delta$	
47314.00	1.0	2	5.5	6	10.14 $^2\Delta$	
47315.62	0.04	1	5.5	6	16.98 $^2\Pi$	
47317.61	0.49		7.5	7	term1	
47318.29	0.39					
47319.26	0.99	2	7.5	7	10.14 $^2\Delta$	
47319.85	0.15	1	5.5	6	16.98 $^2\Pi$	
47326.61	0.10					

47324.28	0.21	1	7.5	7	16.98 $^2\Pi$
47325.00	0.85	2	7.5	8	10.14 $^2\Delta$
47324.83	0.35				
47328.04	0.26	1	5.5	6	17.14 $^2\Delta$
47330.01	0.32	1	7.5	8	16.98 $^2\Pi$
47330.93	0.25				
47333.24	0.35				
47333.79	0.29	1	7.5	7	17.14 $^2\Delta$
47334.65	0.35	1	7.5	7	17.19 $^2\Sigma$
47335.10	0.14				
47336.68	0.42	1	5.5	5	17.36 $^2\Pi$
47337.63	0.41	1	5.5	6	17.36 $^2\Pi$
47338.22	0.11				
47339.47	0.15	1	7.5	8	17.14 $^2\Delta$
47343.90	0.05				
47348.97	0.05				
47349.64	0.07	1	7.5	8	17.36 $^2\Pi$
47351.44	0.10	1	7.5	7	17.55 $^2\Sigma$
47352.54	0.22	2	5.5	5	10.36 $^2\Pi$
47353.81	0.14		5.5	5	term2
47357.21	0.28	2	5.5	6	10.36 $^2\Pi$
47357.54	0.11				
47359.21	0.19				
47359.38	0.37		5.5	6	term3
47360.63	0.10	1	5.5	6	17.98 $^2\Pi$
47361.17	0.05				
47361.37	0.03	1	5.5	5	f $^2\Pi$ (ℓ=-1)
47362.72	0.49		7.5	7	term2
47363.84	0.05	1	5.5	5	18.14 $^2\Delta$
47365.02	0.22	1	7.5	7	17.98 $^2\Pi$
47368.19	0.37	1	5.5	6	18.14 $^2\Delta$
47368.50	0.40	2	7.5	8	10.36 $^2\Pi$
47370.74	0.36	1	7.5	8	17.98 $^2\Pi$
47371.77	0.28	1	7.5	7	f $^2\Pi$ (ℓ=-1)
47373.80	0.25				
47374.20	0.33	1	7.5	7	18.14 $^2\Delta$
47375.53	0.05				
47376.23	0.28	1	5.5	5	18.36 $^2\Pi$
47377.35	0.24	1	5.5	6	18.36 $^2\Pi$

Table 2.1.34 - Autoionization Spectra Observed in the n*=17 and n*=18 Region.

PUMP line - $A^2\Pi$-$X^2\Sigma$ (0,0) Q_2(7.5)   J=7.5, N=8, e-parity

Term Value(cm⁻¹)	Intensity	v'	J'	N'	Λ and n*	comment
47313.06	0.11					
47313.62	0.15					
47314.27	0.11	2	6.5	5	10.14 $^2\Delta$	
47319.23	1.0	2	6.5	7	10.14 $^2\Delta$	
47322.94	0.50					
47324.64	0.13	1	6.5	7	16.98 $^2\Pi$	
47325.11	0.96	2	8.5	8	10.14 $^2\Delta$	
47325.30	0.92		8.5	8	term1	
47326.01	0.21					
47328.33	0.08	1	6.5	6	17.14 $^2\Delta$	
47329.60	0.15	1	8.5	8	16.98 $^2\Pi$	
47331.70	0.52	2	8.5	9	10.14 $^2\Delta$	
47332.95	0.09					
47333.20	0.21					
47333.44	0.23					
47336.23	0.25	1	8.5	9	16.98 $^2\Pi$	
47337.24	0.19					
47339.09	0.42					
47340.09	0.19	1	8.5	8	17.14 $^2\Delta$	
47340.82	0.29	1	8.5	8	17.19 $^2\Sigma$	
47342.52	0.23	1	6.5	6	17.36 $^2\Pi$	
47343.25	0.35	1	6.5	7	17.36 $^2\Pi$	
47344.09	0.15					
47346.26	0.08	1	8.5	9	17.14 $^2\Delta$	
47350.27	0.11					
47355.77	0.08					
47356.65	0.15	1	8.5	9	17.36 $^2\Pi$	blended
47356.65	0.15	2	6.5	6	10.36 $^2\Pi$	blended
47357.78	0.25	1	8.5	8	17.55 $^2\Sigma$	blended
47357.78	0.25		6.5	6	term2	blended
47359.18	0.04					
47360.17	0.04	1	6.5	6	17.98 $^2\Pi$	
47362.53	0.36	2	6.5	7	10.36 $^2\Pi$	
47364.33	0.35		6.5	7	term3	

47365.28	0.11	1	6.5	7	17.98 $^2\Pi$	
47366.19	0.08	1	6.5	6	f $^2\Pi$ ($\ell=-1$)	
47368.45	0.23		8.5	8	term2	
47370.37	0.17	1	8.5	8	17.98 $^2\Pi$	
47373.11	0.10					
47373.71	0.21	1	6.5	7	18.14 $^2\Delta$	
47375.20	0.54	2	8.5	9	10.36 $^2\Pi$	
47376.83	0.21	1	8.5	9	17.98 $^2\Pi$	
47377.97	0.29	1	8.5	8	f $^2\Pi$ ($\ell=-1$)	
47379.32	0.33					
47380.50	0.19	1	8.5	8	18.14 $^2\Delta$	
47381.61	0.08	1	6.5	6	18.36 $^2\Pi$	
47382.97	0.19	1	6.5	7	18.36 $^2\Pi$	
47386.32	0.08					

Table 2.1.35 - Autoionization Spectra Observed in the n*=17 and n*=18 Region.

PUMP line - A$^2\Pi$-X$^2\Sigma$ (0,0) P$_2$(5.5)   J=4.5, N=5, f-parity

Term Value(cm^{-1})	Intensity	v'	J'	N'	Λ and n*	comment
47300.11	0.17		3.5	4	term1	
47302.83	0.21	2	3.5	3	10.14 $^2\Delta$	
47303.63	0.09					
47305.81	0.98	2	3.5	4	10.14 $^2\Delta$	
47306.82	0.15	1	3.5	4	f $^2\Delta$ ($\ell=+1$)	
47309.47	1.0	2.	5.5	5	10.14 $^2\Delta$	
47311.26	0.09	1	5.5	6	term1	
47313.44	0.60	1	5.5	6	f $^2\Delta$ ($\ell=+1$)	
47314.04	0.22					
47315.87	0.34	1	5.5	5	16.98 $^2\Pi$	
47316.34	0.28	1	5.5	5	f $^2\Delta$ ($\ell=0$)	
47319.63	0.47	1	3.5	4	17.14 $^2\Delta$	
47320.95	0.62	1	3.5	4	17.19 $^2\Sigma$	
47323.41	0.41	1	5.5	5	17.14 $^2\Delta$	
47325.66	0.32	1	3.5	3	17.36 $^2\Pi$	
47328.02	0.19	1	3.5	4	f $^2\Sigma$ ($\ell=-3$)	
47328.35	0.19	1	5.5	6	17.14 $^2\Delta$	
47328.70	0.10					
47329.42	0.13	1	5.5	6	17.19 $^2\Sigma$	
47331.62	0.30	1	3.5	4	17.36 $^2\Pi$	

Term Value(cm⁻¹)	Intensity	v'	J'	N'	Λ and n*	comment
47332.81	0.21	1	5.5	5	17.36 $^2\Pi$	
47333.10	0.15					
47334.11	0.04					
47337.17	0.11					
47346.00	0.34	2	3.5	3	10.36 $^2\Pi$	
47348.34	0.08					
47348.98	0.21	1	3.5	4	f $^2\Delta$ (ℓ=+1)	
47350.99	0.09					
47352.78	0.47	2	5.5	5	10.36 $^2\Pi$	
47355.11	0.15					
47356.65	0.49	1	5.5	6	f $^2\Delta$ (ℓ=+1)	blended
47356.65	0.49	1	5.5	5	17.98 $^2\Pi$	blended
47357.35	0.21	1	3.5	4	f $^2\Pi$(ℓ=-1)	
47357.76	0.15		5.5	6	term2	
47359.78	0.51	1	3.5	4	18.14 $^2\Delta$	
47362.12	0.22					
47363.48	0.41					
47365.39	0.13					
47366.26	0.04	1	5.5	6	f $^2\Pi$(ℓ=-1)	
47368.66	0.09	1	3.5	4	f $^2\Sigma$ (ℓ=-3)	blended
47368.66	0.09	1	5.5	6	18.14 $^2\Delta$	blended
47371.29	0.17	1	3.5	4	18.36 $^2\Pi$	
47372.55	0.05	1	3.5	5	18.36 $^2\Pi$	
47374.28	0.09					

Table 2.1.36 - Autoionization Spectra Observed in the n*=17 and n*=18 Region.

PUMP line - $A^2\Pi$-$X^2\Sigma$ (0,0) P_2(6.5)   J=5.5, N=6, f-parity

Term Value(cm⁻¹)	Intensity	v'	J'	N'	Λ and n*	comment
47305.37	0.11		4.5	5	term1	
47305.78	0.24	2	4.5	4	10.14 $^2\Delta$	
47309.43	0.94	2	4.5	5	10.14 $^2\Delta$	
47309.76	0.57	1	4.5	5	f $^2\Delta$ (ℓ=+1)	
47312.55	0.11					
47313.90	1.0	2	6.5	6	10.14 $^2\Delta$	
47315.59	0.04					
47317.53	0.30		6.5	7	term1	
47318.26	0.22	1	6.5	7	f $^2\Delta$ (ℓ=+1)	
47319.18	0.41					
47319.46	0.21	2	6.5	7	10.14 $^2\Delta$	

47319.88	0.47	1	6.5	6	16.98 $^2\Pi$	
47320.40	0.26	1	6.5	6	f $^2\Delta$ ($\mathcal{L}$=0)	
47323.58	0.36	1	4.5	5	17.14 $^2\Delta$	
47324.27	0.26					
47324.86	0.64	1	4.5	5	17.19 $^2\Sigma$	
47328.03	0.39	1	6.5	6	17.14 $^2\Delta$	
47328.82	0.26	1	4.5	4	17.36 $^2\Pi$	
47333.18	0.38	1	4.5	5	f $^2\Sigma$ ($\mathcal{L}$=-3)	
47333.84	0.09	1	6.5	7	17.14 $^2\Delta$	
47331.68	0.07					
47336.73	0.32	1	4.5	5	17.36 $^2\Pi$	
47337.58	0.23	1	6.5	6	17.36 $^2\Pi$	
47338.33	0.15					
47348.99	0.32	2	4.5	4	10.36 $^2\Pi$	blended
47348.99	0.32	1	6.5	7	17.36 $^2\Pi$	blended
47351.41	0.07					
47352.61	0.19	1	4.5	5	f $^2\Delta$ ($\mathcal{L}$=+1)	
47353.82	0.15		4.5	5	term2	
47357.20	0.28	2	6.5	6	10.36 $^2\Pi$	
47359.47	0.32					
47360.66	0.55	1	6.5	6	17.98 $^2\Pi$	
47361.37	0.23	1	4.5	5	f $^2\Pi$ ($\mathcal{L}$=-1)	
47362.70	0.28		6.5	7	term2	
47363.85	0.41	1	4.5	5	18.14 $^2\Delta$	
47365.03	0.32					
47365.77	0.21					
47367.59	0.13	1	6.5	6	18.14 $^2\Delta$	
47368.25	0.39		6.5	6	term5	
47368.61	0.15					
47371.74	0.11	1	6.5	7	f $^2\Pi$ ($\mathcal{L}$=-1)	
47373.75	0.23	1	4.5	5	f $^2\Sigma$ ($\mathcal{L}$=-3)	
47376.22	0.26	1	4.5	5	18.36 $^2\Pi$	
47377.38	0.09	1	6.5	6	18.36 $^2\Pi$	
47378.68	0.09					
47379.58	0.04					

Table 2.1.37 - Autoionization Spectra Observed in the n*=17 and n*=18 Region.
PUMP line - $A^2\Pi$-$X^2\Sigma$ (0,0) P_2(7.5)   J=6.5, N=7, f-parity

Term Value(cm⁻¹)	Intensity	v'	J'	N'	Λ and n*	comment
47309.55	0.21	2	5.5	5	10.14 $^2\Delta$	
47311.30	0.15		5.5	6	term1	
47313.58	0.21	1	5.5	6	f $^2\Delta$ (ℓ=+1)	
47314.16	0.85	2	5.5	6	10.14 $^2\Delta$	
47315.95	0.10	1	5.5	5	16.98 $^2\Pi$	
47316.93	0.06					
47319.18	1.0	2	7.5	7	10.14 $^2\Delta$	
47322.85	0.48	1	7.5	8	f $^2\Delta$ (ℓ=+1)	
47324.58	0.33	1	7.5	7	16.98 $^2\Pi$	
47325.19	0.40	1	7.5	7	f $^2\Delta$ (ℓ=0)	blended
47325.19	0.40		7.5	8	term1	blended
47325.19	0.40	2	7.5	8	10.14 $^2\Delta$	blended
47328.38	0.21	1	5.5	6	17.14 $^2\Delta$	
47329.38	0.52	1	5.5	6	17.19 $^2\Sigma$	
47329.76	0.19					
47330.32	0.08					
47332.86	0.36	1	5.5	5	17.36 $^2\Pi$	
47333.30	0.34	1	7.5	7	17.14 $^2\Delta$	
47339.08	0.23	1	5.5	6	f $^2\Sigma$ (ℓ=-3)	
47340.08	0.06	1	7.5	8	17.14 $^2\Delta$	
47340.85	0.04	1	7.5	8	17.19 $^2\Sigma$	
47342.56	0.15	1	5.5	6	17.36 $^2\Pi$	
47343.20	0.13	1	7.5	7	17.36 $^2\Pi$	
47344.10	0.08					
47345.77	0.06					
47352.71	0.23	2	5.5	5	10.36 $^2\Pi$	
47352.71	0.23	1	7.5	8	f $^2\Sigma$ (ℓ=-3)	
47356.63	0.11	1	5.5	6	f $^2\Delta$ (ℓ=+1)	
47356.63	0.11	1	5.5	5	17.98 $^2\Pi$	
47357.74	0.17		5.5	6	term2	
47362.53	0.31	2	7.5	7	10.36 $^2\Pi$	
47362.53	0.31	1	5.5	5	18.14 $^2\Delta$	
47363.51	0.15					
47364.35	0.23					

Term Value	Intensity	v'	J'	N'	Λ and n*
47365.37	0.36	1	7.5	7	17.98 $^2\Pi$
47366.24	0.23	1	5.5	6	f $^2\Pi(\ell=-1)$
47368.60	0.40	1	5.5	6	18.14 $^2\Delta$
47370.37	0.23				
47372.54	0.15	1	5.5	5	18.36 $^2\Pi$
47373.16	0.13	1	7.5	7	18.14 $^2\Delta$
47373.67	0.21		7.5	7	term5
47377.98	0.10	1	7.5	8	f $^2\Pi(\ell=-1)$
47379.40	0.22	1	5.5	6	f $^2\Sigma(\ell=-3)$
47381.65	0.10	1	5.5	6	18.36 $^2\Pi$
47383.01	0.08	1	7.5	7	18.36 $^2\Pi$

Table 2.1.38 - Autoionization Spectra Observed in the n*=17 and n*=18 Region.

PUMP line - A$^2\Pi$-X$^2\Sigma$ (0,0) P$_2$(8.5) J=7.5, N=8, f-parity

Term Value(cm^{-1})	Intensity	v'	J'	N'	Λ and n*	comment
47313.96	0.23	2	6.5	6	10.14 $^2\Delta$	
47317.57	0.17		6.5	7	term1	
47318.34	0.13	1	6.5	7	f $^2\Delta(\ell=+1)$	
47319.32	0.94	2	6.5	7	10.14 $^2\Delta$	
47325.03	1.0	2	8.5	8	10.14 $^2\Delta$	
47328.04	0.13	1	6.5	6	17.14 $^2\Delta$	
47328.58	0.44	1	8.5	9	f $^2\Delta(\ell=+1)$	
47330.03	0.35	1	8.5	8	16.98 $^2\Pi$	
47330.84	0.25	1	8.5	8	f $^2\Delta(\ell=0)$	
47331.84	0.42	2	8.5	9	10.14 $^2\Delta$	
47333.05	0.06		8.5	9	term1	
47333.79	0.27	1	6.5	7	17.14 $^2\Delta$	
47334.63	0.35	1	6.5	7	17.19 $^2\Sigma$	
47335.06	0.15					
47336.00	0.08					
47337.58	0.27	1	6.5	6	17.36 $^2\Pi$	
47339.43	0.31	1	8.5	8	17.14 $^2\Delta$	
47343.97	0.10					
47344.25	0.08					
47345.55	0.36	1	6.5	7	f $^2\Sigma(\ell=-3)$	
47347.09	0.04	1	8.5	9	17.14 $^2\Delta$	
47347.80	0.08	1	8.5	9	17.19 $^2\Sigma$	
47349.00	0.13	1	6.5	7	17.36 $^2\Pi$	

47349.63	0.17	1	8.5	8	17.36 $^2\Pi$	
47350.37	0.04					
47351.31	0.11					
47357.13	0.31	2	6.5	6	10.36 $^2\Pi$	
47357.50	0.15					
47359.39	0.05					
47361.11	0.08	1	6.5	7	f $^2\Delta$ (ℓ=+1)	
47362.65	0.23		6.5	7	term2	
47368.53	0.38	2	8.5	8	10.36 $^2\Pi$	
47370.09	0.37					
47370.75	0.44	1	8.5	8	17.98 $^2\Pi$	
47371.73	0.43	1	6.5	7	f $^2\Pi$(ℓ=-1)	
47374.18	0.35	1	6.5	7	18.14 $^2\Delta$	
47374.72	0.11		8.5	9	term2	
47375.51	0.11					
47376.43	0.13					
47377.32	0.11	1	6.5	6	18.36 $^2\Pi$	
47379.38	0.23	1	8.5	8	18.14 $^2\Delta$	
47380.00	0.15		8.5	8	term5	
47384.90	0.10	1	8.5	9	f $^2\Pi$(ℓ=-1)	
47385.46	0.27	1	6.5	7	f $^2\Sigma$ (ℓ=-3)	
47387.63	0.10	1	8.5	9	18.14 $^2\Delta$	blended
47387.63	0.10	1	6.5	7	18.36 $^2\Pi$	blended
47389.50	0.06	1	8.5	8	18.36 $^2\Pi$	

Table 2.1.39 - Autoionization Spectra Observed in the n*=17 and n*=18 Region.

PUMP line - $A^2\Pi$-$X^2\Sigma$ (0,0) P_2(9.5)   J=8.5, N=9, f-parity

Term Value(cm^{-1})	Intensity	v'	J'	N'	Λ and n*	comment
47319.23	0.36	2	7.5	7	10.14 $^2\Delta$	
47322.93	0.11	1	7.5	8	f $^2\Delta$ (ℓ=+1)	
47325.15	0.92	2	7.5	8	10.14 $^2\Delta$	blended
47325.15	0.92	1	7.5	7	f $^2\Delta$ (ℓ=0)	blended
47325.36	0.96		7.5	8	term1	
47331.74	1.0	2	9.5	9	10.14 $^2\Delta$	
47333.10	0.10					
47333.37	0.08					
47334.95	0.38	1	9.5	10	f $^2\Delta$ (ℓ=+1)	
47336.17	0.19	1	9.5	9	16.98 $^2\Pi$	

121

Term Value(cm⁻¹)	Intensity	v'	J'	N'	Λ and n*	comment
47337.17	0.27	1	9.5	9	f $^2\Delta$ (ℓ=0)	
47338.09	0.04					
47338.75	0.08					
47339.31	0.36	2	9.5	10	10.14 $^2\Delta$	
47340.18	0.29	1	7.5	8	17.14 $^2\Delta$	
47340.77	0.27	1	7.5	8	17.19 $^2\Sigma$	
47342.80	0.19					
47343.26	0.31	1	7.5	7	17.36 $^2\Pi$	
47346.30	0.25	1	9.5	9	17.14 $^2\Delta$	
47352.68	0.56	1	7.5	8	f $^2\Sigma$ (ℓ=-3)	
47353.78	0.10					
47355.78	0.11	1	7.5	8	17.36 $^2\Pi$	
47356.92	0.15	1	9.5	9	17.36 $^2\Pi$	
47359.09	0.17					
47362.52	0.29	2	7.5	7	10.36 $^2\Pi$	
47366.39	0.08	1	7.5	8	f $^2\Delta$ (ℓ=+1)	
47368.40	0.25		7.5	8	term2	
47372.64	0.11					
47373.71	0.13		7.5	7	term5	
47375.20	0.56	2	9.5	9	10.36 $^2\Pi$	
47375.54	0.31					
47376.95	0.40	1	9.5	9	17.98 $^2\Pi$	
47378.01	0.58	1	7.5	8	f $^2\Pi$(ℓ=-1)	
47380.55	0.23	1	7.5	8	18.14 $^2\Delta$	
47381.63	0.11		9.5	10	term2	
47383.10	0.17	1	7.5	7	18.36 $^2\Pi$	
47386.27	0.17	1	9.5	9	18.14 $^2\Delta$	
47387.18	0.08		9.5	9	term5	
47392.03	0.31	1	7.5	8	f $^2\Sigma$ (ℓ=-3)	
47392.48	0.10	1	9.5	10	f $^2\Pi$(ℓ=-1)	
47394.60	0.11	1	7.5	8	18.36 $^2\Pi$	

Table 2.1.40 - Autoionization Spectra Observed in the n*=17 and n*=18 Region.

PUMP line - $A^2\Pi$-$X^2\Sigma$ (0,0) P_2(10.5)   J=9.5, N=10, f-parity

Term Value(cm⁻¹)	Intensity	v'	J'	N'	Λ and n*	comment
47325.15	0.25	2	8.5	8	10.14 $^2\Delta$	
47328.65	0.06	1	8.5	9	f $^2\Delta$ (ℓ=+1)	
47331.94	1.0	2	8.5	9	10.14 $^2\Delta$	

47333.15	0.15		8.5	9	term1	
47335.93	0.06					
47339.09	0.96	2	10.5	10	10.14 $^2\Delta$	
47342.13	0.42	1	10.5	11	f $^2\Delta$ $(\ell=+1)$	
47343.08	0.17	1	10.5	10	16.98 $^2\Pi$	
47344.27	0.23	1	10.5	10	f $^2\Delta$ $(\ell=0)$	
47345.95	0.06					
47347.17	0.19	1	8.5	9	17.14 $^2\Delta$	
47347.51	0.48	2	10.5	11	10.14 $^2\Delta$	
47347.68	0.19					
47349.66	0.23	1	8.5	8	17.36 $^2\Pi$	
47350.63	0.11		10.5	11	term1	
47353.81	0.23	1	10.5	10	17.14 $^2\Delta$	
47360.29	0.50	1	10.5	11	f $^2\Sigma$ $(\ell=-3)$	
47362.48	0.10					
47363.11	0.10	1	10.5	11	17.36 $^2\Pi$	
47365.11	0.08	1	10.5	10	17.36 $^2\Pi$	
47365.84	0.10					
47368.46	0.21	2	8.5	8	10.36 $^2\Pi$	
47372.22	0.04	1	8.5	9	f $^2\Delta$ $(\ell=+1)$	
47374.73	0.11		8.5	9	term2	
47376.42	0.04					
47379.45	0.15	1	8.5	8	18.14 $^2\Delta$	
47380.04	0.06		8.5	8	term5	
47382.57	0.35	2	10.5	10	10.36 $^2\Pi$	
47383.10	0.36					
47383.77	0.23	1	10.5	10	17.98 $^2\Pi$	
47384.88	0.44	1	8.5	9	f $^2\Pi(\ell=-1)$	
47387.66	0.15	1	8.5	9	18.14 $^2\Delta$	
47389.42	0.13		10.5	11	term2	blended
47389.42	0.13	1	10.5	10	18.36 $^2\Pi$	blended
47390.96	0.13					
47393.87	0.15	1	10.5	10	18.14 $^2\Delta$	
47399.00	0.19	1	8.5	9	f $^2\Sigma$ $(\ell=-3)$	

Table 2.1.41 - Autoionization Spectra Observed in the n*=17 and n*=18 Region.

PUMP line - $A^2\Pi$-$X^2\Sigma$ (0,0) P_2(11.5)   J=10.5, N=11, f-parity

Term Value(cm^{-1})	Intensity	v'	J'	N'	Λ and n*	comment
47331.81	0.15	2	9.5	9	10.14 $^2\Delta$	
47335.02	0.06	1	9.5	10	f $^2\Delta$ (ℓ=+1)	
47339.34	0.63	2	9.5	10	10.14 $^2\Delta$	
47341.61	0.15	1	9.5	10	term1	
47342.96	0.06					
47347.24	1.0	2	11.5	11	10.14 $^2\Delta$	
47348.86	0.25					
47350.52	0.27	1	11.5	12	f $^2\Delta$ (ℓ=+1)	
47350.78	0.21					
47351.70	0.21					
47352.14	0.12					
47353.71	0.10					
47354.94	0.19	1	9.5	10	17.14 $^2\Delta$	
47356.41	0.50	2	11.5	12	10.14 $^2\Delta$	
47356.93	0.23	1	9.5	9	17.36 $^2\Pi$	
47357.72	0.06					
47359.10	0.10					
47360.41	0.04					
47362.08	0.15	1	11.5	11	17.14 $^2\Delta$	
47366.75	0.06					
47368.25	0.40					
47371.34	0.19					
47374.18	0.08	1	11.5	11	17.36 $^2\Pi$	
47374.78	0.10					
47375.19	0.19	2	9.5	9	10.36 $^2\Pi$	
47376.99	0.08	1	9.5	9	17.98 $^2\Pi$	
47379.03	0.08	1	9.5	10	f $^2\Delta$ (ℓ=+1)	
47381.71	0.11		9.5	10	term2	
47383.27	0.08					
47387.16	0.13		9.5	9	term5	
47390.56	0.50	2	11.5	11	10.36 $^2\Pi$	
47391.09	0.35					
47391.73	0.15	1	11.5	11	17.98 $^2\Pi$	
47392.50	0.42	1	9.5	10	f $^2\Pi$(ℓ=-1)	
47394.77	0.08					

Term Value	Intensity	v'	J'	N'	Λ and n*	comment
47395.57	0.11	1	9.5	10	18.14 $^2\Delta$	
47396.95	0.08					
47399.57	0.11					
47402.27	0.11	1	11.5	11	18.14 $^2\Delta$	
47406.57	0.15	1	9.5	10	f $^2\Sigma$ ($\ell=-3$)	

Table 2.1.42 - Autoionization Spectra Observed in the n*=17 and n*=18 Region.

PUMP line - A$^2\Pi$-X$^2\Sigma$ (0,0) P$_2$(12.5)   J=11.5, N=12, f-parity

Term Value(cm⁻¹)	Intensity	v'	J'	N'	Λ and n*	comment
47339.16	0.11	2	10.5	10	10.14 $^2\Delta$	
47342.24	0.06	1	10.5	11	f $^2\Delta$ ($\ell=+1$)	
47347.57	0.73	2	10.5	11	10.14 $^2\Delta$	
47348.66	0.08					
47350.63	0.13		10.5	11	term1	
47351.51	0.08					
47356.06	1.0	2	12.5	12	10.14 $^2\Delta$	
47358.07	0.42					
47359.14	0.10	1	12.5	12	16.98 $^2\Pi$	
47360.36	0.35	1	12.5	13	f $^2\Delta$ ($\ell=+1$)	
47363.21	0.08					
47363.50	0.11					
47365.09	0.15	1	10.5	10	17.36 $^2\Pi$	
47366.07	0.29	2	12.5	13	10.14 $^2\Delta$	
47368.25	0.08	1	9.5	10	f $^2\Sigma$ ($\ell=-3$)	
47371.13	0.08	1	12.5	12	17.14 $^2\Delta$	
47375.29	0.04					
47376.87	0.21	1	10.5	11	f $^2\Sigma$ ($\ell=-3$)	
47380.54	0.13	1	10.5	11	17.36 $^2\Pi$	
47381.04	0.08					
47382.57	0.19	2	10.5	10	10.36 $^2\Pi$	
47383.12	0.03					
47383.37	0.06	1	12.5	12	17.36 $^2\Pi$	
47389.35	0.04		10.5	11	term2	
47390.88	0.10					
47393.77	0.06	1	10.5	10	18.14 $^2\Delta$	
47395.44	0.13					
47399.04	0.42	2	12.5	12	10.36 $^2\Pi$	
47399.64	0.31					

47400.79	0.41	1	12.5 12	17.98	$^2\Pi$	blended
47400.79	0.41	1	10.5 11		f $^2\Pi(\ell=-1)$	blended
47403.11	0.06					
47404.32	0.04					
47405.27	0.08					
47406.92	0.08					
47408.60	0.08					
47409.38	0.08					
47409.90	0.04					
47411.30	0.08	1	12.5 12	18.14	$^2\Delta$	
47414.75	0.08	10	10.5 11		f $^2\Sigma\,(\ell=-3)$	

Part 2.2 - CaF Autoionization Data - C $^2\Pi$ (v=0) State Intermediate

Table 2.2.1 - $C^2\Pi_{3/2}$ (v=0) State PUMP Lines[2]

PUMP line	PUMP Energy (cm^{-1})	Term Value (cm^{-1})
$R_{21}(3.5)$	30234.017	30238.129
$R_{21}(4.5)$	30234.875	30241.727
$R_{21}(5.5)$	30235.701	30245.979
$R_{21}(6.5)$	30236.496	30250.884
$R_{21}(7.5)$	30237.258	30256.442
$R_{21}(8.5)$	30237.992	30262.654
$R_{21}(9.5)$	30238.692	30269.518
$R_{21}(10.5)$	30239.360	30277.035
$R_{21}(11.5)$	30239.997	30285.205
$R_{21}(12.5)$	30240.602	30294.027
$P_2(6.5)$	30222.554	30241.727
$P_2(8.5)$	30220.070	30250.884
$P_2(10.5)$	30217.461	30262.653

Table 2.2.2 - Autoionization Spectra Observed in the n*=13 Region.
PUMP line - $C^2\Pi$-$X^2\Sigma$ (0,0) $R_{21}(3.5)$ J=4.5, N=5, e-parity

Term Value(cm^{-1})	Intensity	v	J'	N'	Λ and n*	comment
74007.80	0.17					
47010.48	0.81	2	3.5	4	g $^2\Phi$ (ℓ=+1)	
47010.78	0.07					
47013.11	0.06	2	3.5	4	8.98 $^2\Pi$	
47013.66	1.0					
47014.84	0.09	2	3.5	4	f $^2\Delta$ (ℓ=0)	
47015.95	0.04					
47016.58	0.17	2	5.5	5	8.98 $^2\Pi$	
47016.75	0.07					
47017.43	0.42	2	5.5	5	f $^2\Delta$ (ℓ=+1)	
47017.81	0.67	2	5.5	6	g $^2\Phi$ (ℓ=+1)	
47019.15	0.07					
47020.38	0.02					
47021.22	0.09					
47021.60	0.41	2	5.5	6	8.98 $^2\Pi$	

47022.83	0.01				
47025.08	0.07				
47025.84	0.02				
47028.25	0.07	2	3.5	3	f $^2\Pi$ (ℓ=-1)
47029.40	0.02				
47029.69	0.06				
47029.98	0.22				
47031.08	0.09				
47031.56	0.11				
47032.42	0.15				
47034.11	0.68	2	5.5	5	f $^2\Pi$ (ℓ=-1)
47034.93	0.74	2	3.5	4	f $^2\Pi$ (ℓ=-2)
47035.52	0.05				
47035.71	0.06				
47036.55	0.07				
47037.69	0.06				
47039.14	0.11	1	5.5	6	f $^2\Phi$ (ℓ=+2)
47039.70	0.03				
47040.60	0.39	1	3.5	4	f $^2\Delta$ (ℓ=0)
47042.37	0.44	1	5.5	5	f $^2\Delta$ (ℓ=+1)
47044.06	0.28	2	5.5	6	f $^2\Pi$ (ℓ=-2)
47044.23	0.40				
47045.30	0.03				
47045.67	0.18				
47045.86	0.17				
47047.50	0.06				
47048.18	0.30	1	5.5	6	f $^2\Delta$ (ℓ=0)
47049.23	0.09				
47049.74	0.04				
47050.45	0.02				
47050.91	0.13	2	5.5	5	f $^2\Sigma$ (ℓ=-3)
47051.18	0.55	1	5.5	5	f $^2\Pi$ (ℓ=-1)
47053.01	0.35	1	3.5	4	f $^2\Pi$ (ℓ=-2)
47054.33	0.22				
47055.15	0.09				
47055.78	0.07				
47057.56	0.04				
47058.49	0.05				
47059.51	0.01				
47063.38	0.04				
47064.08	0.02	1	5.5	6	f $^2\Pi$ (ℓ=-2)

47067.68   0.01

Table 2.2.3 - Autoionization Spectra Observed in the n*=13 Region.
PUMP line - $C^2\Pi$-$X^2\Sigma$ (0,0) $R_{21}(4.5)$ J=5.5, N=6, e-parity

Term Value(cm^{-1})	Intensity	v'	J'	N'	Λ and n*	comment
47004.95	0.01					
47010.41	0.13					
47013.79	0.72	2	4.5	5	g $^2\Phi$ (ℓ=+1)	
47016.29	0.03					
47016.74	0.04	2	4.5	5	8.98 $^2\Pi$	
47017.42	1.0					
47017.77	0.38	2	4.5	5	f $^2\Delta$ (ℓ=0)	
47018.08	0.23					
47019.10	0.02					
47020.33	0.21	2	6.5	6	f $^2\Delta$ (ℓ=+1)	
47021.17	0.50	2	6.5	6	8.98 $^2\Pi$	
47021.60	0.09					
47021.86	0.09					
47022.24	0.34	2	6.5	7	g $^2\Phi$ (ℓ=+1)	pert.
47022.82	0.40	2	6.5	7	g $^2\Phi$ (ℓ=+1)	pert.
47023.75	0.01					
47024.24	0.06					
47025.19	0.02					
47025.46	0.15	2	6.5	7	f $^2\Delta$ (ℓ=0)	
47026.15	0.04					
47026.45	0.30	2	6.5	7	8.98 $^2\Pi$	
47028.13	0.03					
47029.35	0.01					
47031.06	0.14	2	4.5	4	f $^2\Pi$ (ℓ=-1)	
47032.49	0.08					
47034.14	0.07					
47034.96	0.09					
47035.55	0.12					
47036.03	0.01					
47037.01	0.02					
47037.68	0.85	2	6.5	6	f $^2\Pi$ (ℓ=-1)	
47038.50	0.07					
47038.78	0.07					
47039.10	0.96	2	4.5	5	f $^2\Pi$ (ℓ=-2)	
47040.24	0.04					

Term Value(cm⁻¹)	Intensity	v	J'	N'	Λ and n*	comment
47041.79	0.06					
47042.86	0.07	2	6.5	7	$f\,^2\Phi\,(\ell=+2)$	
47043.42	0.02					
47044.03	0.21	1	4.5	5	$f\,^2\Delta\,(\ell=0)$	
47045.66	0.83	1	6.5	6	$f\,^2\Delta\,(\ell=+1)$	
47047.49	0.03	1	4.5	4	$f\,^2\Pi\,(\ell=-1)$	
47048.19	0.07					
47049.24	0.32					
47049.63	0.11	2	6.5	7	$f\,^2\Pi\,(\ell=-2)$	pert
47050.45	0.17	2	6.5	7	$f\,^2\Pi\,(\ell=-2)$	pert
47050.90	0.08					
47051.19	0.11					
47051.79	0.02					
47053.14	0.34	1	6.5	7	$f\,^2\Delta\,(\ell=0)$	
47054.73	0.07					
47055.09	0.06					
47055.51	0.45	1	6.5	6	$f\,^2\Pi\,(\ell=-1)$	
47055.77	0.07					
47057.11	0.26	2	6.5	6	$f\,^2\Sigma\,(\ell=-3)$	
47057.53	0.25	1	4.5	5	$f\,^2\Pi\,(\ell=-2)$	
47058.48	0.25					
47059.51	0.07					
47061.58	0.06					
47063.16	0.04					
47064.38	0.04	1	4.5	4	$f\,^2\Sigma\,(\ell=-3)$	
47067.64	0.07					
47069.78	0.02					
47070.09	0.02					
47073.42	0.01					
47075.67	0.01	1	6.5	6	$f\,^2\Sigma\,(\ell=-3)$	

Table 2.2.4 - Autoionization Spectra Observed in the n*=13 Region. PUMP line - $C\,^2\Pi$-$X\,^2\Sigma$ (0,0) $R_{21}(5.5)$ J=6.5, N=7, e-parity

Term Value(cm⁻¹)	Intensity	v	J'	N'	Λ and n*	comment
47010.41	0.01					
47013.67	0.15					
47017.44	0.07	2	5.5	5	$f\,^2\Delta\,(\ell=+1)$	
47017.80	0.74	2	5.5	6	$g\,^2\Phi\,(\ell=+1)$	
47019.11	0.11					
47020.36	0.03					

47020.88	0.03	2	5.5	6	f $^2\Delta$ (ℓ=0)
47021.57	0.24	2	5.5	6	8.98 $^2\Pi$
47021.84	0.78				
47022.25	0.07				
47022.84	0.09				
47024.24	0.72	2	7.5	7	f $^2\Delta$ (ℓ=+1)
47025.48	0.04				
47026.11	0.31	2	7.5	7	8.98 $^2\Pi$
47026.45	0.09				
47026.66	0.04				
47027.98	0.70	2	7.5	8	g $^2\Phi$ (ℓ=+1)
47028.96	0.07				
47030.66	0.30	2	7.5	8	f $^2\Delta$ (ℓ=0)
47031.85	0.04				
47033.18	0.50				
47032.26	0.30	2	7.5	8	8.98 $^2\Pi$
47034.13	0.17	2	5.5	5	f $^2\Pi$ (ℓ=-1)
47035.71	0.07				
47037.34	0.06				
47038.80	0.09				
47039.15	0.09	1	5.5	6	f $^2\Phi$ (ℓ=+2)
47039.59	0.11				
47041.83	0.53	2	7.5	7	f $^2\Pi$ (ℓ=-1) pert.
47042.28	0.48	2	7.5	7	f $^2\Pi$ (ℓ=-1) pert.
47043.26	0.11				
47044.07	1.0	2	5.5	6	f $^2\Pi$ (ℓ=-2)
47044.70	0.02				
47045.15	0.02				
47045.89	0.05				
47046.26	0.07				
47047.35	0.06	1	7.5	8	f $^2\Phi$ (ℓ=+2)
47047.84	0.01				
47048.20	0.11	1	5.5	6	f $^2\Delta$ (ℓ=0)
47049.70	0.42	1	7.5	7	f $^2\Delta$ (ℓ=+1)
47050.92	0.39	1	5.5	5	f $^2\Sigma$ (ℓ=-3)
47051.20	0.28	1	5.5	5	f $^2\Pi$ (ℓ=-1)
47053.17	0.04				
47054.27	0.02				
47054.44	0.02				
47054.73	0.01				

Term Value(cm⁻¹)	Intensity	v'	J'	N'	Λ and n*	comment
47055.13	0.15					
47055.50	0.02					
47056.65	0.18	2	7.5	8	f $^2\Pi$ (ℓ=-2)	
47057.04	0.07					
47057.47	0.03					
47058.92	0.31	1	7.5	8	f $^2\Delta$ (ℓ=0)	
47059.54	0.07					
47060.31	0.05					
47060.94	0.46	1	7.5	7	f $^2\Pi$ (ℓ=-1)	
47062.47	0.15	1	5.5	6	13.14 $^2\Delta$	
47063.08	0.18					
47063.43	0.24					
47064.12	0.30	1	5.5	6	f $^2\Pi$ (ℓ=-2)	
47068.21	0.01	1	7.5	7	13.14 $^2\Delta$	
47069.69	0.09	1	5.5	5	f $^2\Sigma$ (ℓ=-3)	
47070.30	0.04					
47073.34	0.06					
47075.69	0.01					
47077.16	0.01					

Table 2.2.5 - Autoionization Spectra Observed in the n*=13 Region.
PUMP line - $C^2\Pi$-$X^2\Sigma$ (0,0) R_{21}(6.5) J=7.5, N=8, e-parity

Term Value(cm⁻¹)	Intensity	v'	J'	N'	Λ and n*	comment
47007.94	0.17					
47017.43	0.11					
47018.04	0.03					
47020.32	0.02					
47021.89	0.03	2	6.5	6	f $^2\Delta$ (ℓ=+1)	
47022.24	0.43	2	6.5	7	g $^2\Phi$ (ℓ=+1)	
47022.82	0.51	2	6.5	7	g $^2\Phi$ (ℓ=+1)	
47024.22	0.02					
47025.07	0.01					
47025.44	0.26	2	6.5	7	f $^2\Delta$ (ℓ=0)	
47026.44	0.73	2	6.5	7	8.98 $^2\Pi$	
47027.97	0.07					
47028.93	0.98	2	8.5	8	f $^2\Delta$ (ℓ=+1)	
47030.66	0.04					
47031.81	0.41	2	8.5	9	8.98 $^2\Pi$	
47032.30	0.03					
47033.97	0.68	2	8.5	9	g $^2\Phi$ (ℓ=+1)	

47034.60	0.09			
47035.02	0.02			
47035.57	0.02			
47036.65	0.47	2	8.5 9	f $^2\Delta$ ($\mathcal{L}$=0)
47037.69	0.19	2	6.5 6	f $^2\Pi$ ($\mathcal{L}$=-1)
47038.31	0.02			
47038.73	0.43	2	8.5 9	8.98 $^2\Pi$
47039.01	0.04			
47039.39	0.04			
47040.26	0.04			
47041.83	0.02			
47042.34	0.04			
47042.89	0.03	1	6.5 7	f $^2\Phi$ ($\mathcal{L}$=+2)
47043.37	0.19			
47044.12	0.07			
47046.12	0.26			
47046.76	0.24	2	8.5 9	f $^2\Pi$ ($\mathcal{L}$=-1)
47047.53	1.0	2	8.5 9	f $^2\Pi$ ($\mathcal{L}$=-1)
47049.00	0.03			
47049.24	0.11			
47049.62	0.87	2	6.5 7	f $^2\Pi$ ($\mathcal{L}$=-2)
47050.48	0.60	2	6.5 7	f $^2\Pi$ ($\mathcal{L}$=-2)
47050.70	0.23			
47051.14	0.04			
47052.12	0.02			
47052.64	0.13	1	8.5 9	f $^2\Phi$ ($\mathcal{L}$=+2)
47053.17	0.11	1	6.5 7	f $^2\Delta$ ($\mathcal{L}$=0)
47054.49	0.43	1	8.5 8	f $^2\Delta$ ($\mathcal{L}$=+1)
47054.77	0.21			
47055.53	0.07	1	6.5 6	f $^2\Pi$ ($\mathcal{L}$=-1)
47056.73	0.04			
47057.11	0.56	2	6.5 6	f $^2\Sigma$ ($\mathcal{L}$=-3)
47058.06	0.02			
47058.95	0.04			
47059.84	0.03			
47060.07	0.03			
47060.95	0.04			
47061.60	0.02			
47061.91	0.05			
47063.67	0.06			
47064.09	0.21	2	8.5 9	f $^2\Pi$ ($\mathcal{L}$=-2)

Term Value(cm⁻¹)	Intensity	v'	J'	N'	Λ and n*	comment
47065.51	0.34	1	8.5	9	f $^2\Delta$ (ℓ=0)	
47066.70	0.05					
47067.27	0.53	1	8.5	8	f $^2\Delta$ (ℓ=+1)	
47067.89	0.09	1	6.5	7	13.14 $^2\Delta$	
47068.18	0.15					
47068.79	0.02					
47069.00	0.02					
47070.12	0.36					
47070.77	0.30	1	6.5	7	f $^2\Pi$ (ℓ=-2)	
47074.44	0.02	1	8.5	8	13.14 $^2\Delta$	
47075.61	0.34	1	6.5	6	f $^2\Sigma$ (ℓ=-3)	
47078.60	0.03					
47080.38	0.04					
47081.65	0.01					
47082.41	0.02					
47085.04	0.01					

Table 2.2.6 - Autoionization Spectra Observed in the n*=13 Region. PUMP line - C$^2\Pi$-X$^2\Sigma$ (0,0) R$_{21}$(7.5)   J=8.5, N=9, e-parity

Term Value(cm⁻¹)	Intensity	v'	J'	N'	Λ and n*	comment
47020.41	0.01					
47021.85	0.09					
47024.22	0.04	2	7.5	7	f $^2\Delta$ (ℓ=+1)	
47026.68	0.05					
47027.98	0.50	2	7.5	8	g $^2\Phi$ (ℓ=+1)	
47028.91	0.02					
47030.66	0.24	2	7.5	8	f $^2\Delta$ (ℓ=0)	
47031.43	0.28					
47032.25	0.17	2	7.5	8	8.98 $^2\Pi$	
47033.95	0.05					
47034.56	0.81	2	9.5	9	f $^2\Delta$ (ℓ=+1)	
47036.66	0.04					
47038.27	0.26	2	9.5	9	8.98 $^2\Pi$	
47038.80	0.04					
47039.55	0.03					
47040.61	0.50	2	9.5	10	g $^2\Phi$ (ℓ=+1)	
47041.02	0.06					
47041.84	0.07	2	7.5	7	f $^2\Pi$ (ℓ=-1)	
47042.30	0.12	2	7.5	7	f $^2\Pi$ (ℓ=-1)	
47043.46	0.52	2	9.5	10	f $^2\Delta$ (ℓ=0)	

47044.34	0.07				
47045.99	0.53	2	9.5 10	8.98 $^2\Pi$	
47047.39	0.06	1	7.5 8	f $^2\Phi$ ($\mathcal{L}$=+2)	
47047.73	0.15				
47049.67	0.03	1	7.5 7	f $^2\Delta$ ($\mathcal{L}$=+1)	
47050.58	0.03				
47051.06	0.18				
47053.44	1.0	2	9.5 9	f $^2\Pi$ ($\mathcal{L}$=-1)	
47054.00	0.04				
47054.81	0.07				
47055.09	0.17				
47055.95	0.28				
47056.68	0.83	2	7.5 8	f $^2\Pi$ ($\mathcal{L}$=-2)	
47057.80	0.03				
47058.72	0.11	1	9.5 10	f $^2\Phi$ ($\mathcal{L}$=+2)	
47058.94	0.09	1	7.5 8	f $^2\Delta$ ($\mathcal{L}$=0)	
47060.08	0.33	1	9.5 9	f $^2\Delta$ ($\mathcal{L}$=+1)	
47060.96	0.03	1	7.5 7	f $^2\Pi$ ($\mathcal{L}$=-1)	
47062.71	0.02				
47063.61	0.57	2	7.5 7	f $^2\Sigma$ ($\mathcal{L}$=-3)	
47063.97	0.02				
47064.48	0.02				
47065.49	0.01				
47066.00	0.01				
47066.50	0.01				
47067.17	0.02	1	7.5 7	13.14 $^2\Delta$	
47068.16	0.02				
47069.03	0.03				
47069.57	0.01				
47070.25	0.13				
47070.69	0.03				
47072.15	0.05	2	9.5 10	f $^2\Pi$ ($\mathcal{L}$=-2)	
47072.87	0.35	1	9.5 10	f $^2\Delta$ ($\mathcal{L}$=0)	
47073.77	0.11				
47073.93	0.15	1	7.5 8	13.14 $^2\Delta$	
47074.31	0.48	1	9.5 9	f $^2\Pi$ ($\mathcal{L}$=-1)	
47075.50	0.01				
47075.96	0.01				
47077.10	0.44				
47078.27	0.18	2	9.5 9	f $^2\Sigma$ ($\mathcal{L}$=-3)	blended

Term Value(cm^{-1})	Intensity	v'	J'	N"	Λ and n*	comment
47078.27	0.18	1	7.5	8	f $^2\Pi$ (ℓ=-2)	blended
47081.16	0.02	1	9.5	9	13.14 $^2\Delta$	
47082.29	0.15	1	7.5	7	f $^2\Sigma$ (ℓ=-3)	
47087.90	0.01					
47088.20	0.02					

Table 2.2.7 - Autoionization Spectra Observed in the n*=13 Region.
PUMP line - C$^2\Pi$-X$^2\Sigma$ (0,0)   R$_{21}$(8.5)   J=9.5, N=10, e-parity

Term Value(cm^{-1})	Intensity	v'	J'	N"	Λ and n*
47026.45	0.04				
47028.05	0.02				
47028.92	0.06	2	8.5	8	f $^2\Delta$ (ℓ=+1)
47033.94	0.45	2	8.5	9	g $^2\Phi$ (ℓ=+1)
47034.18	0.09				
47034.56	0.01				
4703.5.37	0.01				
47034.64	0.36				
47036.93	0.15				
47037.63	0.04				
47038.46	0.03				
47038.79	0.11	2	8.5	9	8.98 $^2\Pi$
47040.77	0.23				
47041.04	1.0	2	10.5	10	f $^2\Delta$ (ℓ=+1)
47043.48	0.04				
47044.54	0.03				
47045.41	0.21	2	10.5	10	8.98 $^2\Pi$
47046.83	0.08	2	8.5	8	f $^2\Pi$ (ℓ=-1)
47047.60	0.15	2	8.5	8	f $^2\Pi$ (ℓ=-1)
47047.94	0.38	2	10.5	11	g $^2\Phi$ (ℓ=+1)
47048.22	0.07				
47049.28	0.06				
47049.70	0.06				
47050.51	0.02				
47051.10	0.60	2	10.5	11	f $^2\Delta$ (ℓ=0)
47052.21	0.04				
47052.63	0.08	1	8.5	9	f $^2\Phi$ (ℓ=+2)
47053.51	0.04				
47054.00	0.36	2	10.5	11	8.98 $^2\Pi$
47056.80	0.26				
47057.29	0.03				

Term Value(cm⁻¹)	Intensity	v'	J'	N'	Λ and n*	comment
47059.68	0.13					
47060.22	0.96	2	10.5	10	f $^2\Pi$ (ℓ=-1)	
47061.05	0.11					
47062.10	0.38					
47062.95	0.11					
47064.04	0.89	2	8.5	9	f $^2\Pi$ (ℓ=-2)	
47065.53	0.23	1	8.5	9	f $^2\Delta$ (ℓ=0)	blended
47065.53	0.23	1	10.5	11	f $^2\Phi$ (ℓ=+2)	blended
47066.50	0.26	1	10.5	10	f $^2\Delta$ (ℓ=+1)	
47067.21	0.02	1	8.5	8	f $^2\Pi$ (ℓ=-1)	
47069.81	0.07					
47070.68	0.49	2	8.5	8	f $^2\Sigma$ (ℓ=-3)	
47072.82	0.01					
47074.27	0.04	1	8.5	8	13.14 $^2\Delta$	
47075.37	0.11					
47078.26	0.03					
47078.57	0.04					
47079.11	0.03					
47079.95	0.04					
47080.70	0.12	1	8.5	9	13.14 $^2\Delta$	
47080.70	0.12	1	10.5	11	f $^2\Delta$ (ℓ=0)	
47081.26	0.19	2	10.5	11	f $^2\Pi$ (ℓ=-2)	
47081.61	0.13					
47082.22	0.38	1	10.5	10	f $^2\Pi$ (ℓ=-1)	
47083.34	0.03					
47084.51	0.02					
47084.99	0.32					
47086.23	0.13	1	8.5	9	f $^2\Pi$ (ℓ=-2)	
47089.00	0.02					
47089.89	0.13	1	8.5	8	f $^2\Sigma$ (ℓ=-3)	
47090.55	0.04					

Table 2.2.8 - Autoionization Spectra Observed in the n*=13 Region.
PUMP line - $C^2\Pi$-$X^2\Sigma$ (0,0) R_{21}(9.5) J=10.5, N=11, e-parity

Term Value(cm⁻¹)	Intensity	v'	J'	N'	Λ and n*	comment
47034.54	0.09	2	9.5	9	f $^2\Delta$ (ℓ=+1)	
47038.47	0.01					
47040.70	0.42	2	9.5	10	g $^2\Phi$ (ℓ=+1)	
47042.64	0.04					
47043.13	0.11					

47043.45	0.55	2	9.5	10	f $^2\Delta$ ($\ell=0$)
47046.01	0.14	2	9.5	10	8.98 $^2\Pi$
47048.21	0.99	2	11.5	11	f $^2\Delta$ ($\ell=+1$)
47048.53	0.13				
47051.10	0.06				
47042.30	0.02				
47053.29	0.26	2	11.5	12	8.98 $^2\Pi$
47053.51	0.22	2	9.5	9	f $^2\Pi$ ($\ell=-1$)
47054.02	0.02				
47054.84	0.09				
47055.98	0.41	2	11.5	12	g $^2\Phi$ ($\ell=+1$)
47057.22	0.01				
47057.98	0.08				
47058.32	0.11				
47058.75	0.09	1	9.5	10	f $^2\Phi$ ($\ell=+2$)
47059.52	0.94	2	11.5	12	f $^2\Delta$ ($\ell=0$)
47060.25	0.05				
47060.87	0.04				
47061.29	0.05				
47061.95	0.01				
47062.14	0.01				
47062.69	0.50	2	11.5	12	8.98 $^2\Pi$
47063.20	0.33				
47063.64	0.02				
47064.08	0.05				
47064.59	0.03				
47067.08	0.09				
47067.57	0.81	2	11.5	11	f $^2\Pi$ ($\ell=-1$)
47067.95	0.13				
47069.26	0.83				
47070.01	0.09				
47070.22	0.02				
47070.87	0.09				
47072.11	1.0	2	9.5	10	f $^2\Pi$ ($\ell=-2$)
47072.84	0.24	1	9.5	10	f $^2\Delta$ ($\ell=0$)
47073.12	0.24	1	11.5	12	f $^2\Phi$ ($\ell=+2$)
47073.37	0.02				
47073.71	0.37	1	11.5	11	f $^2\Delta$ ($\ell=+1$)
47074.24	0.04	1	9.5	9	f $^2\Pi$ ($\ell=-1$)
47077.55	0.05				
47078.23	0.50	2	9.5	9	f $^2\Sigma$ ($\ell=-3$)

Term Value (cm⁻¹)	Intensity	v'	J'	N'	Λ and n*
47081.15	0.06	1	9.5	9	13.14 $^2\Delta$
47082.42	0.31				
47082.90	0.04				
47083.63	0.02				
47084.97	0.02				
47086.22	0.04				
47086.74	0.02				
47088.16	0.06	1	9.5	10	13.14 $^2\Delta$
47089.07	0.04	1	11.5	12	f $^2\Delta$ (ℓ=0)
47089.62	0.17				
47090.52	0.05				
47090.82	0.55	1	11.5	11	f $^2\Pi$ (ℓ=-1)
47090.97	0.52	2	11.5	12	f $^2\Pi$ (ℓ=-2)
47091.82	0.02				
47092.68	0.03				
47093.62	0.35				
47094.64	0.11	1	9.5	10	f $^2\Pi$ (ℓ=-2)
47095.54	0.03				
47097.36	0.03				
47098.19	0.18	1	9.5	9	f $^2\Sigma$ (ℓ=-3)
47099.49	0.09				

Table 2.2.9 - Autoionization Spectra Observed in the n*=13 Region.
PUMP line - $C^2\Pi$-$X^2\Sigma$ (0,0) $R_{21}(10.5)$ J=11.5, N=12, e-parity

Term Value(cm⁻¹)	Intensity	v'	J'	N'	Λ and n*	comment
47041.01	0.09	2	10.5	10	f $^2\Delta$ (ℓ=+1)	
47041.45	0.07					
47045.54	0.02					
47047.93	0.28	2	10.5	11	g $^2\Phi$ (ℓ=+1)	
47050.16	0.07					
47050.67	0.07					
47051.10	0.57	2	10.5	11	f $^2\Delta$ (ℓ=0)	
47052.57	0.01					
47053.03	0.01					
47054.03	0.15	2	10.5	11	8.98 $^2\Pi$	
47055.73	0.17					
47056.05	0.99	2	12.5	12	f $^2\Delta$ (ℓ=+1)	
47059.57	0.05					
47060.28	0.23	2	10.5	10	f $^2\Pi$ (ℓ=-1)	
47060.85	0.02					

47061.09	0.09				
47061.87	0.21	2	12.5	12	$f\,^2\Delta\,(\ell=+1)$
47062.13	0.06				
47063.51	0.04				
47064.25	0.11				
47064.76	0.32	2	12.5	13	$g\,^2\Phi\,(\ell=+1)$
47065.56	0.11	1	10.5	11	$f\,^2\Phi\,(\ell=+2)$
47066.76	0.04				
47067.07	0.11				
47068.81	0.90	2	12.5	13	$f\,^2\Delta\,(\ell=0)$
47069.32	0.02				
47070.31	0.41				
47070.67	0.06				
47072.11	0.58	2	12.5	13	$8.98\;^2\Pi$
47074.05	0.02				
47075.10	0.13				
47075.36	0.38	2	12.5	12	$f\,^2\Pi\,(\ell=-1)$
47075.56	0.15				
47076.79	0.13				
47077.54	1.0				
47078.69	0.07				
47079.63	0.15				
47080.68	0.53	1	10.5	11	$f\,^2\Delta\,(\ell=0)$
47081.23	0.83	2	10.5	11	$f\,^2\Pi\,(\ell=-2)$
47081.40	0.43	1	12.5	13	$f\,^2\Phi\,(\ell=+2)$
47081.55	0.45				
47081.75	0.41	1	12.5	12	$f\,^2\Delta\,(\ell=+1)$
47082.74	0.06				
47085.75	0.04				
47086.18	0.47	2	10.5	10	$f\,^2\Sigma\,(\ell=-3)$
47088.86	0.05	1	10.5	10	$13.14\;^2\Delta$
47089.92	0.03				
47090.40	0.60				
47091.17	0.02				
47092.55	0.01				
47093.64	0.01				
47094.61	0.01				
47096.37	0.11	1	10.5	11	$13.14\;^2\Delta$
47098.34	0.07	1	12.5	13	$f\,^2\Delta\,(\ell=0)$
47099.21	0.26				
47099.38	0.06				

Term Value(cm^{-1})	Intensity	v'	J'	N'	Λ and n*	comment
47100.20	0.55	1	12.5	12	f $^2\Pi$ (ℓ=-1)	
47101.16	0.06					
47101.36	0.26	2	12.5	13	f $^2\Pi$ (ℓ=-2)	
47102.17	0.03					
47103.06	0.57					
47103.67	0.05	1	10.5	11	f $^2\Pi$ (ℓ=-2)	
47106.56	0.03	1	12.5	12	13.14 $^2\Delta$	
47107.35	0.19	1	10.5	10	f $^2\Sigma$ (ℓ=-3)	
47109.26	0.09					

Table 2.2.10 - Autoionization Spectra Observed in the n*=13 Region.

PUMP line - C$^2\Pi$-X$^2\Sigma$ (0,0) P$_2$(6.5)   J=5.5, N=6, f-parity

Term Value(cm^{-1})	Intensity	v'	J'	N'	Λ and n*	comment
47026.16	0.53	2	6.5	7	8.98 $^2\Pi$	
47026.44	0.17					
47027.55	0.11					
47027.73	0.26					
47028.15	0.14					
47028.88	0.18					
47029.12	0.07					
47029.42	0.04					
47029.61	0.13					
47030.75	0.30					
47032.04	0.14					
47032.33	0.16					
47033.24	0.04					
47033.76	0.23					
47034.07	0.86	2	4.5	5	f $^2\Pi$ (ℓ=-1)	
47034.57	0.46					
47034.91	0.99	2	4.5	4	f $^2\Pi$ (ℓ=-2)	
47035.24	0.67					
47035.68	0.23					
47036.52	0.04					
47037.15	0.48					
47037.66	0.07					
47038.35	0.03					
47038.72	0.44					
47039.08	0.13	1	6.5	6	f $^2\Phi$ (ℓ=+2)	
47039.51	0.11					
47040.17	0.21					

47040.37	0.23			
47040.91	0.44			
47041.44	0.06			
47041.81	0.44	2	6.5	7	f $^2\Pi$ ($\mathcal{L}$=-1)
47042.26	0.08	1	4.5	5	f $^2\Delta$ ($\mathcal{L}$=+1)
47043.36	0.88			
47043.67	0.23			
47044.10	0.80	2	6.5	6	f $^2\Pi$ ($\mathcal{L}$=-2)
47044.78	0.05			
47045.31	0.06			
47045.69	0.06			
47045.90	0.14			
47046.08	0.14			
47046.28	0.11			
47047.00	0.38			
47047.41	0.86			
47047.82	0.28			
47048.22	0.78	1	6.5	6	f $^2\Delta$ ($\mathcal{L}$=0)
47049.03	0.58			
47049.74	0.51	1	6.5	7	f $^2\Delta$ ($\mathcal{L}$=+1)
47050.90	0.71	2	4.5	5	f $^2\Sigma$ ($\mathcal{L}$=-3)
47051.19	1.0	1	4.5	5	f $^2\Pi$ ($\mathcal{L}$=-1)
47052.98	0.37	1	4.5	4	f $^2\Pi$ ($\mathcal{L}$=-2)
47055.11	0.30			
47055.88	0.51			
47056.78	0.46			
47057.51	0.04			
47057.74	0.04			
47059.53	0.14			
47059.90	0.10			
47061.16	0.07			
47061.89	0.13			
47062.50	0.23	1	6.5	6	13.14 $^2\Delta$
47063.11	0.28			
47063.53	0.07			
47064.06	0.14	1	6.5	6	f $^2\Pi$ ($\mathcal{L}$=-2)
47064.93	0.08			
47065.61	0.06			
47066.04	0.34			
47066.82	0.48			
47068.36	0.24			

Term Value(cm⁻¹)	Intensity	v'	J'	N'	Λ and n*	comment
47068.88	0.28					
47069.06	0.24					
47069.23	0.11					
47069.65	0.51	1	4.5	5	f $^2\Sigma$ (ℓ=-3)	
47070.20	0.07					
47070.95	0.07					
47071.99	0.28					
47072.27	0.14					
47072.95	0.03					
47073.43	0.13					
47073.76	0.23					
47074.80	0.03					
47075.56	0.17					
47075.78	0.11					
47076.24	0.06					
47078.14	0.07					
47078.75	0.14					
47079.59	0.14					
47080.76	0.13					
47081.91	0.06					
47083.22	0.03					
47085.17	0.06					

Table 2.2.11 - Autoionization Spectra Observed in the n*=13 Region.

PUMP line - C$^2\Pi$-X$^2\Sigma$ (0,0) P$_2$(8.5)   J=7.5, N=8, f-parity

Term Value(cm⁻¹)	Intensity	v'	J'	N'	Λ and n*	comment
47015.87	0.16					
47016.23	0.11					
47017.75	0.09	2	6.5	6	g $^2\Phi$ (ℓ=+1)	
47018.43	0.04					
47018.81	0.23					
47020.35	0.03					
47021.83	0.36					
47022.19	0.04					
47024.16	0.32	2	6.5	7	f $^2\Delta$ (ℓ=+1)	
47026.64	0.09					
47026.72	0.10					
47027.30	0.09					
47027.42	0.13					
47027.92	0.83	2	8.5	8	g $^2\Phi$ (ℓ=+1)	
47028.27	0.16					

47028.87	0.03				
47029.18	0.03				
47030.65	0.38	2	8.5	8	f $^2\Delta$ (ℓ=0)
47031.50	0.39				
47032.26	0.42	2	8.5	8	8.98 $^2\Pi$
47033.42	0.39				
47033.70	0.16				
47034.57	0.74	2	8.5	9	f $^2\Delta$ (ℓ=+1)
47034.71	0.32				
47036.97	0.03				
47037.24	0.06				
47037.48	0.04				
47038.29	0.33	2	8.5	9	8.98 $^2\Pi$
47038.73	0.09				
47039.54	0.07				
47040.65	0.06				
47041.79	0.32	2	6.5	7	f $^2\Pi$ (ℓ=-1)
47042.02	0.25				
47042.27	0.46	2	6.5	7	f $^2\Pi$ (ℓ=-1)
47042.92	0.29				
47043.25	0.11				
47044.09	0.58	2	6.5	6	f $^2\Pi$ (ℓ=-2)
47044.29	0.16				
47044.65	0.04				
47045.18	0.03				
47045.91	0.04				
47046.36	0.10				
47047.34	0.12	1	8.5	8	f $^2\Phi$ (ℓ=+2)
47047.66	0.09				
47050.01	0.11				
47050.41	0.03				
47050.90	0.33				
47051.00	0.32				
47052.93	0.49				
47053.44	0.13	2	8.5	9	f $^2\Pi$ (ℓ=-1)
47054.27	0.14				
47055.09	0.09				
47055.94	0.09				
47056.53	0.38				
47056.67	0.64	2	8.5	8	f $^2\Pi$ (ℓ=-2)
47057.33	0.36				

47057.85	0.02				
47058.94	0.43	1	8.5	8	f $^2\Delta$ (ℓ=0)
47059.19	0.38				
47060.04	0.64	1	6.5	7	f $^2\Delta$ (ℓ=+1)
47060.43	0.30				
47060.92	0.51	1	6.5	7	f $^2\Pi$ (ℓ=-1)
47061.67	0.51				
47061.83	0.22				
47062.42	0.11	1	6.5	6	13.14 $^2\Delta$
47063.39	0.32				
47063.62	1.0	2	6.5	7	f $^2\Sigma$ (ℓ=-3)
47065.50	0.03				
47067.67	0.14				
47068.24	0.07	1	6.5	7	13.14 $^2\Delta$
47069.04	0.09				
47069.35	0.07				
47070.30	0.35				
47073.59	0.09				
47073.78	0.07				
47074.38	0.16	1	8.5	9	f $^2\Pi$ (ℓ=-1)
47075.03	0.07				
47077.10	0.14				
47080.50	0.02				
47082.32	0.58	1	6.5	7	f $^2\Sigma$ (ℓ=-3)
47083.52	0.03				
47084.60	0.25				
47084.89	0.17				
47085.15	0.09				

Table 2.2.12 - Autoionization Spectra Observed in the n*=13 Region.

PUMP line - $C^2\Pi$-$X^2\Sigma$ (0,0) P_2(10.5)   J=9.5, N=10, f-parity

Term Value(cm^{-1})	Intensity	v'	J'	N'	Λ and n*	comment
47027.88	0.08	2	8.5	8	g $^2\Phi$ (ℓ=+1)	
47030.60	0.05	2	8.5	8	f $^2\Delta$ (ℓ=0)	
47031.38	0.12					
47032.66	0.12					
47033.77	0.14					
47034.51	0.49	2	8.5	9	f $^2\Delta$ (ℓ=+1)	
47036.43	0.03					
47036.67	0.04					

47067.22	0.03				
47039.12	0.04				
47040.57	0.55	2	10.5	10	g $^2\Phi$ ($\mathcal{L}=+1$)
47041.23	0.12				
47042.22	0.19				
47043.20	0.11				
47043.49	0.94	2	10.5	10	f $^2\Delta$ ($\mathcal{L}=0$)
47044.87	0.04				
47046.04	0.61	2	10.5	10	8.98 $^2\Pi$
47046.28	0.28				
47047.15	0.26				
47047.52	0.05				
47047.72	0.10				
47048.20	0.47	2	10.5	11	f $^2\Delta$ ($\mathcal{L}=+1$)
47048.70	0.14				
47051.05	0.04				
47051.24	0.04				
47053.30	0.47				
47053.46	1.0	2	8.5	9	f $^2\Pi$ ($\mathcal{L}=-1$)
47054.50	0.19				
47054.68	0.17				
47054.79	0.18				
47055.07	0.14				
47055.94	0.22				
47056.72	0.76	2	8.5	8	f $^2\Pi$ ($\mathcal{L}=-2$)
47057.18	0.07				
47057.93	0.04				
47058.31	0.08				
47058.73	0.30	1	10.5	10	f $^2\Phi$ ($\mathcal{L}=+2$)
47059.83	0.04				
47060.10	0.10	1	8.5	9	f $^2\Delta$ ($\mathcal{L}=+1$)
47061.80	0.07				
47063.12	0.44				
47063.67	0.03				
47064.02	0.03				
47064.43	0.03				
47067.69	0.04				
47069.23	0.21				
47069.48	0.42				
47072.08	0.78	2	10.5	10	f $^2\Pi$ ($\mathcal{L}=-2$)
47072.82	0.47	1	10.5	10	f $^2\Delta$ ($\mathcal{L}=0$)

47073.04	0.22				
47073.67	0.42				
47073.78	0.14	1	10.5	11	f $^2\Delta$ (ℓ=+1)
47074.25	0.69	1	8.5	9	f $^2\Pi$ (ℓ=-1)
47074.84	0.21				
47075.56	0.60				
47076.32	0.22				
47077.06	0.36				
47077.91	0.32				
47078.22	0.83	1	8.5	8	f $^2\Pi$ (ℓ=-2) blended
47078.22	0.83	2	8.5	9	f $^2\Delta$ (ℓ=-3) blended
47079.36	0.50				
47080.39	0.03				
47081.25	0.17	1	8.5	9	13.14 $^2\Delta$
47081.47	0.42				

Table 2.2.13 - Autoionization Spectra Observed in the n*=14 Region.

PUMP line - $C^2\Pi$-$X^2\Sigma$ (0,0) R_{21}(3.5)   J=4.5, N=5, e-parity

Term Value(cm^{-1})	Intensity	v′	J′	N′	Λ and n*	comment
47110.37	0.07	3	3.5	3	7.55 $^2\Sigma$	
47113.30	0.04					
47116.92	0.36	3	3.5	5	7.55 $^2\Sigma$	
47121.05	0.26	2	3.5	3	9.36 $^2\Pi$	
47123.56	0.50					
47123.90	0.17	2	3.5	4	9.36 $^2\Pi$	
47124.99	0.05					
47126.01	0.14					
47126.20	0.04					
47126.60	0.14					
47127.29	0.14	1	5.5	5	g $^2\Phi$ (ℓ=+2)	
47127.82	0.36	2	5.5	5	9.36 $^2\Pi$	
47128.69	0.03					
47129.28	0.19					
47130.73	0.62	1	3.5	4	f $^2\Delta$ (ℓ=0)	
47132.05	0.50	2	5.5	6	9.36 $^2\Pi$	
47132.30	0.95	1	5.5	5	f $^2\Delta$ (ℓ=0)	
47134.02	0.21					
47134.96	0.09					
47135.30	0.02					
47135.76	0.09					
47136.27	0.01					
47136.75	0.19					
47138.46	0.67	1	5.5	6	f $^2\Delta$ (ℓ=0)	
47139.41	0.12	1	5.5	6	13.98 $^2\Pi$	
47140.42	1.0	1	5.5	5	f $^2\Pi$ (ℓ=-1)	
47142.25	0.83	1	3.5	4	f $^2\Pi$ (ℓ=-2)	
47142.48	0.62	1	3.5	3	14.19 $^2\Sigma$	
47143.94	0.02	1	3.5	4	14.14 $^2\Delta$	
47146.31	0.07					
47146.78	0.02					
47147.52	0.08	1	3.5	3	f $^2\Sigma$ (ℓ=-3)	
47148.93	0.02	4	3.5	3	6.55 $^2\Sigma$	
47150.35	0.11					
47151.80	0.01	1	5.5	6	14.14 $^2\Delta$	

Term Value(cm^{-1})	Intensity	v'	J'	N'	Λ and n*	comment
47152.14	0.02					
47155.41	0.11	4	5.5	5	6.55 $^2\Sigma$	
47167.90	0.07	2	3.5	3	9.55 $^2\Sigma$	
47170.72	0.02					
47174.67	0.12	2	5.5	5	9.55 $^2\Sigma$	

Table 2.2.14 - Autoionization Spectra Observed in the n*=14 Region.

PUMP line - C$^2\Pi$-X$^2\Sigma$ (0,0) R$_{21}$(4.5)   J=5.5, N=6, e-parity

Term Value(cm^{-1})	Intensity	v'	J'	N'	Λ and n*	comment
47113.25	0.07	3	4.5	4	7.55 $^2\Sigma$	
47116.91	0.03					
47121.28	0.19	3	6.5	6	7.55 $^2\Sigma$	
47123.67	0.15					
47124.09	0.10	2	4.5	4	9.36 $^2\Pi$	
47125.08	0.02					
47126.25	0.17					
47126.84	0.15	1	6.5	6	g $^2\Gamma$ (ℓ=+4)	
47127.61	0.10	2	4.5	5	9.36 $^2\Pi$	
47128.67	0.20	1	6.5	6	f $^2\Phi$ (ℓ=+3)	
47129.26	0.01					
47129.45	0.01					
47129.63	0.01					
47129.82	0.01					
47130.63	0.13	1	6.5	6	g $^2\Phi$ (ℓ=+2)	
47132.02	0.19					
47132.44	0.19	1	6.5	6	9.36 $^2\Pi$	
47133.08	0.18					
47134.17	0.37	1	4.5	5	f $^2\Delta$ (ℓ=0)	
47135.24	0.02	1	4.5	5	13.98 $^2\Pi$	
47135.70	0.57	1	6.5	6	f $^2\Delta$ (ℓ=+1)	
47136.69	0.04	1	4.5	4	f $^2\Pi$ (ℓ=-1)	
47134.29	0.15					
47138.47	0.09					
47139.08	0.07					
47140.03	0.04					
47140.46	0.06					
47142.07	0.02					
47142.27	0.06					
47143.49	0.41	1	6.5	7	f $^2\Delta$ (ℓ=0)	

Term Value	Intensity	v'	J'	N'	Λ and n*	comment
47144.29	0.11	1	6.5	7	13.98 $^2\Pi$	
47145.11	1.0	1	6.5	6	f $^2\Pi$ (ℓ=-1)	
47146.32	0.37	1	4.5	4	14.19 $^2\Sigma$	
47146.80	0.49	1	4.5	5	f $^2\Pi$ (ℓ=-2)	
47147.98	0.15	1	4.5	5	14.14 $^2\Delta$	
47150.60	0.03					
47151.81	0.06	1	4.5	4	6.55 $^2\Sigma$	
47152.18	0.15	1	4.5	4	f $^2\Sigma$ (ℓ=-3)	
47153.20	0.01					
47155.42	0.07	1	6.5	6	14.19 $^2\Sigma$	
47157.37	0.04					
47159.79	0.09	4	6.5	6	6.55 $^2\Sigma$	
47170.85	0.06	2	4.5	4	9.55 $^2\Sigma$	
47174.62	0.02					
47179.07	0.11	2	6.5	6	9.55 $^2\Sigma$	

Table 2.4.15 - Autoionization Spectra Observed in the n*=14 Region.
PUMP line - $C^2\Pi$-$X^2\Sigma$ (0,0) R_{21}(5.5)   J=6.5, N=7, e-parity

Term Value(cm^{-1})	Intensity	v'	J'	N'	Λ and n*	comment
47108.88	0.03					
47116.96	0.09	3	5.5	5	7.55 $^2\Sigma$	
47121.32	0.01					
47126.40	0.28	3	7.5	7	7.55 $^2\Sigma$	
47126.61	0.12					
47127.32	0.07	1	5.5	5	g $^2\Phi$ (ℓ=+2)	
47127.84	0.07	2	5.5	5	9.36 $^2\Pi$	
47129.26	0.07					
47129.85	0.21	1	7.5	7	g $^2\Gamma$ (ℓ=+4)	
47130.65	0.01					
47132.07	0.52	2	5.5	6	9.36 $^2\Pi$	blended
47132.07	0.52	1	7.5	7	f $^2\Phi$ (ℓ=+3)	blended
47132.64	0.01					
47133.08	0.01					
47134.79	0.12	1	7.5	7	g $^2\Phi$ (ℓ=+2)	
47135.71	0.05					
47136.26	0.04					
47137.39	0.38	2	7.5	7	9.36 $^2\Pi$	
47137.67	0.33					

Term Value(cm⁻¹)	Intensity	v'	J'	N'	Λ and n*	comment
47138.45	0.31	1	5.5	6	$f\,^2\Delta\,(\ell=0)$	
47139.39	0.02	1	5.5	6	$13.98\,^2\Pi$	
47139.96	0.36	1	7.5	7	$f\,^2\Delta\,(\ell=+1)$	
47140.41	0.05	1	5.5	5	$f\,^2\Pi\,(\ell=-1)$	
47143.26	0.17	2	7.5	8	$9.36\,^2\Pi$	
47143.51	0.05					
47143.94	0.05					
47145.10	0.07					
47146.81	0.01					
47147.72	0.01					
47149.28	0.40	1	7.5	8	$f\,^2\Delta\,(\ell=0)$	
47149.85	0.12	1	7.5	8	$13.98\,^2\Pi$	
47150.61	1.0	1	5.5	5	$14.19\,^2\Sigma$	blended
47150.61	1.0	1	7.5	7	$f\,^2\Pi\,(\ell=-1)$	blended
47151.77	0.24	1	5.5	6	$14.14\,^2\Delta$	
47153.16	0.38	1	5.5	6	$f\,^2\Pi\,(\ell=-2)$	
47155.42	0.05	4	5.5	5	$6.55\,^2\Sigma$	
47157.38	0.21	1	5.5	5	$f\,^2\Sigma\,(\ell=-3)$	
47161.73	0.05					
47163.37	0.02	1	7.5	8	$14.14\,^2\Delta$	
47164.86	0.05	4	7.5	7	$6.55\,^2\Sigma$	
47170.23	0.01	1	7.5	7	$f\,^2\Sigma\,(\ell=-3)$	
47174.58	0.05	2	5.5	5	$9.55\,^2\Sigma$	
47179.11	0.01					
47184.31	0.09	2	7.5	7	$9.55\,^2\Sigma$	

Table 2.2.16 - Autoionization Spectra Observed in the n*=14 Region.

PUMP line - $C\,^2\Pi$-$X\,^2\Sigma$ (0,0) $R_{21}(6.5)$ J=7.5, N=8, e-parity

Term Value(cm⁻¹)	Intensity	v'	J'	N'	Λ and n*	comment
47121.35	0.06	3	6.5	6	$7.55\,^2\Sigma$	
47126.46	0.01					
47129.48	0.01					
47130.65	0.13	1	6.5	6	$g\,^2\Phi\,(\ell=+2)$	
47132.32	0.30	3	8.5	8	$7.55\,^2\Sigma$	
47133.11	0.15					
47133.42	0.13	1	8.5	8	$g\,^2\Gamma\,(\ell=+4)$	
47134.77	0.02					
47135.68	0.01	1	6.5	6	$f\,^2\Delta\,(\ell=+1)$	

47136.28	0.53	1	8.5	8	f $^2\Phi$ (ℓ=+3)
47136.37	0.32				
47136.99	0.02				
47137.28	0.10	2	6.5	7	9.36 $^2\Pi$
47137.69	0.02				
47139.57	0.11	1	8.5	8	g $^2\Phi$ (ℓ=+2)
47140.15	0.06				
47141.22	0.03				
47142.30	0.02				
47143.06	0.77	2	8.5	8	9.36 $^2\Pi$
47143.46	0.28	1	6.5	7	f $^2\Delta$ (ℓ=0)
47144.29	0.04	1	6.5	7	13.98 $^2\Pi$
47145.11	0.10	1	6.5	6	f $^2\Pi$ (ℓ=-1)
47145.23	0.17	1	8.5	8	f $^2\Delta$ (ℓ=+1)
47149.31	0.06				
47149.51	0.06				
47149.91	0.20	2	8.5	9	9.36 $^2\Pi$
47150.63	0.04				
47153.21	0.02				
47154.19	0.03				
47155.36	0.19	1	6.5	6	14.19 $^2\Sigma$
47155.82	0.34	1	8.5	9	f $^2\Delta$ (ℓ=0)
47156.17	0.24	1	8.5	9	13.98 $^2\Pi$
47156.95	1.0	1	8.5	8	f $^2\Pi$ (ℓ=-1)
47157.25	0.19	1	6.5	7	14.14 $^2\Delta$
47158.10	0.02				
47158.53	0.02				
47159.43	0.62	1	6.5	7	f $^2\Pi$ (ℓ=-2)
47159.79	0.06	4	6.5	6	6.55 $^2\Sigma$
47163.41	0.27	1	6.5	6	f $^2\Sigma$ (ℓ=-3)
47168.96	0.04				
47170.29	0.02	1	8.5	9	14.14 $^2\Delta$
47170.67	0.06	4	8.5	8	6.55 $^2\Sigma$
47177.90	0.01	1	8.5	8	f $^2\Sigma$ (ℓ=-3)
47179.08	0.07	2	6.5	6	9.55 $^2\Sigma$
47184.32	0.01				
47184.64	0.01				
47187.97	0.01				
47189.15	0.01				
47190.28	0.17	2	8.5	8	9.55 $^2\Sigma$

Table 2.2.17 - Autoionization Spectra Observed in the n*=14 Region.

PUMP line - $C^2\Pi$-$X^2\Sigma$ (0,0) R_{21}(7.5)   J=8.5, N=9, e-parity

Term Value(cm^{-1})	Intensity	v'	J'	N'	Λ and n*	comment
47126.48	0.14	3	7.5	7	7.55 $^2\Sigma$	
47129.89	0.01	1	7.5	7	g $^2\Gamma$ (ℓ=+4)	
47132.10	0.01	1	7.5	7	f $^2\Phi$ (ℓ=+3)	
47132.31	0.01					
47134.78	0.09	1	7.5	7	g $^2\Phi$ (ℓ=+2)	
47137.46	0.17	2	7.5	7	9.36 $^2\Pi$	blended
47137.46	0.17	1	9.5	9	g $^2\Gamma$ (ℓ=+4)	blended
47137.69	0.21					
47138.87	0.31	3	9.5	9	7.55 $^2\Sigma$	
47139.82	0.02					
47141.21	0.76	1	9.5	9	f $^2\Phi$ (ℓ=+3)	
47141.82	0.01					
47143.20	0.12	2	7.5	8	9.36 $^2\Pi$	
47145.00	0.12	1	9.5	9	g $^2\Phi$ (ℓ=+2)	
47145.32	0.09					
47148.61	0.02					
47149.12	0.67	1	9.5	9	f $^2\Delta$ (ℓ=+1)	
47149.21	0.86	1	9.5	10	f $^2\Phi$ (ℓ=+2)	blended
47149.21	0.86	1	7.5	8	f $^2\Delta$ (ℓ=0)	blended
47149.83	0.05	1	7.5	8	13.98 $^2\Pi$	
47150.60	0.06	1	7.5	7	f $^2\Pi$ (ℓ=-1)	
47151.54	0.05	2	9.5	9	9.36 $^2\Pi$	
47155.81	0.07					
47157.18	0.19	2	9.5	10	9.36 $^2\Pi$	
47157.75	0.02	1	9.5	10	g $^2\Phi$ (ℓ=+1)	
47160.75	0.12	1	7.5	7	14.19 $^2\Sigma$	
47162.50	0.05					
47163.25	0.59	1	9.5	10	f $^2\Delta$ (ℓ=0)	
47164.08	1.0	1	9.5	9	f $^2\Pi$ (ℓ=-1)	
47164.93	0.05	4	7.5	7	6.55 $^2\Sigma$	
47166.53	0.83	1	7.5	8	f $^2\Pi$ (ℓ=-2)	
47168.26	0.01					
47170.22	0.38	1	7.5	7	f $^2\Sigma$ (ℓ=-3)	
47176.90	0.01					

Term Value(cm⁻¹)	Intensity	v'	J'	N'	Λ and n*	comment
47177.19	0.12	1	9.5	9	6.55 $^2\Sigma$	
47177.87	0.01	1	9.5	10	14.14 $^2\Delta$	
47184.32	0.07	2	7.5	7	9.55 $^2\Sigma$	
47186.31	0.01	1	9.5	9	f $^2\Sigma$ (ℓ=-3)	
47192.30	0.01	1	9.5	9	14.36 $^2\Pi$	
47197.19	0.14	1	9.5	9	9.55 $^2\Sigma$	

Table 2.2.18 - Autoionization Spectra Observed in the n*=14 Region.

PUMP line - C$^2\Pi$-X$^2\Sigma$ (0,0) R$_{21}$(8.5)   J=9.5, N=10, e-parity

Term Value(cm⁻¹)	Intensity	v'	J'	N'	Λ and n*	comment
47129.19	0.03					
47132.37	0.11	3	8.5	8	7.55 $^2\Sigma$	
47136.33	0.01	1	8.5	8	f $^2\Phi$ (ℓ=+3)	
47139.60	0.07	1	8.5	8	g $^2\Phi$ (ℓ=+2)	
47142.15	0.06	1	10.5	10	g $^2\Gamma$ (ℓ=+4)	
47143.03	0.30	2	8.5	8	9.36 $^2\Pi$	
47145.26	0.02	1	8.5	8	f $^2\Delta$ (ℓ=+1)	
47146.19	0.32	3	10.5	10	7.55 $^2\Sigma$	
47146.84	0.75	1	10.5	10	f $^2\Phi$ (ℓ=+3)	
47147.43	0.04					
47149.12	0.04					
47149.87	0.11	2	8.5	9	9.36 $^2\Pi$	
47151.14	0.10	1	10.5	10	g $^2\Phi$ (ℓ=+2)	
47151.30	0.10					
47153.17	0.03					
47155.99	0.89	1	10.5	10	f $^2\Delta$ (ℓ=+1)	
47155.99	0.89	1	10.5	11	f $^2\Phi$ (ℓ=+2)	
47156.88	0.04	1	8.5	8	f $^2\Pi$ (ℓ=-1)	
47158.84	0.01	1	10.5	10	9.36 $^2\Pi$	
47162.95	0.04					
47163.33	0.02					
47164.12	0.03					
47164.91	0.07	1	10.5	11	g $^2\Phi$ (ℓ=+1)	
47165.63	0.11	2	10.5	11	9.36 $^2\Pi$	
47166.30	0.02					
47166.58	0.02					
47166.94	0.06	1	8.5	8	14.19 $^2\Sigma$	
47170.33	0.09	1	8.5	9	14.14 $^2\Delta$	

Term Value(cm⁻¹)	Intensity	v'	J'	N'	Λ and n*	comment
47170.72	0.04	4	8.5	8	6.55 $^2\Sigma$	
47171.32	0.49	1	10.5	11	f $^2\Delta$ (ℓ=0)	
47172.01	1.0	1	10.5	10	f $^2\Pi$ (ℓ=-1)	
47173.06	0.03					
47174.51	0.68	1	8.5	9	f $^2\Pi$ (ℓ=-2)	
47172.76	0.02					
47177.92	0.34	1	8.5	8	f $^2\Sigma$ (ℓ=-3)	
47184.44	0.07	4	10.5	10	6.55 $^2\Sigma$	
47186.29	0.01	1	10.5	11	14.14 $^2\Delta$	
47190.37	0.06	2	8.5	8	9.55 $^2\Sigma$	
47195.45	0.01	1	10.5	10	f $^2\Sigma$ (ℓ=-3)	
47200.68	0.02	1	10.5	10	14.36 $^2\Pi$	
47204.45	0.07	2	10.5	10	9.55 $^2\Sigma$	
47205.92	0.02					

Table 2.2.19 - Autoionization Spectra Observed in the n*=14 Region.

PUMP line - C$^2\Pi$-X$^2\Sigma$ (0,0) R$_{21}$(9.5)   J=10.5, N=11, e-parity

Term Value(cm⁻¹)	Intensity	v'	J'	N'	Λ and n*	comment
47137.54	0.02					
47138.96	0.09	3	9.5	9	7.55 $^2\Sigma$	
47141.22	0.01	1	9.5	9	f $^2\Phi$ (ℓ=+3)	
47145.01	0.09	1	9.5	9	g $^2\Phi$ (ℓ=+2)	
47147.52	0.02	1	11.5	11	g $^2\Gamma$ (ℓ=+4)	
47149.12	0.36	1	9.5	9	f $^2\Delta$ (ℓ=+1)	
47151.54	0.02	2	9.5	9	9.36 $^2\Pi$	
47153.17	0.76	1	11.5	11	f $^2\Phi$ (ℓ=+3)	
47153.71	0.03					
47154.26	0.26	1	11.5	11	7.55 $^2\Sigma$	
47155.95	0.02					
47157.18	0.09	1	9.5	10	9.36 $^2\Pi$	
47157.75	0.03	1	9.5	10	g $^2\Phi$ (ℓ=+1)	
47157.95	0.12	1	11.5	11	g $^2\Phi$ (ℓ=+2)	
47160.15	0.01					
47162.83	0.04					
47163.48	0.74	1	11.5	11	f $^2\Delta$ (ℓ=+1)	blended
47163.48	0.74	1	11.5	12	f $^2\Phi$ (ℓ=+2)	blended
47164.07	0.04	1	9.5	9	f $^2\Pi$ (ℓ=-1)	
47166.94	0.02	2	11.5	11	9.36 $^2\Pi$	

Term Value(cm⁻¹)	Intensity	v'	J'	N'	Λ and n*	comment
47170.79	0.05					
47171.31	0.01					
47171.99	0.03					
47173.11	0.05	1	11.5	12	g $^2\Phi$ (ℓ=+1)	
47173.43	0.05	1	9.5	9	14.19 $^2\Sigma$	
47174.48	0.14	2	11.5	12	9.36 $^2\Pi$	
47177.24	0.02	4	9.5	9	6.55 $^2\Sigma$	
47177.95	0.07	1	9.5	10	14.14 $^2\Delta$	
47178.86	0.07					
47179.27	0.03	1	11.5	12	13.98 $^2\Pi$	
47180.15	0.52	1	11.5	11	f $^2\Pi$ (ℓ=-1)	
47180.68	1.0					
47182.35	0.04					
47182.55	0.03					
47183.13	0.90	1	9.5	10	f $^2\Pi$ (ℓ=-2)	
47186.28	0.38	1	9.5	9	f $^2\Sigma$ (ℓ=-3)	
47192.42	0.09	4	11.5	11	6.55 $^2\Sigma$	
47195.39	0.01	1	11.2	12	14.14 $^2\Delta$	
47197.25	0.09	2	9.5	9	9.55 $^2\Sigma$	
47205.16	0.01	1	11.5	11	f $^2\Sigma$ (ℓ=-3)	
47209.71	0.05	1	11.5	11	14.36 $^2\Pi$	
47211.31	0.01					
47213.07	0.09	2	11.5	11	9.55 $^2\Sigma$	
47213.82	0.01					

Table 2.2.20 - Autoionization Spectra Observed in the n*=14 Region.

PUMP line - C$^2\Pi$-X$^2\Sigma$ (0,0) R$_{21}$(10.5) J=11.5, N=12, e-parity

Term Value(cm⁻¹)	Intensity	v'	J'	N'	Λ and n*	comment
47146.27	0.13	3	10.5	10	7.55 $^2\Sigma$	
47146.88	0.02	1	10.5	10	f $^2\Phi$ (ℓ=+3)	
47151.17	0.04	1	10.5	10	g $^2\Phi$ (ℓ=+2)	
47151.51	0.02					
47153.60	0.03	1	12.5	12	g $^2\Gamma$ (ℓ=+4)	
47155.37	0.02					
47155.98	0.36	1	10.5	10	f $^2\Delta$ (ℓ=+1)	
47156.63	0.02					
47158.83	0.03	2	10.5	10	9.36 $^2\Pi$	
47159.81	0.02					

47160.20	0.62	1	12.5	12	f $^2\Phi$ (ℓ=+3)
47160.69	0.04				
47161.78	0.02				
47163.03	0.30	3	12.5	12	7.55 $^2\Sigma$
47163.50	0.01				
47164.89	0.03	1	10.5	11	g $^2\Phi$ (ℓ=+1)
47165.44	0.11	1	12.5	12	g $^2\Phi$ (ℓ=+2)
47165.62	0.11	2	10.5	11	9.36 $^2\Pi$
47167.90	0.02				
47171.02	0.06				
47171.34	0.15	1	10.5	11	f $^2\Delta$ (ℓ=0)
47171.59	0.51	1	12.5	12	f $^2\Delta$ (ℓ=+1)
47171.84	0.57	1	12.5	13	f $^2\Phi$ (ℓ=+2)
47172.31	0.02				
47172.73	0.02				
47175.78	0.04	2	12.5	12	9.36 $^2\Pi$
47179.49	0.05				
47180.17	0.01				
47180.98	0.03				
47182.03	0.03	1	12.5	13	g $^2\Phi$ (ℓ=+1)
47184.10	0.23	2	12.5	13	9.36 $^2\Pi$
47184.53	0.04	4	10.5	10	6.55 $^2\Sigma$
47186.30	0.06	1	10.5	11	14.14 $^2\Delta$
47187.69	0.02				
47188.21	0.06				
47188.49	0.04	1	12.5	13	13.98 $^2\Pi$
47189.73	0.45	1	12.5	13	f $^2\Delta$ (ℓ=0)
47190.05	1.0	1	12.5	12	f $^2\Pi$ (ℓ=-1)
47190.66	0.06				
47192.03	0.04				
47192.59	0.90	1	10.5	11	f $^2\Pi$ (ℓ=-2)
47193.83	0.01				
47194.63	0.02				
47195.37	0.35	1	10.5	10	f $^2\Sigma$ (ℓ=-3)
47199.94	0.01				
47201.11	0.13	4	12.5	12	6.55 $^2\Sigma$
47202.75	0.01				
47204.54	0.06	2	10.5	10	9.55 $^2\Sigma$
47205.98	0.05				
47215.54	0.02				

Term Value(cm^{-1})	Intensity	v'	J'	N'	Λ and n*	comment
47219.35	0.07	1	12.5	12	f$^2\Sigma$ (ℓ=-3)	
47222.48	0.06	1	12.5	12	14.36 $^2\Pi$	
47223.22	0.01					
47223.59	0.02					

Table 2.2.21 - Autoionization Spectra Observed in the n*=14 Region.

PUMP line - $C^2\Pi$-$X^2\Sigma$ (0,0) R_{21}(11.5)   J=12.5, N=13, e-parity

Term Value(cm^{-1})	Intensity	v'	J'	N'	Λ and n*	comment
47153.22	0.01	1	11.5	11	f$^2\Phi$ (ℓ=+3)	
47154.37	0.12	3	11.5	11	7.55 $^2\Sigma$	
47156.47	0.02					
47157.98	0.05	1	11.5	11	g$^2\Phi$ (ℓ=+2)	
47160.41	0.02	2	13.5	13	g$^2\Gamma$ (ℓ=+4)	
47163.02	0.01					
47163.52	0.38	1	11.5	11	f$^2\Delta$ (ℓ=+1)	
47164.16	0.01					
47166.93	0.04	2	11.5	11	9.36 $^2\Pi$	
47167.55	0.03					
47167.91	0.67	1	13.5	13	f$^2\Phi$ (ℓ=+3)	
47168.38	0.02					
47172.54	0.28	3	13.5	13	7.55 $^2\Sigma$	
47173.07	0.01	1	11.5	12	g$^2\Phi$ (ℓ=+1)	
47173.59	0.07	1	13.5	13	g$^2\Phi$ (ℓ=+2)	
47173.72	0.09					
47174.46	0.12	2	11.5	12	9.36 $^2\Pi$	
47179.25	0.01	1	11.5	12	13.98 $^2\Pi$	
47179.75	0.01					
47180.14	0.12	1	11.5	12	f$^2\Delta$ (ℓ=0)	
47180.51	0.48	1	13.5	13	f$^2\Delta$ (ℓ=+1)	
47180.87	0.57	1	13.5	14	f$^2\Phi$ (ℓ=+2)	
47181.35	0.02					
47181.82	0.03					
47185.32	0.05	1	13.5	13	9.36 $^2\Pi$	
47188.97	0.02					
47189.23	0.02					
47191.67	0.02					
47192.54	0.02					
47194.49	0.19	2	13.5	14	9.36 $^2\Pi$	

47195.41	0.05	1	11	12	14.14 $^2\Delta$	
47197.93	0.01					
47198.30	0.06	1	13.5	14	13.98 $^2\Pi$	
47200.17	1.0	1	13.5	13	f $^2\Pi$ (ℓ=-1)	blended
47200.17	1.0	1	13.5	14	f $^2\Delta$ (ℓ=0)	blended
47200.74	0.04					
47202.25	0.05					
47202.80	0.76	1	11.5	12	f $^2\Pi$ (ℓ=-2)	
47205.16	0.31	1	11.5	11	f $^2\Sigma$ (ℓ=-3)	
47205.61	0.05					
47210.58	0.07	4	13.5	13	6.55 $^2\Sigma$	
47213.18	0.07	2	11.5	11	9.55 $^2\Sigma$	
47216.89	0.02					
47217.16	0.01					
47225.64	0.01					
47226.51	0.01	1	13.5	13	f $^2\Sigma$ (ℓ=-3)	
47229.65	0.07	1	13.5	13	14.36 $^2\Pi$	
47230.36	0.01					
47233.09	0.03					
47233.38	0.03					

Table 2.2.22 - Autoionization Spectra Observed in the n*=14 Region.

PUMP line - C $^2\Pi$ - X $^2\Sigma$ (0,0) P$_2$(6.5)   J=5.5, N=6, f-parity

Term Value(cm^{-1})	Intensity	v'	J'	N'	Λ and n*	comment
47110.87	0.23					
47113.00	0.06					
47114.30	0.06					
47116.91	0.30	3	4.5	5	7.55 $^2\Sigma$	
47119.54	0.11					
47120.09	0.17					
47123.57	0.11					
47124.06	0.57					
47124.45	0.63					
47126.45	0.09	3	6.5	7	7.55 $^2\Sigma$	
47126.63	0.21					
47127.31	0.16	1	4.5	5	g $^2\Phi$ (ℓ=+2)	
47127.79	0.11	2	4.5	5	9.36 $^2\Pi$	
47129.08	0.16					
47129.27	0.24					

47129.84	0.18	1	6.5	7	g $^2\Gamma$ ($\ell=+4$)	
47130.18	0.11					
47130.54	0.17					
47130.99	0.12					
47131.82	0.13					
47132.10	0.46	2	6.5	6	9.36 $^2\Pi$	blended
47132.10	0.46	1	6.5	7	f $^2\Phi$ ($\ell=+3$)	blended
47133.98	0.06					
47134.91	0.04					
47135.74	0.08					
47136.68	0.07					
47137.03	0.31					
47137.41	0.80	2	6.5	7	9.36 $^2\Pi$	
47137.87	0.26					
47138.36	0.66					
47138.47	1.0	1	6.5	6	f $^2\Delta$ ($\ell=0$)	
47139.49	0.14	1	6.5	6	13.98 $^2\Pi$	
47140.02	0.38	1	6.5	7	f $^2\Delta$ ($\ell=+1$)	
47140.47	0.68	1	4.5	5	f $^2\Pi$ ($\ell=-1$)	
47141.84	0.31					
47142.29	0.38	1	4.5	4	f $^2\Pi$ ($\ell=-2$)	
47143.93	0.05	1	4.5	4	14.14 $^2\Delta$	
47145.10	0.05					
47146.20	0.05					
47150.60	0.28	1	4.5	5	14.19 $^2\Sigma$	blended
47150.60	0.28	1	6.5	7	f $^2\Pi$ ($\ell=-1$)	blended
47151.02	0.13					
47151.80	0.13	1	6.5	6	14.14 $^2\Delta$	
47152.36	0.15					
47152.86	0.14					
47153.26	0.21	1	6.5	6	f $^2\Pi$ ($\ell=-2$)	
47153.65	0.17					
47155.43	0.08	4	4.5	5	6.55 $^2\Sigma$	
47155.90	0.50					
47156.69	0.60					
47157.06	0.17					
47157.37	0.24					
47157.77	0.03					
47158.74	0.43					
47159.32	0.50					
47159.99	0.07					

Term Value(cm⁻¹)	Intensity	v'	J'	N'	Λ and n*	comment
47160.85	0.06					
47161.49	0.57					
47161.65	0.30					
47161.73	0.28					
47163.27	0.18					
47164.87	0.03	4	6.5	7	6.55 $^2\Sigma$	
47167.13	0.06					
47167.94	0.10					
47169.70	0.08					
47170.33	0.08	1	6.5	7	f $^2\Sigma$ (ℓ=-3)	
47174.33	0.17					
47174.61	0.17	2	4.5	5	9.55 $^2\Sigma$	
47178.88	0.07					
47184.34	0.03	2	6.5	7	9.55 $^2\Sigma$	
47186.17	0.03					

Table 2.2.23 - Autoionization Spectra Observed in the n*=14 Region.

PUMP line - $C^2\Pi$-$X^2\Sigma$ (0,0) P_2(8.5)   J=7.5, N=8, f-parity

Term Value(cm⁻¹)	Intensity	v'	J'	N'	Λ and n*	comment
47117.80	0.04					
47120.19	0.10					
47120.39	0.13					
47121.12	0.03					
47121.49	0.04					
47126.46	0.31	2	6.5	7	7.55 $^2\Sigma$	
47127.09	0.03					
47127.60	0.14					
47127.91	0.07					
47129.88	0.05	1	6.5	7	g $^2\Gamma$ (ℓ=+4)	
47130.25	0.04					
47131.91	0.06					
47132.13	0.14	2	6.5	6	9.36 $^2\Pi$	blended
47132.13	0.14	1	6.5	7	f $^2\Phi$ (ℓ=+3)	blended
47132.70	0.41					
47132.89	0.21					
47133.90	0.01					
47134.80	0.26	1	6.5	7	g $^2\Phi$ (ℓ=+2)	
47136.28	0.02					
47137.36	0.18	2	6.5	7	9.36 $^2\Pi$	blended
47137.36	0.18	1	8.5	9	g $^2\Gamma$ (ℓ=+4)	blended

47137.68	0.44				
47138.88	0.06	2	8.5	9	7.55 $^2\Sigma$
47139.97	0.04	1	6.5	7	f $^2\Delta$ ($\mathcal{l}$=+1)
47140.18	0.04				
47140.55	0.04				
47141.21	0.66	1	8.5	9	f $^2\Phi$ ($\mathcal{l}$=+3)
47142.80	0.10				
47143.23	0.18	2	8.5	8	9.36 $^2\Pi$
47143.88	0.17				
47144.47	0.13				
47145.36	0.08				
47148.51	0.04				
47149.08	0.18	1	8.5	9	f $^2\Delta$ ($\mathcal{l}$=+1)
47149.27	1.0	1	8.5	8	f $^2\Delta$ ($\mathcal{l}$=0)
47149.67	0.27				
47149.91	0.17	1	8.5	8	13.98 $^2\Pi$
47150.15	0.30				
47150.62	0.94	1	6.5	7	f $^2\Pi$ ($\mathcal{l}$=-1)
47150.81	0.57				
47151.82	0.20	1	6.5	6	14.14 $^2\Delta$
47153.21	0.30	1	6.5	6	f $^2\Pi$ ($\mathcal{l}$=-2)
47155.39	0.03				
47155.81	0.03				
47156.94	0.08				
47158.20	0.03	1	6.5	7	14.19 $^2\Sigma$
47159.43	0.03	1	8.5	8	14.14 $^2\Delta$
47160.79	0.20	1	8.5	9	f $^2\Pi$ ($\mathcal{l}$=-1)
47163.43	0.06	4	6.5	7	6.55 $^2\Sigma$
47164.09	0.08				
47164.88	0.08				
47165.56	0.04				
47166.53	0.40				
47167.23	0.13				
47169.71	0.24				
47170.26	0.57	1	6.5	7	f $^2\Sigma$ ($\mathcal{l}$=-3)
47172.16	0.33				
47172.86	0.18				
47174.34	0.51				
47175.13	0.37				
47175.38	0.40				
47176.66	0.14				

Term Value(cm⁻¹)	Intensity	v'	J'	N'	Λ and n*	comment
47177.53	0.63					
47178.77	0.08					
47179.08	0.17					
47180.48	0.04					
47181.69	0.08					
47182.10	0.06					
47182.89	0.16					
47184.34	0.23	2	6.5	7	9.55 $^2\Sigma$	
47187.05	0.04					

Table 2.2.24 - Autoionization Spectra Observed in the n*=14 Region.

PUMP line - C$^2\Pi$-X$^2\Sigma$ (0,0) P$_2$(10.5)   J=9.5, N=10, f-parity

Term Value(cm⁻¹)	Intensity	v'	J'	N'	Λ and n*	comment
47132.79	0.05					
47133.06	0.03					
47133.27	0.04					
47136.81	0.03					
47137.48	0.02					
47138.90	0.35	3	8.5	9	7.55 $^2\Sigma$	
47139.07	0.18					
47141.23	0.10	1	8.5	9	f $^2\Phi$ (ℓ=+3)	
47143.24	0.10	2	8.5	8	9.36 $^2\Pi$	
47143.71	0.33					
47145.02	0.12	1	8.5	9	g $^2\Phi$ (ℓ=+2)	
47146.88	0.01					
47147.51	0.04	1	10.5	11	g $^2\Gamma$ (ℓ=+4)	
47148.32	0.01					
47149.11	0.69	1	8.5	9	f $^2\Delta$ (ℓ=+1)	
47149.87	0.02	1	8.5	8	13.98 $^2\Pi$	
47151.50	0.06	2	8.5	9	9.36 $^2\Pi$	
47153.15	0.83	1	10.5	11	f $^2\Phi$ (ℓ=+3)	
47154.24	0.15	3	10.5	11	7.55 $^2\Sigma$	
47155.80	0.03					
47157.19	0.12	2	10.5	10	9.36 $^2\Pi$	
47157.99	0.17	1	10.5	11	g $^2\Phi$ (ℓ=+2)	
47159.21	0.05					
47159.86	0.12					
47161.74	0.07					
47163.28	0.68	1	10.5	10	f $^2\Delta$ (ℓ=0)	

47163.40	0.47	1	10.5	11	f $^2\Delta$ ($\ell=+1$)
47164.09	1.0	1	8.5	9	f $^2\Pi$ ($\ell=-1$)
47164.48	0.17				
47165.22	0.30				
47165.96	0.11				
47166.54	0.46				
47166.64	0.36				
47170.78	0.03				
47172.05	0.03				
47173.54	0.06				
47174.62	0.03				
47177.22	0.07	4	8.5	9	6.55 $^2\Sigma$
47177.90	0.04	1	10.5	10	14.14 $^2\Delta$
47179.96	0.01				
47180.68	0.11	1	10.5	11	f $^2\Pi$ ($\ell=-1$)
47183.18	0.35				
47186.28	0.49	1	8.5	9	f $^2\Sigma$ ($\ell=-3$)
47186.49	0.19				
47189.00	0.10				
47190.26	0.06				
47190.67	0.21				
47192.58	0.14				
47193.04	0.17				
47194.27	0.33				
47194.34	0.28				
47195.47	0.15				
47196.81	0.21				
47197.24	0.24	1	8.5	9	9.55 $^2\Sigma$
47198.01	0.08				
47198.39	0.04				
47198.95	0.01				
47200.56	0.02				
47202.26	0.06				
47203.82	0.04				
47206.15	0.04				

Part 2.3 - CaF Autoioniozation Spectra - A $^2\Pi$ State Intermediate, High-n* Spectra

Table 2.3.1 - Autoionization Spectra Observed in the n*=20-32 Region.

PUMP line - A$^2\Pi$-X$^2\Sigma$ (0,0) Q$_2$(1.5)   J=1.5, N=2, e-parity

Term Value(cm^{-1})	v	J'	N'	Λ and n*	comment
47381.43					
47383.44					
47384.55					
47385.64					
47386.58					
47388.09					
47390.40					
47391.54					
47394.06					
47411.80					
47412.49					
47413.52	1			n* = 20.01[a]	
47415.32					
47415.97					
47417.23	1			n* = 20.15[a]	
47419.42					
47421.94					
47433.70					
47435.06					
47438.00					
47438.87	1			n* = 21.01[a]	
47441.37					
47442.37	1			n* = 21.16[a]	
47444.50					
47446.25					
47458.17					
47458.49					
47459.22					
47459.54					
47460.06					
47460.86					
47461.60	1			n* = 22.04[a]	
47461.95					

47463.24			
47463.80			
47464.20			
47467.36			
47469.51			
47477.98			
47479.50			
47480.43	1		$n* = 23.02$[a]
47482.07			
47482.52	1		$n* = 23.14$[a]
47483.19			
47484.95			
47485.60	2	2.5 2	11.14 $^2\Delta$
47487.76			
47494.57			
47495.09			
47496.35			
47497.07			
47497.40	1		$n* = 24.03$[a]
47498.88			
47499.19	1		$n* = 24.14$[a]
47500.17			
47501.93			
47506.03			
47510.20			
47511.32			
47512.24	1		$n* = 25.02$[a]
47513.91	1		$n* = 25.14$[a]
47514.68			
47515.79			
47516.05			
47520.01			
47521.63			
47523.67			
47524.75			
47525.59	1		$n* = 26.03$[a]
47527.02	1		$n* = 26.15$[a]
47529.41			
47535.36			
47535.76			
47537.28			

47537.86	1	$n* = 27.03$[a]
47538.78		
47540.20	1	$n* = 27.16$[a]
47540.55		
47540.86		
47546.09		
47547.80	1	$n* = 28.03$[a]
47549.15	1	$n* = 28.16$[a]
47555.76		
47556.65		
47557.30	1	$n* = 29.03$[a]
47558.63		
47559.00		
47559.66		
47563.52		
47564.46		
47565.81	1	$n* = 30.03$[a]
47567.06		
47571.81		
47573.49	1	$n* = 31.02$[a]
47574.65		
47578.91		
47580.54	1	$n* = 32.03$[a]
47581.56		
47582.21		
47584.51		
47585.51		
47585.37		
47590.12		
47591.38		
47592.49		
47593.93		
47596.67		
47597.73		
47599.47		
47601.49		
47602.48		
47604.19		
47605.72		
47607.99		
47608.96		
47612.99		

Term Value(cm^{-1})	v	J'	N'	Λ and n*	comment
47613.75					
47616.59					
47620.08					
47621.93					
47622.76					
47624.70	2	2.5	2	12.14 $^2\Delta$	
47626.64					
47628.18					
47632.54					
47635.44					

[a]I.P. = 47687.5 cm^{-1}

Table 2.3.2 - Autoionization Spectra Observed in the n*=20-32 Region.

PUMP line - $A^2\Pi$-$X^2\Sigma$ (0,0) Q$_2$(2.5)   J=2.5, N=3, e-parity

Term Value(cm^{-1})	v	J'	N'	Λ and n*	comment
47385.13					
47386.23					
47387.28					
47388.02					
47388.40					
47388.86					
47390.68					
47391.33					
47392.05					
47392.80					
47393.57					
47394.62					
47395.57					
47395.94					
47409.86					
47411.52					
47412.59					
47413.50					
47415.18					
47416.95					
47417.65					
47418.28					
47419.82	1			n* = 20.16[a]	
47421.69					
47422.67					
47423.60					

47426.80
47429.39
47430.77
47433.85
47435.39
47436.77
47437.79
47438.85
47440.48
47442.02
47443.14
47443.59
47445.00
47447.30
47447.68
47447.89
47450.50
47452.54
47453.73
47455.04
47458.15
47459.15
47560.02
47461.56
47462.17
47463.00
47463.78
47464.14
47464.63
47465.61
47466.99
47468.06
47469.05
47472.67
47478.80
47479.48
47480.05
47482.08
47482.50
47483.51
47484.26
47484.47
47485.55

47485.85				
47486.88				
47487.56				
47487.87	2	3.5 3	11.14	$^2\Delta$
47488.17				
47490.70				
47492.79				
47495.29				
47496.56				
47498.92				
47499.32				
47499.56				
47499.93				
47501.25				
47501.60				
47502.25				
47503.40				
47503.89				
47505.11				
47511.40	1		$n^* = 24.96$[b]	
47511.94				
47513.80				
47516.02				
47516.34				
47516.74				
47519.90				
47521.30				
47521.98				
47522.45				
47524.13				
47524.91	1		$n^* = 25.98$[b]	
47526.61				
47527.38				
47529.28				
47529.49	1		$n^* = 26.16$[a]	
47529.98				
47536.19				
47536.82	1		$n^* = 26.99$[b]	
47538.62				
47538.90				
47541.12	1		$n^* = 27.17$[a]	
47541.47				

47542.00		
47542.84		
47547.14	1	$n^* = 27.96$[b]
47547.56		
47549.51		
47551.54	1	$n^* = 28.17$[a]
47552.38		
47556.76	1	$n^* = 28.97$[b]
47558.16		
47559.00		
47559.58		
47560.82	1	$n^* = 29.17$[a]
47561.33		
47561.53		
47565.29	1	$n^* = 29.96$[b]
47567.06		
47567.96		
47569.20	1	$n^* = 30.16$[a]
47569.43		
47569.85		
47573.22	1	$n^* = 30.98$[b]
47574.78		
47575.64		
47576.32		
47576.99		
47577.36		
47578.03		
47579.99		
47580.36		
47583.01		
47583.94		
47584.22		
47586.29		
47586.96		
47589.19		
47590.26		
47592.11		
47593.07		
47594.13		
47596.06		
47547.20		
47597.50		

47601.28					
47602.74					
47604.39					
47606.01					
47606.75					
47607.24					
47608.10					
47610.76					
47614.74					
47615.55					
47618.54					
47619.07					
47621.94					
47622.48					
47624.67					
47626.92	2	3.5	3	12.14 $^2\Delta$	
47629.97					
47633.32					
47637.39					

[a]I.P. = 47689.8 cm^{-1}
[b]I.P. = 47687.5 cm^{-1}

Table 2.3.3 - Autoionization Spectra Observed in the n*=20-32 Region.

PUMP line - $A^2\Pi$-$X^2\Sigma$ (0,0) Q_2(3.5) **J=3.5, N=4, e-parity**

Term Value(cm^{-1})	v	J'	N'	Λ and n*	comment
47383.48					
47384.54					
47385.61					
47386.59					
47387.56					
47388.10					
47388.47					
47390.46					
47390.83					
47391.39					
47392.11					
47394.02	1			n* = 19.15[a]	
47395.00					
47395.77					
47396.94					

47397.45
47397.99
47413.83
47417.70
47419.45
47420.85
47421.53
47423.21   1 $n^* = 20.15^a$
47424.56
47425.48
47426.11
47426.53
47437.99
47438.97
47439.26
47442.83
47444.51
47446.22
47446.90
47448.20   1 $n^* = 21.15^a$
47450.26
47450.52
47451.64
47457.25
47459.52
47462.11
47462.77
47463.66
47464.92
47465.58
47466.35
47467.38
47467.73
47468.03
47468.80
47469.69   1 $n^* = 22.15^a$
47471.10
47471.68
47471.94
47473.41
47476.76
47477.34

47480.95		
47481.72		
47484.53		
47485.00		
47485.62		
47487.36		
47487.64		
47487.74		
47488.44	1	$n^* = 23.14$[a]
47490.45		
47490.87		
47492.09		
47494.43		
47497.03		
47498.39		
47501.34		
47502.91		
47504.27	1	$n^* = 24.13$[a]
47504.78		
47505.58		
47512.82		
47513.57		
47516.20		
47519.03		
47519.39		
47519.62	1	$n^* = 25.14$[a]
47521.52		
47523.58		
47525.74		
47526.84		
47527.36		
47528.11		
47529.98		

[a]I.P. = 47693.3 cm^{-1}

Part 3 - CaCl Spectra
Part 3.1 - CaCl Fluorescence Spectra - B $^2\Sigma$ (v=0) State Intermediate and REMPI - A $^2\Pi_{3/2}$ (v=0) State Intermediate

Spectra recorded using the fluorescence dip detection scheme and one state recorded by the direct fluorescence detection method are presented graphically in Figures 5.1-5.5 at the end of this chapter. Those spectra were recorded using the B$^2\Sigma$ (v=0) state as the intermediate state.

The direct fluorescence spectra recorded in the 37,000 cm^{-1} - 39,000 cm^{-1} region are presented in Table 3.1 along with the REMPI spectra recorded in the same region using the A $^2\Pi_{3/2}$ (v=0) state as the intermediate state. Only one PUMP transition was used to record the REMPI spectra in this region and the spectra are of low quality compared to the CaF autoionization spectra (see Figure 3.7). The same is true of the direct fluorescence spectra recorded using the B $^2\Sigma$ (v=0) state as the intermediate state in this region. The energies are only approximate term values for each state. These values are accurate to about ±10 cm^{-1} (absolute energy).

Table 3.1 - PUMP + PROBE Energy for REMPI and Fluorescence Spectra Recorded in the 37,000 cm^{-1} - 39,000 cm^{-1} Region

REMPI (PUMP + PROBE Energy (cm^{-1}))	Fluorescence (PUMP + PROBE Energy (cm^{-1}))	Λ and n*	(v",v')
36919		G$^2\Delta$	0,0
37021		F$^2\Pi$	3,0
	37109	3.15 $^2\Sigma$	0,1
	37140	3.16 $^2\Pi$	0,1
37174		G$^2\Delta$	1,0
37465	37470	3.15 $^2\Sigma$	0,0
37496	37500	3.16 $^2\Pi$	0,0
37605		G$^2\Delta$	2,0
37912	37917	3.15 $^2\Sigma$	1,0
37946		3.16 $^2\Pi$	1,0
38034		G$^2\Delta$	3,0
	39211	3.51 $^2\Sigma$	0,1

Part 3.2 - CaCl Autoionization data - A $^2\Pi_{3/2}$ (v=0) State Intermediate

Only the spectra in the n*=16 region were of high enough quality to provide reliable intensity information. The intensities were not measured for the spectra recorded in the n*=17-43 region.

Table 3.2 - A$^2\Pi_{3/2}$ (v=0) State PUMP Lines[4]

PUMP line	PUMP Energy (cm^{-1})	Term Value (cm^{-1})
$P_2(7.5)$	16163.846	16174.78
$P_2(8.5)$	16163.397	16177.06
$P_2(9.5)$	16162.963	16179.66
$P_2(10.5)$	16162.544	16182.58
$P_2(11.5)$	16162.137	16185.76
$P_2(12.5)$	16161.470	16189.37
$P_2(13.5)$	16161.353	16193.23
$P_2(14.5)$	16160.971	16197.40

Table 3.2.1 - Autoionization Spectra Observed in the n*=16 Region. PUMP line - A$^2\Pi$-X$^2\Sigma$ (0,0) $P_2(8.5)$ J=7.5, N=8, f-parity

Term Value(cm^{-1})	Intensity	v	J'	N'	Λ and n*	comment
48490.10	0.15					
48495.27	0.03					
48498.79	0.06					
48501.09	0.39	2	6.5	7	11.06 $^2\Delta$	
48503.74	0.15	2	8.5	8	11.06 $^2\Delta$	
48505.39	0.06					
48506.65	0.09	2	8.5	9	11.06 $^2\Delta$	
48512.95	0.13					
48515.53	0.09					
48516.68	0.13					
48517.72	0.15					
48519.04	0.72	2	6.5	7	11.16 $^2\Sigma$	
48520.20	0.19					
48520.61	0.17					
48522.59	0.38	1	6.5	7	16.06 $^2\Delta$	
48524.17	0.41	2	8.5	9	11.16 $^2\Sigma$	

Term Value(cm^{-1})	Intensity	v	J'	N'	Λ and n*	comment
48525.40	1.0	1	8.5	8	16.06 $^2\Delta$	
48527.38	0.43	1	6.5	7	16.16 $^2\Sigma$	
48528.15	0.24					
48529.39	0.06	1	8.5	9	16.10	
48531.70	0.09					
48532.68	0.23	1	8.5	9	16.16 $^2\Sigma$	
48534.42	0.30					

Table 3.2.2 - Autoionization Spectra Observed in the n*=16 Region.
PUMP line - $A^2\Pi$-$X^2\Sigma$ (0,0) P$_2$(9.5) J=8.5, N=9, f-parity

Term Value(cm^{-1})	Intensity	v	J'	N'	Λ and n*	comment
48503.73	0.29	2	7.5	8	11.06 $^2\Delta$	
48506.79	0.06	2	9.5	9	11.06 $^2\Delta$	
48508.87	0.07					
48510.03	0.07	2	9.5	10	11.06 $^2\Delta$	
48512.97	0.12					
48515.56	0.11					
48519.49	0.16					
48520.70	0.25					
48521.54	1.0	2	7.5	8	11.16 $^2\Sigma$	
48522.08	0.37					
48524.00	0.23					
48525.26	0.32	1	7.5	8	16.06 $^2\Delta$	
48527.33	0.56	2	9.5	10	11.16 $^2\Sigma$	
48528.45	0.99	1	9.5	9	16.06 $^2\Delta$	
48529.92	0.59	1	7.5	8	16.16 $^2\Sigma$	
48531.47	0.28	1	9.5	10	16.06 $^2\Delta$	
48532.76	0.18	1	9.5	10	16.10	
48535.84	0.32	1	9.5	10	16.16 $^2\Sigma$	
48537.84	0.18					

Table 3.2.3- Autoionization Spectra Observed in the n*=16 Region.
PUMP line - $A^2\Pi$-$X^2\Sigma$ (0,0) P$_2$(10.5) J=9.5, N=10, f-parity

Term Value(cm^{-1})	Intensity	v	J'	N'	Λ and n*	comment
48495.82	0.13					
48498.75	0.07					
48502.83	0.04					
48506.71	0.40	2	8.5	9	11.06 $^2\Delta$	

Term Value(cm⁻¹)	Intensity	v	J'	N'	Λ and n*	comment
48510.03	0.19	2	10.5	10	11.06 $^2\Delta$	
48513.71	0.04	2	10.5	11	11.06 $^2\Delta$	
48516.22	0.07					
48516.66	0.10					
48517.65	0.03					
48518.52	0.03					
48520.61	0.04					
48522.41	0.07					
48524.15	1.0	2	8.5	9	11.16 $^2\Sigma$	
48525.43	0.09	1	8.5	8	16.16 $^2\Delta$	
48527.39	0.13					
48528.05	0.18	1	8.5	9	16.06 $^2\Delta$	
48530.64	0.44	2	10.5	11	11.16 $^2\Sigma$	
48531.65	0.99	1	10.5	10	16.16 $^2\Delta$	
48532.57	0.42	1	8.5	9	16.16 $^2\Sigma$	
48534.99	0.36	1	10.5	11	16.06 $^2\Delta$	
48536.28	0.10	1	10.5	11	16.10	
48539.49	0.18	1	10.5	11	16.16 $^2\Sigma$	
48541.63	0.09					

Table 3.2.4 - Autoionization Spectra Observed in the n*=16 Region.
PUMP line - $A^2\Pi$-$X^2\Sigma$ (0,0) P_2(11.5)   J=10.5, N=11, f-parity

Term Value(cm⁻¹)	Intensity	v	J'	N'	Λ and n*	comment
48510.03	0.30	2	9.5	10	11.06 $^2\Delta$	
48513.01	0.22					
48513.59	0.17	2	11.5	11	11.06 $^2\Delta$	
48517.61	0.19	2	11.5	12	11.06 $^2\Delta$	
48520.45	0.17					
48521.84	0.10					
48522.08	0.07					
48524.02	0.04					
48525.88	0.11					
48527.30	0.98	2	9.5	10	11.16 $^2\Sigma$	
48528.79	0.10					
48531.37	0.22	1	9.5	10	16.06 $^2\Delta$	
48533.80	0.33					
48531.85	0.39					
48534.49	0.50	2	11.5	12	11.16 $^2\Sigma$	
48535.42	1.0	1	11.5	11	16.06 $^2\Delta$	
48535.84	0.72	1	9.5	10	16.16 $^2\Sigma$	

Term Value(cm⁻¹)	Intensity	v	J'	N'	Λ and n*	comment
48539.01	0.42	1	11.5	12	16.06 $^2\Delta$	
48540.42	0.25	1	11.5	12	16.10	
48543.18	0.29	1	11.5	12	16.16 $^2\Sigma$	
48544.20	0.14					
48545.86	0.25					
48548.40	0.04					
48549.40	0.08					

Table 3.2.5 - Autoionization Spectra Observed in the n*=16 Region. **PUMP line** - $A^2\Pi$-$X^2\Sigma$ (0,0) P$_2$(12.5)   J=11.5,   N=12, f-parity

Term Value(cm⁻¹)	Intensity	v	J'	N'	Λ and n*	comment
48502.85	0.15					
48507.23	0.15					
48511.25	0.06					
48513.65	0.13	2	10.5	11	11.06 $^2\Delta$	
48516.70	0.15					
48517.53	0.11	2	10.5	10	11.06 $^2\Delta$	
48521.84	0.11	2	12.5	13	11.06 $^2\Delta$	
48523.85	0.11					
48521.72	0.15					
48524.40	0.15					
48529.55	0.13					
48530.68	0.83	2	10.5	11	11.16 $^2\Sigma$	
48532.57	0.07					
48535.06	0.32	1	10.5	11	16.06 $^2\Delta$	
48537.31	0.19					
48538.53	0.31	2	12.5	13	11.16 $^2\Sigma$	
48539.37	1.0	1	12.5	12	16.06 $^2\Delta$	blended
48539.37	1.0	1	10.5	11	16.16 $^2\Sigma$	blended
48543.25	0.21	1	12.5	13	16.06 $^2\Delta$	
48544.72	0.26	1	12.5	13	16.10	
48547.38	0.21	1	12.5	13	16.16 $^2\Sigma$	
48548.86	0.26					
48550.42	0.11					
48553.39	0.09					

Table 3.2.6 - Autoionization Spectra Observed in the n*=16 Region.
PUMP line - $A^2\Pi$-$X^2\Sigma$ (0,0) P_2(13.5)   J=12.5, N=13, f-parity

Term Value(cm⁻¹)	Intensity	v	J'	N'	Λ and n*	comment
48517.62	0.21	2	11.5	12	11.06 $^2\Delta$	
48520.42	0.19					
48521.21	0.10					
48522.13	0.07	2	13.5	13	11.06 $^2\Delta$	
48526.59	0.11	2	13.5	14	11.06 $^2\Delta$	
48527.28	0.05					
48529.14	0.14					
48513.12	0.05					
48533.85	0.17					
48534.51	0.68	2	11.5	12	11.16 $^2\Sigma$	
48535.36	0.30	1	11.5	11	16.06 $^2\Delta$	
48537.02	0.18					
48539.01	0.25	1	11.5	12	16.06 $^2\Delta$	
48539.80	0.22					
48541.34	0.19					
48542.88	0.54	2	13.5	14	11.16 $^2\Sigma$	
48543.19	1.0	1	11.5	12	16.16 $^2\Sigma$	
48543.79	0.72	1	13.5	13	16.06 $^2\Delta$	
48545.53	0.11					
48545.86	0.05					
48547.96	0.22	1	13.5	14	16.06 $^2\Delta$	
48549.50	0.25	1	13.5	14	16.10	
48552.00	0.26	1	13.5	14	16.16 $^2\Sigma$	
48552.75	0.04					
48553.87	0.11					
48555.54	0.12					

Table 3.2.7 - Autoionization Spectra Observed in the n*=16 Region.
PUMP line - $A^2\Pi$-$X^2\Sigma$ (0,0) P_2(14.5)   J=13.5, N=14, f-parity

Term Value(cm⁻¹)	Intensity	v	J'	N'	Λ and n*	comment
48505.12	0.13					
48511.29	0.17					
48513.61	0.07					
48515.60	0.06					
48517.18	0.07					
48517.75	0.06					

48521.99	0.23	2	12.5	13	11.06	$^2\Delta$
48523.95	0.09					
48524.76	0.26					
48526.77	0.11	2	14.5	14	11.06	$^2\Delta$
48531.55	0.60	2	14.5	15	11.06	$^2\Delta$
48532.84	0.13					
48533.94	0.19					
48534.85	0.07					
48536.26	0.07					
48538.46	0.49	2	12.5	13	11.16	$^2\Sigma$
48539.92	0.23					
48541.74	0.11					
48543.24	0.11	1	12.5	13	16.06	$^2\Sigma$
48544.61	0.21	1	12.5	13	16.10	
48454.71	0.41					
48547.44	1.0	1	12.5	13	16.16	$^2\Sigma$
48548.18	0.64	2	14.5	15	11.16	$^2\Sigma$
48548.50	0.62	1	14.5	14	16.06	$^2\Delta$
48552.89	0.34	1	14.5	15	16.06	$^2\Delta$
48554.55	0.55	1	14.5	15	16.10	
48556.92	0.30	1	14.5	15	16.16	$^2\Sigma$
48559.11	0.23					
48560.95	0.15					
48562.51	0.14					

Table 3.2.8- Autoionization Spectra Observed in the n*=17 Region.
PUMP line - $A^2\Pi$-$X^2\Sigma$ (0,0) P_2(7.5)   J=6.5, N=7, f-parity

Term Value(cm⁻¹)	v	J'	N'	Λ and n*	comment
48563.40					
48563.76					
48564.70					
48565.84	1	7.5	7	16.93 $^2\Pi$	
48566.64					
48568.54	1	5.5	6	17.06 $^2\Delta$	
48570.89	1	7.5	7	17.06 $^2\Delta$	
48572.63	1	5.5	6	17.16 $^2\Delta$	
48573.39	1	7.5	8	17.06 $^2\Delta$	
48574.56	1	7.5	8	17.10	
48575.41					
48576.06					
48576.79					
48577.24	1	7.5	8	17.16 $^2\Delta$	
48578.32					
48578.92					

Table 3.2.9- Autoionization Spectra Observed in the n*=17 Region.
PUMP line - $A^2\Pi$-$X^2\Sigma$ (0,0) P_2(8.5)   J=7.5, N=8, f-parity

Term Value(cm⁻¹)	v	J'	N'	Λ and n*	comment
48568.35	1	8.5	8	16.93 $^2\Pi$	
48569.78					
48570.72	1	6.5	7	17.06 $^2\Delta$	
48571.38					
48572.49					
48573.31	1	8.5	8	17.06 $^2\Delta$	
48574.73	1	6.5	7	17.16 $^2\Sigma$	
48576.30	1	8.5	9	17.06 $^2\Delta$	
48577.38	1	8.5	9	17.10	
48578.31					
48579.86	1	8.5	9	17.16 $^2\Sigma$	
48580.19					
48582.01					

Table 3.2.10- Autoionization Spectra Observed in the n*=17 Region.

PUMP line - A$^2\Pi$-X$^2\Sigma$ (0,0) P$_2$(9.5)   J=8.5, N=9, f-parity

Term Value(cm^{-1})	v	J'	N'	Λ and n*	comment
48558.10					
48564.14					
48565.07					
48568.25					
48569.99					
48570.93	1	9.5	9	16.93 $^2\Pi$	
48573.40	1	7.5	8	17.06 $^2\Delta$	
48575.49					
48576.45	1	9.5	9	17.06 $^2\Delta$	
48577.19	1	7.5	8	17.16 $^2\Sigma$	
48579.57	1	9.5	10	17.06 $^2\Delta$	
48580.76	1	9.5	10	17.10	
48583.16	1	9.5	10	17.16 $^2\Sigma$	
48584.03					
48585.32					
48591.34					
48597.65					
48600.03					

Table 3.2.11- Autoionization Spectra Observed in the n*=17 Region.

PUMP line - A$^2\Pi$-X$^2\Sigma$ (0,0) P$_2$(10.5)   J=9.5, N=10, f-parity

Term Value(cm^{-1})	v	J'	N'	Λ and n*	comment
48556.54					
48560.99					
48567.92					
48568.14					
48568.33	1	8.5	8	16.93 $^2\Pi$	
48568.82					
48571.34					
48573.39	1	8.5	8	17.06 $^2\Delta$	
48574.33	1	10.5	10	16.93 $^2\Pi$	
48576.38	1	8.5	9	17.06 $^2\Delta$	
48578.43					
48579.81	1	8.5	9	17.16 $^2\Sigma$	blended

Term Value(cm⁻¹)	v	J'	N'	Λ and n*	comment
48579.81	1	10.5	10	17.06 $^2\Delta$	blended
48570.15					
48582.53					
48583.28	1	10.5	11	17.06 $^2\Delta$	
48584.44	1	10.5	11	17.10	
48585.31					
48586.68	1	10.5	11	17.16 $^2\Sigma$	

Table 3.2.12- Autoionization Spectra Observed in the n*=17 Region.

PUMP line - $A^2\Pi$-$X^2\Sigma$ (0,0) P$_2$(12.5) J=11.5, N=12, f-parity

Term Value(cm⁻¹)	v	J'	N'	Λ and n*	comment
48556.60					
48557.69					
48558.91					
48562.33					
48563.91					
58567.83					
48574.91					
48575.56					
48575.54					
48578.36					
48579.86	1	10.5	10	17.06 $^2\Delta$	
48580.42					
48581.51	1	12.5	12	16.93 $^2\Pi$	
48582.09					
48583.29	1	10.5	11	17.06 $^2\Delta$	
48584.41	1	10.5	11	17.10	
48585.36					
48586.75	1	10.5	11	17.16 $^2\Sigma$	
48587.23	1	12.5	12	17.06 $^2\Delta$	
48587.73					
48590.40					
48591.56					
48592.80	1	12.5	13	17.10	
48594.80	1	12.5	13	17.16 $^2\Sigma$	

Table 3.2.13- Autoionization Spectra Observed in the n*=18 Region.

PUMP line - $A^2\Pi$-$X^2\Sigma$ (0,0) $P_2(7.5)$ J=6.5, N=7, f-parity

Term Value(cm⁻¹)	v	J'	N'	Λ and n*	comment
48592.85					
48595.27					
48600.11					
48601.89					
48605.98	1	7.5	7	17.93 $^2\Pi$	
48607.02					
48608.62					
48608.92	1	5.5	6	18.06 $^2\Delta$	
48610.60					
48611.29	1	7.5	7	18.06 $^2\Delta$	
48612.32	1	5.5	6	18.16 $^2\Sigma$	
48613.85	1	7.5	8	18.06 $^2\Delta$	
48614.91	1	7.5	8	18.10	
48616.94	1	7.5	8	18.16 $^2\Delta$	
48617.56					
48618.81					
48624.33					
48624.77					

Table 3.2.14- Autoionization Spectra Observed in the n*=18 Region.

PUMP line - $A^2\Pi$-$X^2\Sigma$ (0,0) $P_2(9.5)$ J=8.5, N=9, f-parity

Term Value(cm⁻¹)	v	J'	N'	Λ and n*	comment
48597.57					
48600.04					
48605.99					
48608.32					
48610.58					
48611.22	1	9.5	9	17.93 $^2\Pi$	
48612.12					
48612.44					
48613.78	1	7.5	8	18.06 $^2\Delta$	
48514.44					
48615.64					
48616.81	1	7.5	8	18.16 $^2\Sigma$	blended

Term Value(cm⁻¹)	v	J'	N'	Λ and n*	comment
48616.81	1	9.5	9	18.06 $^2\Delta$	blended
48620.04	1	9.5	10	18.06 $^2\Delta$	
48621.16	1	9.5	10	18.10	
48622.99	1	9.5	10	18.16 $^2\Sigma$	
48624.53					
48625.78					
48629.27					

Table 3.2.15- Autoionization Spectra Observed in the n*=18 Region.

PUMP line - $A^2\Pi$-$X^2\Sigma$ (0,0) P₂(10.5)   J=9.5, N=10, f-parity

Term Value(cm⁻¹)	v	J'	N'	Λ and n*	comment
48588.84					
48589.42					
48594.62					
48600.56					
48602.99					
48608.44					
48609.63					
48611.35					
48612.21					
48614.46	1	10.5	10	17.93 $^2\Pi$	
48615.26					
48615.75					
48616.72	1	8.5	9	18.06 $^2\Delta$	
48617.82					
48518.64					
48619.90	1	8.5	9	18.16 $^2\Sigma$	blended
48619.90	1	10.5	10	18.06 $^2\Delta$	blended
48621.82					
48623.77	1	10.5	11	18.06 $^2\Delta$	
48624.90	1	10.5	11	18.10	
48626.58	1	10.5	11	18.16 $^2\Sigma$	
48628.29					
48632.38					
48632.87					
48634.62					
48636.70					

Table 3.2.16- Autoionization Spectra Observed in the n*=18 Region.

PUMP line - $A^2\Pi$-$X^2\Sigma$ (0,0) P_2(12.5)   J=11.5, N=12, f-parity

Term Value(cm^{-1})	v	J'	N'	Λ and n*	comment
48596.80					
48598.68					
48603.30					
48607.47					
48609.66					
48615.62					
48617.99					
48618.47					
48619.93	1	10.5	10	18.06 $^2\Delta$	
48621.70	1	12.5	12	17.93 $^2\Pi$	
48622.71					
48623.68	1	10.5	11	18.06 $^2\Delta$	
48625.62					
48626.64	1	10.5	11	18.16 $^2\Sigma$	
48627.81	1	12.5	12	18.06 $^2\Delta$	
48632.24	1	12.5	13	18.06 $^2\Delta$	
48633.25	1	12.5	13	18.10	
48634.83	1	12.5	13	18.16 $^2\Sigma$	
48636.96					

Table 3.2.17- Autoionization Spectra Observed in the n*=19 Region.

PUMP line - $A^2\Pi$-$X^2\Sigma$ (0,0) $P_2(7.5)$ J=6.5, N=7, f-parity

Term Value(cm^{-1})	v	J'	N'	Λ and n*	comment
48629.27					
48632.47					
48637.12					
48639.85	2	5.5	5	12.06 $^2\Delta$	
48640.92					
48641.60	2	5.5	6	12.06 $^2\Delta$	
48641.95					
48643.61					
48644.16	2	7.5	7	12.06 $^2\Delta$	
48644.99					
48646.09					
48646.75	2	7.5	8	12.06 $^2\Delta$	
48647.15					
48648.60					
48649.11					
48650.81					
48651.83					
48652.94					
48653.91					
48655.07					
48655.78					
48656.15					
48659.52					
48663.20					

Table 3.2.18- Autoionization Spectra Observed in the n*=19 Region.

PUMP line - $A^2\Pi$-$X^2\Sigma$ (0,0) $P_2(9.5)$ J=8.5, N=9, f-parity

Term Value(cm^{-1})	v	J'	N'	Λ and n*	comment
48630.99					
48632.36					
48635.75					
48637.21					
48643.12					
48644.15	2	7.5	7	12.06 $^2\Delta$	
48646.69	2	7.5	8	12.06 $^2\Delta$	

48547.20					
48648.39					
48649.30					
48649.83	2	9.5	9	12.06	$^2\Delta$
48650.76					
48653.02	2	9.5	10	12.06	$^2\Delta$
48653.79					
48655.41					
48656.11					
48656.90					
48658.46					
48659.49					
48660.06					
48661.41					
48665.27					
48666.02					
48667.13					
48667.75					

Part 3.3 - CaCl Autoionization Data - A $^2\Pi_{3/2}$ (v=0) State Intermediate, High-n* Spectra

Table 3.3.1 - Autoionization Spectra Observed in the n*=20-43 Region.

PUMP line - $A^2\Pi$-$X^2\Sigma$ (0,0) P_2(9.5) J=8.5, N=9, f-parity

Term Value(cm^{-1})	v	J'	N'	Λ and n*	comment
48673.59					
48675.98					
48676.77					
48677.23	1	7.5	8	n* = 20.06[a]	
48678.07					
48678.86					
48679.53					
48680.37					
48683.80					
48684.56	1	9.5	10	n* = 20.13[b]	
48685.82					
48687.16					
48688.70					
48693.79					
48696.21					
48696.88					
48698.76					
48699.84					
48701.52					
48702.30	1	7.5	8	n* = 21.05[a]	
48702.67					
48703.36					
48703.91					
48704.45					
48705.56					
48709.74	1	9.5	10	n* = 21.13[b]	
48711.81					
48713.13					
48722.45					
48723.71					
48724.51	1	7.5	8	n* = 22.06[a]	
48725.24					
48725.82					

48726.26
48727.41
48729.77
48731.51   1   9.5 10 $n* = 22.13^b$
48732.84
48734.34
48735.11
48736.82
48737.31
48737.82
48738.76
48740.20
48740.77
48742.36   1   7.5 8 $n* = 23.07^a$
48742.94
48743.83
48744.35
48745.01
48745.60
48746.12
48748.57
48750.55   1   9.5 10 $n* = 23.14^b$
48754.06
48755.05
48756.78
48757.19
48759.55
48760.43   1   7.5 8 $n* = 24.06^a$
48761.05
48761.84
48762.55
48763.32
48766.69
48767.29
48773.11   1   9.5 10 $n* = 24.15^b$
48774.88   1   7.5 8 $n* = 25.03^a$
48775.75
48776.79
48777.45
48778.21
48782.04   1   9.5 10 $n* = 25.15^b$
48788.32   1   7.5 8 $n* = 26.05^a$

48790.75					
48793.24					
48795.16	1	9.5	10	$n^* = 26.16^b$	
48800.25	1	7.5	8	$n^* = 27.07^a$	
48802.90					
48804.58					
48805.57					
48806.67	1	9.5	10	$n^* = 27.15^b$	
48810.67	1	7.5	8	$n^* = 28.06^a$	
48811.44					
48815.36					
48817.19	1	9.5	10	$n^* = 28.16^b$	
48819.93	1	7.5	8	$n^* = 29.05^a$	
48820.90					
48821.47					
48823.62					
48824.17					
48826.58	1	9.5	10	$n^* = 29.17^b$	
48828.52	1	7.5	8	$n^* = 30.05^a$	
48834.90					
48836.23					
48837.03					
48836.00					
48842.83	1	9.5	10	$n^* = 31.21^b$	
48843.20	1	7.5	8	$n^* = 32.05^a$	
48845.60					
48848.32					
48849.52	1	9.5	10	$n^* = 32.18^b$	blended
48849.52	1	7.5	8	$n^* = 33.05^a$	blended
48849.65					
48850.64					
48852.82					
48853.02					
48854.05					
48855.13					
48855.36	1	7.5	8	$n^* = 34.06^a$	
48855.87	1	9.5	10	$n^* = 33.18^b$	
48858.66					
48859.57					
48860.60	1	7.5	8	$n^* = 35.03^a$	
48861.72	1	9.5	10	$n^* = 34.21^b$	

48865.60	1	7.5	8	$n^* = 36.03$[a]
48867.00	1	9.5	10	$n^* = 35.21$[b]
48867.78				
48870.08	1	7.5	8	$n^* = 37.05$[a]
48872.72				
48874.24	1	7.5	8	$n^* = 38.06$[a]
48876.30				
48876.76				
48878.04	1	7.5	8	$n^* = 39.05$[a]
48881.62	1	7.5	8	$n^* = 40.05$[a]
48884.90	1	7.5	8	$n^* = 40.06$[a]
48888.04	1	7.5	8	$n^* = 41.06$[a]
48891.06	1	7.5	8	$n^* = 42.08$[a]
48895.82				
48905.34				
48907.11				
48908.98				
48910.08				
48912.99				
48914.79				
48917.29				
48917.62				
48920.40				
48923.24				
48923.55				
48925.06				
48926.68				
48927.40				
48929.00				
48949.29				
48968.47				
48969.82				
48971.37				
48972.15				
48973.24				
48974.58				
48975.48				
48977.72				
48979.29				
48980.77				
48982.13				
48985.22				

48987.22					
48988.42					
49015.45					
49019.30	2				
49020.40	2	9.5	9	16.93	$^2\Pi$
49022.70	2	7.5	8	17.06	$^2\Delta$
49024.90					
49025.90	2	9.5	9	17.06	$^2\Delta$
49026.60	2	7.5	8	17.16	$^2\Sigma$
49029.00	2	9.5	10	17.06	$^2\Delta$
49030.20	2	9.5	10	17.10	
49032.50	2	9.5	10	17.16	$^2\Sigma$
49033.40	2				
49034.80	2				

[a]I.P. = 48950.0

[b]I.P. = 48955.5

References

[1]N. A. Harris and R. W. Field , J. Chem. Phys. **98**, 2642-2646 (1993).

[2]C. M. Gittins, N. A. Harris, R. W. Field, J. Verges, C. Effantin, A. Bernard, J. D'Incan, W. E. Ernst, P. Bundgen, and B. Engels, J. Mol. Spec. **161**, 303-311 (1993).

[3]J. Nakagawa, P. J. Domaille, T. C. Steimle, and D. O. Harris, J. Mol. Spec. **70**, 374-385 (1978).

[4] L. E. Berg, L. Klynning, and H. Martin, "Laboratory Measurements of the Red Band Spectrum of the CaCl Molecule: Wavelengths and Molecular Constants of the $A^2\Pi$-$X^2\Sigma$ System", unpublished work.

Figure Captions

Figure 5.1   Spectra recorded using the direct fluorescence detection scheme.   These spectra were recorded using the B $^2\Sigma$ (v=0) State as the intermediate state.   This is the highest energy state observed using direct fluorescence in CaCl.

Figure 5.2   Spectra recorded using the direct fluorescence detection scheme.   These spectra were recorded using the B $^2\Sigma$ (v=0) State as the intermediate state.   This is the highest energy state observed using direct fluorescence in CaCl.

Figure 5.3   Spectra recorded using the fluorescence dip detection scheme.   These spectra were recorded using the $B^2\Sigma$ (v=0) state as the intermediate state.

Figure 5.4   Spectra recorded using the fluorescence dip detection scheme.   These spectra were recorded using the $B^2\Sigma$ (v=0) state as the intermediate state.

Figure 5.5   Spectra recorded using the fluorescence dip detection scheme.   These spectra were recorded using the $B^2\Sigma$ (v=0) state as the intermediate state.   These are the strongest transitions observed using the fluorescence dip detection scheme in CaCl.

Figure 5.1 Highest Energy State Observed by Direct Fluorescence in CaCl
$v=1$, $n^*=3.8$ $^2\Sigma$

P (Δ J = -1)
24,441.2 cm^{-1}

R (Δ J = 1)
24,452.6 cm^{-1}

B$^2\Sigma$(0,0), R$_1$(16) PUMP
16,860.463 cm^{-1}

24,442 cm^{-1}

24,453 cm^{-1}

B$^2\Sigma$(0,0), R$_1$(15) PUMP
16860.109 cm^{-1}

24,443 cm^{-1}

24,448 cm^{-1}

B$^2\Sigma$(0,0), R$_1$(7) PUMP
16857.462 cm^{-1}
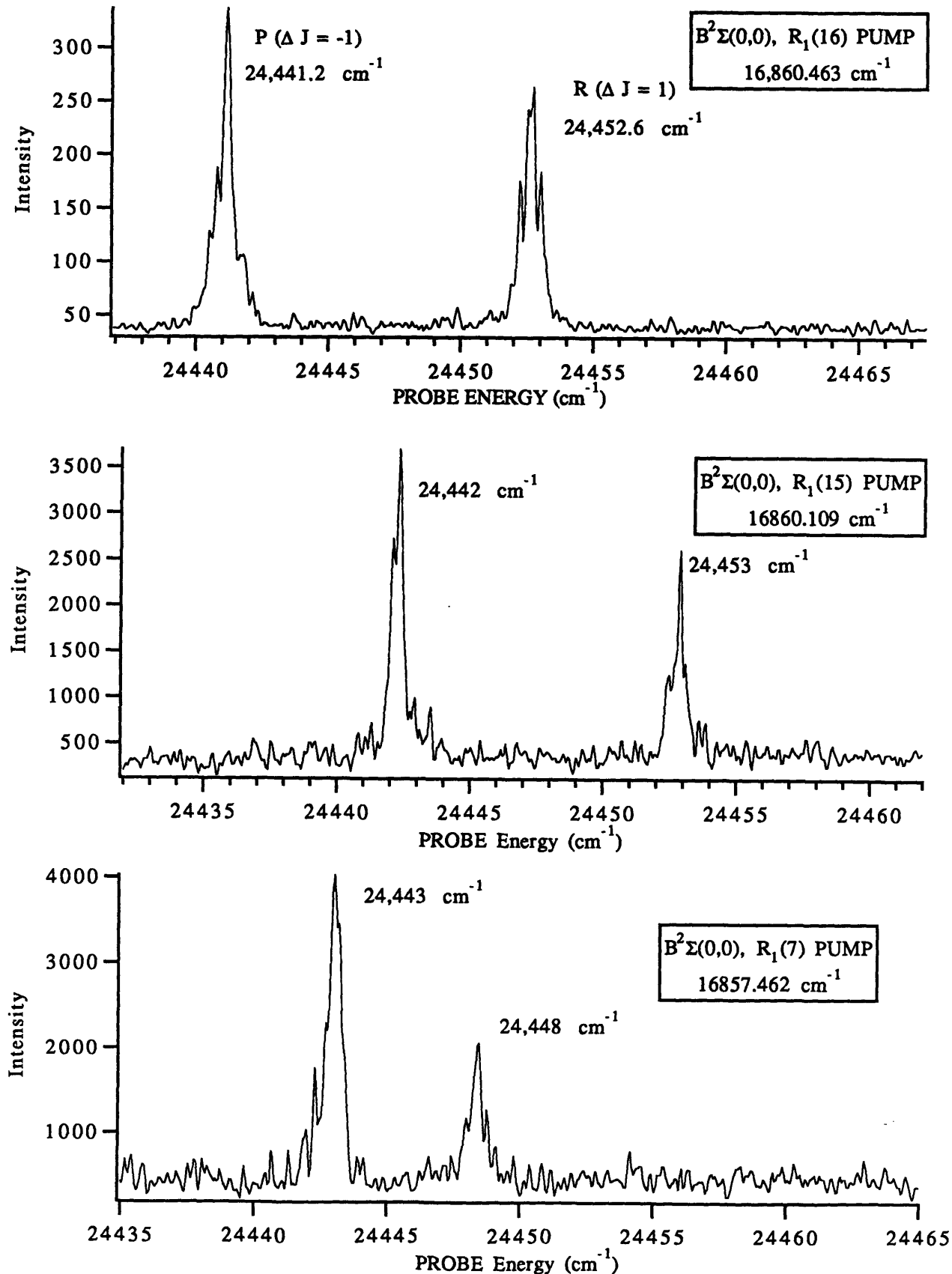
Figure 5.2 Highest Energy State Observed by Direct Fluorescence in CaCl - $v=1$, $n^*=3.8$ $^2\Sigma$

B$^2\Sigma$(1,1), R$_1$(25) and R$_2$(21) blended with (0,0), R$_1$(16)

24,080 cm^{-1}

24,097 cm^{-1}

24,078 cm^{-1}

24,092 cm^{-1}

PROBE Energy (cm^{-1})

24,444 cm^{-1}

24,447 cm^{-1}

24,446 cm^{-1}

B$^2\Sigma$(0,0), R$_2$(3) + R$_1$(4) PUMP
16856.557 cm^{-1}(blended line)

PROBE Energy (cm^{-1})
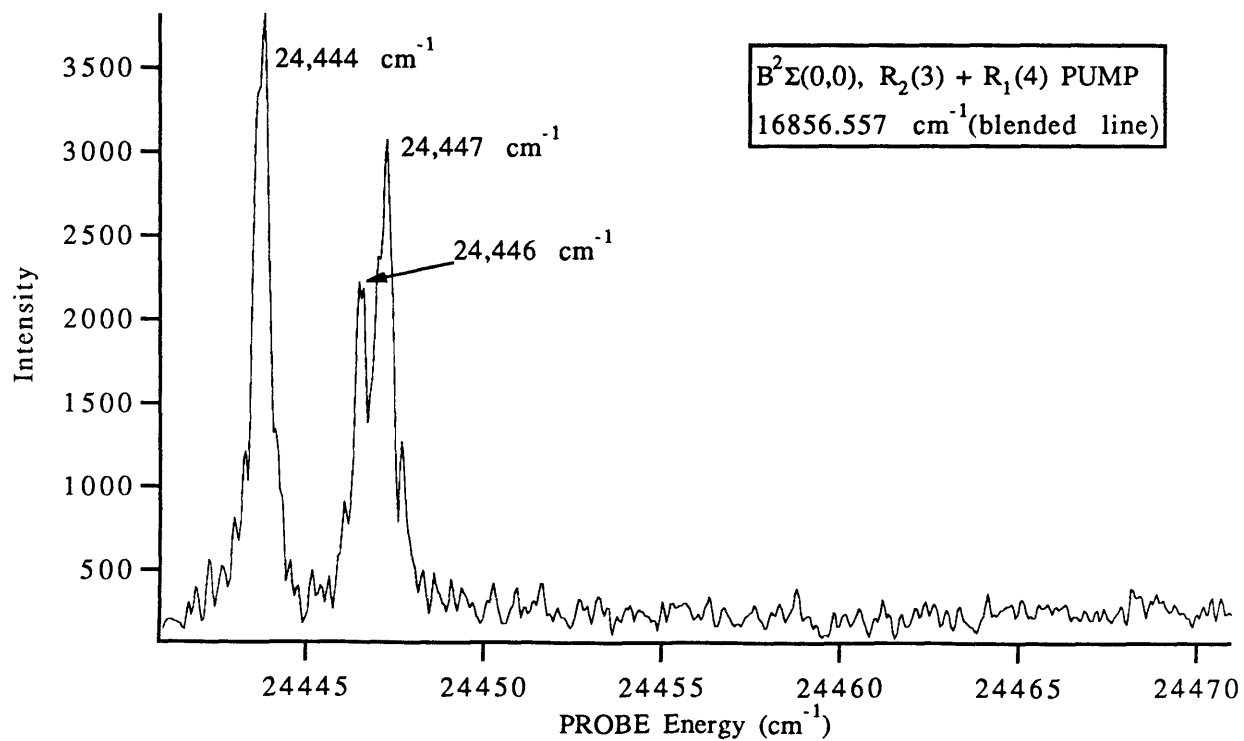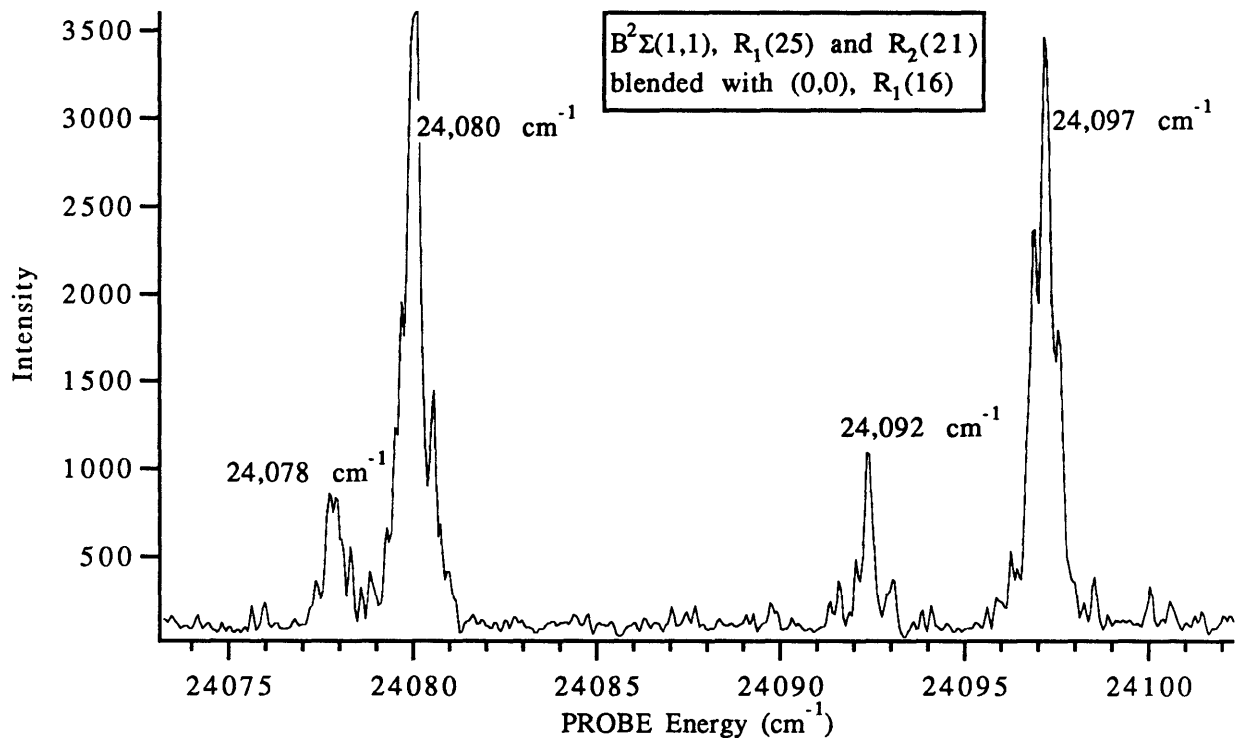
Figure 5.3   CaCl Florescence Dip Spectra

B$^2\Sigma$(0,0), R$_1$(16) PUMP
16860.463 cm^{-1}

26,666 cm^{-1}

26,677 cm^{-1}

PROBE Energy (cm^{-1})

27,237 cm^{-1}

27,248 cm^{-1}

B$^2\Sigma$(0,0), R$_1$(16) PUMP
16860.463 cm^{-1}

PROBE Energy (cm^{-1})

B$^2\Sigma$(0,0), R$_1$(16) PUMP
16860.463 cm^{-1}

27,281 cm^{-1}

27,293 cm^{-1}

PROBE Energy (cm^{-1})

198
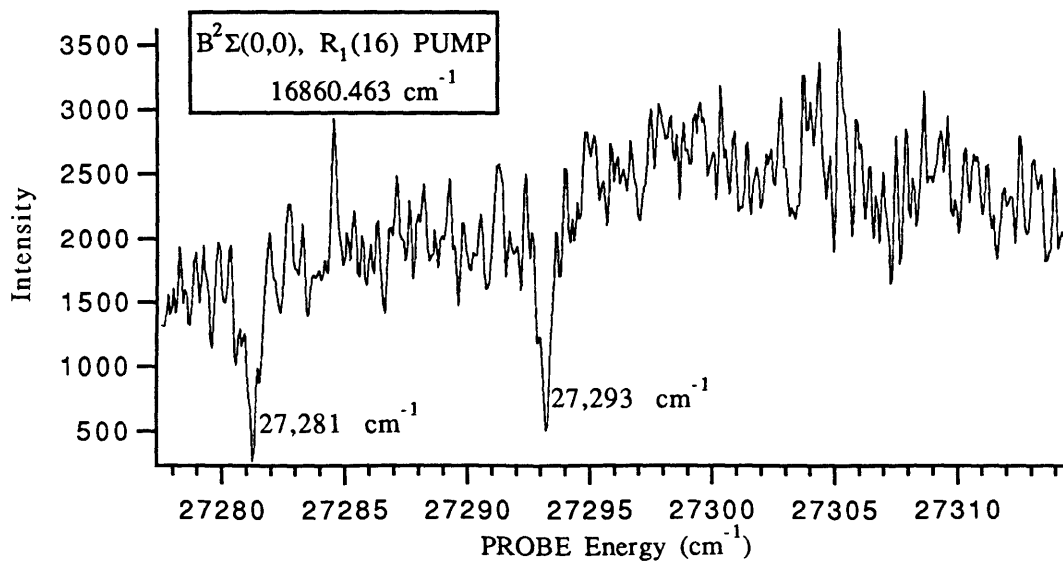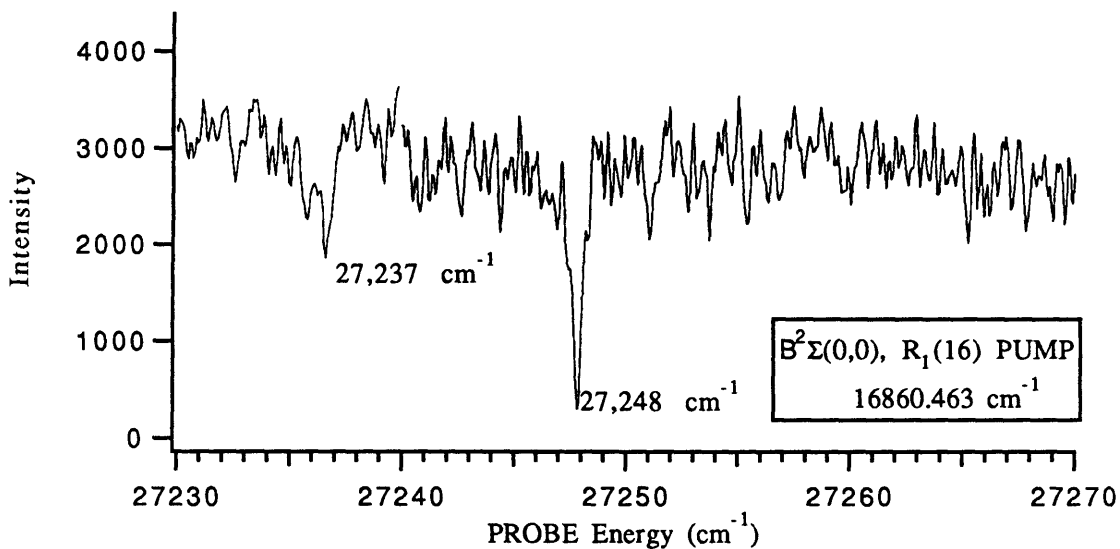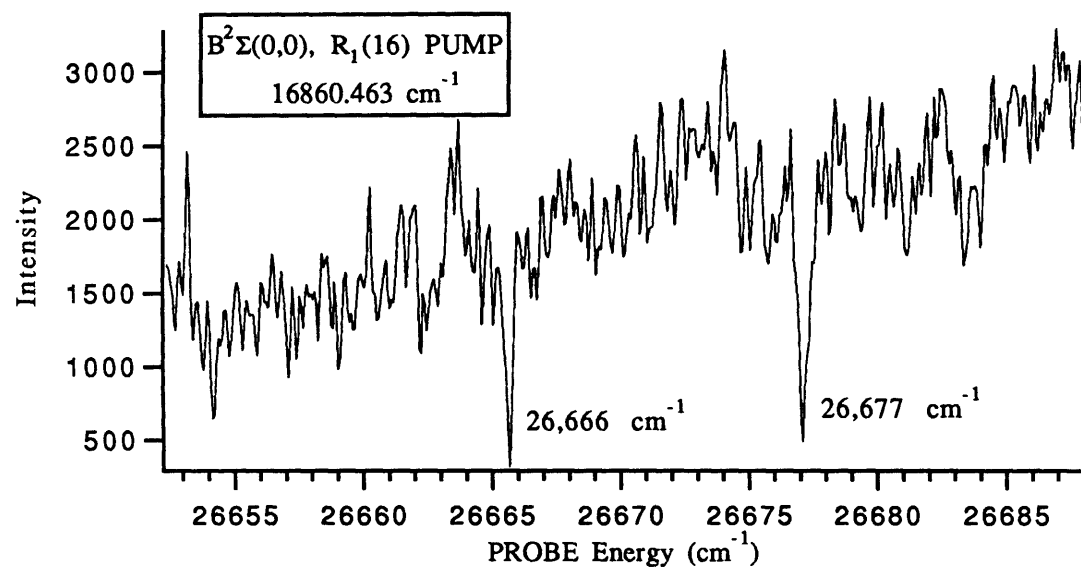
Figure 5.4   CaCl Fluorescence Dip Spectra

$B^2\Sigma(0,0)$, $R_1(16)$ PUMP
16860.463 cm^{-1}

27,753 cm^{-1}

27,755 cm^{-1}

27,767 cm^{-1}

PROBE Energy (cm^{-1})

28,006 cm^{-1}

27,998 cm^{-1}

27,994 cm^{-1}

27,996 cm^{-1}

$B^2\Sigma(0,0)$, $R_1(24)$ PUMP
16863.451 cm-1

PROBE Energy (cm^{-1})
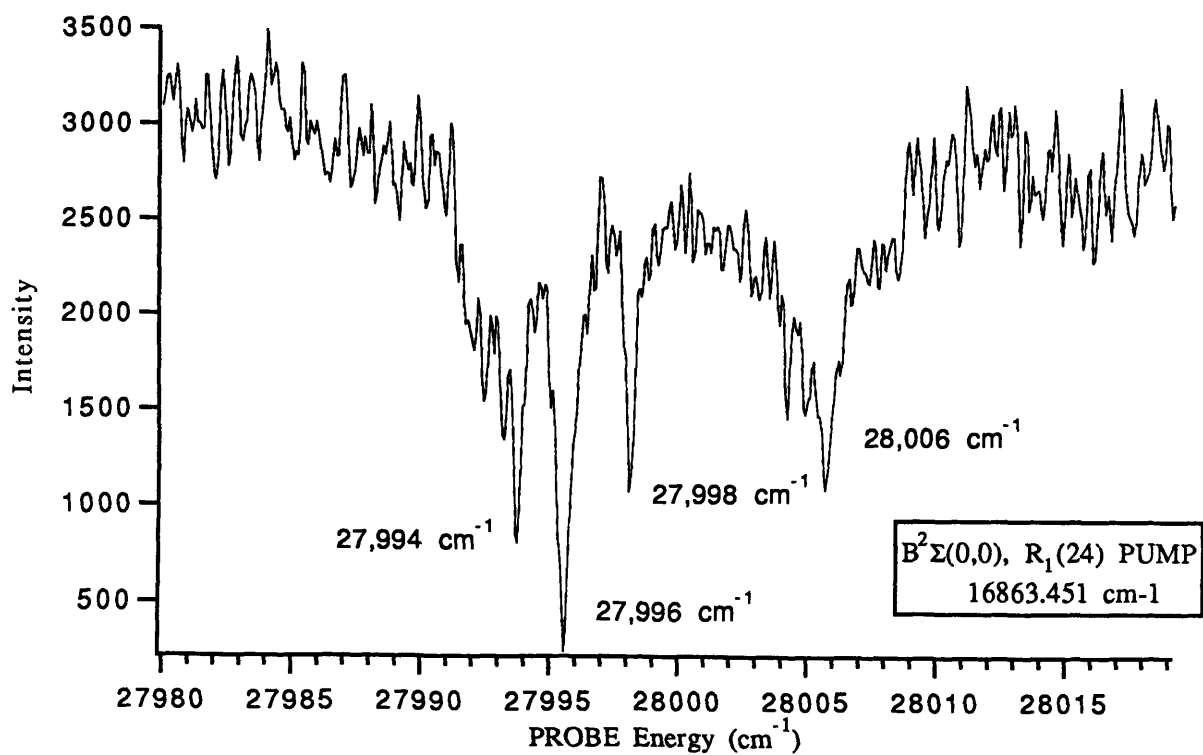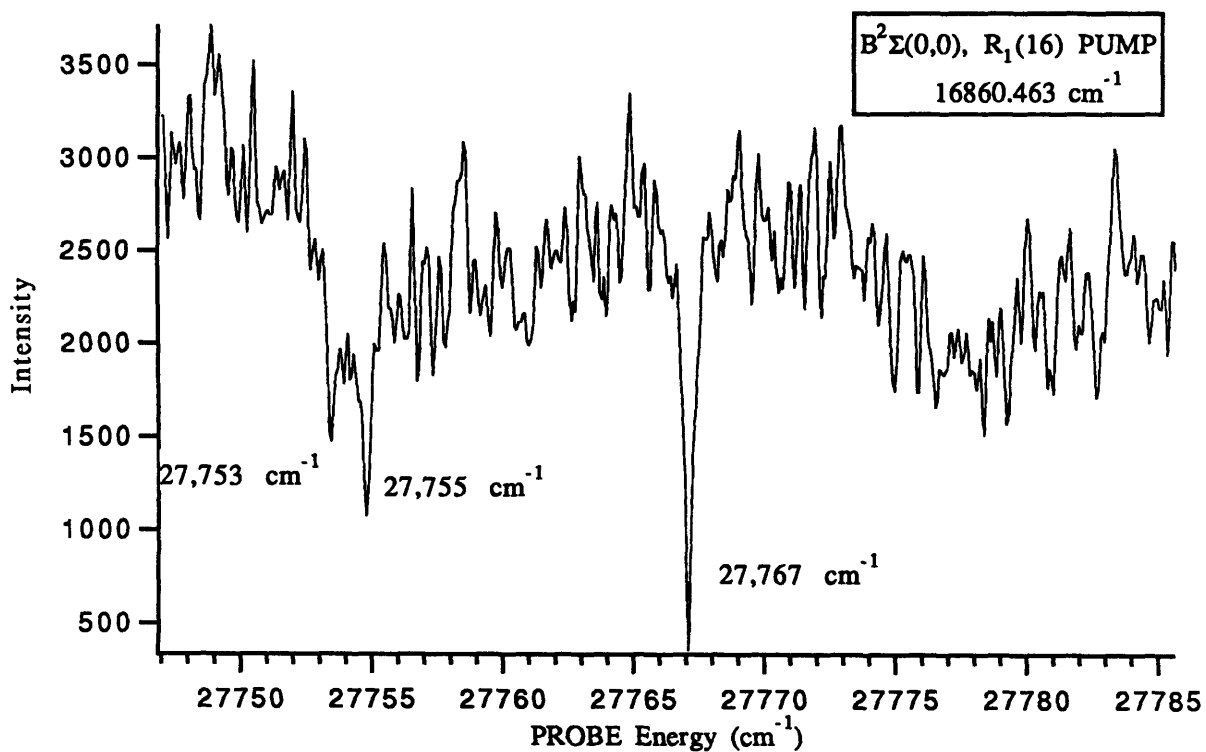
Figure 5.5   Stongest Transition Observed by Fluorescence Dip in CaCl

$R_1(28)$ 16865.060 cm^{-1}

27,553.2 cm^{-1}

27,571.9 cm^{-1}

27,584.9 cm^{-1}

27,557.4 cm^{-1} 27,564.7 cm^{-1}

27,554.4 cm^{-1}

27,550.7 cm^{-1}

$R_1(24)$

27,555.7 cm^{-1}

16863.451 cm^{-1}

27,570.3 cm^{-1}

27,552.1 cm^{-1}

27,546.3 cm^{-1}

27,551.7 cm^{-1} $R_1(16)$

16860.463 cm^{-1}

27,547.6 cm^{-1}

27540   27550   27560   27570   27580   27590

PROBE Energy (cm^{-1})

2000

1800

Intensity

1600

27,550.0 cm^{-1}

27,553.7 cm^{-1}

$B^2\Sigma(0,0)$, $R_2(24)$ PUMP

16865.154 cm^{-1}

1400

27545   27550   27555   27560   27565   27570   27575

PROBE Energy (cm^{-1})

Chapter 6
Analysis and Discussion

Part 6.1 - Assigning Spectra

The CaF double resonance Rydberg spectra recorded previously, in the intermediate n* region, were relatively sparse, therefore vibronic states could be usually be individually identified.[1-4] Vibronic states were assigned by their n* values and the P and R branches of each vibronic state were identified based on the expected P-R spacing. It was assumed that the rotational constant was approximately the same for all of the Rydberg states and therefore the P-R spacing was known. This assumption is valid, but only for the core penetrating states at intermediate n*.

Murphy also assumed, since the spectra were not dense, that only a few low-J (near 1.5), a few intermediate-J (near 11.5) and a few high-J (near 48.5) PUMP lines were needed to characterize each vibronic state. Spectra were not recorded using consecutive-J PUMP transitions. This did not appear to be a problem when the spectra were initially assigned and fitted. We now know that important perturbations by core-nonpenetrating states were missed by this coarse-grained-in-J approach. Those perturbations would have allowed us to locate the core-nonpenetrating states sooner and at lower n*-values.

Murphy's method of recording spectra from only a few PUMP transitions and identifying branches by the P-R spacing did not work for our spectra in the n*=13-18 region because the spectra were too congested. It also did not work for the core-nonpenetrating states because they have anomalous effective rotational constants due to rapid ℓ-uncoupling. Since the vibronic states were no longer isolated and we could not assume we knew the P-R spacings, different methods of recording and assigning spectra were required. These methods are described below.

The methods described below were also used to analyze the CaCl autoionization spectra, however the amount and quality of the spectra available were inferior to the CaF spectra, making the analysis and interpretation more difficult.

Part 6.1.1 - Identifying Branches

One goal of the analysis was to make n*- and Λ-assignments and identify the previously unobserved core-nonpenetrating states. To accomplish this goal, rotationless term values were needed for each observed vibronic state. Plots of the reduced term value (term value - $BJ(J+1)$) vs. $J(J+1)$ and the reduced term value vs. $N(N+1)$ (see Figures 6.20-6.34) enabled the determination of the rotationless term values. Discussion of how these reduced term value plots aided in assignments is given in Parts 6.1.6 and 6.1.7.

Stacking the spectra using only the PROBE energy helped us to identify rotational branches, each member of which, once assigned, is represented by one point on the reduced term value plots. These stacks of spectra were particularly helpful in the cases where only the P(ΔJ=-1) or R(ΔJ=+1) branch showed up in the spectrum (it is common near case d for the branches at the top and bottom of a complex to have little or no intensity). Our unusual methods of making J-and N-assignments would have left such "orphan" transitions unassigned. These stacked spectra also aided in the location of perturbations. Figures 6.1-6.13 show the stacked plots for each observed n*-complex .

Part 6.1.2 - J-Assignments

In order to make J-assignments, we needed to assign each transition as a P(ΔJ=-1), Q(ΔJ=0), or R(ΔJ=1) branch. Assignments were made by comparing the term values (PROBE energy plus the term value of the upper level of the PUMP transition) of two spectra recorded from J and J+2 intermediate levels, for example Q_2(3.5) and Q_2(5.5). The term value for the upper level of an R branch from the Q_2(3.5) PUMP transition would match the term value of a P branch from the Q_2(5.5) PUMP transition. Figure 6.14 shows why these term values should agree. This method worked because our states are near case b (the splitting of the J-levels within an N level is small). This method enabled only P and R branches to be assigned and only when both P and R branches have appreciable intensity. In our spectra, the Q-form R (ΔN=0, ΔJ=1) and Q (ΔN=0, ΔJ=0) transitions could not be resolved. The same was true for the P-form Q (ΔN=-1, ΔJ=0) and P (ΔN=-1, ΔJ=-1) transitions. This was helpful because the Q (ΔJ=0) branch was more intense than the P or R branch for all $\Delta \Lambda \neq 1$ transitions. The fact the these transitions were not resolved ensured

that one member of this composite transition would always be detected. If the splitting of the two J-levels within each N-level had been much larger than the calibration error of about 0.02 cm^{-1}, assigning the P and R transitions could have been more difficult for the $\Delta\Lambda \neq 1$ transitions. It is important to be aware of the relative rotational branch intensity pattern as well as the Q form R - Q and the P form Q - P splitting before assuming that this method of assigning spectra will work. Figure 6.15 shows sample spectra with some assignments.

Part 6.1.3 - N-Assignments

In order to make N-assignments, we needed to assign the transitions as O(ΔN=-2), P(ΔN=-1), Q(ΔN=0) or R(ΔN=1) form branches. N-assignments were important for two reasons. First, because N is the pattern forming quantum number in case b, the term value plots vs. N(N+1) are easier to interpret than those vs. J(J+1) (see Figures 6.24 and 6.25). Second, N-assignments are logically equivalent to +/- Kronig symmetry assignments that appear on the term value plots.

The J-assignments were helpful in making N-assignments, however some ambiguity remains. A P-R pair in J can be an O-Q pair or a P-R pair in N (see Fig. 6.14). If the states are near case b rather than near case d (large ℓ-uncoupling), the term values of spectra recorded from J, J+1, J+2 and J+3, for example $Q_2(3.5)$, $Q_2(4.5)$, $Q_2(5.5)$, and $Q_2(6.5)$ PUMP transitions could be compared in order to assign N. The term value of the O (ΔN=-2) transition from the $Q_2(6.5)$ PUMP transition should match the term value of the P (ΔN=-1) from the $Q_2(5.5)$ PUMP transition which should match the term value of the Q (ΔN=0) from the $Q_2(4.5)$ PUMP transition which finally, should match the term value of the R (ΔN=1) from the $Q_2(3.5)$ PUMP transition (see Figure 6.16). As the ℓ-uncoupling increases (the splitting of the + and - total parity levels increases), comparing spectra from consecutive Q_2 PUMP transitions will no longer reveal the diagnostic patterns (see Figures 6.16 and 6.17). Also, any perturbation caused by states near case d could render this method useless since these perturbations usually affect only one of the parity components. Figure 6.16 shows how, when spectra are recorded from consecutive Q PUMP transitions, the +/- total parities of the final states alternate. When comparing spectra recorded from alternating P_2 and Q_2 branch PUMP lines, for example $Q_2(3.5)$, $P_2(5.5)$, $Q_2(5.5)$, and $P_2(7.5)$, the +/- total parity remains the same for each final state. Figures 6.17 and 6.18 show why the comparison of spectra from P_2 and Q_2 PUMP

transitions avoids problems with perturbations and ℓ-uncoupling. See Figure 6.19a for an example of how the term values of the ΔN transitions line up when comparing spectra recorded from P_2 and Q_2 PUMP transitions. Figure 6.19b shows a comparison of spectra recorded from only Q_2 PUMP transitions, notice how the term values of the ΔN transitions do not match for one of the states. This is the 14.14 $^2\Delta$ which is perturbed by the f Π state.

Part 6.1.5 - Kronig +/- Symmetry Assignments

The +/- labels on Figures 6.14 and 6.16-6.18 are *total parity* labels. These are related to, but not necessarily identical to the +/- Kronig symmetry assignments which appear on the term value plots. All the levels of $^2\Sigma^+$ states have + Kronig symmetry.[5,6] For the $\Lambda > 0$ states of CaF, the P form and R form transitions terminate on - Kronig symmetry levels, and the O form and Q form transitions terminate on + Kronig symmetry levels when spectra are recorded via both an $A^2\Pi$-$X^2\Sigma^+$ P_2 PUMP transition and $C^2\Pi$-$X^2\Sigma^+$ P_2 PUMP transition. When spectra are recorded via an $A^2\Pi$-$X^2\Sigma^+$ Q_2 PUMP transition and $C^2\Pi$-$X^2\Sigma^+$ R_{21} PUMP transition the pattern is reversed. O-form and Q-form transitions terminate on + Kronig symmetry levels and P-form and R-form transitions terminate on - Kronig symmetry levels.

Part 6.1.6 - n*- and Λ-Assignments

Once the J- and N-assignments were made, reduced term value plots were constructed in order to identify the rotationless term value of each observed vibronic state. n* was calculated from these rotationless term values using Eq. 3.1. Since we identify and group states based on their n*-value, the reduced term value plots allowed immediate identification of each of the core-penetrating states. These plots also helped to identify states with anomalous rotational constants. Assigning the core-penetrating states and identifying those with anomalous rotational constants, by a process of elimination, enabled us to assign a complete f complex (see figure 6.31) which had not been observed or identified previously.

The reduced term value plots for n*=13, 14, 17 and 18 spectra, recorded using the $A^2\Pi$-$X^2\Sigma^+$(0,0) PUMP transitions are presented in Figure 6.20-6.25. Those for n*=7, 13, and 14, recorded using the $C^2\Pi$-$X^2\Sigma^+$(0,0) PUMP transitions are presented in Figures 6.26-6.30.

CaCl reduced term value plots for n*=16, 17, and 18 are presented in Figures 6.33 and 6.34.

Part 6.1.7 - $\mathcal{L}$-Assignments

For case d states, $\mathcal{L}$ is used to label the states rather than Λ (which is not a good quantum number for case d). The pattern forming quantum number for case d is R (R = N - $\mathcal{L}$) which represents the rotation of the CaF^+ core.[7,8] Figure 6.31 shows the f and g states observed in the n*=14 region. Reduced term value plots vs. N(N+1) and R(R+1) are presented. The reduced term value plot vs R(R+1) is compressed to 12 cm^{-1} from 70 cm^{-1} in the N(N+1) plot (this suggests that R, not N, is the pattern forming quantum number for these case d states).

Three pieces of information were used to make $\mathcal{L}$ assignments, the Kronig symmetry, the slope of the term on the reduced term value vs. N(N+1) plot and the location of the term on the reduced term value vs. R(R+1). Each of the $\mathcal{L}$ components in an f or g complex has an a priori known Kronig symmetry. Table 6.1 summerizes these Kronig symmetry. The expected slope of the reduced term value vs. N(N+1) plot, which is also included in Table 6.1, is also a priori known based on the expected location of the component within the complex. The components with negative $\mathcal{L}$ values are at the top of the complex in CaF and will have a positive slope. Those with a positive $\mathcal{L}$ value will be at the bottom of the complex and have a negative slope. Finally, the location of the term on the reduced term value vs. R(R+1) plot is also an indication of a correct assignment. R is defined in terms of $\mathcal{L}$ so when all the components are correctly assigned, all the term curves will be within a 12 cm^{-1} (this value is for the CaF n*=14 f complex, the size of the energy region will not be the same for other molecules and other n* values) region on the reduced term value vs. R(R+1) plot. If $\mathcal{L}$ is incorrectly assigned for one of the components, its curve will fall outside the energy region where all the other components are located.

Table 6.1 Kronig Symmetry and Predicted Slope on the Reduced Term Value Plots for the Different Members of an f and g Complex

ℓ value	Kronig symmetry for f component and slope	Kronig symmetry for g component and slope
-4	*	+, strongly positive
-3	+, strongly positive	-, positive
-2	-, positive	+, positive
-1	+, slightly positive	-, slightly positive
0	-, zero	+, zero
+1	+, slighly negative	-, slighly negative
+2	-, negative	+, negative
+3	+, strongly negative	-, negative
+4	*	+, strongly negative

* an f complex does not have an ℓ = +4 or -4 component

Part 6.1.7 - Vibrational Assignments

The vibrational assignments for CaF were made based on the known vibrational constant for the CaF^+ ion (683 ± 2 cm^{-1})^4 and the calculated n* values. For CaCl the vibrational constant had not been determined but we had an additional piece of information not available for CaF. We recorded both $Ca^{35}Cl$ and $Ca^{37}Cl$ spectra simultaneously which enabled us to make vibrational assignments based on isotope shifts. We were also able to approximate the vibrational constant of the $CaCl^+$ ion from our spectra which is 450 ± 2 cm^{-1}. Figure 6.38 show the isotope shifts for v=1 and v=2 of the n*=17 complex.

Part 6.2 Discussion

For all the spectra discussed below the uncertainty of the assignments increased as the congestion of the spectra increases. The least congested spectra discussed below were recorded in the n*=14 region.

Part 6.2.1 Spectra Recorded from the $A^2\Pi$ State

In the n*=13 region (Figures 6.20 and 6.21) all of the predicted states were observed except the v=2 9.14 $^2\Delta$ state. This state is predicted to be very near the location as the 13.14 $^2\Delta$ state. It is possible that an interference effect ,like the one seen between the

v=0 7.36 $^2\Pi$ and the v=1 6.36 $^2\Pi$ state[1], made this state difficult to observe. There is an "extra" state where the 9.14 $^2\Delta$ state should be, but it was assigned as the v=3 7.36 $^2\Pi$ state based on of the size of its λ-doubling(the splitting between the + and - Kronig symmetry levels). It is unlikely that the 9.14 $^2\Delta$ state could have a λ-doubling larger than that of the 13.14 $^2\Delta$ state since the λ-doubling of the q-parameter is expected to scale as n^{*3}.

The identification of the state which perturbs the v=3 7.36 $^2\Pi$ state is unknown. It is most likely a v=2 f or g state that has not yet been assigned. The assignments for this energy region are presented on Figure 6.21 and in Tables 2.1.2-2.1.14. The perturbation in the 13.36 $^2\Pi$ state is due to the ℓ = +4 g state.

In the n*=14 region (Figures 6.22 and 6.23) all of the predicted states were observed. The perturbation in the 14.36$^2\Pi$ state is again due to the ℓ = +4 g state. The assignments for this energy region are presented on Figure 6.23 and in Tables 2.1.15-2.1.27.

The n*=17 and n*=18 regions were very difficult to assign because those spectra were so congested and there are also so many perturbations. An attempt was made to assign all terms, but the assignments in this region were not as certain as those in the n*=13 and n*=14 regions. Terms which could not be assigned that appear on the reduced term value plot (Figure 6.25) were given labels Term1, Term2 etc. A similar system was used in the n*=7 region but these labels are not related to those in the n*=7 region. They are only for book keeping purposes. The assignments for this energy region are presented on Figure 6.25 and in Tables 2.1.28-2.1.42.

The high-n* spectra recorded out of the A$^2\Pi$ state was a good test for the value of the ionization potential determined by Murphy[1-3]. A value for the v=1 ionization potential of 47,687 $\pm$ 0.5 cm^{-1} was determined from the states in the n*= 27-32 region. Figure 6.35 shows a sample of the spectra recorded in this region with some of the n* assignments. Since spectra from only three PUMP transitions (Q$_2$(1.5), Q$_2$(2.5), Q$_2$(3.5)) were recorded, no Λ, J, or N assignments were made for these spectra. The ionization potential determined from each series identified in this region is at the bottom of Tables 2.3.1-2.3.3. The value of the ionization potential depends on which N the series terminates on, so the value is slightly different for each series.

Part 6.2.2 Spectra Recorded from the $C^2\Pi$ State

The spectra in the n*=7 region were very difficult to assign because transition into the f and g states from v=0, 1 and 3 could all occur in this region. Three of the terms were assigned. The v=0 f $^2\Delta$ is the only v=0 f state which has been detected and assigned (the autoionization spectra all terminate v>0 levels). Terms 14 and 15 could be the v=3 f Π state. Since very few terms were assigned, each term was given a labels such as Term1, Term2, etc. These labels are for book keeping purposes only. The assignments for this energy region are presented on Figures 6.26 and 6.27 and in Tables 1.2-1.13. Since N assignments are less reliable in this region due to the complexity of the spectra, both a reduced term value vs. J(J+1) and a reduced term value vs. N(N+1) are presented.

The spectra in the n* = 13 region were difficult to assign because both v=1 (n*=13) and v=2 (n*= 9) f and g states are expected to occur in this region. The assignments are not as certain here as in the n*=14 region. The assignments for this energy region are presented on Figure 6.28 and in Tables 2.2.2-2.2.12. "Pert" in the comment section of the tables means that the state is perturbed by an unassigned state.

The spectra in the n*=14 region were much easier to assign because there were no problems with v>1 states making the spectra congested. The assignments for this energy region are presented on Figures 6.29-6.31 and in Tables 2.2.13-2.2.24.

Part 6.2.3 CaCl Spectra

The quality and quantity of the CaCl spectra provided only limited insights into the electronic structure of CaCl. In the low energy region, the first member of the third Σ series (the n*=3.15 $^2\Sigma$ state) was located (see Chapter 3). In the n*=16-18 region, five series were located, all of which can be traced back to one of the "valence"- state precursors of CaCl. The 0.10 series, which has no Λ assignment, could be a member of the series which terminates on the $C^2\Pi$ state.

The high-n* spectra, in the n*=20-24 region, enabled us to determine the ionization potential of CaCl. This value of 48489 ± 2 cm^{-1} had not been determinedpreviously. Two series were identified in this n* region. The 0.05 series could be the part of the 0.06 Δ series and the 0.16 series could be part of the 0.16 Σ series.

There is no text material missing here.
Pages have been incorrectly numbered.

p. 208

Figure 6.36 shows a sample of the spectra recorded in this region with some of the n* assignments. The ionization potential determined from each series identified in this region is at the bottom of Table 3.3.1. The value of the ionization potential depends on which N the series terminates on, so the value is slightly different for each series.

Part 6.3 MQDT Fitting

In order to determine which theoretical model appropriately describes the core-nonpenetrating states of CaF a model is needed to fit the data and determine the zero order quantum defects. The f and g states are perturbed by the core-penetrating series. We need to be sure that the quantum defects we come with theory reflect only the effect of the multipole moments unless the theoretical model includes the effects of the core-penetrating series.

Multichannel quantum defect theory (MQDT)[9] is the most reasonable model since it is specifically designed for fitting Rydberg states. This fitter has been successfully used to fit H_2[10,11] and N_2[12] Rydberg spectra. MQDT treats each Rydberg series as a channel instead of treating each Rydberg state individually. This drastically reduced the number of terms needed to fit a group of states. The concern of n mixing is also removed by this approach because n mixing is taken in account when series are treated as channels.

MQDT fits will be used to fit the spectra presented in this thesis. These fits are not complete but the initial results look promising. The final results will be discussed in a future publication. The results from the initial MQDT fits of the n*=14 (- Kronig symmetry) states are presented in Figure 6.37 and in Tables 6.2-6.6 below. Each table corresponds to a term curve in Figure 6.37 and is labeled to match a curve on that reduced term value plot.

Table 6.2 Results of MQDT Fit for 14.36 Π^-

N	Observed	Calculated
1	47154.22	47154.22
2	47155.72	47155.75
3	47157.98	47158.04
4	47161.03	47161.10
5	47164.94	47164.91
6	47169.55	47169.50

7	47174.86	47174.85
8	47181.07	47180.97

Table 6.3 Results of MQDT Fit for $\ell = -2$

N	Observed	Calculated
2	47138.36	47138.37
3	47140.67	47140.71
4	47143.88	47143.88
5	47147.95	47147.97
6	47153.16	47153.17
7	47159.43	47159.39
8	47166.53	47166.47

Table 6.4 Results of MQDT Fit for 14.14 Δ^-

N	Observed	Calculated
4	47142.22	47142.27
5	47146.76	47146.77
6	47151.76	47151.72
7	47157.21	47152.20
8	47163.39	47163.35

Table 6.5 Results of MQDT Fit for 13.98 Π^-

N	Observed	Calculated
1	47125.62	47125.58
2	47126.97	47126.97
3	47129.04	47129.04
4	47131.80	47131.81
5	47135.25	47135.26
6	47139.42	47139.41
7	47144.27	47144.27
8	47149.85	47149.82

Table 6.6 Results of MQDT Fit for $\ell = 0$

N	Observed	Calculated
4	47130.73	47130.73
5	47134.17	47134.21
6	47138.46	47138.45
7	47143.49	47143.48
8	47149.28	47149.27

References

[1] J. E. Murphy, Ph.D. thesis, Massachusetts Institute of Technology, 1992.

[2] N. A. Harris and R. W. Field, J. Chem. Phys. **98**, 2642 (1993).

[3] J. E. Murphy, J. M. Berg, N. A. Harris, and R. W. Field, Phys. Rev. Lett. **65**, 1861 (1990).

[4] J. M. Berg, J. E. Murphy, N. A. Harris, and R. W. Field, Phys. Rev. A **48**, 3012 (1993).

[5] R de L. Kronig, Ch. 2, "Band Spectra and Molecular Structure", Cambridge University Press (1930).

[6] J. T. Hougen, Monograph 115, Nat. Bur. Stand. (US), (1970).

[7] E. Miecher, Can. J. Phys. **54**, 2074 (1976).

[8] Ch. Jungen and E. Miecher, Can. J. Phys. **47**, 1769 (1969).

[9] C. H. Greene and Ch. Jungen, Adv. At. Mol. Phys. **21**, 51 (1985).

[10] S.C. Ross and Ch. Jungen Phys. Rev. A **49**, 4364 (1994).

[11] S.C. Ross and Ch. Jungen Phys. Rev. A **49**, 4353 (1994).

[12] K. P. Huber, Ch. Jungen, K. Joshino, K. Ito and G. Stark, J. Chem. Phys., **100**, 7957 (1994).

Figure Captions

Figure 6.1 n*=13 stacked plot for CaF. PUMP transitions from Q_2 of $A^2\Pi - X^2\Sigma$. This type of plot is discussed in Part 6.1.1. It is used to identify branches. Some of the assigned branches are labeled with ΔN, n* and Λ.

Figure 6.2 n*= 13 stacked plot for CaF. PUMP transitions from P_2 of $A^2\Pi - X^2\Sigma$. This type of plot is discussed in Part 6.1.1. It is used to identify branches.

Figure 6.3 n*=14 stacked plot for CaF. PUMP transitions from Q_2 of $A^2\Pi - X^2\Sigma$. This type of plot is discussed in Part 6.1.1. It is used to identify branches. Some of the assigned branches are labeled with ΔN, n* and Λ.

Figure 6.4 n*=14 stacked plot for CaF. PUMP transitions from

P_2 of $A^2\Pi$ - $X^2\Sigma$. This type of plot is discussed in Part 6.1.1. It is used to identify branches.

Figure 6.5 n*=17 and n*=18 stacked plot for CaF. PUMP transitions from Q_2 of $A^2\Pi$ - $X^2\Sigma$. This type of plot is discussed in Part 6.1.1. It is used to identify branches. Some of the assigned branches are labeled with ΔN, n* and Λ.

Figure 6.6 n*=17 and n*=18 stacked plot for CaF. PUMP transitions from P_2 of $A^2\Pi$ - $X^2\Sigma$. This type of plot is discussed in Part 6.1.1. It is used to identify branches.

Figure 6.7 n*=7 stacked plot for CaF. PUMP transitions from Q_2 of $C^2\Pi$ - $X^2\Sigma$. This type of plot is discussed in Part 6.1.1. It is used to identify branches. Some of the assigned branches are labeled with ΔN and ℓ labels.

Figure 6.8 n*=7 stacked plot for CaF. PUMP transitions from Q_2 of $C^2\Pi$ - $X^2\Sigma$. This type of plot is discussed in Part 6.1.1. It is used to identify branches. Some of the assigned branches are labeled with ΔN, n* and Λ.

Figure 6.9 n*=13 stacked plot for CaF. PUMP transitions from R_{21} of $C^2\Pi$ - $X^2\Sigma$. This type of plot is discussed in Part 6.1.1. It is used to identify branches. Some of the assigned branches are labeled with ΔN and ℓ labels.

Figure 6.10 n*=14 stacked plot for CaF. PUMP transitions from R_{21} of $C^2\Pi$ - $X^2\Sigma$. This type of plot is discussed in Part 6.1.1. It is used to identify branches. Some of the assigned branches are labeled with ΔN and ℓ labels.

Figure 6.11 n*=16 stacked plot for CaCl. PUMP transitions from P_2 of $A^2\Pi$ - $X^2\Sigma$. This type of plot is discussed in Part 6.1.1. It is used to identify branches.

Figure 6.12 n*=17 stacked plot for CaCl. PUMP transitions from P_2 of $A^2\Pi$ - $X^2\Sigma$. This type of plot is discussed in Part 6.1.1. It is used to identify branches. The spectra from the $P_2(11.5)$ PUMP transition are missing because they were never recorded.

Figure 6.13 n*=18 stacked plot for CaCl. PUMP transitions from P$_2$ of A$^2\Pi$ - X$^2\Sigma$. This type of plot is discussed in Part 6.1.1. It is used to identify branches. The spectra from the P$_2$(8.5) and P$_2$(11.5) PUMP transitions are missing because they were never recorded.

Figure 6.14 This figure shows why comparing two spectra recorded from J and J+2 intermediate levels allows J to be assigned . The open arrows terminate on - total parity levels. The filled arrows terminate on + total parity levels. The horizontal arrows identify pairs of levels which will have the same term value. The R-P label above the arrow describes the transitions in terms of ΔJ. The O-Q and R-P labels above the ΔJ labels describe the transitions in terms of ΔN.

Figure 6.15 A sample of spectra with P(ΔJ=-1) and R(ΔJ=1) assignments. This type of plot is discussed in Part 6.1.2. This plot shows how the R lines from the Q$_2$(2.5) PUMP transition are at the same term value as the P lines from the Q$_2$(4.5) PUMP transition and the P lines from the Q$_2$(6.5) PUMP transition are at the same term value as the R lines from the Q$_2$(4.5) PUMP transition (comparing two spectra recorded from J and J+2 intermediate levels allows J to be assigned).

Figure 6.16 This figure shows how comparing a series of spectra recorded from J, J+1, J+2 and J+3 allows N to be assigned (if the +/- total parity splitting is small). The open arrows terminate on - total parity levels. The filled arrows terminate on + total parity levels.

Figure 6.17 This figure shows what happens to the +/- total parity splitting as the spin splitting and ℓ-uncoupling vary for Λ>0 states. The top line shows how the + and - total parity levels split as the ℓ-uncoupling increases. If the spin-splitting remains constant, the separation between the two - levels and the two + levels will remain constant but the separation between each pair + and - levels will increase. The right side shows what happens if the ℓ-uncoupling remains constant and the spin splitting decreases. When the spin is zero there will only be one + and one - total parity level, this is represented by the overlap of the dashed and solid gray line. The bottom of the figure shows how this pair of + and - levels behaves if the ℓ-uncoupling increases.

Figure 6.18   This figure shows why comparing spectra from P_2 and Q_2 PUMP transitions allow N-assignments to be made, even in the presence of strong ℓ-uncoupling.   The open arrows terminate on - total parity levels.   The filled arrows terminate on + total parity levels.

Figures 6.19a and 6.19b   A sample of spectra with O(ΔN=-2), P(ΔN=-1), Q(ΔN=0) or R(ΔN=1) assignments.   This type of plot is discussed in Part 6.1.3.   These figures illustrate the importance of comparing alternating P_2 and Q_2 PUMP transitions vs. Q_2 PUMP transitions only. In Figure 19a the O, P, Q and R lines of the state in the middle of the plot match, however when only the Q_2 branch is used as in Figure 6.19b, these lines no longer match because this state is perturbed by a case d state (see discussion is in Part 6.1.3).   The first state on these plots is close to case b so there is little difference in Figures 6.19a and 6.19b.

Figure 6.20   Reduced term value vs. N(N+1) for n*=13 of CaF.   These spectra were recorded out of the $A^2\Pi$ state.   The +/- labels in the legend box are Kronig symmetry.

Figure 6.21   Reduced term value vs. N(N+1) for n*=13 of CaF.   These spectra were recorded out of the $A^2\Pi$ state.

Figure 6.22 Reduced term value vs N(N+1) for n*=14 of CaF.   These spectra were recorded out of the $A^2\Pi$ state.   The +/- labels in the legend box are Kronig symmetry.

Figure 6.23   Reduced term value vs N(N+1) for n*=14 of CaF.   These spectra were recorded out of the $A^2\Pi$ state. The ℓ=+1 state in these plots is a v=1 state.   It has a v=2 symbol because it is perturbed by a v=2 state (in order to keep smooth, continuous curves).

Figure 6.24   Reduced term value vs J(J+1) for n*=17 and n*=18 of CaF.   These spectra were recorded out of the $A^2\Pi$ state.

Figure 6.25   Reduced term value vs N(N+1) for n*=17 and n*=18 of CaF.   These spectra were recorded out of the $A^2\Pi$ state.

Figure 6.26   Reduced term value vs J(J+1) for n*=7 of CaF.   These spectra were recorded out of the $C^2\Pi$ state.

Figure 6.27 Reduced term value vs N(N+1) for n*=7 of CaF. These spectra were recorded out of the $C^2\Pi$ state.

Figure 6.28 Reduced term value vs N(N+1) for n*=13 of CaF. These spectra were recorded out of the $C^2\Pi$ state. The +/- labels in the legend box are Kronig symmetry.

Figure 6.29 Reduced term value vs N(N+1) for n*=14 of CaF. These spectra were recorded out of the $C^2\Pi$ state. The +/- labels in the legend box are Kronig symmetry.

Figure 6.30 Reduced term value vs N(N+1) for n*=14 of CaF. These spectra were recorded out of the $C^2\Pi$ state. The ℓ=+1 and ℓ= +1 g states in these plots are v=1 states. They have v=2 symbols because they are perturbed by v=2 states (in order to keep smooth, continuos curves).

Figure 6.31 Reduced term value vs N(N+1), and reduced term value vs R(R+1) for n*=14 f and g states of CaF. These spectra were recorded out of the $C^2\Pi$ state.

Figure 6.32 The $0.36^2\Pi$ and ℓ=-3 states of n*= 13-18 for CaF. This figure shows how the basic pattern is repeated at each value of n*.

Figure 6.33 Reduced term value vs N(N+1) for n*=16 of CaCl. These spectra were recorded out of the $A^2\Pi$ state. The +/- labels in the legend box are Kronig symmetry.

Figure 6.34 Reduced term value vs N(N+1) for n*=17 and n*=18 of CaCl. These spectra were recorded out of the $A^2\Pi$ state. The +/- labels in the legend box are Kronig symmetry.

Figure 6.35 High-n* spectra of CaF showing a few members of the Rydberg series that were used to determine the v=1 ionization potential. These spectra were recorded out of the $A^2\Pi$ (0,0) state.

Figure 6.36 High-n* spectra of CaCl showing a few members of the Rydberg series that were used to determine the v=1 ionization potential. These spectra were recorded out of the $A^2\Pi$ (0,0) state. The $Ca^{37}Cl$ spectra which was used to determine vibrational

assignments (from the expected isotope shift) is also included in this figure.

Figure 6.37   Preliminary results of MQDT fit.   Only those terms on the plot have been fit (the - Kronig Symmetry states) so only those are presented on this plot.

Figure 6.38   n*=17 complex of $Ca^{35}Cl$ and $Ca^{37}Cl$ showing isotope shifts for v=1 and v=2.   The numbers identify the peaks that the $Ca^{35}Cl$ and $Ca^{37}Cl$ spectra have in common.   These spectra were recorded out of the $A^2\Pi$ (0,0) state.   The isotope shift is 7.2 cm^{-1} and 13.7 cm^{-1} for v=1 and v=2 respectively.   The vibrational constant for $CaCl^+$ is 450 ± 2 cm^{-1}.

Figure 6.1 n*=13 Stacked Plot for CaF A$^2\Pi$ State PUMP
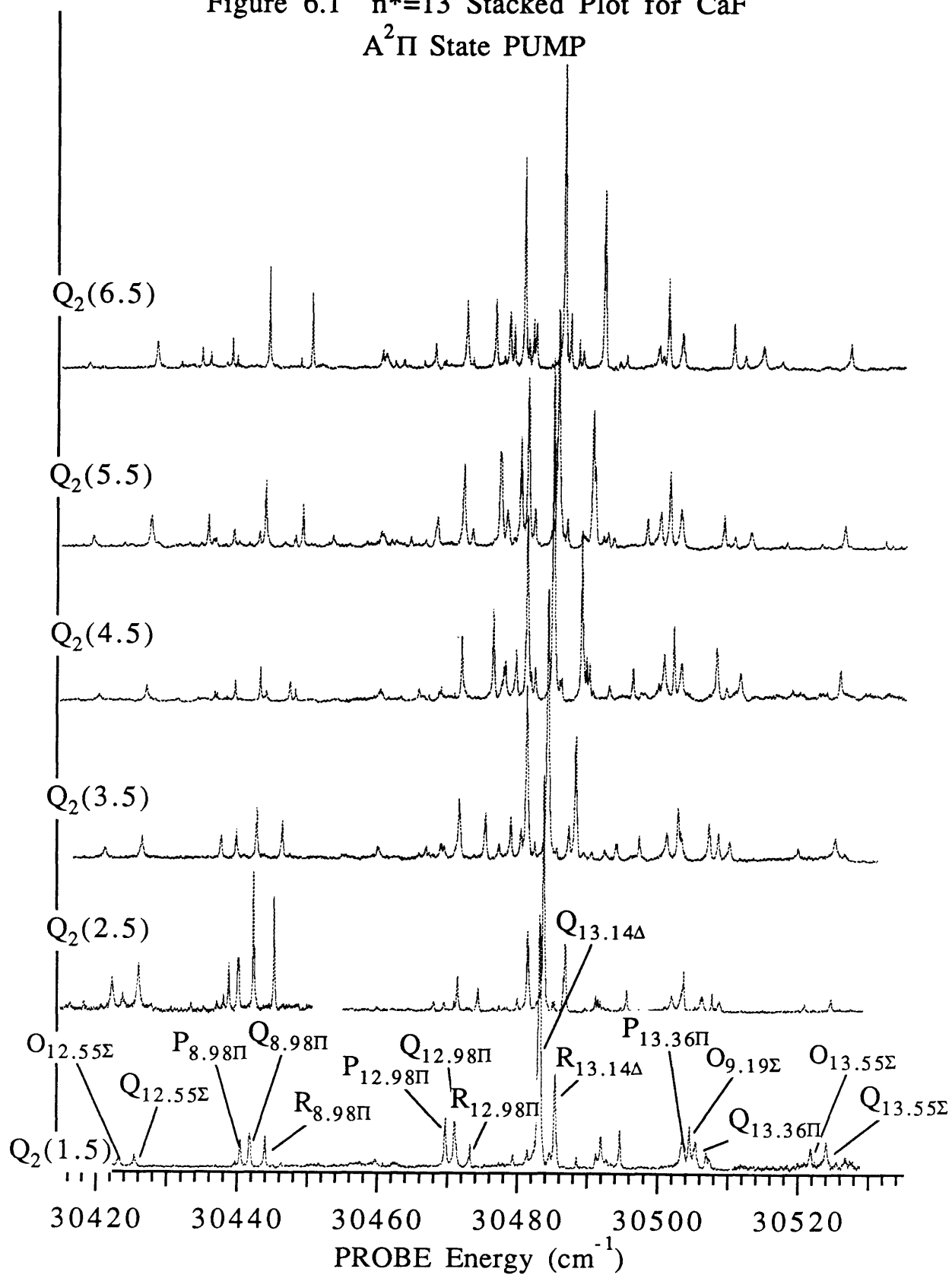
Figure 6.2 n*=13 Stacked Plot for CaF A$^2\Pi$ State PUMP

P$_2$(11.5)

P$_2$(10.5)

P$_2$(9.5)

P$_2$(8.5)

P$_2$(7.5)

P$_2$(6.5)

P$_2$(5.5)

30450   30500   30550

PROBE Energy (cm^{-1})

Figure 6.3 n*=14 Stacked Plot for CaF, $A^2\Pi$ State PUMP

$Q_2(6.5)$

$Q_2(5.5)$

$Q_2(4.5)$

$Q_2(3.5)$

$Q_2(2.5)$

$Q_2(1.5)$

$P_{9.36\Pi}$ $Q_{9.36\Pi}$ $R_{9.36\Pi}$ $Q_{13.98\Pi}$ $Q_{14.14\Delta}$ $O_{9.55\Sigma}$ $Q_{9.55\Sigma}$

$P_{13.98\Pi}$ $R_{13.98\Pi}$ $R_{14.14\Delta}$ $P_{14.36\Pi}$ $Q_{14.36\Pi}$

540   560   580   600

$\nu_{PROBE} - 30000\ cm^{-1}$
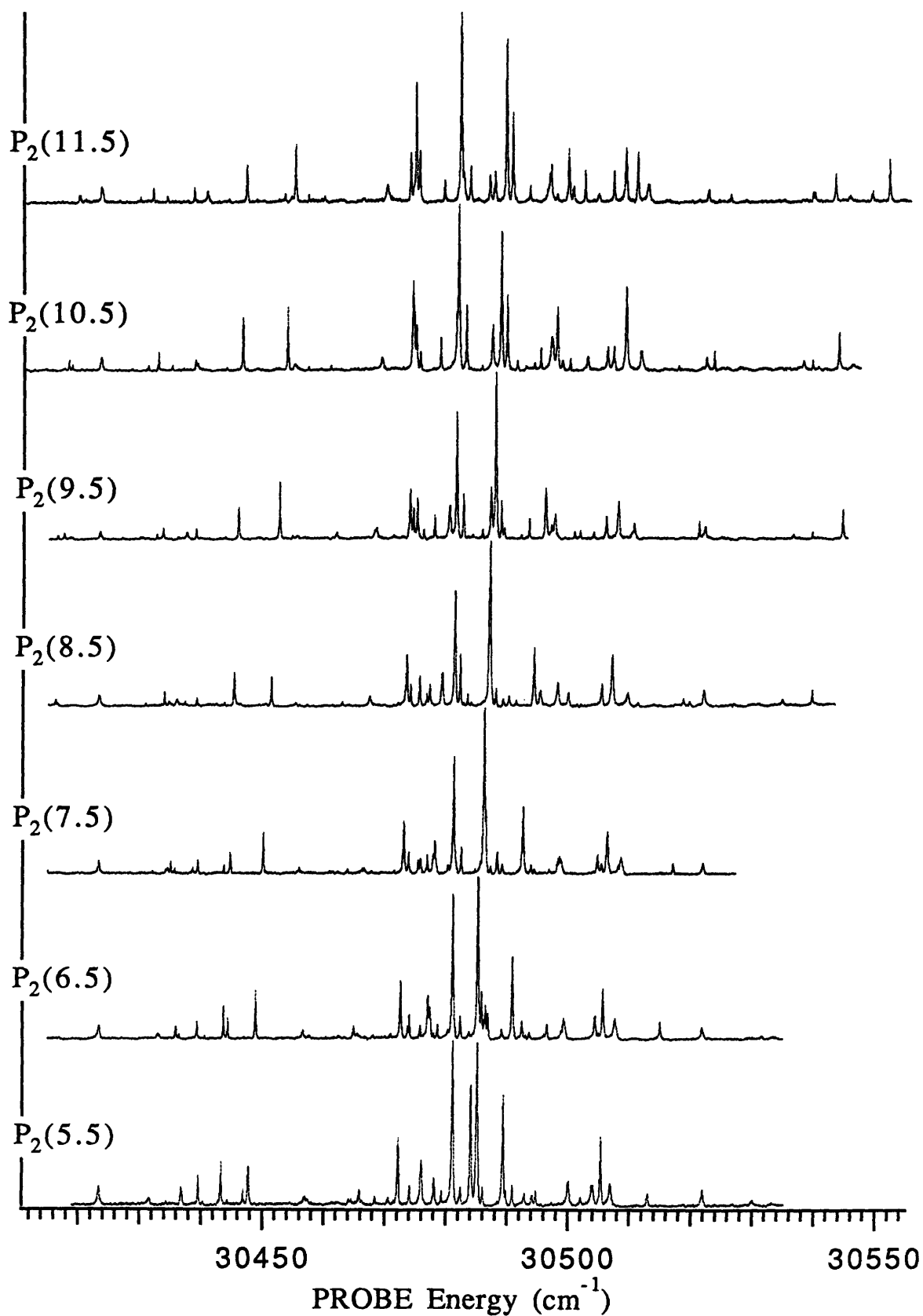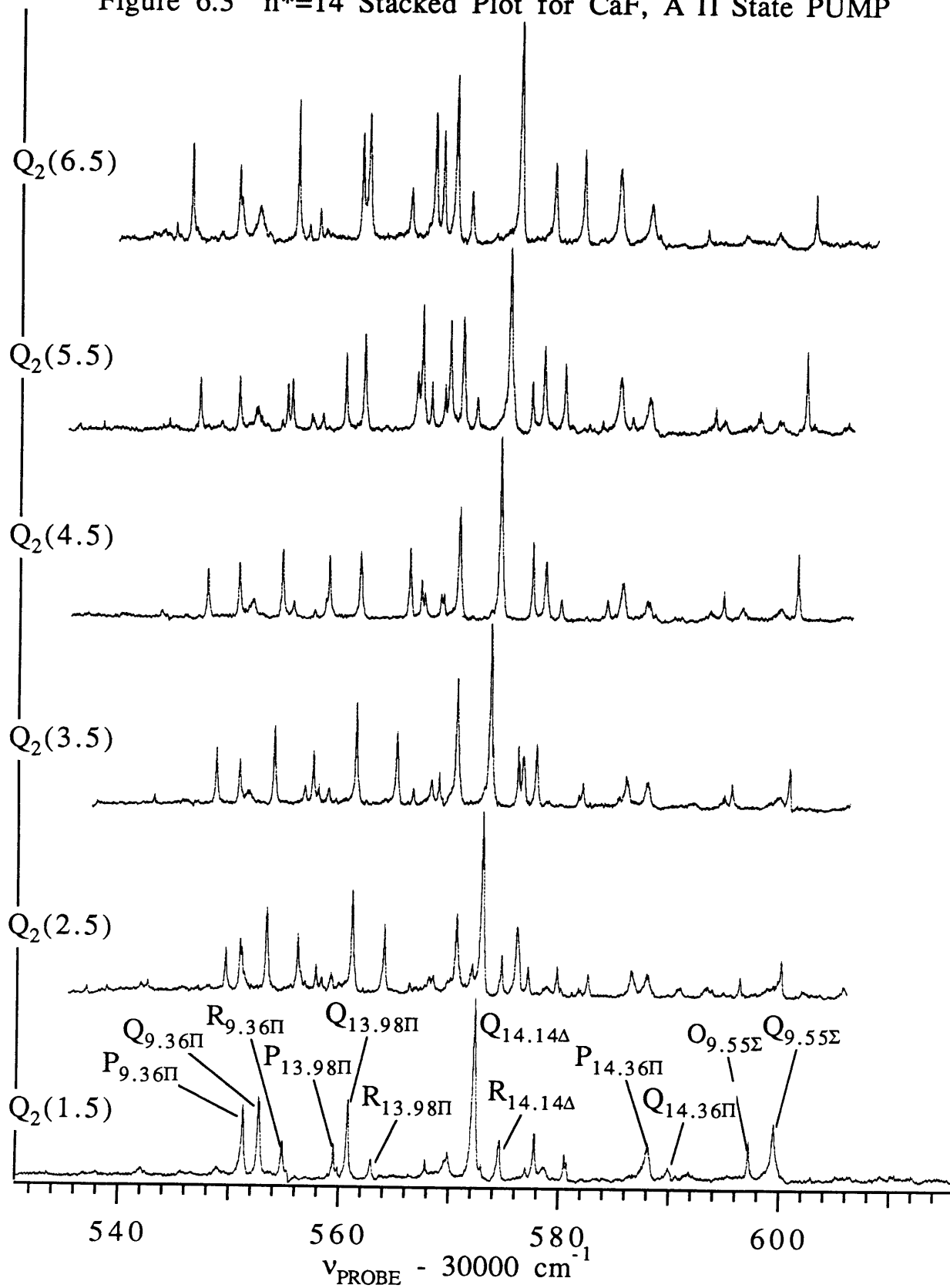
Figure 6.4   n*=14 Stack for CaF, A²Π State PUMP

P₂(11.5)

P₂(10.5)

P₂(9.5)

P₂(8.5)

P₂(7.5)

P₂(6.5)

P₂(5.5)

30540   30560   30580   30600

PROBE Energy (cm⁻¹)

221
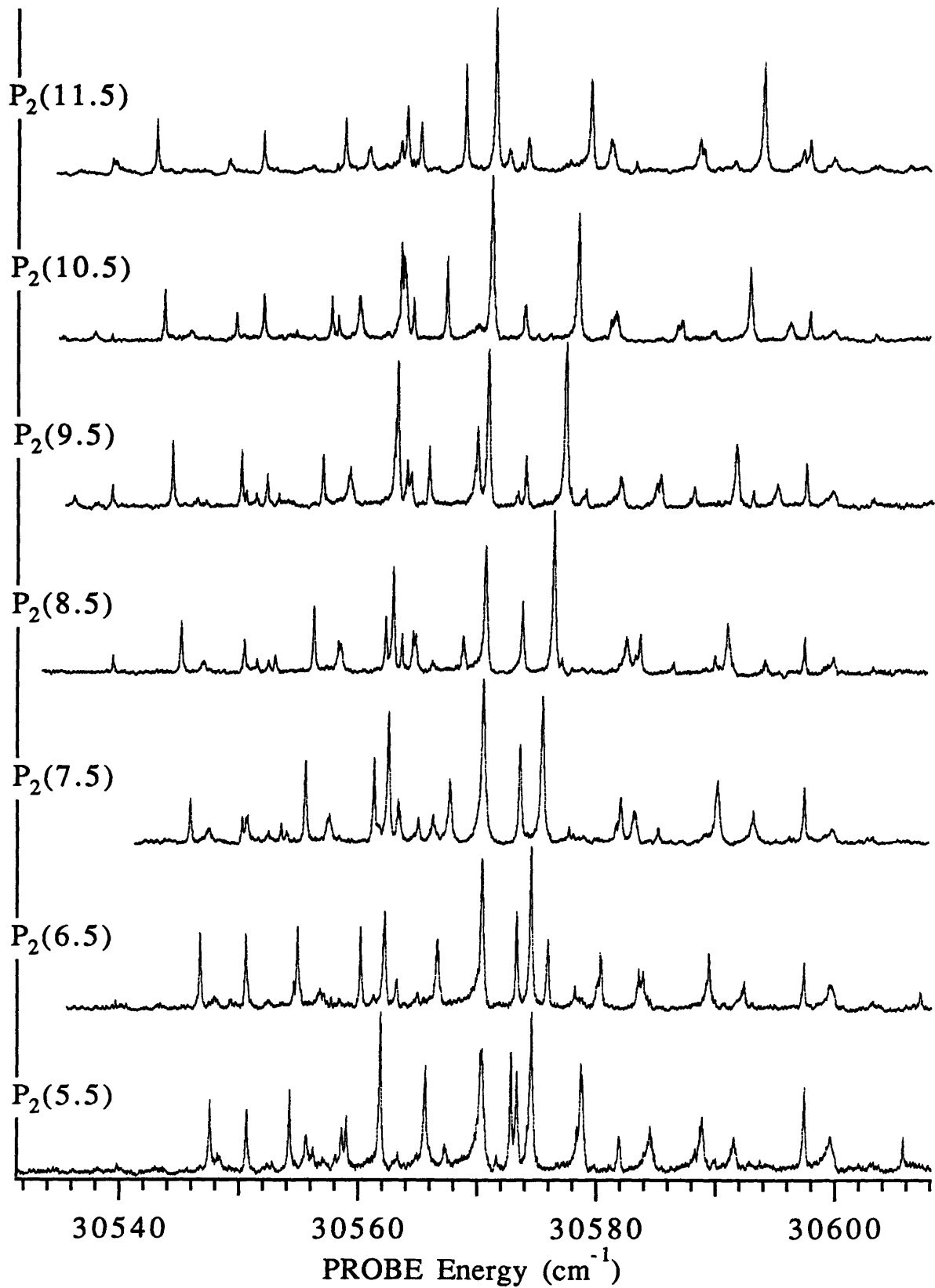
Figure 6.5 n* =17 and n*=18 for CaF, $A^2\Pi$ State PUMP

$Q_2(7.5)$

$Q_2(6.5)$

$Q_2(5.5)$

$Q_2(4.5)$

$Q_2(3.5)$

$Q_2(2.5)$

$10.19\,^2\Sigma$

$10.14\,^2\Delta$

$16.98\,^2\Pi$

$17.14\,^2\Delta$

$17.36\,^2\Pi$

$17.55\,^2\Sigma$

$10.36\,^2\Pi$

$17.98\,^2\Pi$

$18.14\,^2\Delta$

$Q_2(1.5)$

730   740   750   760   770   780   790   800

ν_{PROBE} − 30000 cm^{-1}

222
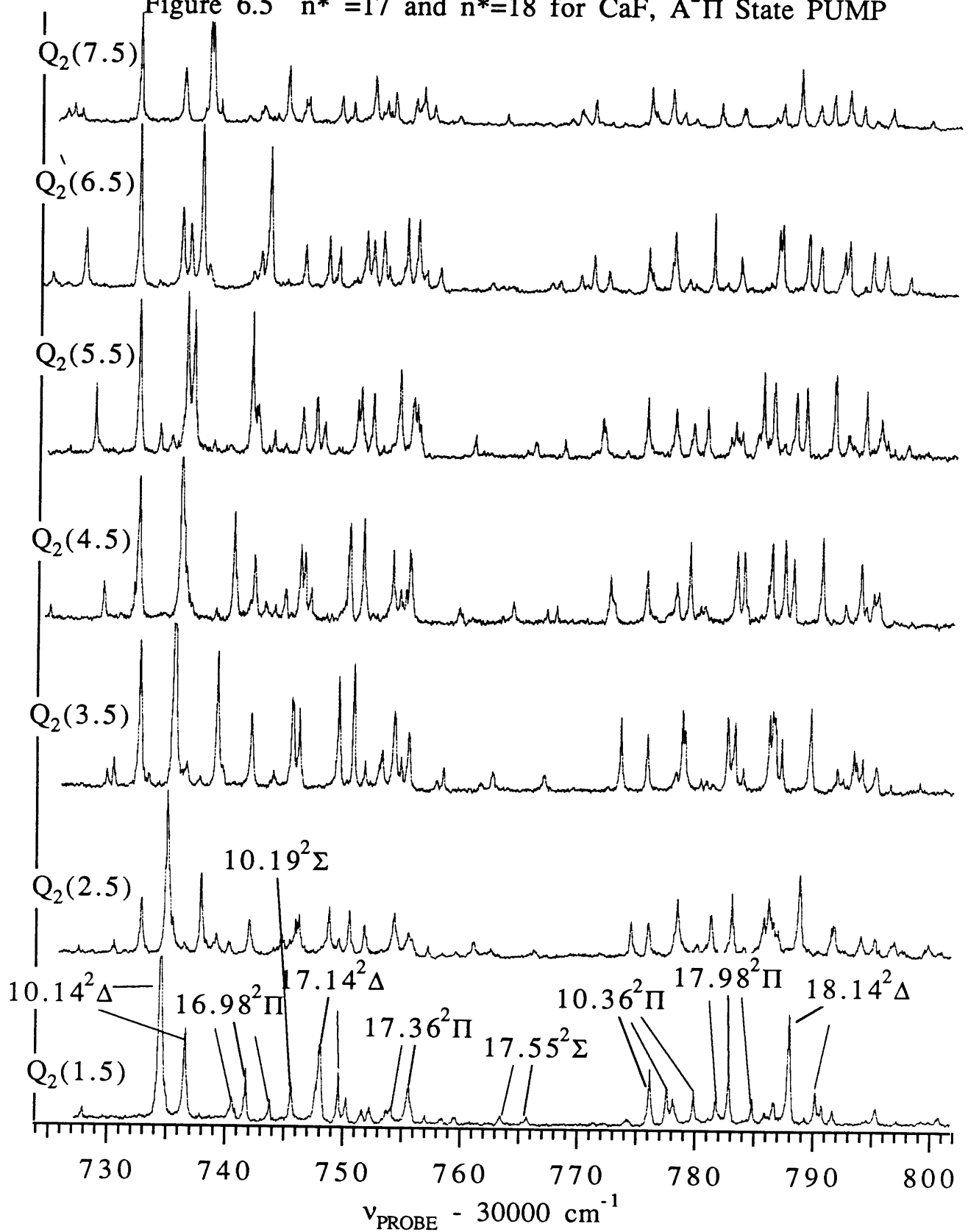
Figure 6.6   n*=17 and n*=18 for CaF, $A^2\Pi$ State PUMP
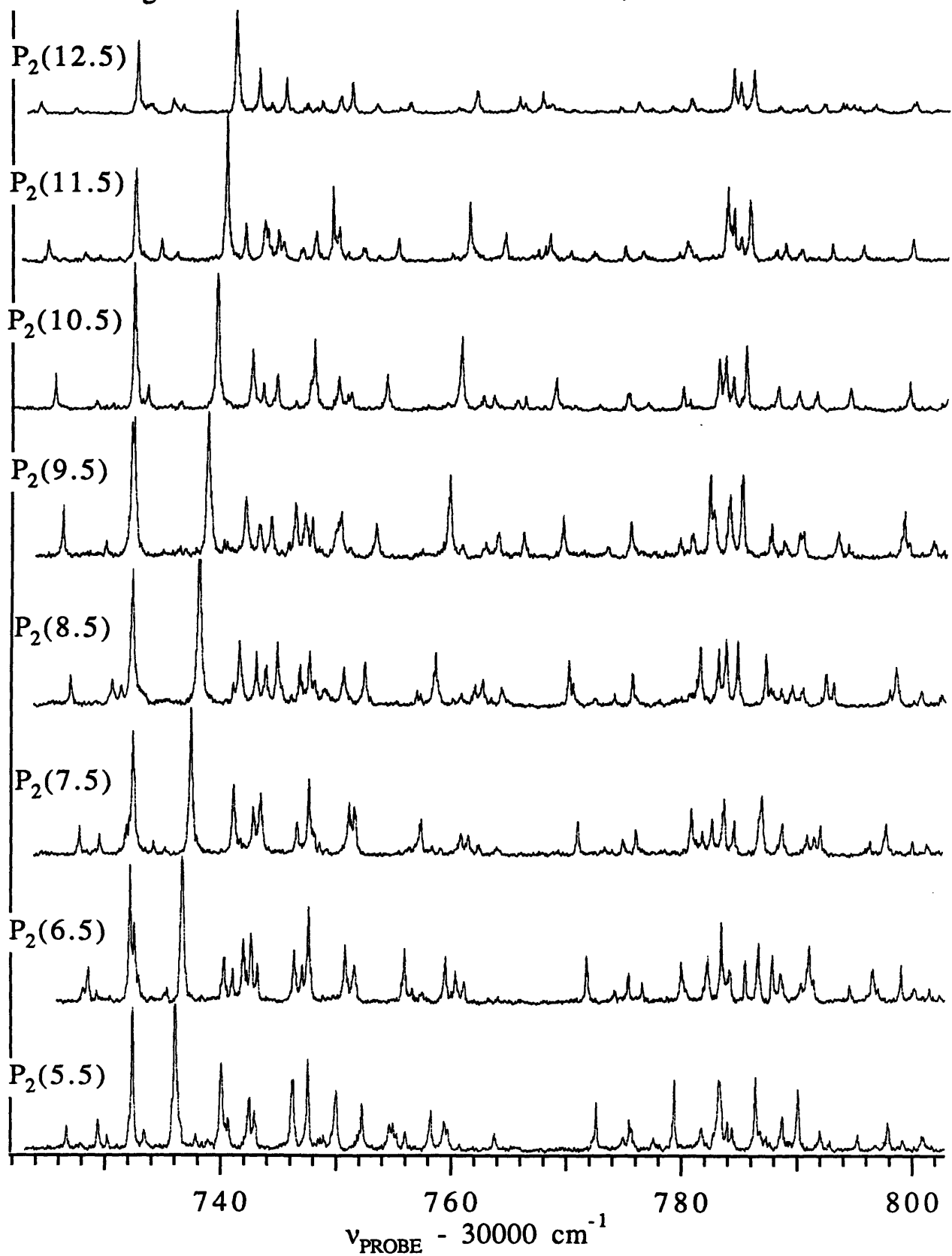
$P_2(12.5)$

$P_2(11.5)$

$P_2(10.5)$

$P_2(9.5)$

$P_2(8.5)$

$P_2(7.5)$

$P_2(6.5)$

$P_2(5.5)$

740   760   780   800

ν_{PROBE} - 30000 cm^{-1}

Figure 6.7 n*=7 Stacked Plot for CaF, $C^2\Pi$ State PUMP

$O_{\ell = +1}$

$P_{\ell = 0}$

$Q_{\ell = +1}$

$R_{\ell = 0}$

$Q_2(13.5)$

$Q_2(12.5)$

$Q_2(11.5)$

$Q_2(10.5)$

$Q_2(9.5)$

$Q_2(8.5)$

$Q_2(7.5)$

$Q_2(6.5)$

$Q_2(5.5)$

470 480 490 500 510 520

$\nu_{PROBE} - 14000 \text{ cm}^{-1}$

Figure 6.8 n*=7 Stacked Plot for CaF, $C^2\Pi$ State PUMP

$Q_2(13.5)$

$O_{5.55\Sigma}$

$Q_{5.55\Sigma}$

$Q_2(11.5)$

$Q_2(10.5)$

$Q_2(9.5)$

$Q_2(8.5)$

$Q_2(7.5)$

$Q_2(6.5)$

530   540   550   560   570   580

$\nu_{PROBE} - 14000 \text{ cm}^{-1}$
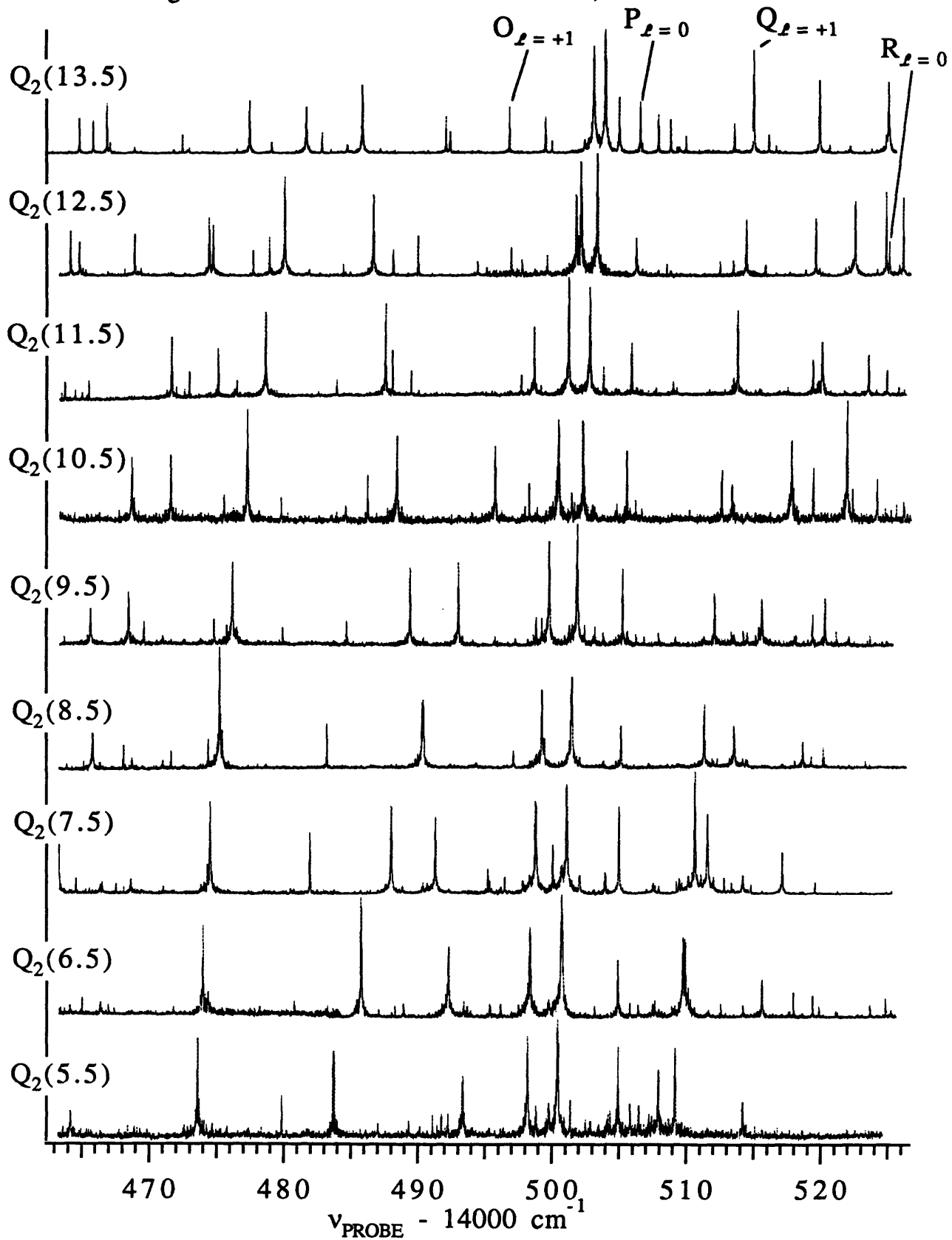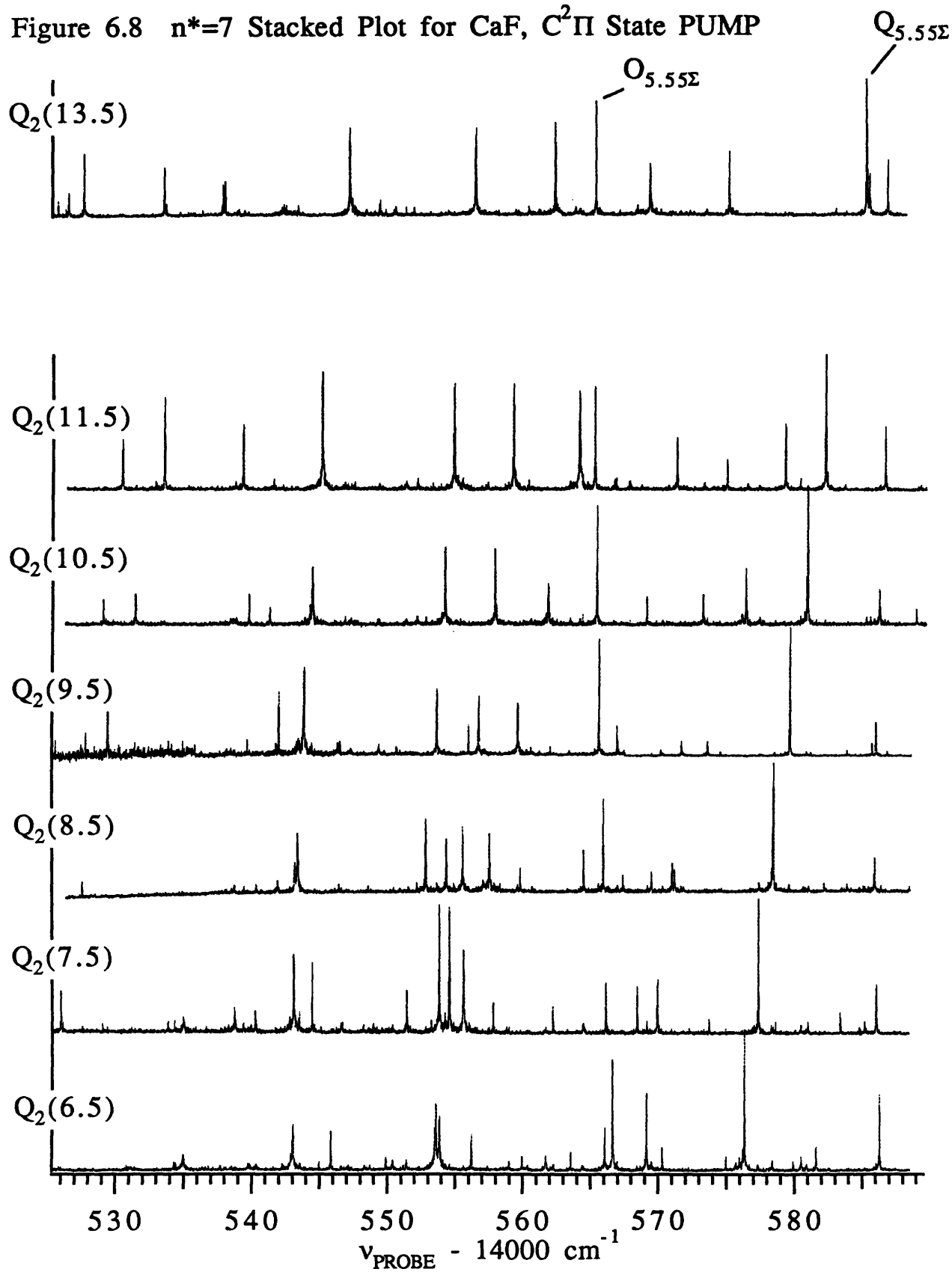
Figure 6.9 n*=13 for CaF, $C^2\Pi$ State PUMP
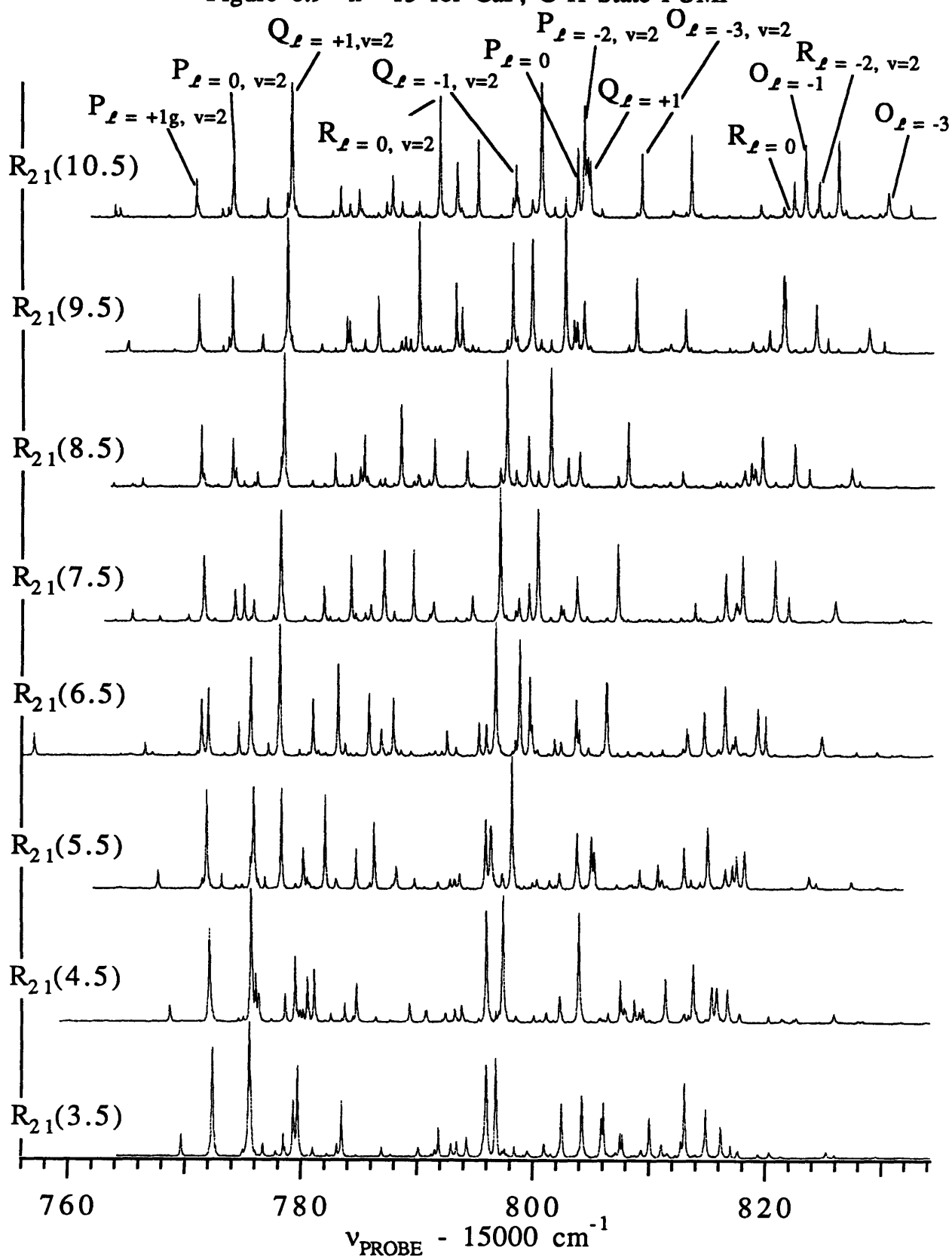
Figure 6.10   n*=14 for CaF, $C^2\Pi$ State PUMP
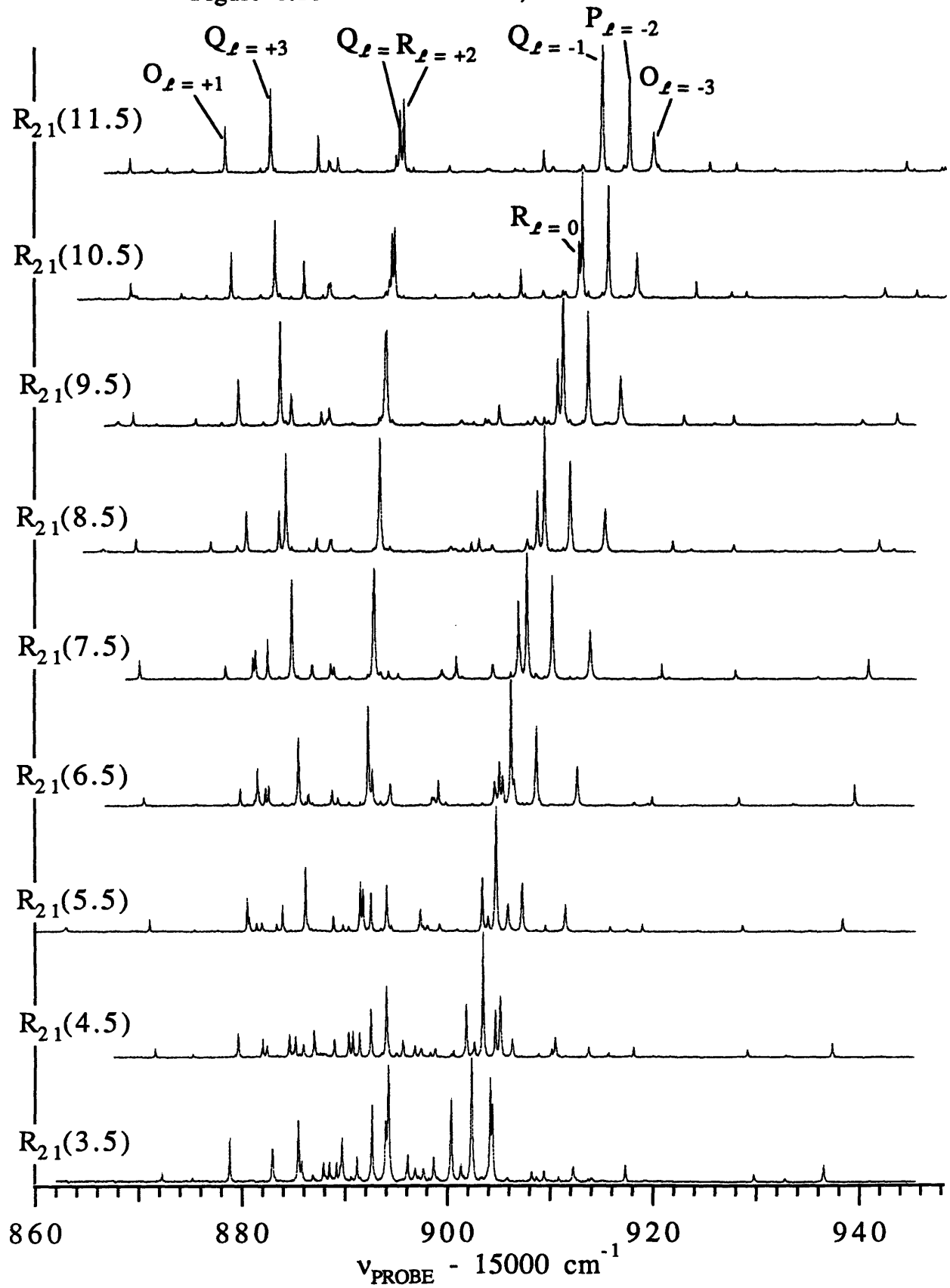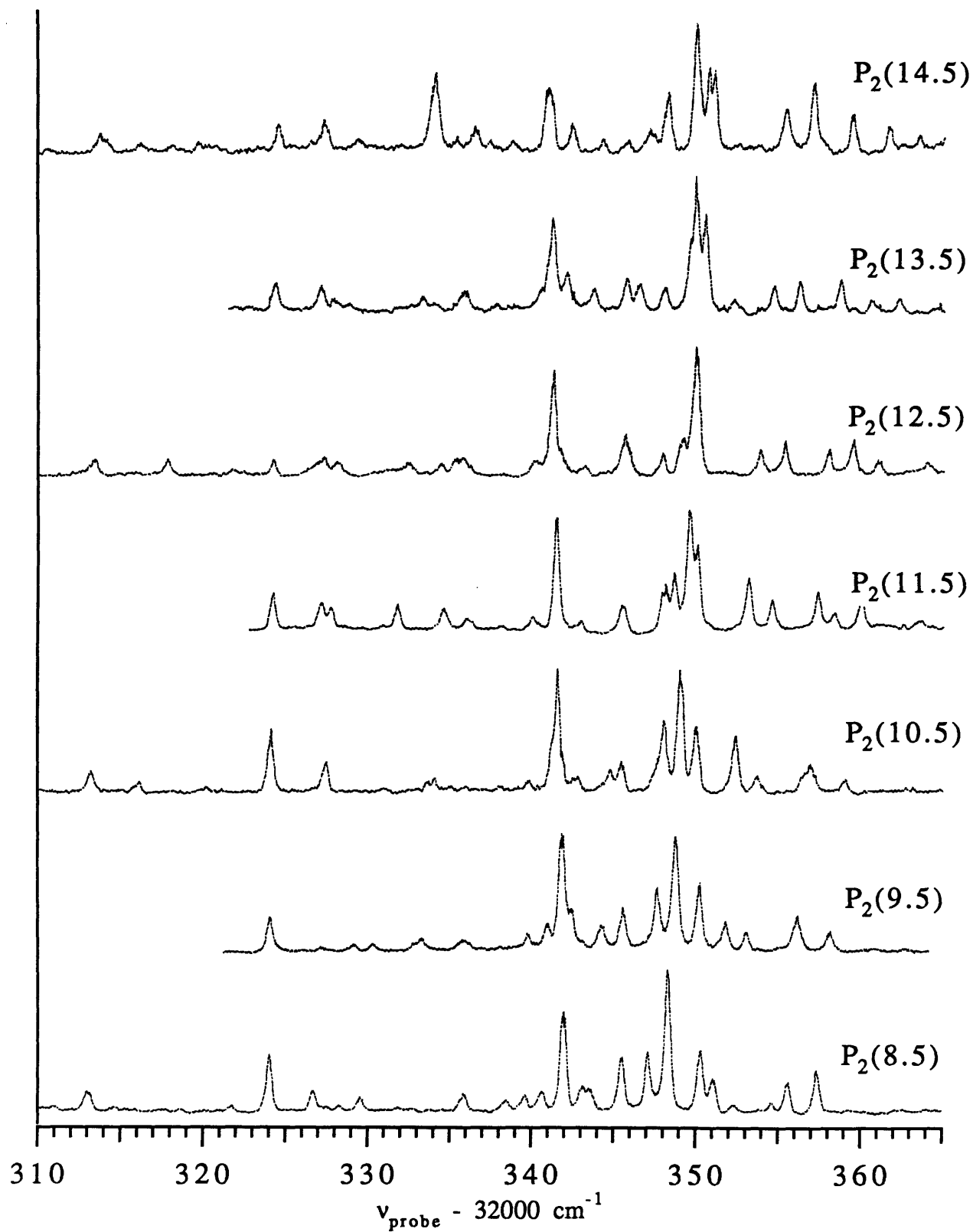
v_{PROBE} - 15000 cm^{-1}

227

Figure 6.11 n*=16 Stacked Plot for CaCl, $A^2\Pi$ State PUMP

$P_2(14.5)$

$P_2(13.5)$

$P_2(12.5)$

$P_2(11.5)$

$P_2(10.5)$

$P_2(9.5)$

$P_2(8.5)$

310   320   330   340   350   360

$\nu_{probe} - 32000$ cm^{-1}

228

Figure 6.12   n*=17 Stacked plot for CaCl, $A^2\Pi$ State PUMP

$P_2(12.5)$

$P_2(10.5)$

$P_2(9.5)$

$P_2(8.5)$

$P_2(7.5)$

32388   32392   32396   32400   32404   32408

PROBE Energy (cm^{-1})

Figure 6.13 n*=18 Stacked plot for CaCl, $A^2\Pi$ State PUMP

$P_2(12.5)$

$P_2(10.5)$

$P_2(9.5)$

$P_2(7.5)$

PROBE Energy (cm^{-1})

32410   32420   32430   32440   32450   32460
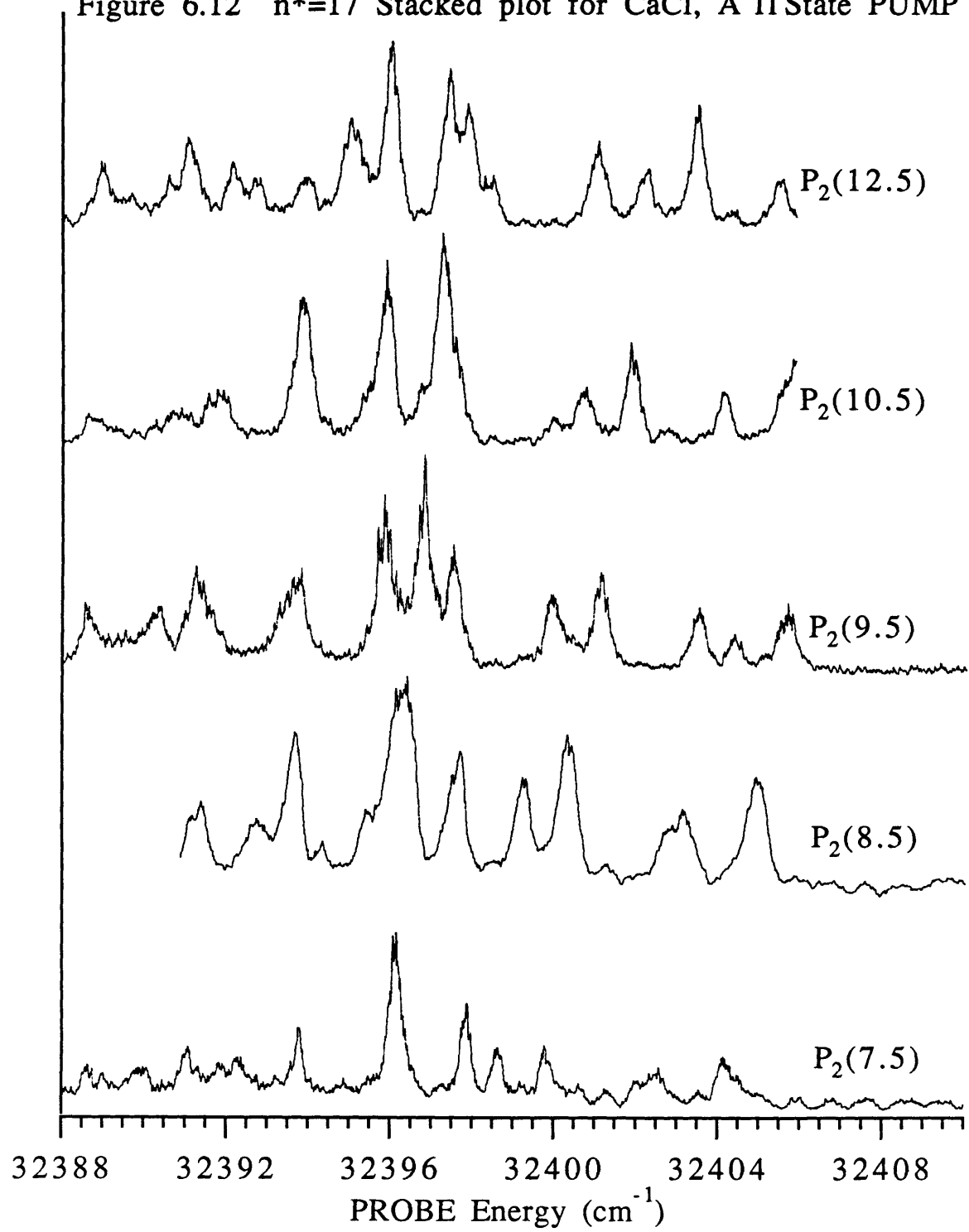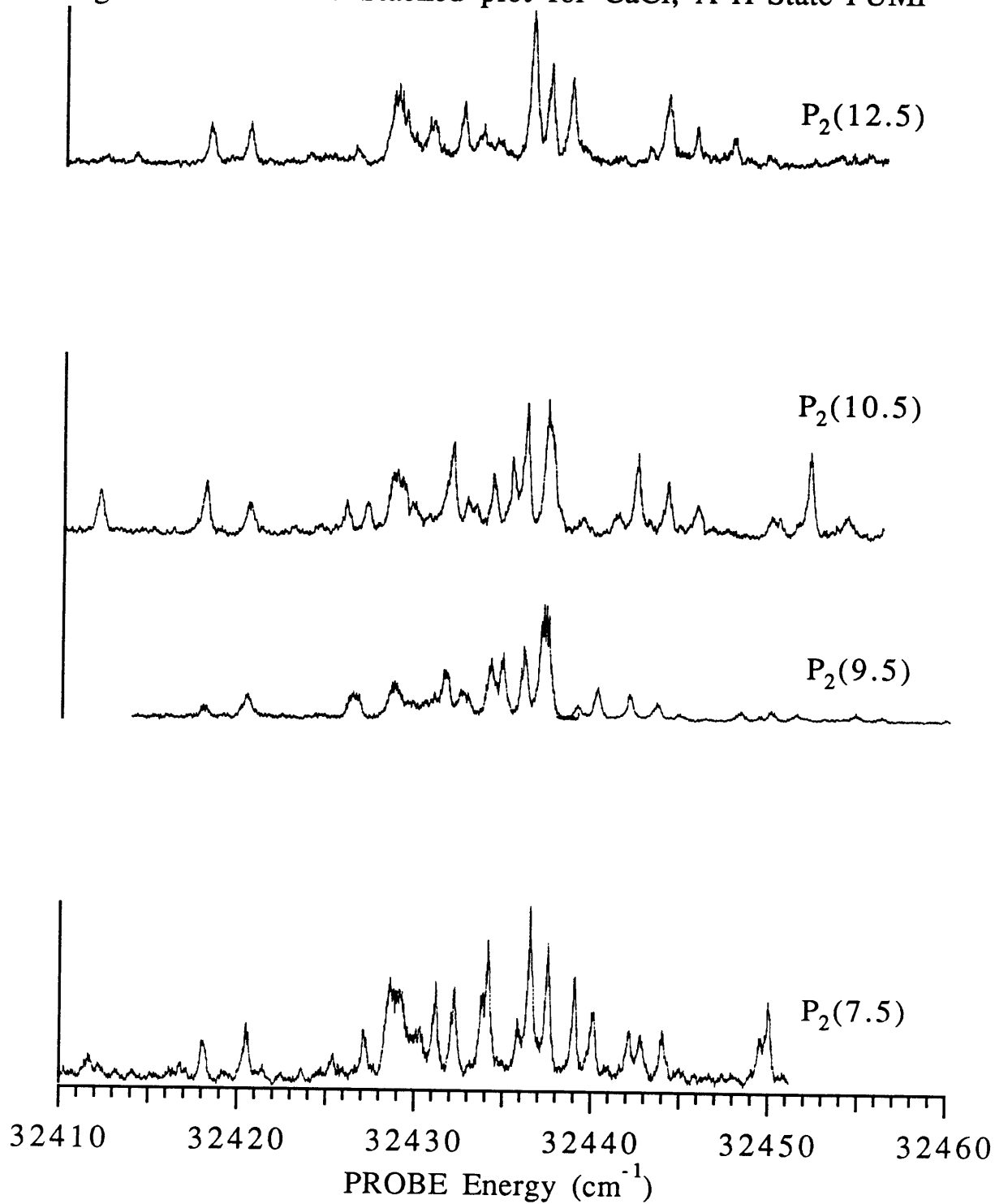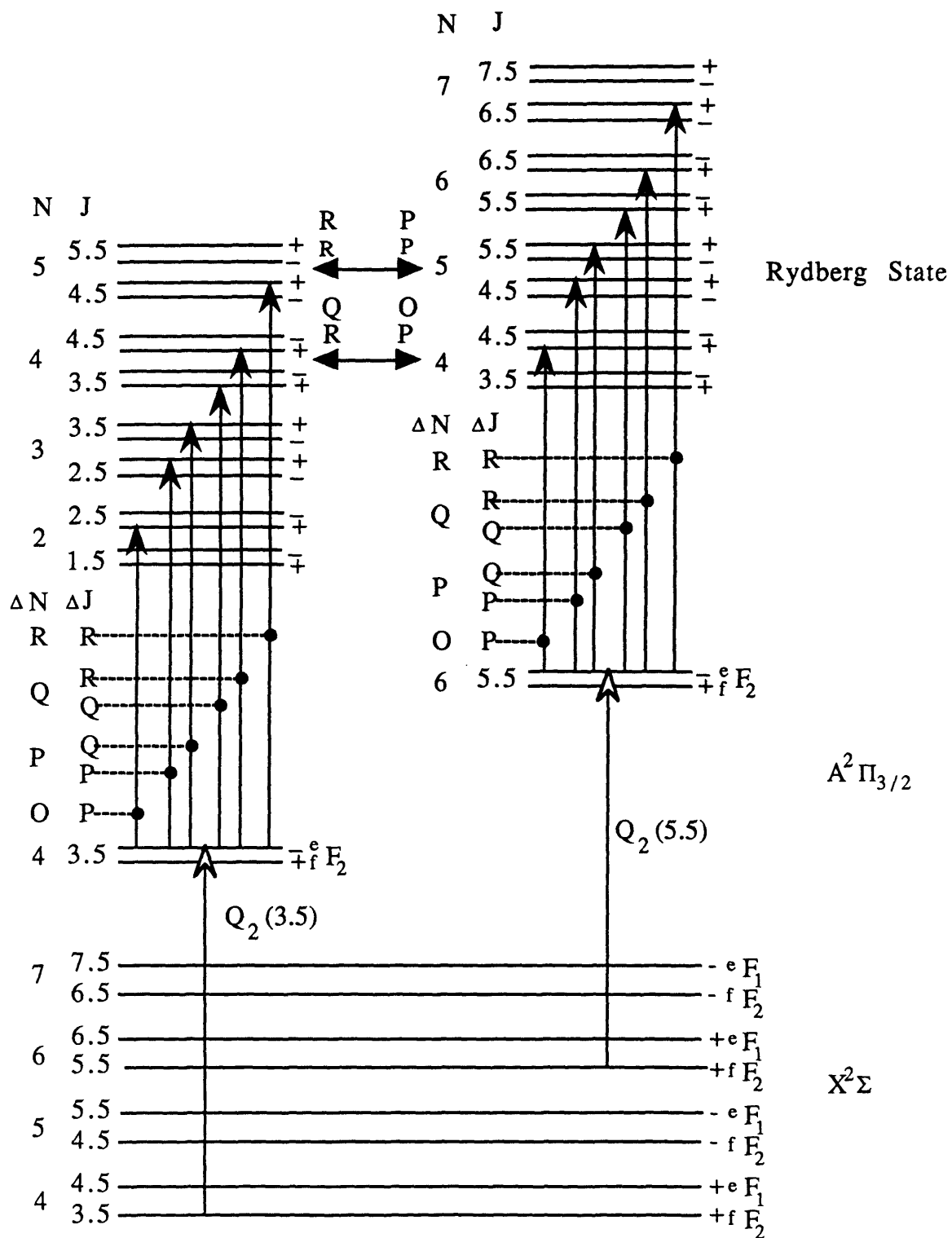
Figure 6.14 Typical $\Lambda > 0$, Case b Rydberg State for CaF

Figure 6.15 n*=14

Term Value - 47000 cm^{-1}
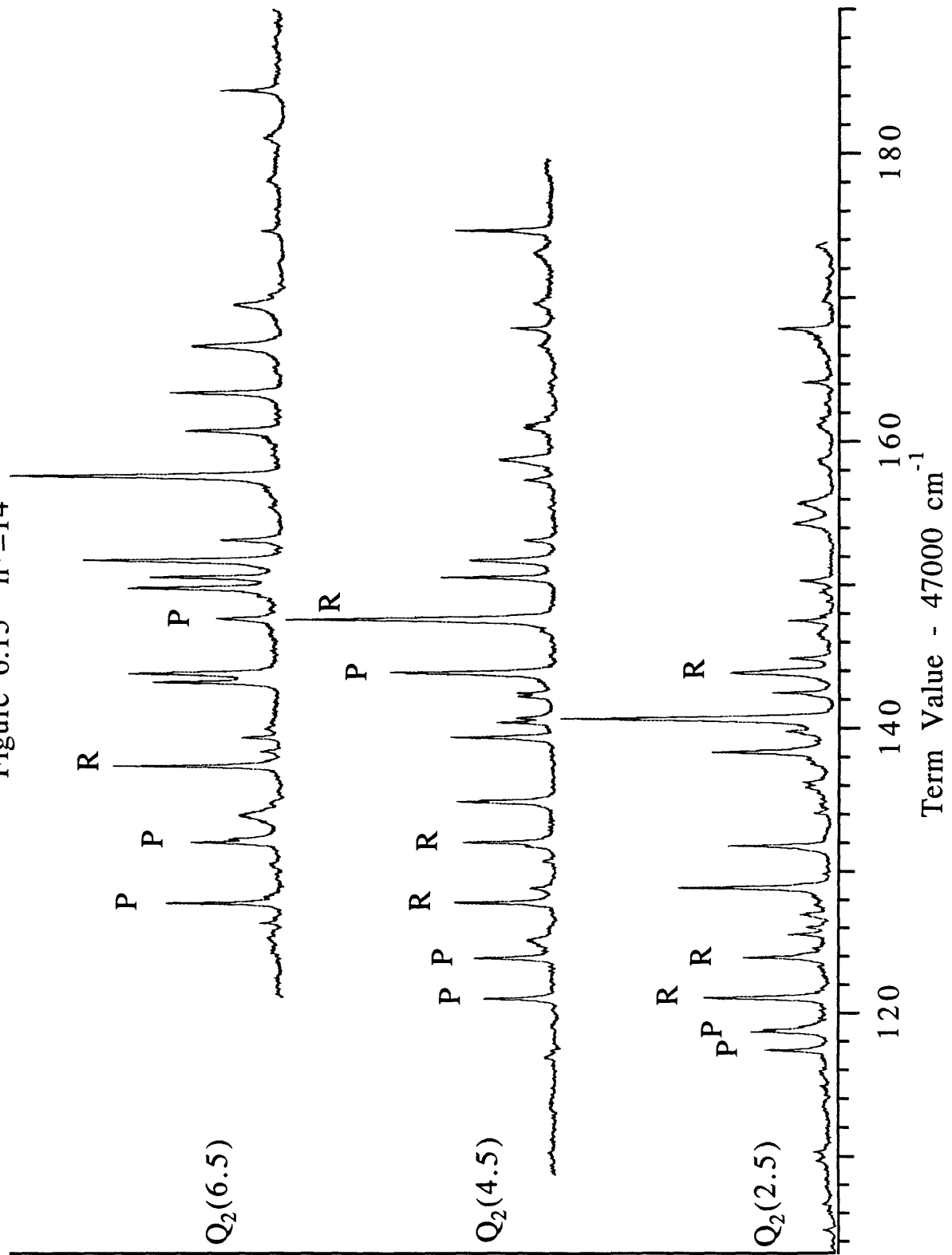
Figure 6.16 Typical Λ > 0, Case b Rydberg State for CaF
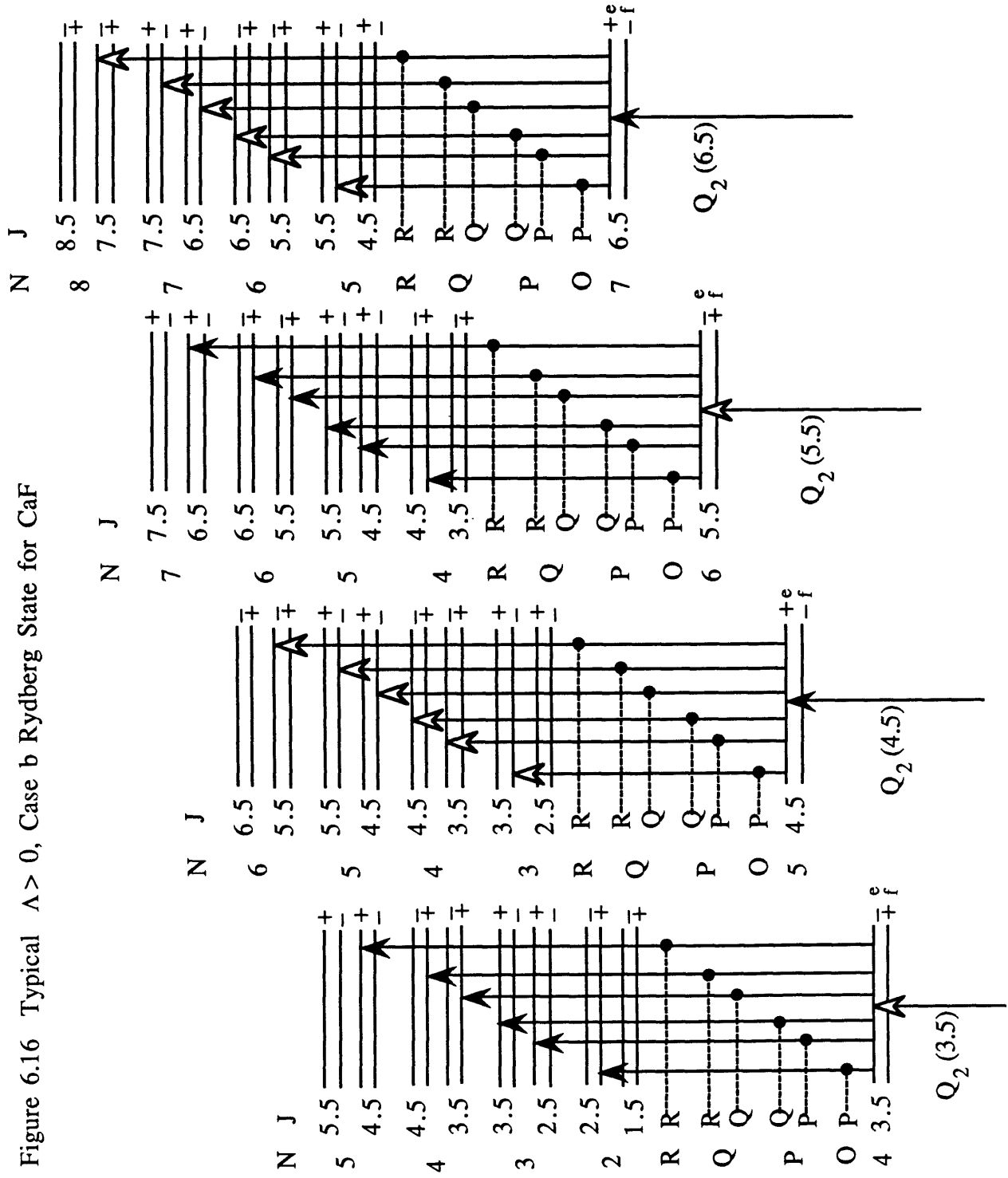
Figure 6.17

Figure 6.18 Typical Λ> 0, Case b Rydberg State for CaF

Figure 6.19a

$P_2(7.5)$ N=7

$Q_2(5.5)$ N=6

$P_2(5.5)$ N=5

$Q_2(3.5)$ N=4

Term Value - 47000 cm^{-1}

110   120   130   140   150   160   170   180
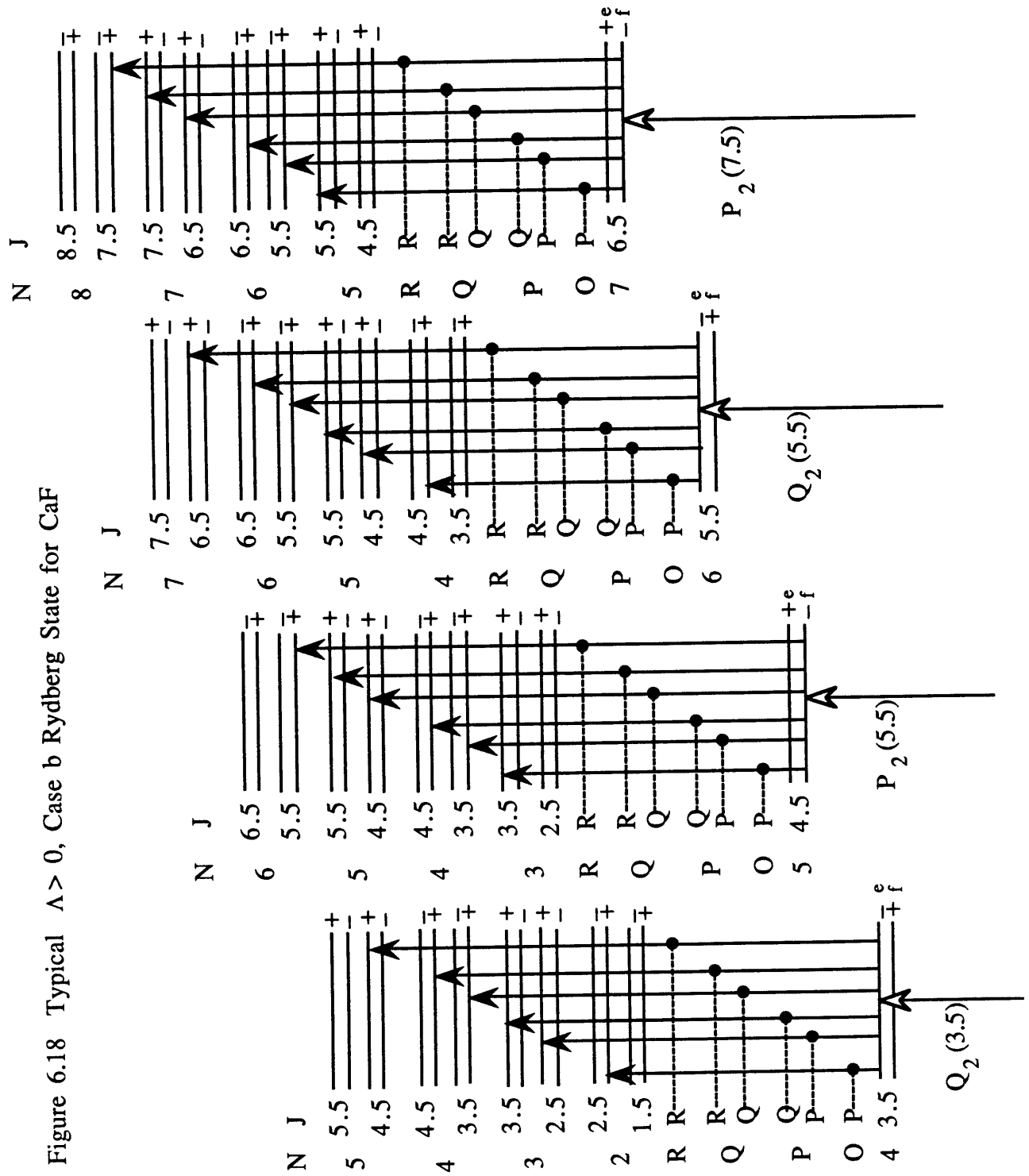
Figure 6.19b
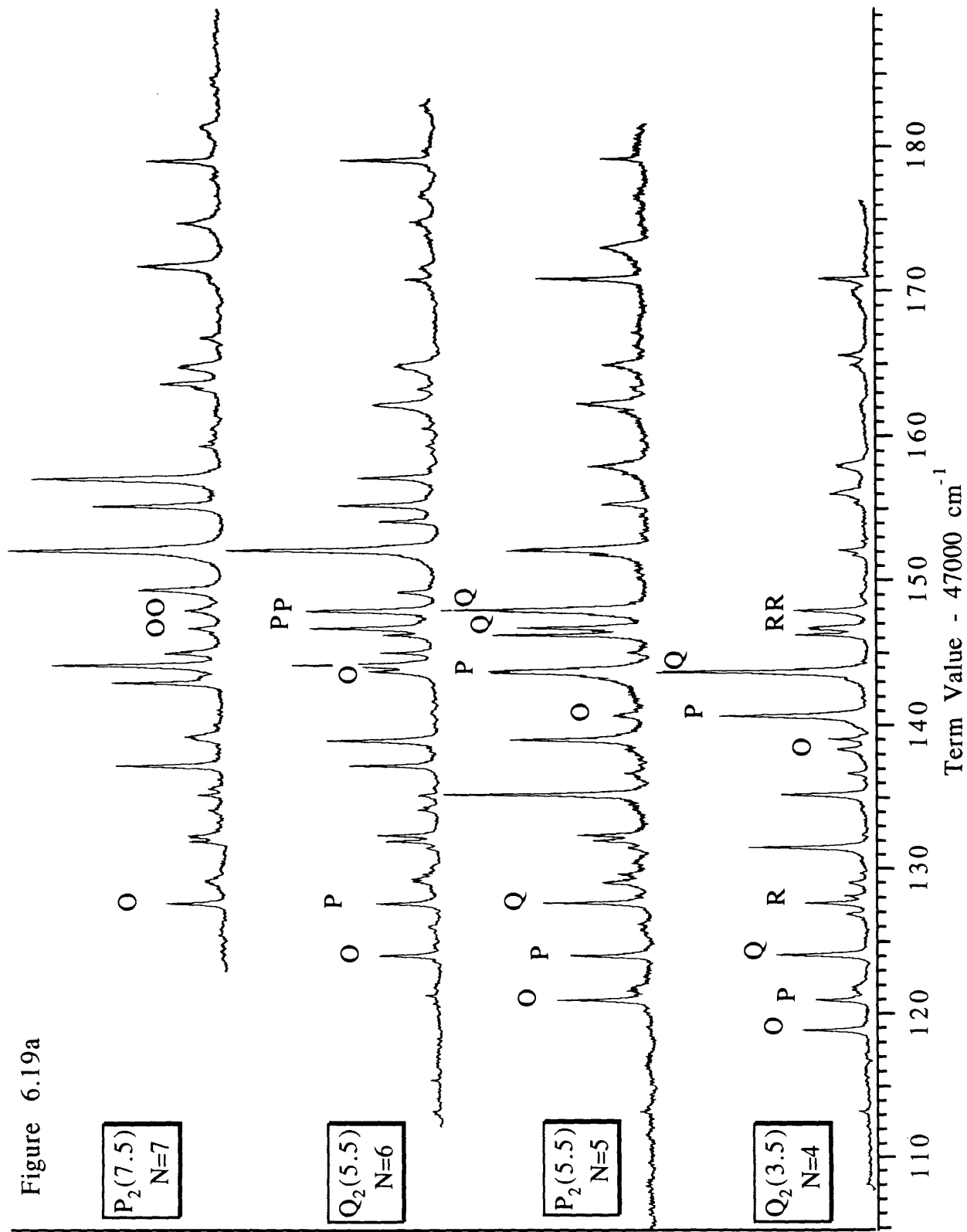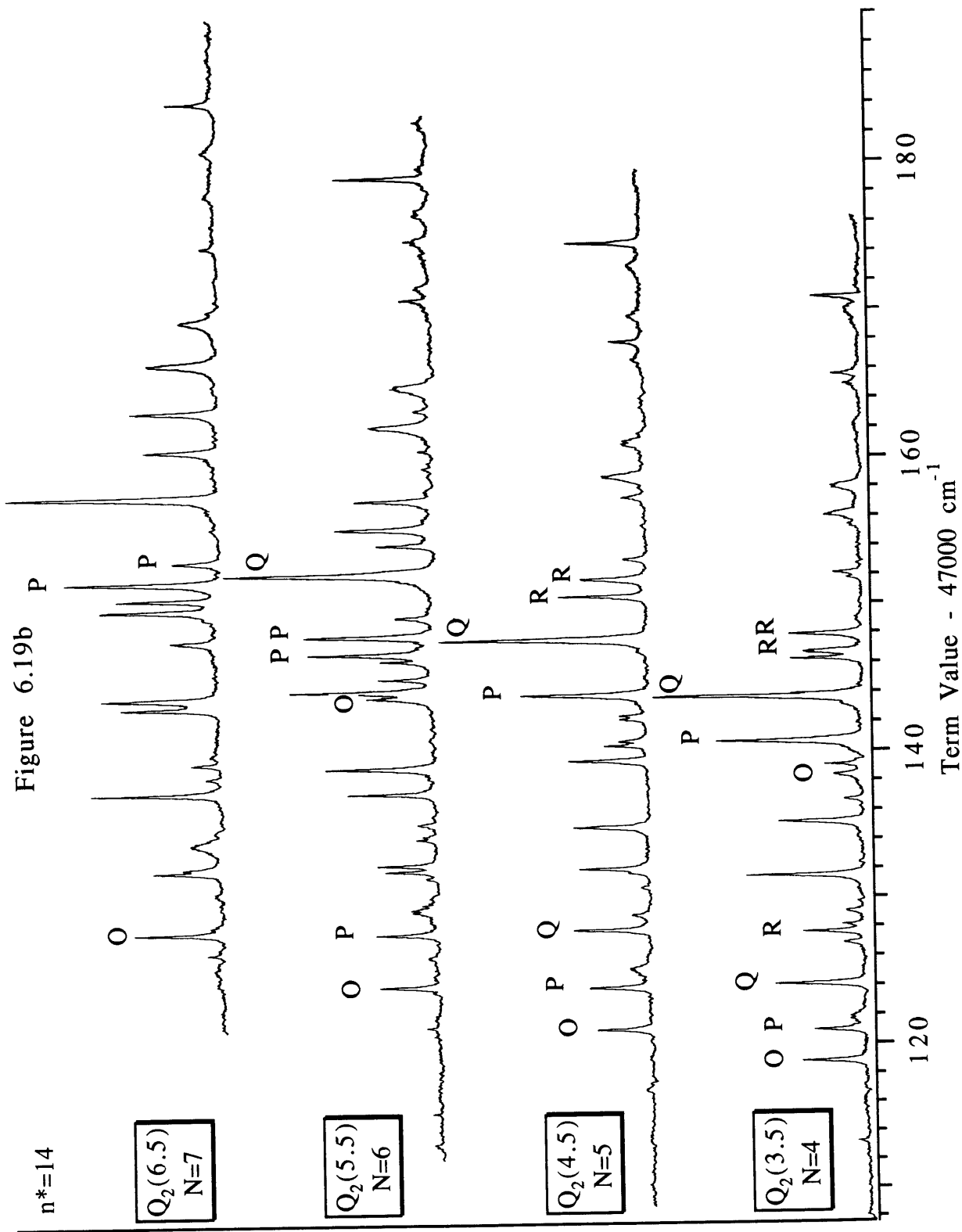
Figure 6.20   n*=13 Term Value Plot for CaF
$A^2\Pi$ state PUMP

Legend:
- ⊕ v=1 +
- ○ v=1 −
- ⊞ v=2 +
- □ v=2 −
- △ v=3 +
- ▽ v=3 −

Reduced Term Value − 47000 cm^{-1}

N(N+1)
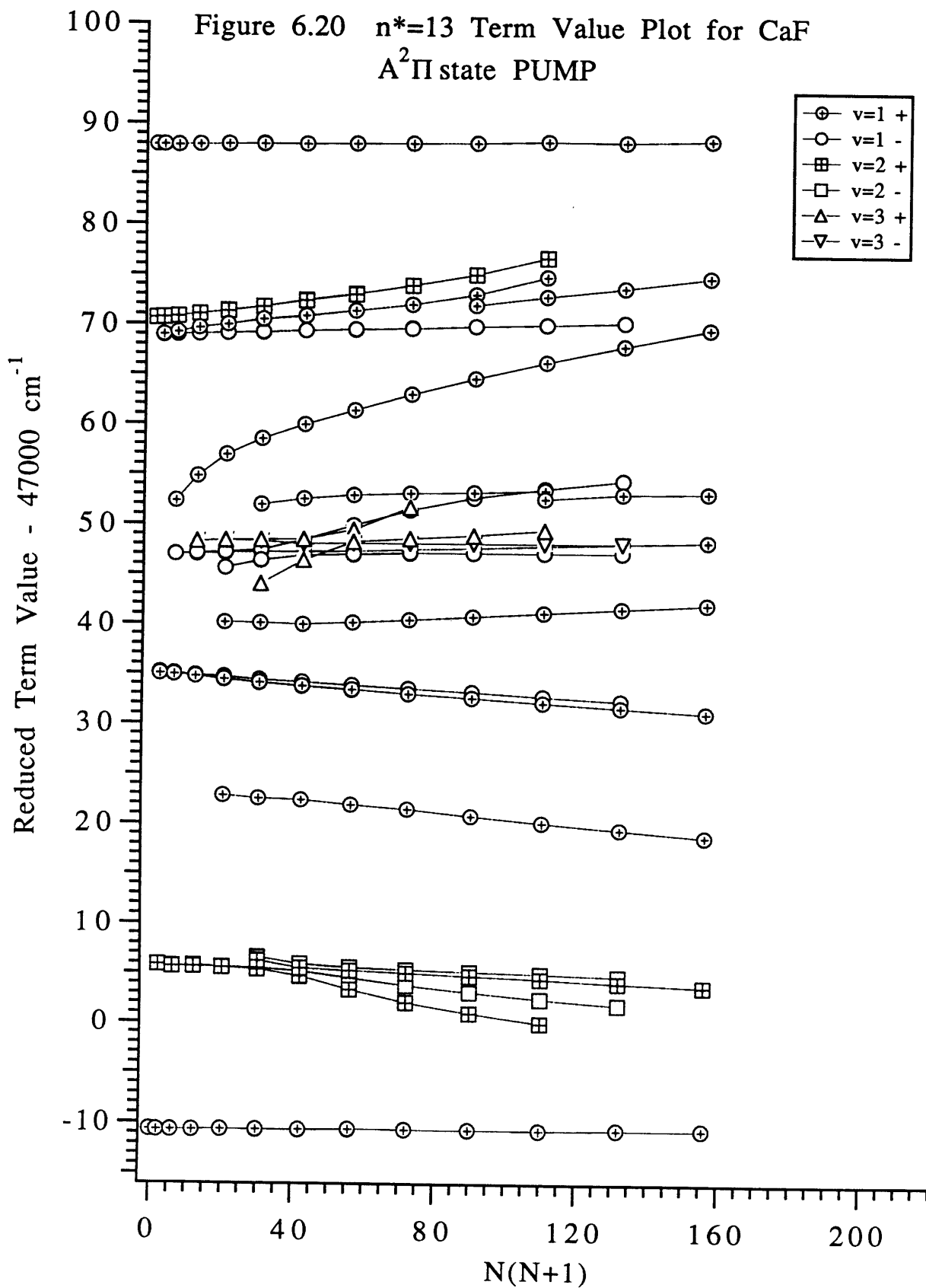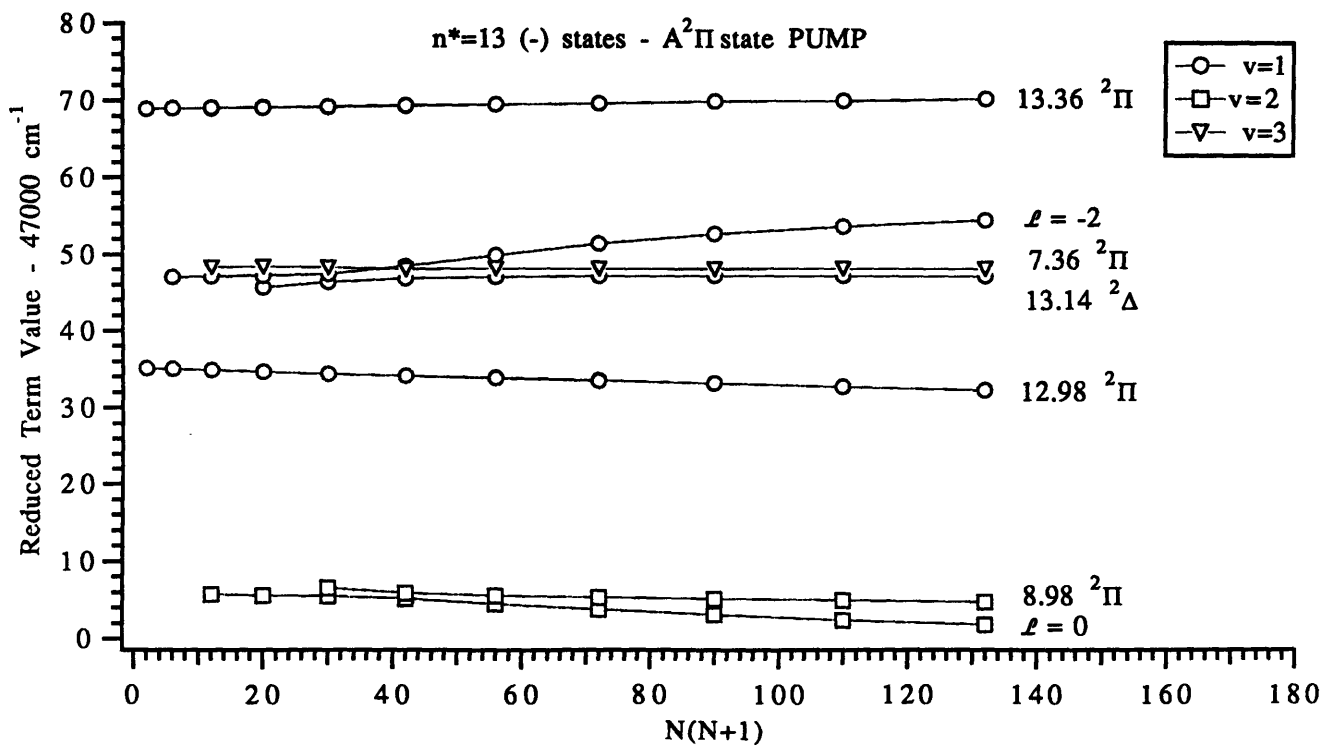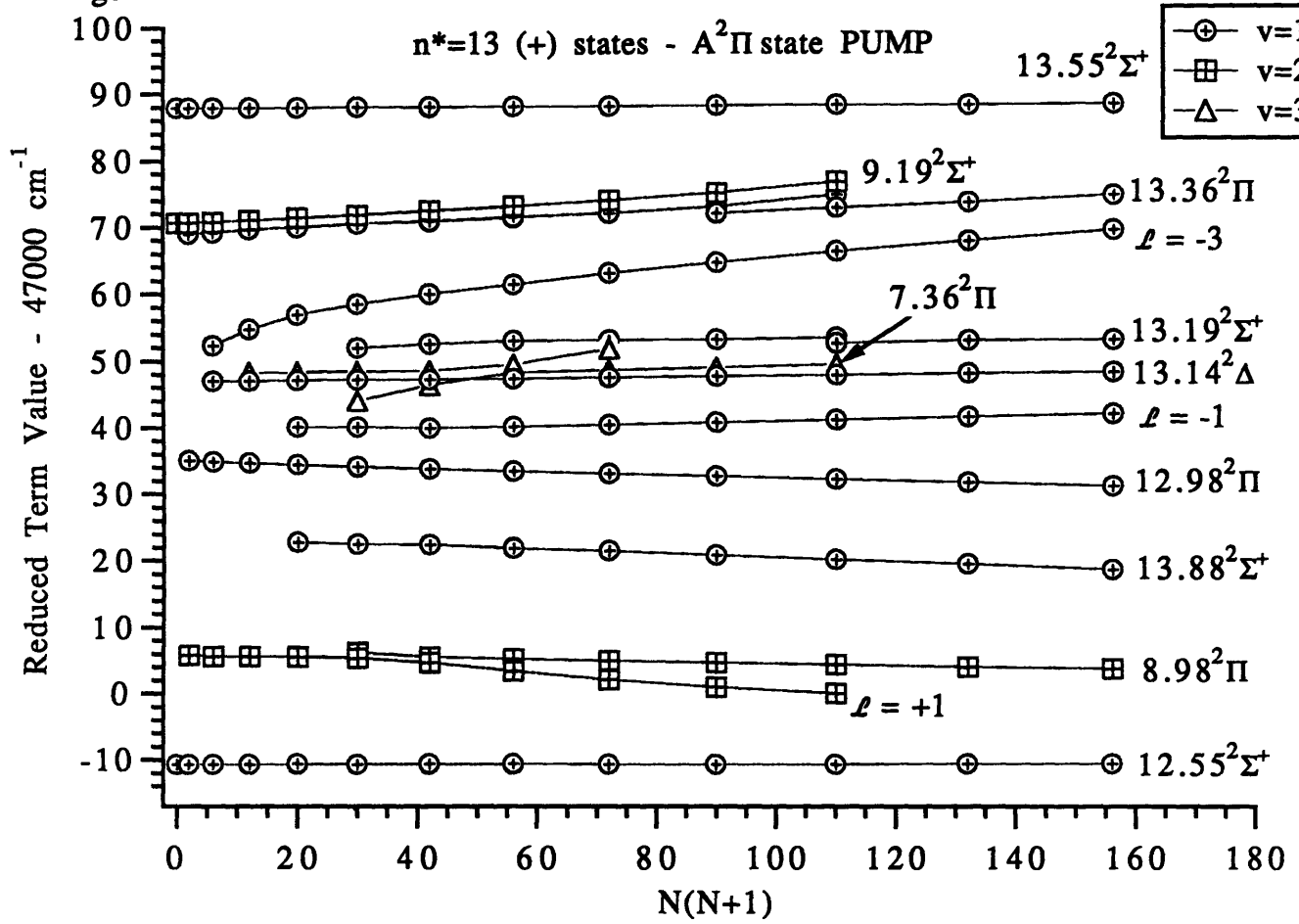
Figure 6.21

Figure 6.22   n*=14   Reduced Term Value Plot for CaF
$A^2\Pi$ State PUMP

Figure 6.23

n*=14 (+) - A$^2\Pi$ State PUMP

n*=14 (-) states - A$^2\Pi$ State PUMP

241
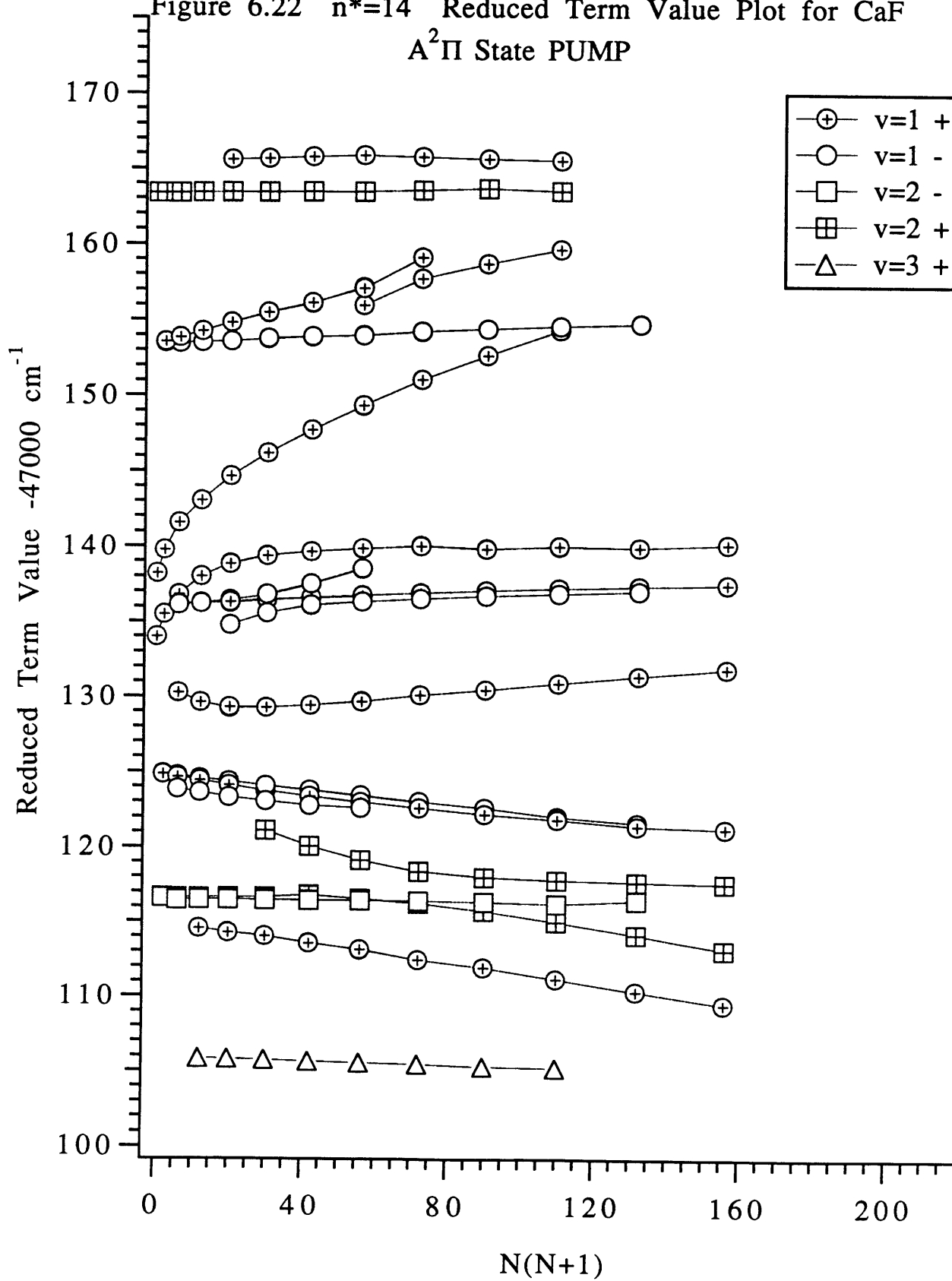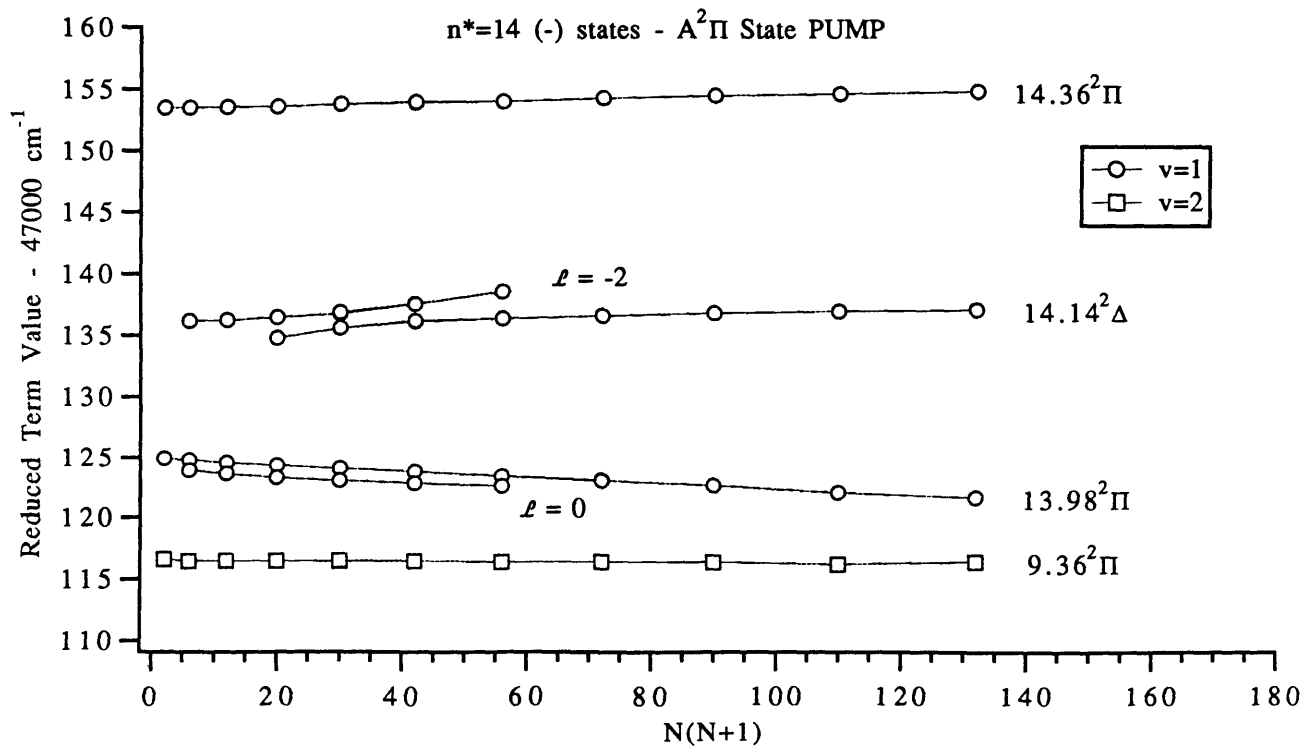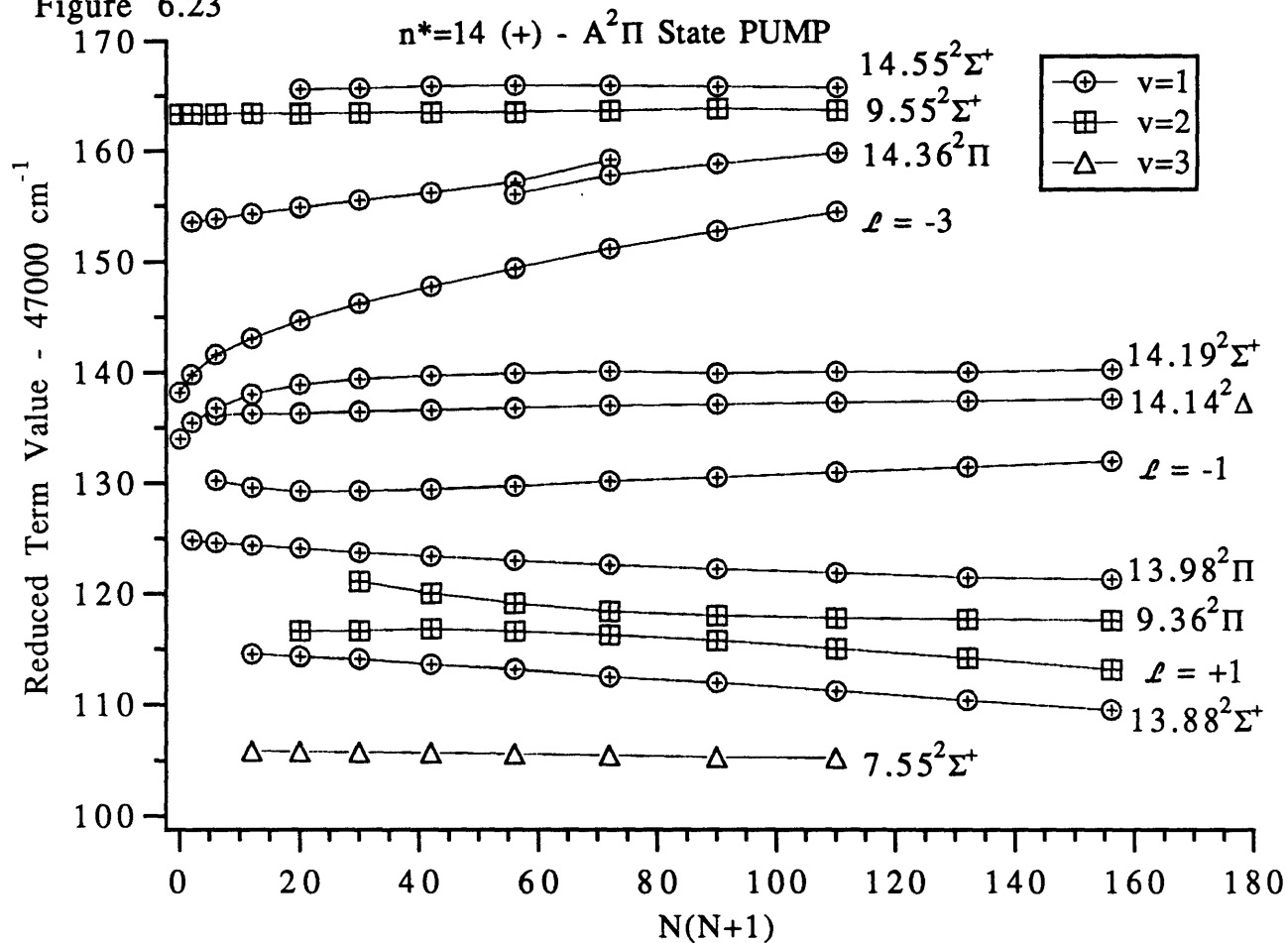
Figure 6.24   n*= 17 and 18 Term Value Plot for CaF
$A^2\Pi$ State PUMP

Figure 6.25 n*=17 and 18 Term Value Plot for CaF A$^2\Pi$ State PUMP

Figure 6.26
n*=7 Reduced Term Value Plot for CaF, C$^2\Pi$ State PUMP

term1
5.55 $^2\Sigma^+$
term3
term4
term5
term6
term7
term8
term9
term10
term11
$\ell=0$, f $^2\Delta$
$\ell=+1$, f $^2\Delta$
term14
term15
term16
term17
term18
term19
term20
term21
term22

Reduced Term Value -44000 cm^{-1}

J(J+1)

Figure 6.27

n*=7 Reduced Term Value Plot for CaF, $C^2\Pi$ State PUMP
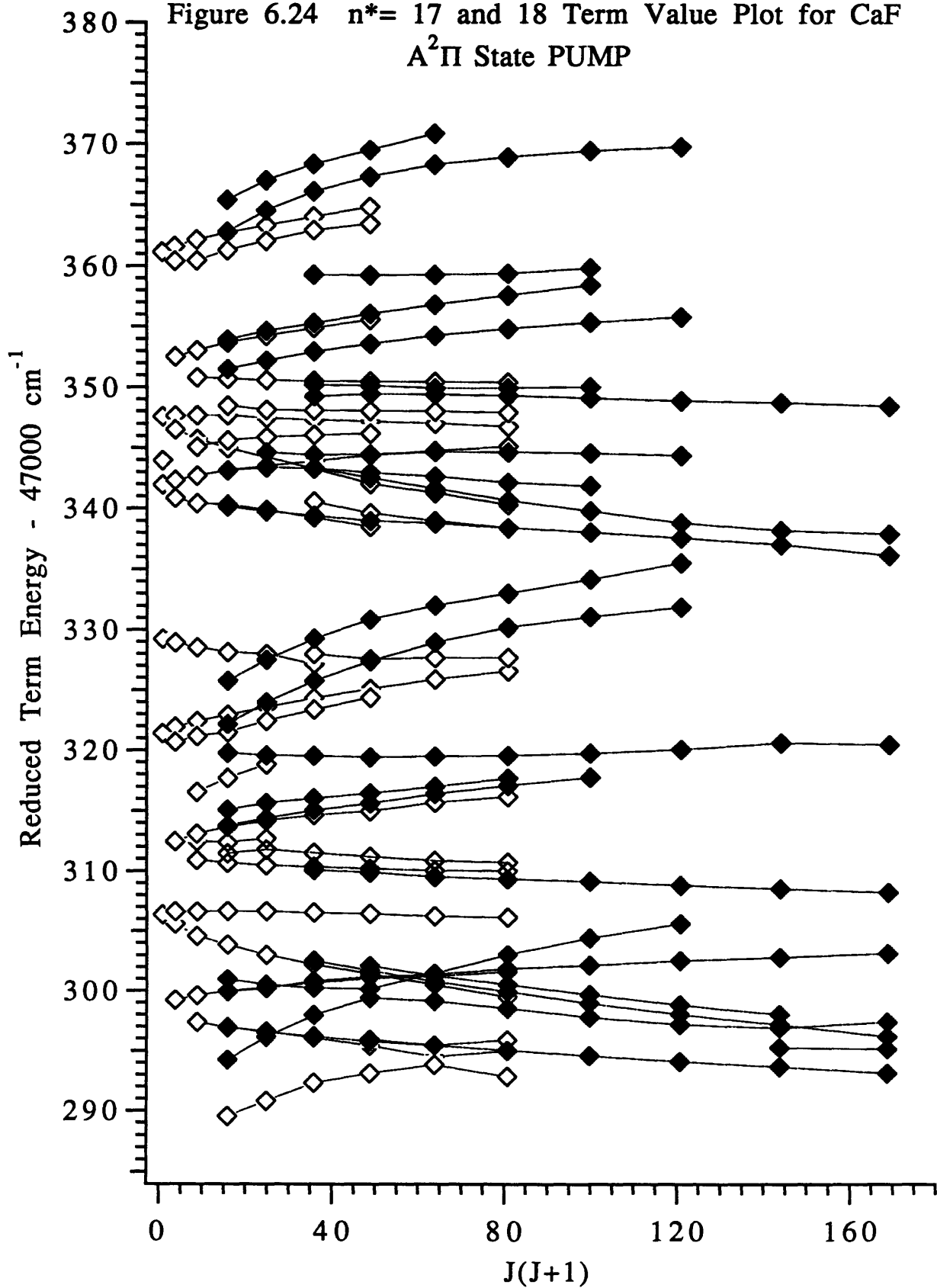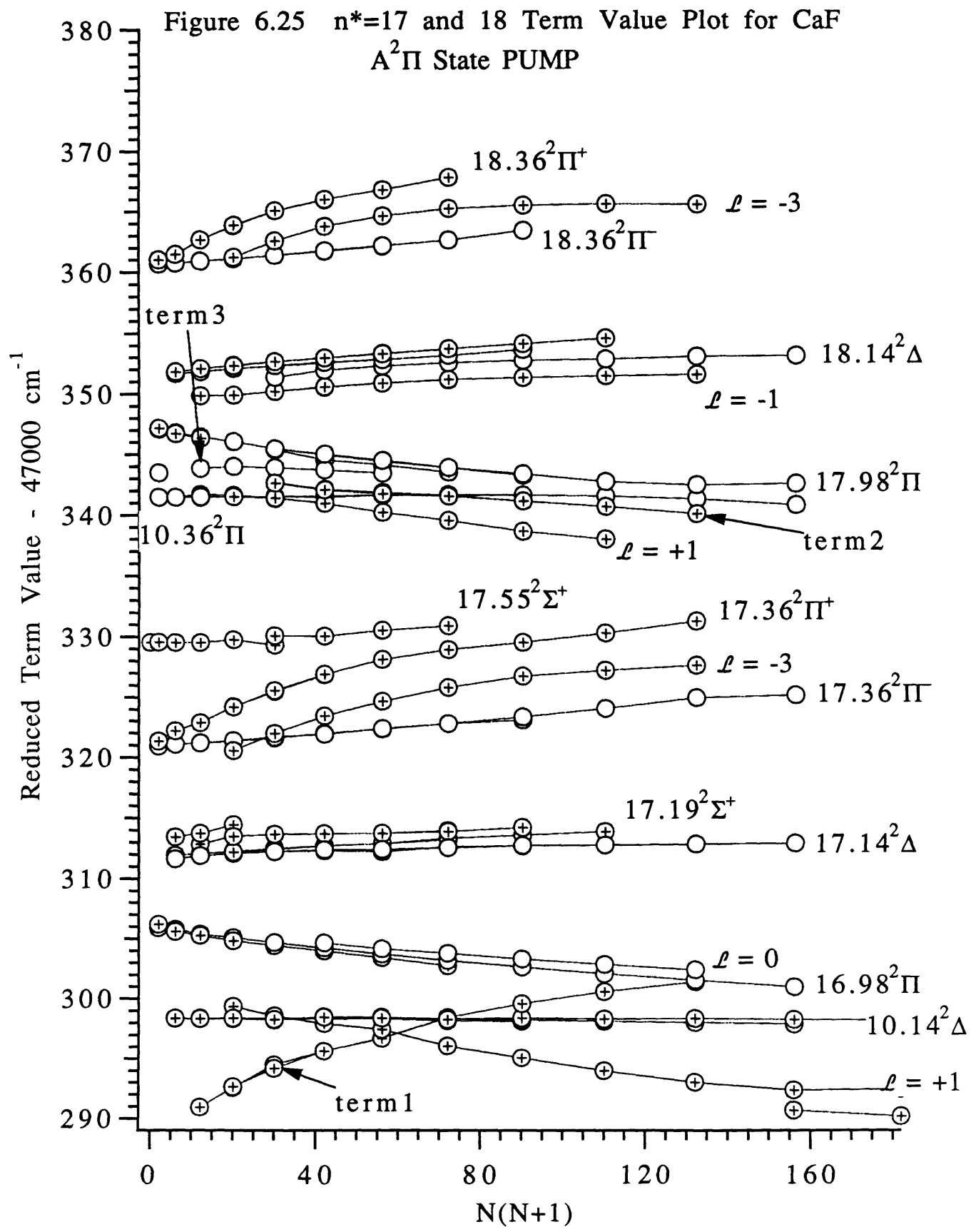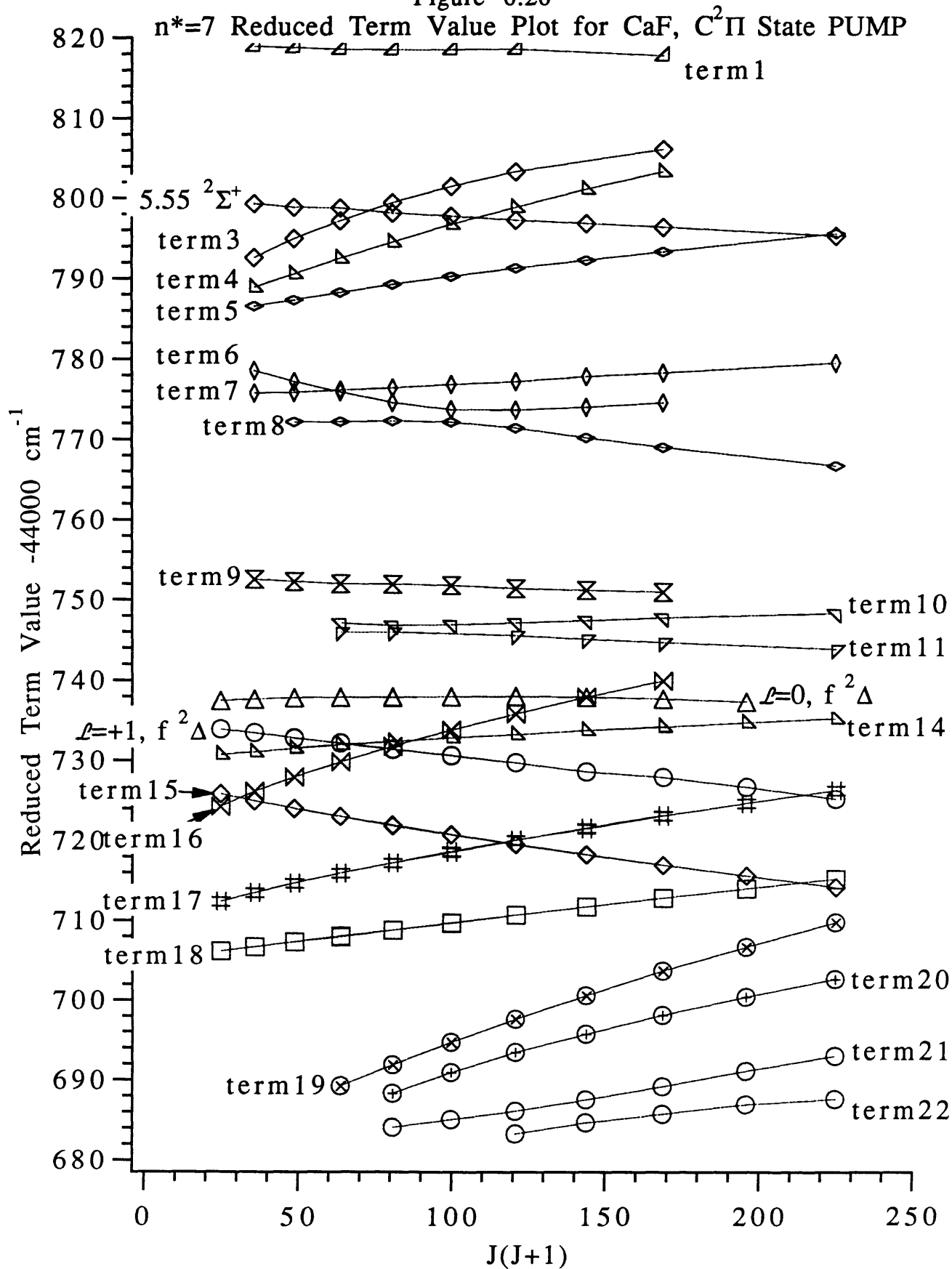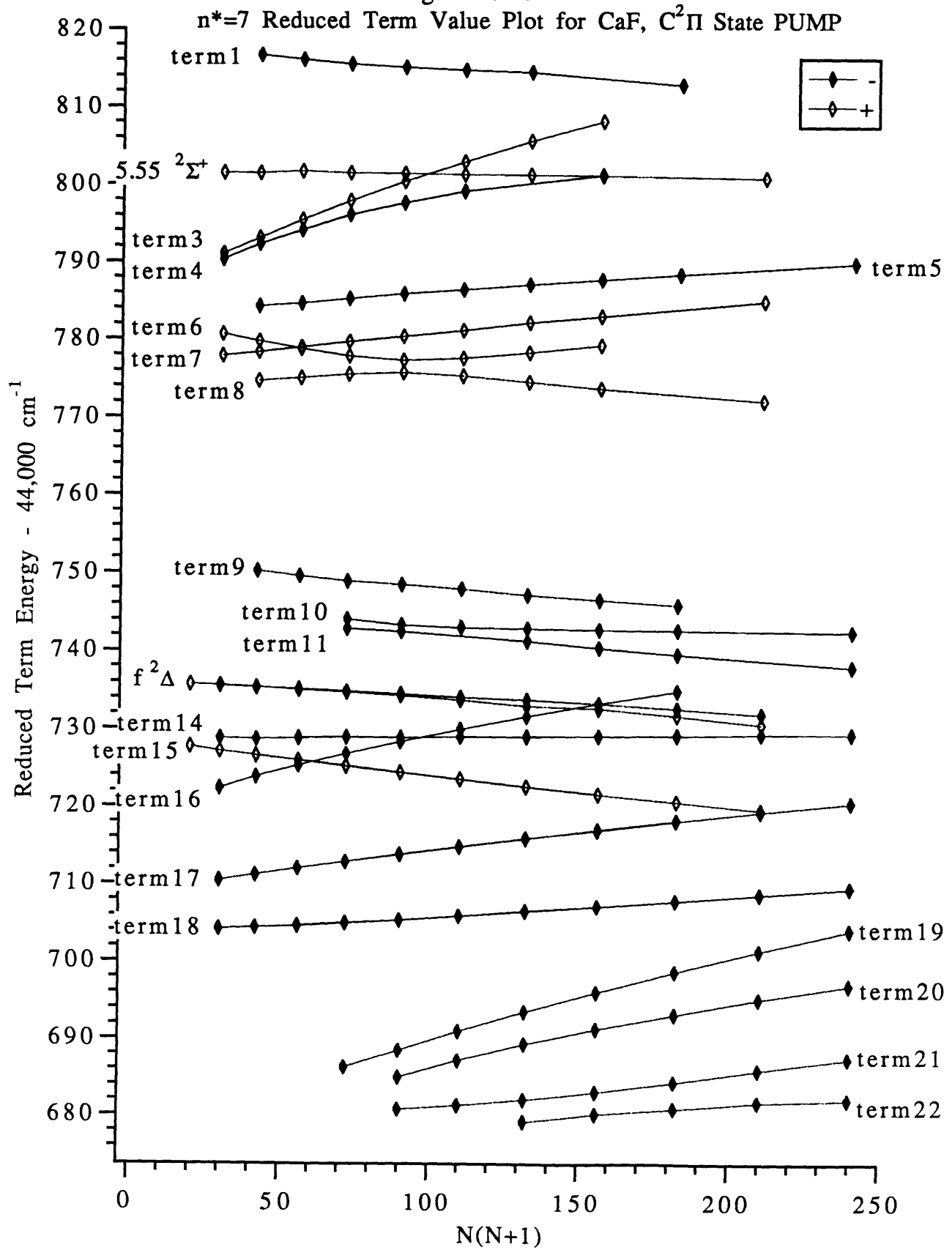
Figure 6.28 n*=13 Reduced Term Value Plot for CaF $C^2\Pi$ State PUMP
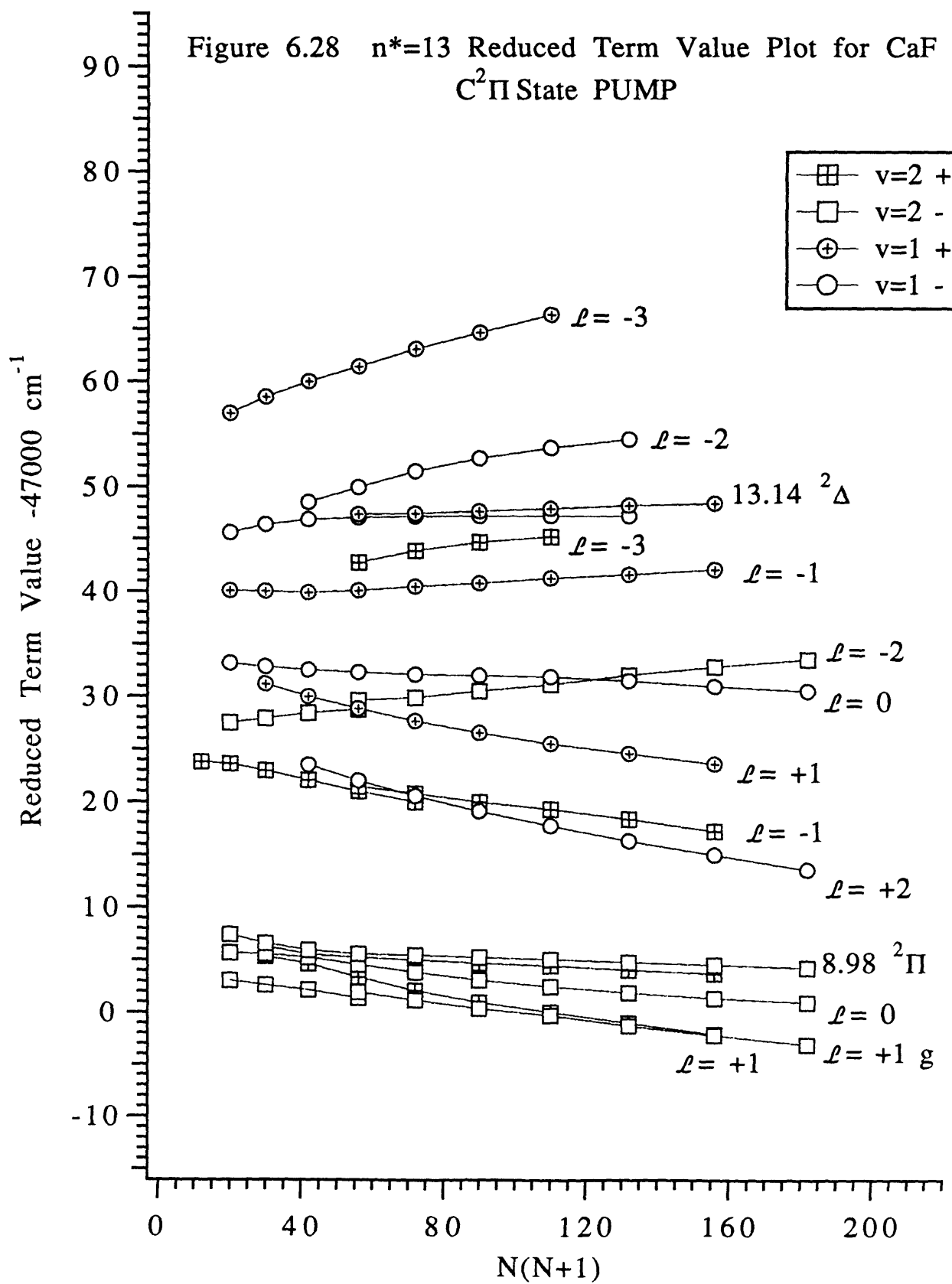
Figure 6.29   n*=14 Reduced Term Value Plot for CaF $C^2\Pi$ State PUMP
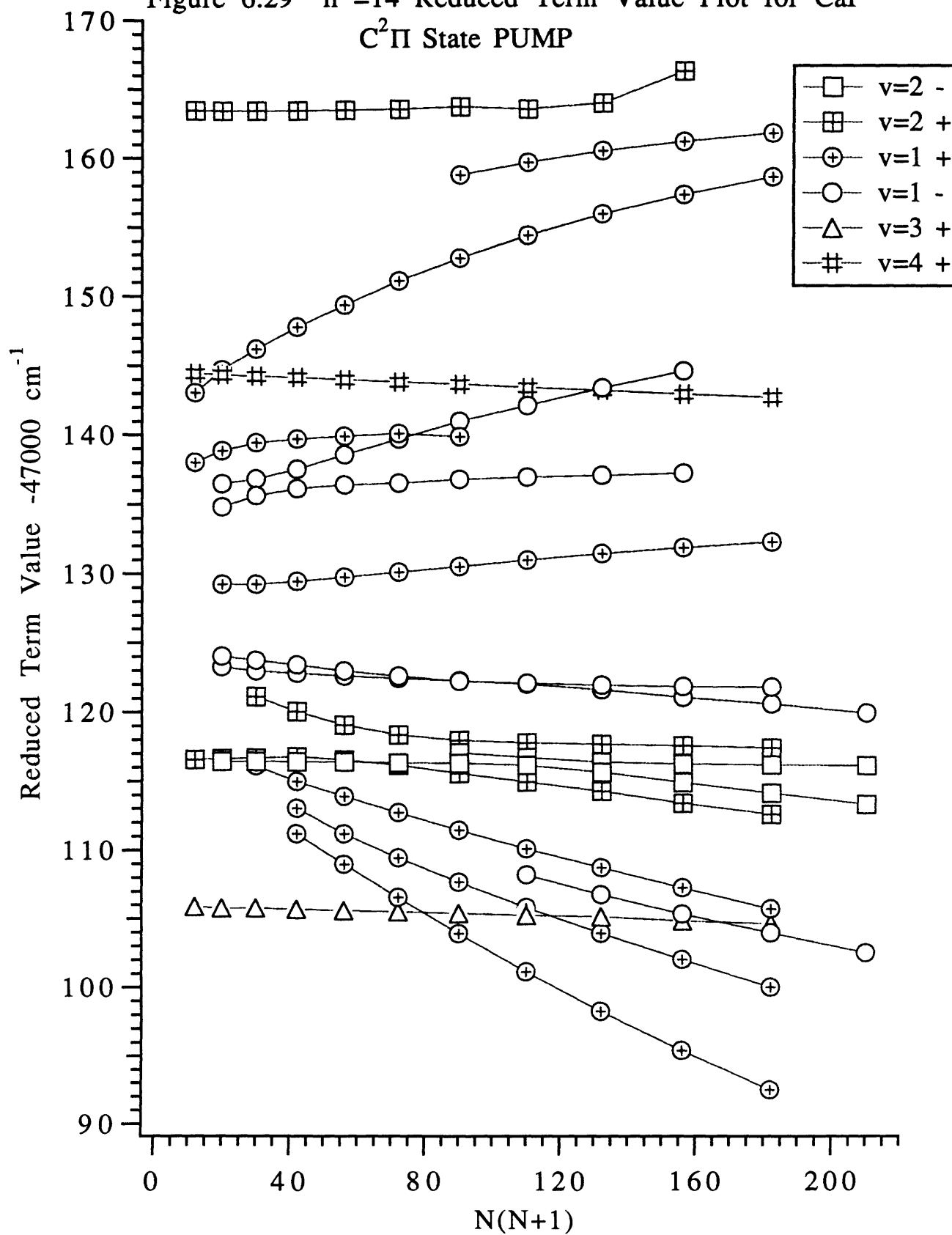
Figure 6.30

n*=14 (+) states - C$^2\Pi$ state PUMP

9.55$^2\Sigma^+$

14.36$^2\Pi$

ℓ = -3

6.55$^2\Sigma^+$

14.19$^2\Sigma^+$

ℓ = -1

9.36$^2\Pi$

ℓ = +1

ℓ = +2 g

7.55$^2\Sigma^+$

ℓ = +3

ℓ = +4 g

Legend: v=2, v=1, v=3, v=4

Y-axis: Reduced Term Value - 47000 cm^{-1}

X-axis: N(N+1)

n*=14 (-) states - C$^2\Pi$ State PUMP

ℓ = -2

14.14$^2\Delta$

ℓ = 0

13.98$^2\Pi$

9.36$^2\Pi$

ℓ = +1 g

ℓ = +2

Legend: v=2, v=1

Y-axis: Reduced Term Value - 47000 cm^{-1}

X-axis: N(N+1)
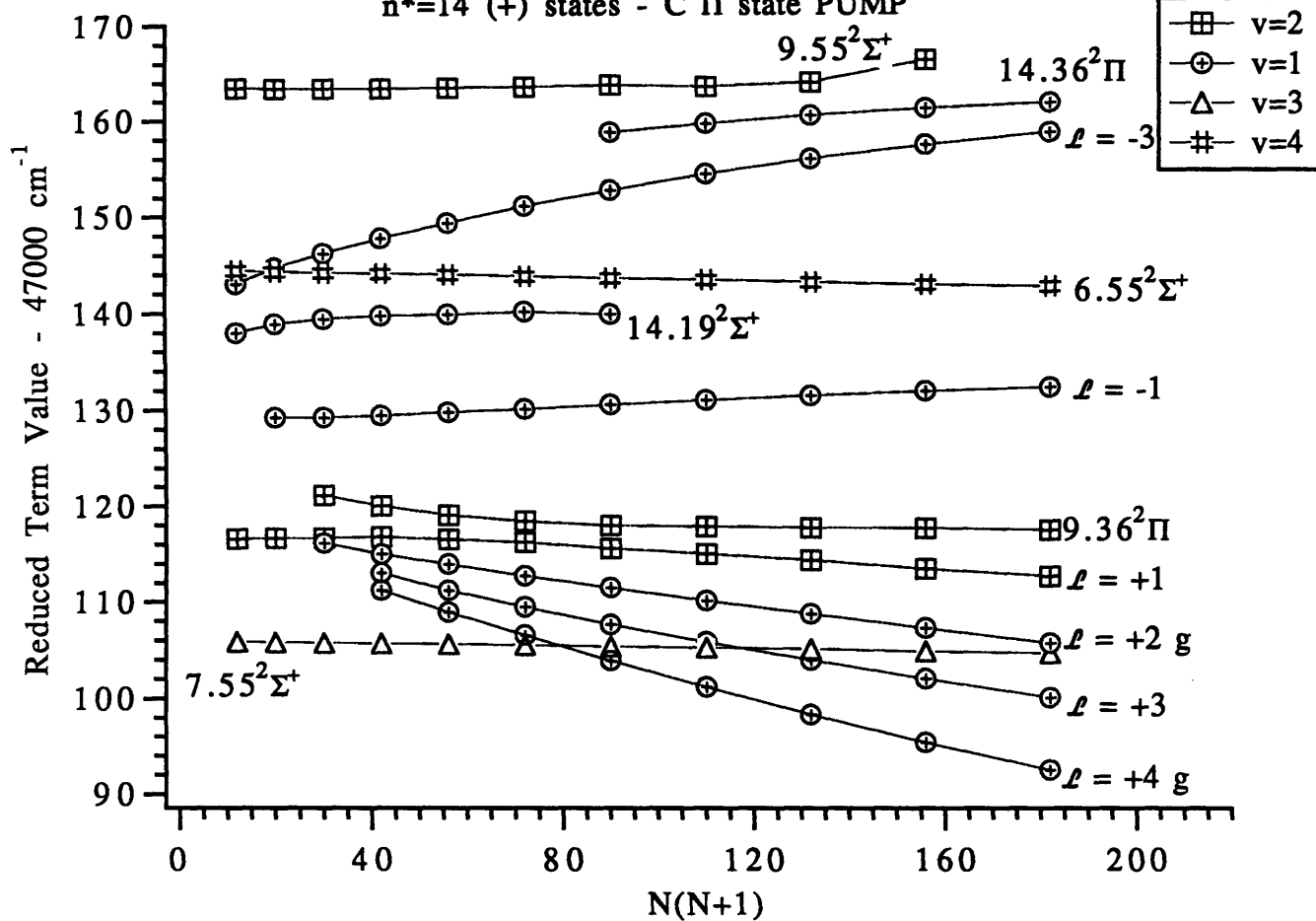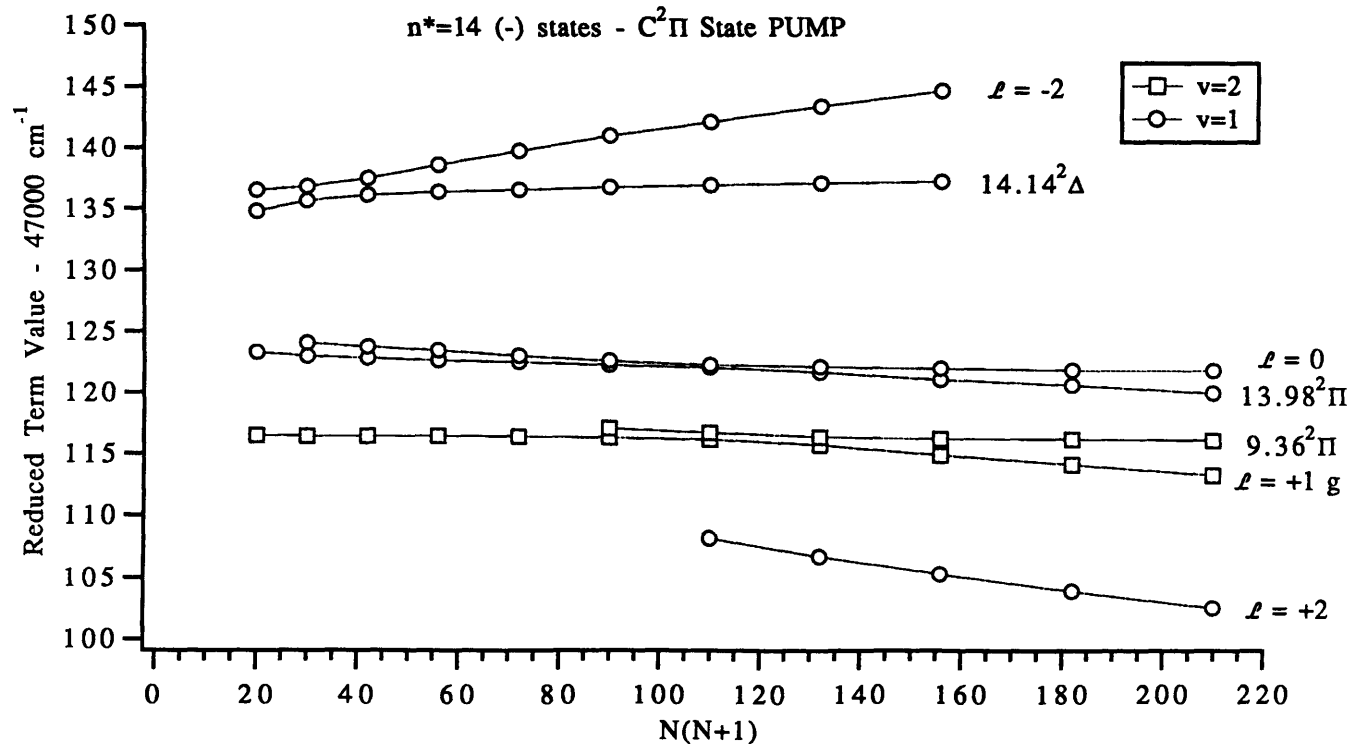
Figure 6.31 n*=14 f Complex
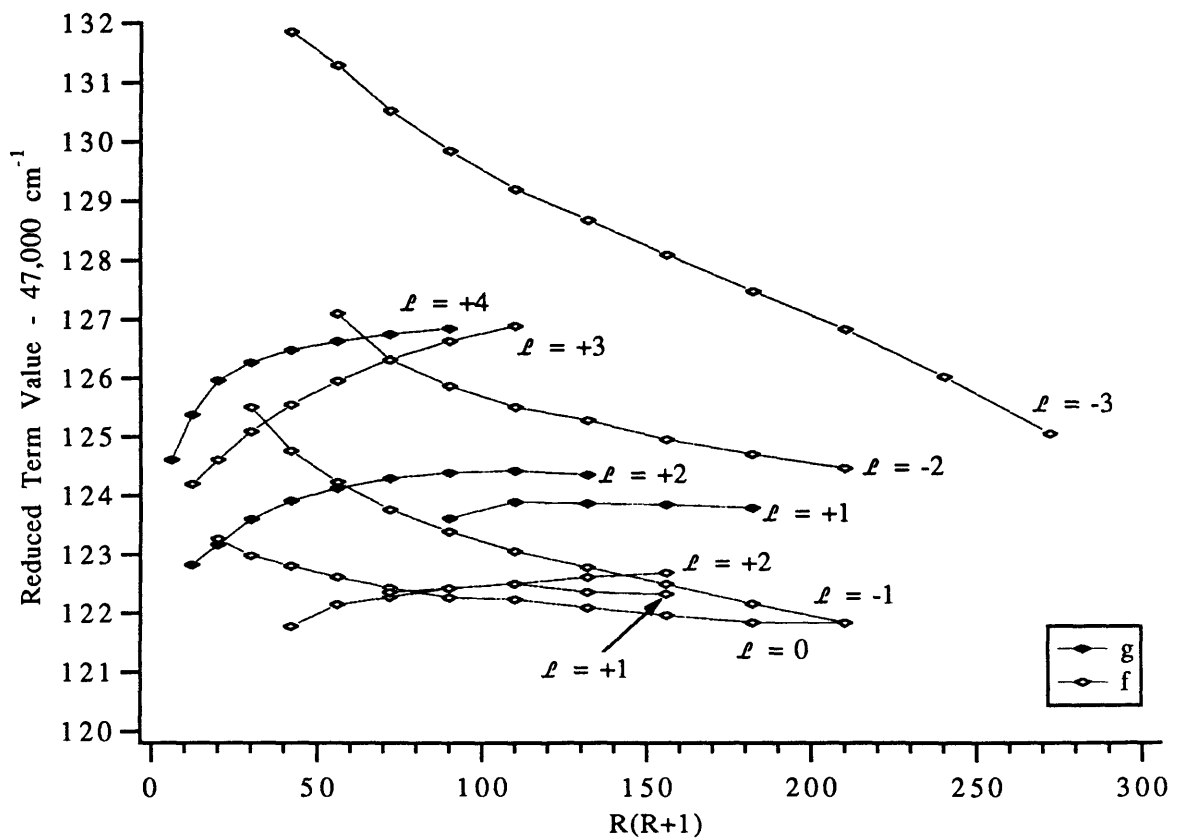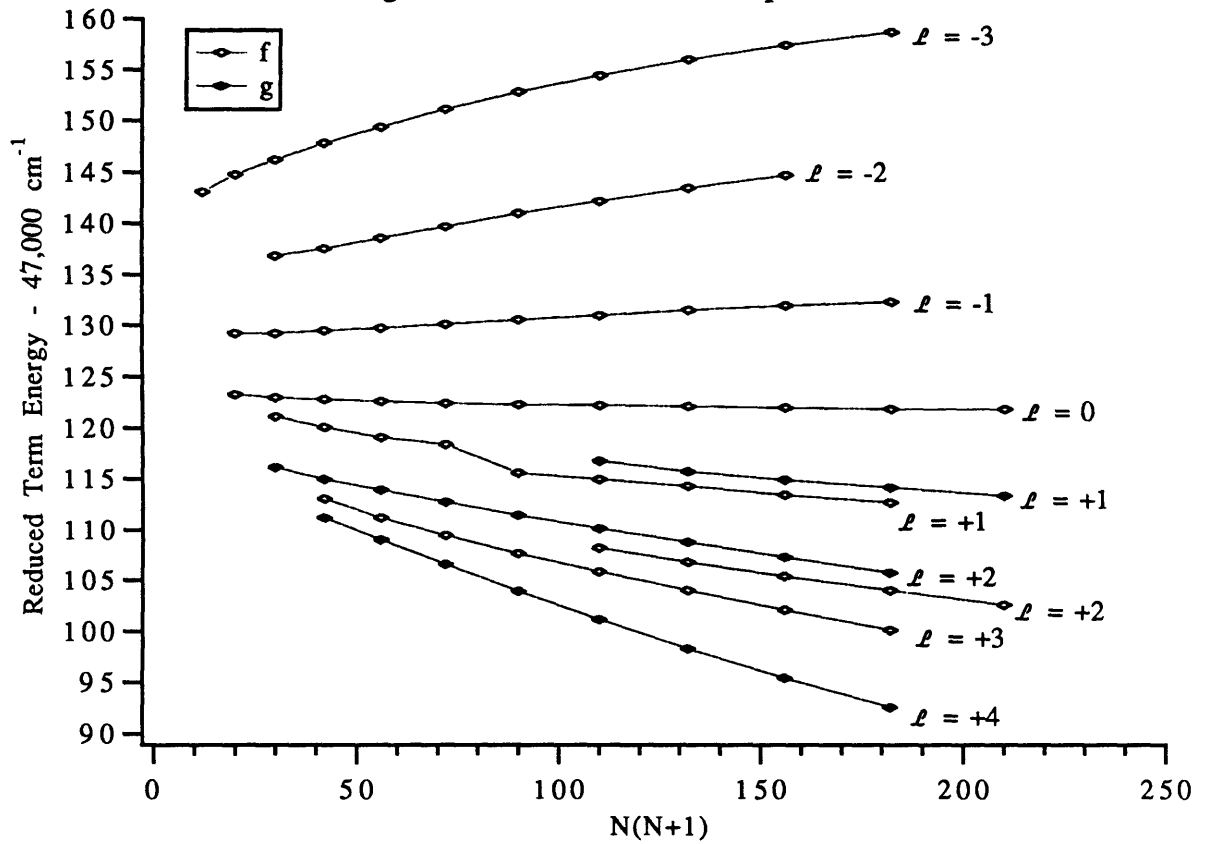
Figure 6.32 $0.36\,^2\Pi$ and $\mathcal{L} = -3$ States for n*=13-18 of CaF

250
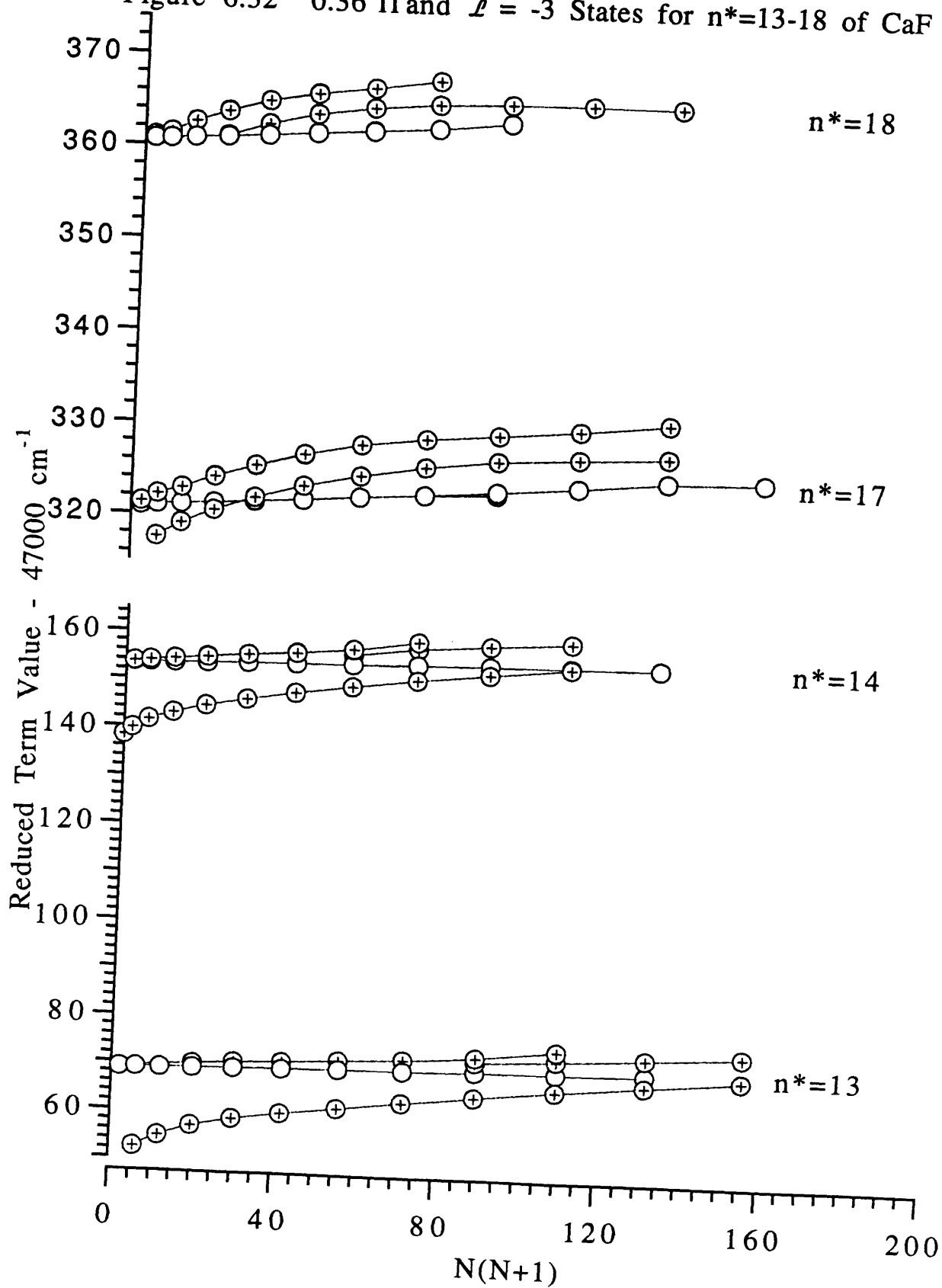
Figure 6.33 CaCl Term Value Plot
A$^2\Pi$ State PUMP

Figure 6.34   CaCl Term Value Plot
$A^2\Pi$ State PUMP

$n^*=18$

$18.16\ ^2\Sigma^+$

$n^*=18.10$

$18.06\ ^2\Delta$

$17.93\ ^2\Pi$

$n^*=17$

$17.16\ ^2\Sigma^+$

$n^*=17.10$

$17.06\ ^2\Delta$

$16.93\ ^2\Pi$

v=1 +
v=1 -

N(N+1)

Reduced Term Value -48,000 cm^{-1}

252

Figure 6.35   High-n* Spectra of CaF

Figure 6.36 High-n* Spectra of CaCl

n*=27.07
n*=30.05
n*=29.05
n*=28.06
n*=28.16
n*=27.15
n*=26.16
n*=26.05
n*=25.15
n*=25.03

$Ca^{35}Cl$

n*=30.05
n*=29.05
n*=28.04

$Ca^{37}Cl$

Term Value (cm^{-1})

Intensity

254

Figure 6.37   MQDT Fit Result for CaF n*=14 (-) States
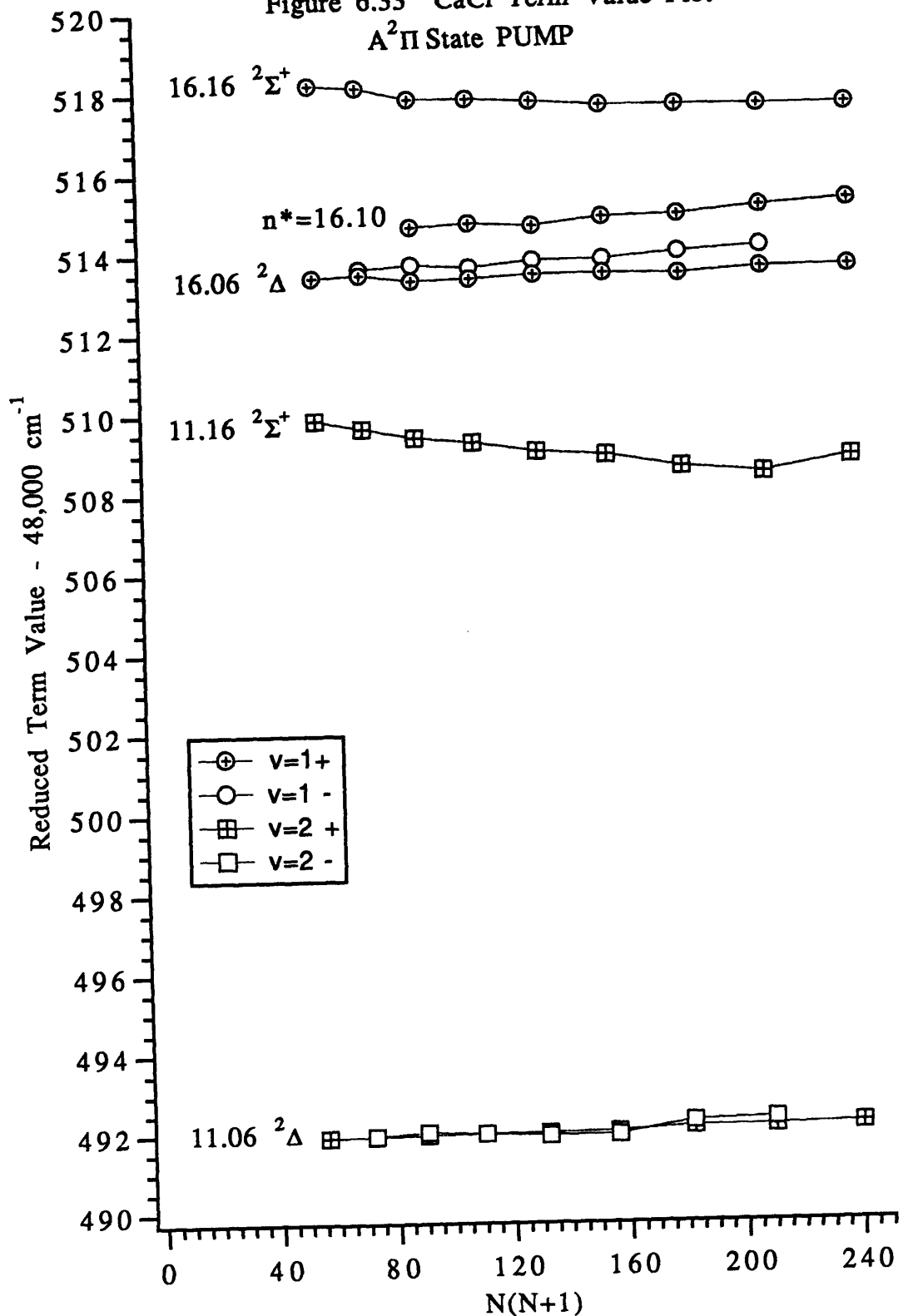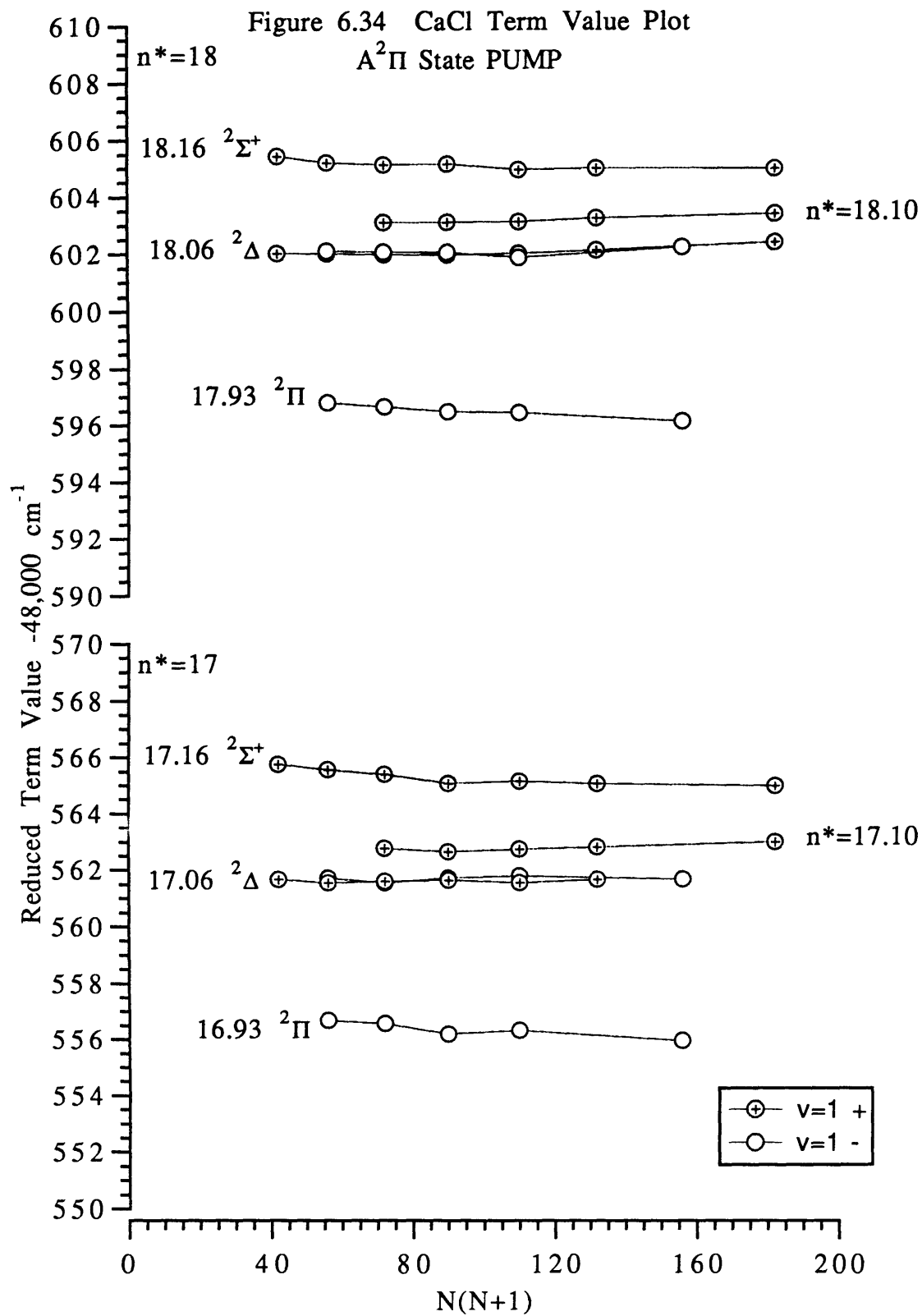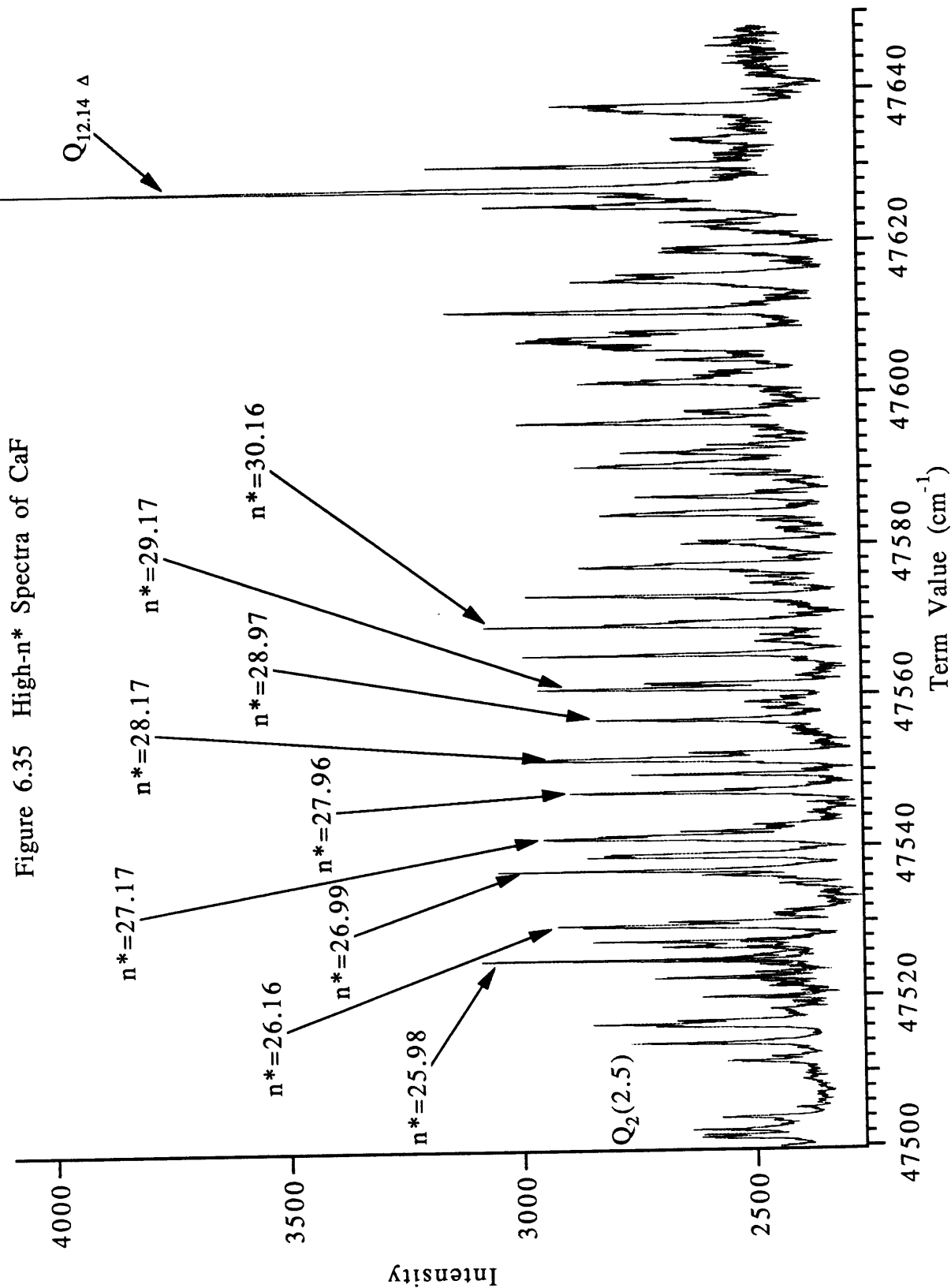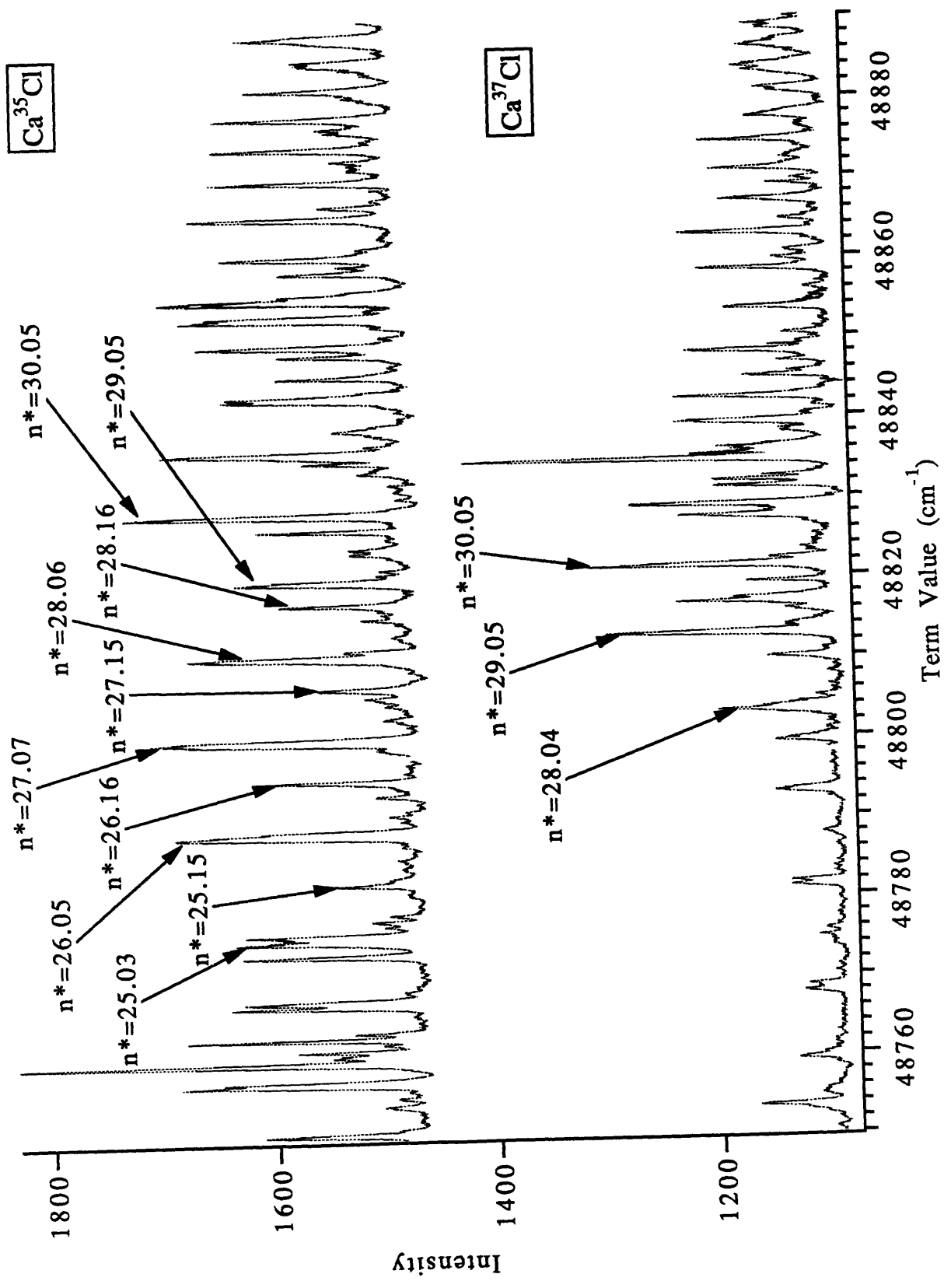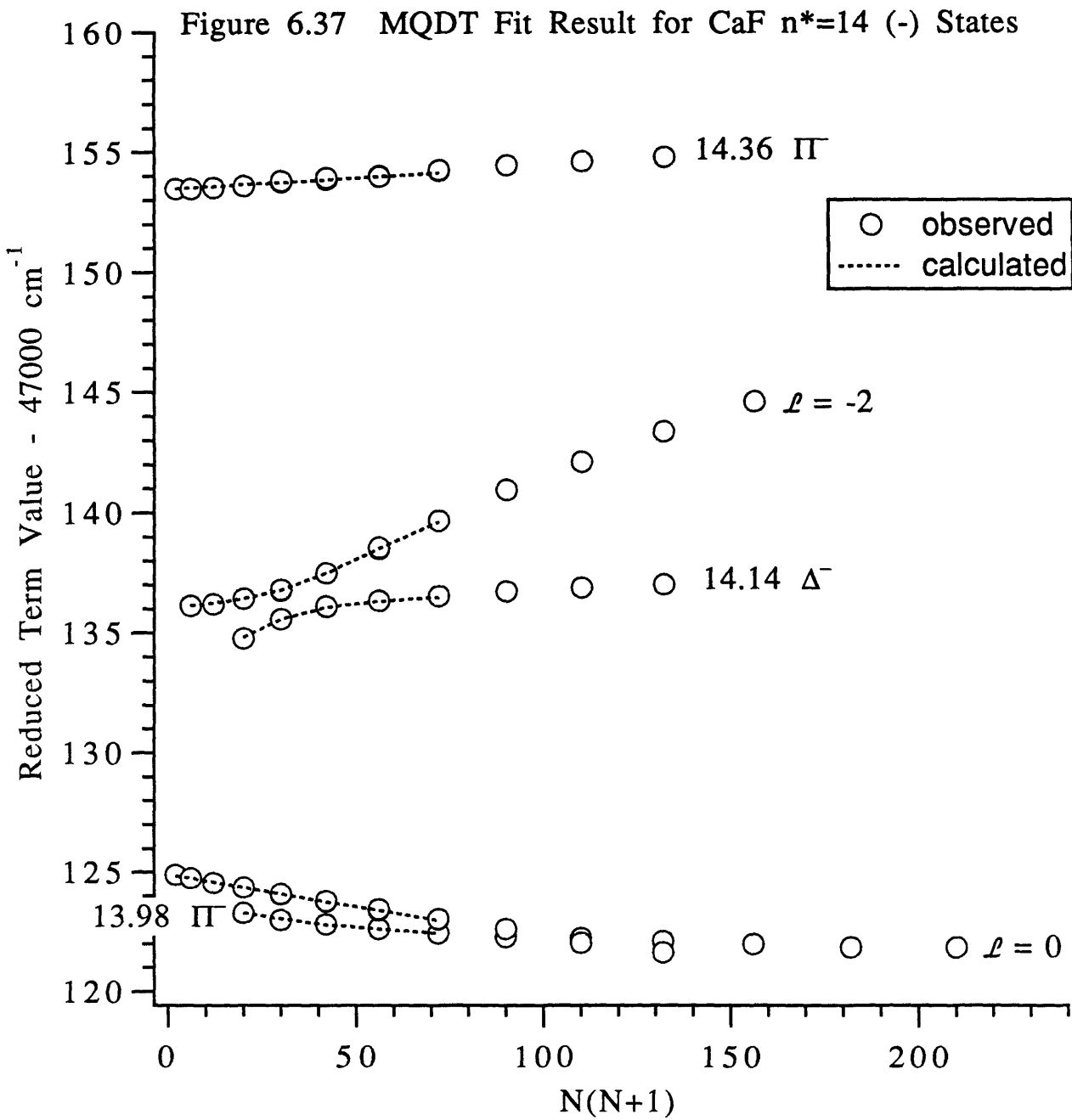
Figure 6.38
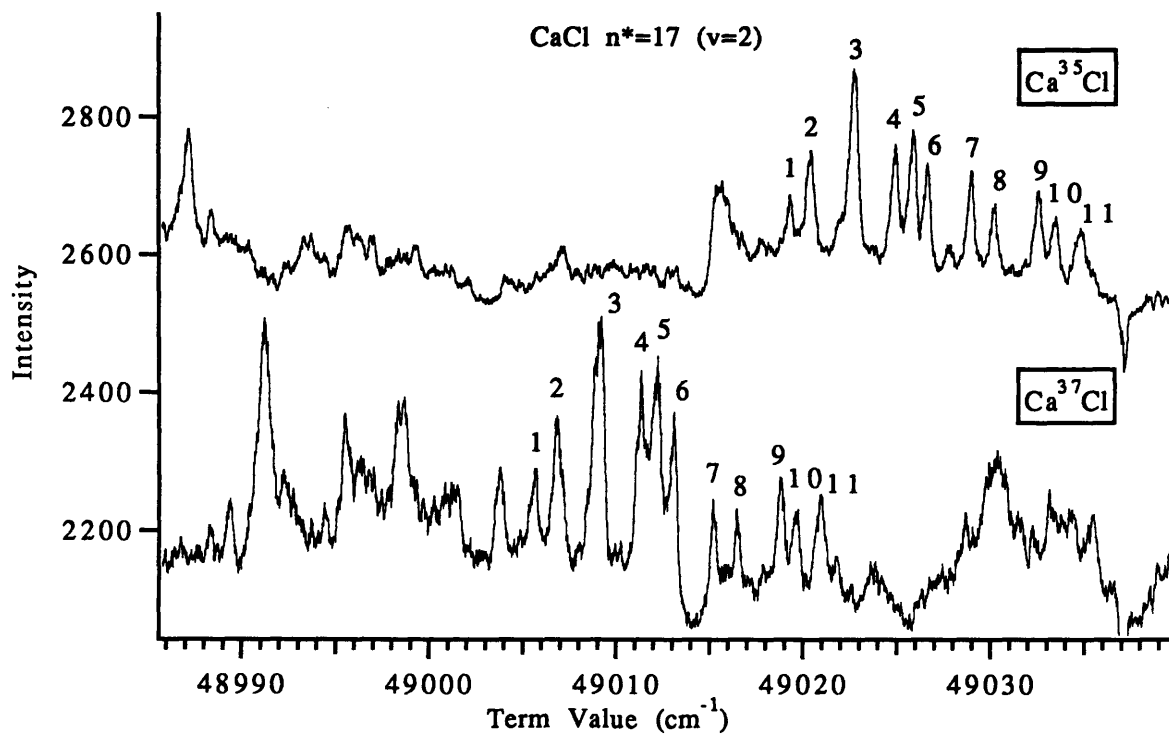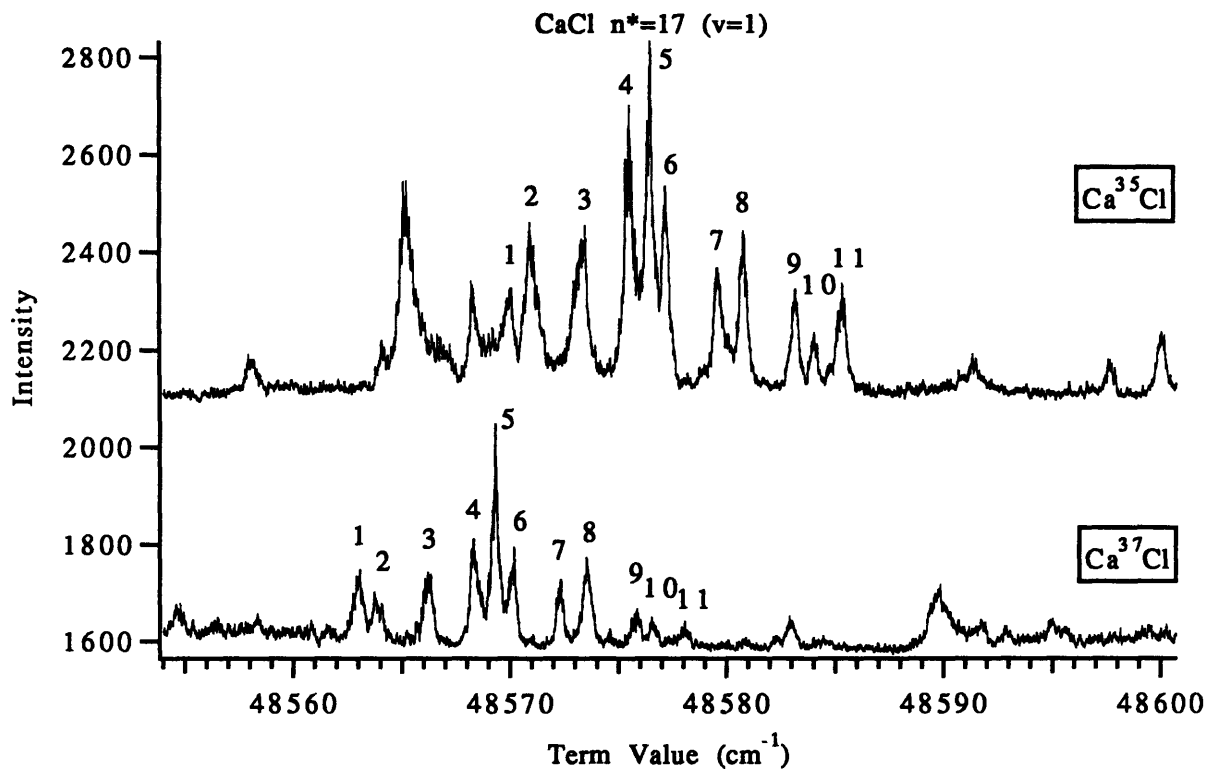
Chapter 7
Conclusion

Part 7.1 - Summary of Results

In summary, autoionization spectra of core-penetrating as well as core-nonpenetrating states have been recorded and assigned in the $n^*=13$, $n^*=14$, $n^*=17$, and $n^*=18$ region of CaF. Autoionization spectra have also been recorded and assigned in the $n^*=16-18$ and regions of CaCl. High-n^* spectra ($n^*=20-30$) have been recorded and some high-n^* series have been identified for both CaCl and CaF.

Molecular constants which were not previously known for CaCl have been measured. These constants include the vibrational constant (450 ± 2 cm^{-1}) of the CaCl$^+$ ion, the rotational constant (0.164 cm^{-1}) of the CaCl$^+$ ion, and the ionization potential of CaCl [48950 ± 0.5 cm^{-1}(N=8, v=1)].

The lowest member of the third $^2\Sigma^+$ series has been observed in CaCl, so all the "valence"-state precursors are now accounted for in CaCl.

The first example of a complete core-nonpenetrating f-complex in a highly polar molecule has been recorded and assigned in the $n^*=14$ region of CaF. MQDT fits of this spectra look promising.

Part 7.2 - New Experiments

Although this thesis contains new information about more than 4,000 rovibronic transitions in the CaF and CaCl molecules that has brought us closer to understanding of the electronic structure of these molecules, the spectroscopic task is far from complete. Two fairly easy experiments (one on CaF and one on CaCl) and one relatively difficult experiment (on CaCl) could offer the keys to a better understanding of how the single nonbonding electron interacts with the highly polar core composed of two closed shell atomic ions. The spectra presented here and that of Murphy[1-4] provide a large pool of spectra that can be used to test theoretical models of CaF. Certain aspects that would be needed to test a comprehensive model remain undetected. It would be unfortunate if the last few pieces of information were not pursued.

One critical piece of information that is still missing for CaF is an understanding of how the pattern of states within a core-nonpenetrating ℓ complex changes with vibrational quantum number (v). The autoionization data gives us information about v>0 states.

It also gives us information at relatively high n* (n*>12) where the spectra are complicated by numerous perturbations. The n*=7 data contains information about v=0 states, however, v=1 (n*=6) and v=3 (n*=5) are also in this region, making the data difficult to assign with confidence. If v=0 data could be obtained for the n*=4 or 5 complex, it would provide a foundation upon which the higher n* complexes could be understood like the low n*-spectra from the core-penetrating states of CaF helped us assign and understand the high-n* spectra. This experiment which is similar to the one described in Chapter 2, Part 2.1.1 would involve PUMPing the C $^2\Pi$ state. It would be nearly identical to the experiment that was done in the n*=7 region of CaF. The n*=4 region would not be at a convenient wavelength, but the n*=5 region could be reached with LDS821 in the Lambda Physik 3002E dye laser. Important information could also be obtained from the n*=6 and 8 complexes which could be reached with LDS750 and LDS698 respectively. The autoionization data from the n*=13 and 14 (v=1) complexes should make the analysis relatively easy. The only difficulty with the experiment might be finding a suitable calibration source.

We do not have the same amount of information about the CaCl molecule, therefore the analysis and understanding is not as good as it is for the CaF molecule. The intermediate n* (4-10) cannot be observed by direct fluorescence, and has not been observed by any other method, so it is difficult to make a smooth connection from the lowest states to the states observed at and above n*=16. The survey scans done in the 37,000-39,000 cm^{-1} energy region (n*=3-4) using the B$^2\Sigma$ state as the PUMP provide a hint about some states which can be observed by direct fluorescence and could help to build the bridge to the low energy valence states. States have been seen in this region by REMPI and direct fluorescence. Energies for those states are provided in Chapter 5, Table 3.1. A careful direct fluorescence experiment would not be difficult and could provide enough information to assign those states. Those states could help provide the connection from the lowest states to the states at n*=16 and above, and provide useful information for the experiment described below.

One way to observe these states above n*=4 which are severely predissociated would be to probe the products of dissociation. Calcium atoms could be ionized and detected in the time of flight mass spectrometer. Observation of these states would aid in the analysis of the current data state as discussed above. Another more interesting aspect of this data is that is could provide an

understanding of the mechanism for predissociation of the highly polar core. For the v=0 states a systematic study of linewidths would provide information on the Λ, ℓ and n* dependences of the predissociation. For states above v=0, the data would compliment the autoionization data that already exists and provide information about the competition between autoionization and predissociation. The CaF dissociation limit is about $44,000 cm^{-1}$ so it is also possible that Rydberg states of CaF could be detected by this method as well. Since the Rydberg states of CaF are so well characterized, assignments would be easy and information about Λ, ℓ and n* dependence of the predissociation could be readily extracted from the data. Once the information about the dependences of Λ, ℓ and n* is understood, it could be used to help interpret the CaCl data.

The experiment described above would provide an enormous amount of useful data but it would not be as easy as the double resonance experiments described previously. This experiment would require at least three dye lasers, pumped by at least two Nd:YAG lasers.

The CaCl fluorescence dip data provide in Chapter 5, Figures 5.3-5.5, could serve as a guide on where to find the predissociated states of CaCl which should help in obtaining the first calcium atomic ion signal. No predissociation has been detected in CaF, however, the states above n*=10 are very weak in direct fluorescence. This could be evidence of the onset of predissociation.

References

[1] J. E. Murphy, J. M. Berg, N. A. Harris, and R. W. Field, Phys. Rev. Lett. **65**, 1861 (1990).

[2] J. M. Berg, J. E. Murphy, N. A. Harris, and R. W. Field, Phys. Rev. A **48**, 3012 (1993).

[3] J. E. Murphy, Ph.D. thesis, Massachusetts Institute of Technology, 1992.

[4] N. A. Harris and R. W. Field, J. Chem. Phys. **98**, 2642 (1993).

Appendix 1

The core-penetrating Rydberg series of the CaF molecule: At the borderline between valence and Rydberg states

Nicole A. Harris and Robert W. Field[a]
Department of Chemistry, Massachusetts Institute of Technology, Cambridge, Massachusetts 02139

This paper reports the results of a pulsed optical–optical double resonance study of three new low energy Rydberg states and the previously known but not rotationally analyzed $F\,^2\Pi$ state [C. A. Fowler, Phys. Rev. 59, 645 (1941)] of the CaF molecule. The $v=0$ levels of these four electronic states are in the energy region 36 000–39 800 cm^{-1} ($n^*\approx 3$-4). Molecular constants (A,p,q) or γ, and B were measured for all of the states. The $F'\,^2\Sigma^+$ state at 36 125 cm^{-1} ($n^*=3.177$) is particularly important because it is the lowest and previously unobserved member of the $'p'\,^2\Sigma^+$ Rydberg series. The assignment of the F' state as the lowest member of the $'p'\,^2\Sigma^+$ series corrects a mistaken assignment of the $C'\,^2\Sigma^+$ state as the lowest member of the $'p'\,^2\Sigma^+$ series [J. E. Murphy, J. M. Berg, A. J. Merer, N. A. Harris, and R. W. Field, Phys. Rev. Lett. 65, 1861 (1990)].

INTRODUCTION

Calcium monofluoride is a relatively simple molecule consisting of two closed shell atomic ions (Ca^{2+} and F^-) and a single outer electron. However, the dipole moment of the CaF^+ ion core, which is calculated to be about 11 D, is much larger than that of any other molecule with a well understood Rydberg spectrum. The electronic spectrum of calcium monofluoride should therefore serve as a paradigm for Rydberg spectra of more complicated dipolar-core molecules.

The lowest electronic states of CaF are well represented by a ligand-field atomic-ion-in-molecule model.[1] In this model the CaF states are described as Ca^+ atomic ion states perturbed by a point charge, the F^-, which causes the atomic $Ca^+ nl\lambda$ states to mix and thereby destroys $'l'$. Each of the lowest states of CaF is represented as a linear combination of $Ca^+ nl\lambda$ atomic-ion states.

In a recent letter we showed that each of the Rydberg series can be extrapolated back to its "valence"-state precursor.[2] In the "valence"-state precursor the unpaired electron occupies an orbital which consists only of the intra-core loops of the Rydberg orbital. It is in this sense that we say the Rydberg orbital collapses into the core (for the lowest states). This collapse of the Rydberg orbital into the molecular-ion core is accompanied by only a relatively small deviation in the quantum defect (see Fig. 1). The quantum defect (μ) is defined by the familiar Rydberg formula

$$E_{n*} = \text{I.P.} - \frac{R}{n^{*2}},$$

where

$$n^* = n - \mu.$$

In this equation, n^* is the effective principal quantum number, R is the Rydberg constant (a value of 109 737 cm^{-1}

was used), I.P. is the ionization potential, and μ is the quantum defect.[3] The ionization potential for the CaF molecule was determined to be 46 998 cm^{-1}.[4,5]

"Valence states" embody the effects of the Rydberg orbital collapse into the molecular core. In the CaF molecule the most prominent of these effects could be (i) a decrease in the quantum defect caused by the extra repulsion by the F^- ion, (ii) an increase in the quantum defect due to the extra attraction by the $+2$ charge on the Ca^{2+} atomic ion [as opposed to the $+1$ charge on the CaF^+ molecular ion], and (iii) large energy denominator effects manifested in second-order fine-structure parameters [as the states shift due to the stronger interaction of the electron with the Ca^{2+} and F^- ions, the states can approach each other (in energy) causing unusually large fine structure parameters and large deviations from the expected n^*-scaling of these parameters].

The largest such low-n^* deviation of the quantum defect is seen in the series which terminates on the $C\,^2\Pi$ state.[6] This deviation is a result of the "reverse" polarization of the C state. The π orbital is polarized toward the fluorine ion which causes the C state to be destabilized and thus appear at higher energy (smaller quantum defect).[2] The $F\,^2\Pi$ state (the second member of this reverse polarized series) shows some effects of reverse polarization, but these effects become less important at higher n^* (because the amplitude in the loop of the radial wave function where the overlap with F^- is large, decreases as $\sim n^{*-3/2}$) and the quantum defect becomes constant (see Fig. 1).

We previously[2] invoked reverse polarization effects to justify what turned out to be an incorrect assignment of the $C'\,^2\Sigma^+$ state as the lowest member of the $'p'\,^2\Sigma^+$ series (the $F'\,^2\Sigma^+$ state had not been observed). Theoretical calculations[7,8] indicate that the $C'\,^2\Sigma^+$ and $D\,^2\Sigma^+$ states cannot be two separate electronic states. Experiments by J. Verges *et al.*,[9] Gittins *et al.*,[10] and Ernst *et al.*[6] confirm these predictions. Verges and Gittins found that the "$D\,^2\Sigma^+$ ($v=0$)" state is in fact $v=1$ of the $C'\,^2\Sigma^+$ state. Previously, we incorrectly assigned the C' state as the lowest member of the $'p'\,^2\Sigma^+$ series and the D state as the
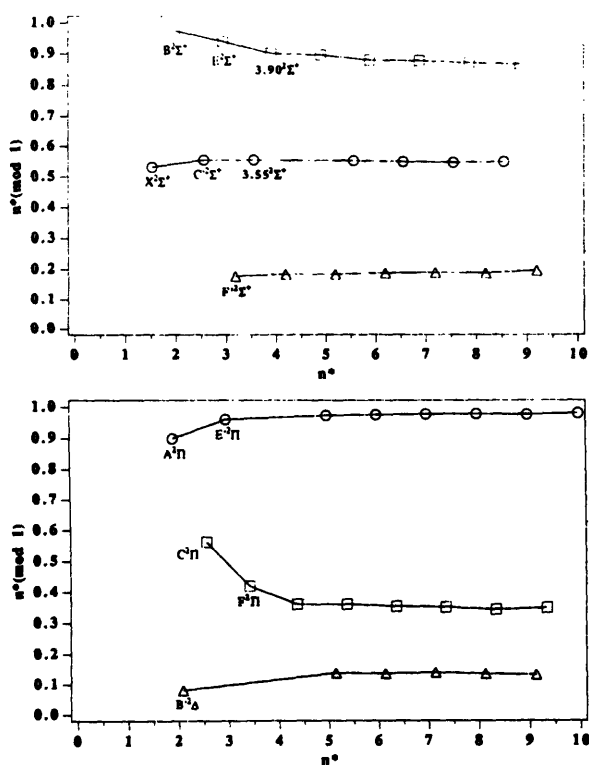
FIG. 1. Plot of n^* (mod 1) vs n^*; $n^* = n - \mu$. This plot shows how the quantum defects (μ) of the valence states connect smoothly to the core-penetrating Rydberg states with only modest changes in quantum defect at low n^*. The new states discussed in this paper are in bold type. The $B'\,^2\Delta$ state in this figure was recently observed by J. d'Incan et al. (Ref. 12).

TABLE I. Molecular constants (cm^{-1}).

	$F\,^2\Sigma^+$	$F\,^2\Pi$	$3.55\,^2\Sigma^+$	$3.90\,^2\Sigma^+$
n^{*a}	3.177	3.418	3.553	3.901
T_0	36 125.976(7)	37 604.597(7)	38 305.052(7)	39 785.856(7)
B_0	0.37317(2)	0.359871(5)	0.36974(2)	0.36795(2)
γ	$-0.0066(2)$		0.0053(2)	0.0269(1)
A		9.184(3)		
p		$3.5(9) \times 10^{-4}$		
q		$2.20(1) \times 10^{-4}$		
$D_0 \times 10^6$	0.330(8)	0.384(2)	0.441(6)	0.443(9)
$\Delta G_{1/2}$	692.80(1)	675.58(1)	671.13(1)	
$\Delta G_{3/2}$	686.17(1)		665.36(1)	

$^a n^*$ is unitless.

The temperature in the oven is approximately 1400 °C. The pressure is maintained at about 200 mTorr by a constant flow of argon which is used as a carrier gas. The Rydberg states were observed by pulsed Optical–Optical Double Resonance (OODR) fluorescence excitation spectroscopy using the $A\,^2\Pi_{3/2}$, $v=0$ state as the intermediate level.[4] We detected direct fluorescence to the $X\,^2\Sigma^+$ ground state using a solar blind photomultiplier (Hamamatsu model 250S) behind a broadband (330–250 nm) interference filter. Various $A\,^2\Pi - X\,^2\Sigma^+$ (0,0) rotational transitions terminating on levels from $J = 1.5$ to 52.5 (both e and f parity) in the $A\,^2\Pi_{3/2}$ state were used as PUMP transitions. The PUMP was a Lambda Physik FL3002E pulsed dye laser. The PROBE was a Spectra Physics PDL-1 pulsed dye laser. The PUMP and the PROBE dye lasers were pumped by the same Spectra Physics DCR2A Nd:YAG laser.

second member of the $'s'\,^2\Sigma^+$ series.[2] It is now clear that the C' state is the second member of the $'s'\,^2\Sigma^+$ series, which leaves the $'p'\,^2\Sigma^+$ series without a "valence"-state precursor.

The primary objective of the present experimental study was to locate and characterize the lowest member of the $'p'\,^2\Sigma^+$ series. We also hoped to characterize all of the low-n^* members of the core penetrating Rydberg series in CaF which had not been observed in this previously unexplored energy region.

Molecular fine structure constants, such as the spin-rotation constant, γ, have proven very useful in helping to arrange Rydberg states into series.[4,5] We expect the molecular constants to scale with n^* in a predictable manner within a series. For example, we expect the spin-rotation constant to be nearly constant within a series. The low-n^* deviations from n^*-scaling relations provide diagnostically valuable information about how the Rydberg orbital collapses into the molecular ion core. Such deviations can provide the crucial tests of a unified atomic-ion-in-molecule model whereby all molecular electronic properties are derived from atomic data.

EXPERIMENT

Gaseous calcium monofluoride was produced from crystalline calcium difluoride in a high temperature oven.

RESULTS

The results are summarized in Table I. The molecular constants presented in Table I were determined using the nonlinear least squares fitting procedure described by Berg et al. to fit the Rydberg$\leftarrow A\,^2\Pi_{3/2}$ transition frequencies of CaF.[4] The data used in the fits is given in Table II. The Hamiltonian used by Berg et al. is presented in Table III.

The $v=0$ level of the $F\,^2\Sigma^+$ state was observed at about 36 125 cm^{-1} (see Table I). This state was assigned as a $^2\Sigma^+$ state from the pattern in its fluorescence excitation spectrum. From the $A\,^2\Pi$ intermediate state, OODR spectra of $^2\Sigma^+$ states typically have a two line pattern (three lines when the spin-rotation splitting is resolvable). $^2\Pi$ and $^2\Delta$ states have a four (case b) or six (case a) line pattern. The $F\,^2\Sigma^+$ state was assigned as the lowest member of the $'p'\,^2\Sigma^+$ series from its n^* value (see Fig. 1) and the sign (negative) and magnitude of its spin-rotation constant. The $'p'\,^2\Sigma^+$ series is the only series observed to have a negative spin-rotation constant.

At higher energy, 37 604 cm^{-1}, the $v=0$ level of the $F\,^2\Pi$ state previously observed by Fowler[11] at low resolution was observed and rotationally analyzed. Fowler correctly assigned this state as a $^2\Pi$ state. However, he reported only the T_0 value and the $\Delta G_{1/2}$ vibrational interval for the F state. The F state has been assigned as the second member of the $'d'\,^2\Pi$ series.[2] The measured spin–orbit

J. Chem. Phys., Vol. 98, No. 4, 15 February 1993

263

TABLE II. Observed and calculated line positions (in cm^{-1}). Numbers in parentheses are (obs–calc) in 10^{-3} cm^{-1}.

	$F'^2\Sigma^+ - A\,^2\Pi_{3/2}$				
$P_{12}(3.5)$	19 557.921(19)	$Q_2(3.5)$	19 563.141(−8)	$R_{12}(3.5)$	19 563.141(21)
$P_{12}(5.5)$	19 556.130(−11)	$Q_2(5.5)$	19 564.372(−15)	$R_{12}(5.5)$	19 564.372(28)
$P_{12}(46.5)$	19 563.572(1)	$Q_2(46.5)$	19 633.032(9)	$R_{12}(46.5)$	19 632.713(3)
$P_{12}(48.5)$	19 566.145(17)	$Q_2(48.5)$	19 638.548(5)	$R_{12}(48.5)$	19 638.205(−12)
$P_{12}(50.5)$	19 568.902(4)	$Q_2(50.5)$	19 644.269(−4)	$R_{12}(50.5)$	19 643.919(−15)
$P_2(15.5)$	19 561.549(−7)	$Q_{12}(15.5)$	19 561.440(−13)	$R_2(15.5)$	19 586.158(−22)

	$F\,^2\Pi - A\,^2\Pi_{3/2}$				
$P_2(3.5)$	21 041.530(4)	$Q_2(1.5)$	21 043.837(−2)	$R_2(1.5)$	21 045.717(3)
$P_2(5.5)$	21 040.521(−17)	$Q_2(3.5)$	21 044.148(−2)	$R_2(3.5)$	21 047.520(3)
$P_2(9.5)$	21 039.112(5)	$Q_2(5.5)$	21 044.648(−5)	$R_2(5.5)$	21 049.508(6)
$P_2(15.5)$	21 038.070(−1)	$Q_2(9.5)$	21 046.160(1)	$R_2(9.5)$	21 053.979(5)
$P_2(21.5)$	21 038.129(−2)	$Q_2(15.5)$	21 049.477(10)	$R_2(15.5)$	21 061.684(0)
$P_2(24.5)$	21 038.534(4)	$Q_2(21.5)$	21 053.825(9)	$R_2(21.5)$	21 070.413(−7)
$P_2(46.5)$	21 047.709(−6)			$R_2(24.5)$	21 075.135(−6)
$P_2(50.5)$	21 050.707(3)			$R_2(46.5)$	21 115.727(−14)
$P_2(53.5)$	21 053.207(−5)			$R_2(50.5)$	21 124.384(−16)
				$R_2(53.5)$	21 131.117(−34)
$P_{12}(3.5)$	21 032.846(26)	$Q_{12}(3.5)$	21 035.239(0)	$R_{12}(3.5)$	21 038.357(9)
$P_{12}(5.5)$	21 031.358(−11)	$Q_{12}(5.5)$	21 035.188(11)	$R_{12}(5.5)$	21 039.690(9)
$P_{12}(9.5)$	21 028.465(0)	$Q_{12}(9.5)$	21 035.084(2)	$R_{12}(9.5)$	21 042.401(11)
$P_{12}(15.5)$	21 024.329(−6)	$Q_{12}(15.5)$	21 035.228(−7)	$R_{12}(15.5)$	21 046.771(−5)
$P_{12}(21.5)$	21 020.722(−25)	$Q_{12}(21.5)$	21 035.983(10)	$R_{12}(46.5)$	21 080.791(−21)
$P_{12}(46.5)$	21 014.125(3)	$Q_{12}(24.5)$	21 036.596(−9)	$R_{12}(50.5)$	21 086.794(−6)
$P_{12}(50.5)$	21 014.449(11)			$R_{12}(53.5)$	21 091.537(−13)
$P_{12}(53.5)$	21 014.949(4)				

	$3.55\,^2\Sigma^+ - A\,^2\Pi_{3/2}$				
$P_{12}(2.5)$	21 737.950(17)	$Q_2(2.5)$	21 741.615(−2)	$R_{12}(2.5)$	21 741.615(−20)
$P_{12}(48.5)$	21 737.164(3)	$Q_2(48.5)$	21 808.222(−9)	$R_{12}(48.5)$	21 808.486(−6)
$P_{12}(50.5)$	21 739.170(−4)	$Q_2(50.5)$	21 813.155(17)	$R_{12}(50.5)$	21 813.406(−4)
$P_2(21.5)$	21 742.232(−7)	$Q_{12}(21.5)$	21 742.367(14)	$R_2(21.5)$	21 775.477(6)
$P_2(24.5)$	21 744.060(−15)	$Q_{12}(24.5)$	21 744.214(10)	$R_2(24.5)$	21 781.723(−1)

	$3.90\,^2\Sigma^+ - A\,^2\Pi_{3/2}$				
$P_{12}(3.5)$	23 217.804(15)	$Q_2(3.5)$	23 222.840(−6)	$R_{12}(3.5)$	23 222.963(−4)
$P_{12}(5.5)$	23 215.999(11)	$Q_2(5.5)$	23 223.922(−13)	$R_{12}(5.5)$	23 224.107(−2)
$P_{12}(48.5)$	23 214.439(2)	$Q_2(48.5)$	23 284.105(−3)	$R_{12}(48.5)$	23 285.438(−4)
$P_{12}(50.5)$	23 216.130(6)	$Q_2(50.5)$	23 288.637(5)	$R_{12}(50.5)$	23 290.015(5)

constant of about 9 cm^{-1} is what one would predict from the other members of that series because the spin–orbit constant is expected to scale as n^{*-3}.[4]

The $v=0$ level of the next higher energy state, the 3.55 $^2\Sigma^+$ state, was observed at 38 305 cm^{-1}. This state was assigned as the third member of the $'s'\,^2\Sigma^+$ series. Its spin-rotation constant is positive and small like those of the other members of the $'s'\,^2\Sigma^+$ series.

Finally, the $v=0$ level of the 3.90 $^2\Sigma^+$ state was observed at 39 785 cm^{-1}. This state was assigned as the third member of the $'d'\,^2\Sigma^+$ series. Its spin-rotation constant is also positive but a factor of 4 larger than that of the $'s'\,^2\Sigma^+$ series, which is consistent with the γ values of other members of the $'d'\,^2\Sigma^+$ series.

Higher vibrational levels were examined for the $F'\,^2\Sigma^+$

state ($v=1$ and $v=2$), the $F\,^2\Pi$ state ($v=1$), and the 3.55 $^2\Sigma^+$ state ($v=1$ and $v=2$) (see Table I). The $\Delta G_{1/2}$ and $\Delta G_{3/2}$ vibrational intervals for all three of these electronic states are similar to those measured for higher Rydberg states of the CaF molecule. The average $\Delta G_{1/2}$ vibrational interval measured for the Rydberg states above $n^*=4$ is about 683 cm^{-1}.[4] We expect the potential curves and thus the vibrational constants to be similar for all of the Rydberg states, with the exception of the lowest members of core penetrating series, as discussed later. The molecular constants for the $n^*=3.55$, 3.90, and the F (3.41) states are exactly what we would have predicted by extrapolation from higher-n^* members of the respective series; these constants confirm our assignments and analyses of the core-penetrating series.

J. Chem. Phys., Vol. 98, No. 4, 15 February 1993

263

TABLE III. Hamiltonian matrix elements for $^2\Sigma^+$ and $^2\Pi$ states. Letting $0 \rightarrow {}^2\Sigma^+$, $1 \rightarrow {}^2\Pi_{3/2}$, $2 \rightarrow {}^2\Pi_{1/2}$, the matrix elements are constructed by summing over the appropriate interaction; $x \equiv J + \frac{1}{2}$. Matrix elements are written f parity over e. The elements in this table were taken directly from Ref. 14.

	$(0,0) = 1$		
E	$(1,1) = 1$	p	$(1,2) = (-1/2)(x^2 - 1)$
	$(2,2) = 1$		$(2,2) = (1/2)(1 \pm x)$
A	$(1,1) = \frac{1}{2}$		$(1,1) = (1/2)(x^2 - 1)$
	$(2,2) = -\frac{1}{2}$	q	$(1,2) = (-1/2)(1 \pm x)(x^2 - 1)^{1/2}$
			$(2,2) = (1/2)(1 \pm x)^2$
	$(0,0) = x(x \pm 1)$		
B	$(1,1) = x^2 - 2$	γ	$(0,0) = (-1/2)(1 \pm x)$
	$(1,2) = -(x^2 - 1)^{1/2}$		
	$(2,2) = x^2$		
	$(0,0) = x^2(x \pm 1)^2$		
D	$(1,1) = (1 - x^2) - (x^2 - 2)^2$		
	$(1,2) = 2(x^2 - 1)^{3/2}$		
	$(2,2) = (1 - x^4) - x^2$		

FIG. 2. Plots of B_0 vs n^* and $\Delta G_{1/2}$ vs n^* for all the electronic states of CaF for which these values are known. These plots show how the CaF ionic bond is weakened due to shielding by the Rydberg electron, which causes a decrease in B_0 and $\Delta G_{1/2}$ when the Rydberg orbital starts to collapse into the core region. The horizontal dashed lines on the B_0 vs n^* and the $\Delta G_{1/2}$ vs n^* plots represent the B_0 and $\Delta G_{1/2}$ values, respectively, of the CaF$^+$ ion estimated from our study of the higher n^* Rydberg states of CaF (Ref. 4). Deviations in B_0 values at high n^* are due to l-uncoupling effects (Ref. 5). Such deviations are expected. These high-n^* deviations can provide information about the interactions between Rydberg series and the resultant mixed-l character of the series (Refs. 5 and 13). The B_0 and $\Delta G_{1/2}$ values for the states above $n^* = 4$ were taken from Refs. 4 and 5.

DISCUSSION

One characteristic feature of Rydberg states is that, for the members of a series, the nodes of the wave functions line up inside the core. In other words, the Rydberg electron samples the core in the same way for each member of a series. This nodal structure is the basis for scaling relations for molecular constants, such as the spin–orbit and spin–rotation constant. Therefore, by characterizing only a few states, we expect to be able to predict the behavior of many states. This is why the lowest members ("valence"-state precursors) are so important. Each member of each core-penetrating Rydberg series has a nodal structure inside the ion core that resembles the nodal structure of one of these "valence" states.

Although all of the electronic states of the CaF molecule can be treated as Rydberg states, diagnostically important deviations occur in the molecular constants as n^* decreases. One such deviation is seen in the rotational and vibrational constants (Fig. 2). CaF is ionically bound, thus when the Rydberg orbital collapses into the molecular core region the Rydberg electron partially shields the Ca^{2+} ion from the F$^-$ ion and thereby weakens the ionic bond. This weakening of the ionic bond causes a decrease in the rotational and vibrational constants at low n^*. The $C\,^2\Pi$ state orbital is polarized toward the F$^-$ ion, so the $C\,^2\Pi$ state has higher electron density between (e.g., shielding) the two ions than any of the other electronic states of CaF. This increased electron density between the ions causes the $C\,^2\Pi$ state to have the smallest rotational and vibrational constants of all known states of CaF (see Fig. 2).

Since we expected the previously unobserved $F'\,^2\Sigma^+$ state to be the lowest member of the $^2\Sigma^+$ series which is most strongly (reverse) polarized toward the fluorine, one might expect that, like the $C\,^2\Pi$ state, the $F'\,^2\Sigma^+$ state should also have rotational and vibrational constants smaller than those of the all the other known $^2\Sigma^+$ states of CaF. One might also expect that the $F'\,^2\Sigma^+$ state would be located at higher energy than would be predicted from a

simple extrapolation to the lowest member of the series that contains the F' state. Interestingly, this is not what is found. The Rydberg orbital in the $F'\,^2\Sigma^+$ state is polarized toward the F$^-$, but this state is pushed so high in energy due to repulsion by the F$^-$ that the corresponding orbital is essentially pushed out of the core region.

This is evident by its n^* value (see Fig. 1) and its rotational and vibrational constants (see Fig. 2). The F' state is the only "valence"-state Rydberg precursor whose rotational and vibrational constants are nearly equal to those of the CaF$^+$ ion, indicating that the F' state has the least (of all the valence states) electron density between the two nuclei. If we use the Bohr model to estimate the average distance of the Rydberg electron from the Ca^{2+} ion core, we conclude that $\langle r \rangle \approx 2R_e$ at $n^* \approx 3$. This result suggests that the reverse polarization of the F' state actually places most of the electron density in the "$4p$" orbital on the far side of the F$^-$ ion. This also explains why the F' state has low electron density between the two nuclei.

In the energy region examined ($36\,000$–$39\,800$ cm^{-1}), one $^2\Delta$ state is expected. We did not observe this $^2\Delta$ state. Our detection scheme involves recording direct fluorescence to the ground state ($X\,^2\Sigma^+$). Since the $^2\Delta$ state cannot decay directly to the ground state, it was not observed in our OODR spectra. The $^2\Delta$ state can decay directly to $^2\Pi$ and $^2\Delta$ states below it, but the UV passing, visible absorbing interference filter blocked the wavelengths of

transitions which occur in the visible and near IR regions. We predict that the $v=0$ level of the $'4d'$ $^2\Delta$ state will be found at about 35 650 cm^{-1} and will have a spin–orbit constant of about 3 cm^{-1}.

CONCLUSION

Four low-lying Rydberg states, one $^2\Pi$ and three $^2\Sigma^+$ states, of the calcium fluoride molecule have been observed and rotationally analyzed. These states are on the border-line between valence and Rydberg states. The results from the rotational analyses of three of these states were pre-dictable from the molecular constants we measured for the higher Rydberg states of the calcium fluoride molecule.[4] The present results confirmed our previous assignments and analyses.

The results of the rotational and vibrational analyses of the 3.18 $^2\Sigma^+$ state (the F state) were surprising. The 3.18 $^2\Sigma^+$ state did not have the smallest rotational and vibra-tional constants of all the $^2\Sigma^+$ states in this region, as we expected for a $^2\Sigma^+$ state polarized toward the fluorine, instead, it had the largest constants. These results are shown to be consistent with the expected reverse polariza-tion, but where the "$4p$" orbital is so large that its reverse polarization is primarily into the region behind the F^- ion. We now understand the characteristics of this lowest mem-ber of the $'p'$ $^2\Sigma^+$ series and thus understand the charac-teristics of the $'p'$ $^2\Sigma^+$ series.

All of the electronic states of the CaF molecule below 38 900 cm^{-1} (approximately $n^*=4$, where the first mem-bers of the non-core penetrating $'f'$ series should appear) have now been observed, with the exception of the $^2\Delta$ state

mentioned above. *Each* core-penetrating series now has a fairly well characterized "valence"-state precursor.

[1] S. F. Rice, H. Martin, and R. W. Field, J. Chem. Phys. **82**, 5023 (1985).
[2] J. E. Murphy, J. M. Berg, A. J. Merer, N. A. Harris, and R. W. Field, Phys. Rev. Lett. **65**, 1861 (1990).
[3] G. Herzberg and Ch. Jungen, J. Mol. Spectrosc. **41**, 425 (1972).
[4] J. M. Berg, J. E. Murphy, N. A. Harris, and R. W. Field (unpub-lished).
[5] J. E. Murphy, Ph.D. thesis, Massachusetts Institute of Technology, 1992.
[6] W. E. Ernst, J. Kandler, and O. Knüppel, J. Mol. Spectrosc. **153**, 81 (1992).
[7] Ch. Jungen and N. A. Harris (unpublished).
[8] B. Engels, private communication.
[9] J. Vergès, C. Effantin, A. Bernard, A. Topouzkhanian, A. R. Allouche, J. d'Incan, and R. F. Barrow (unpublished).
[10] C. M. Gittins, N. A. Harris, R. W. Field, J. Vergès, C. Effantin, A. Bernard, J. d'Incan, W. Ernst, P. Bundgen, and B. Engels (unpub-lished).
[11] C. A. Fowler, Phys. Rev. **59**, 645 (1941).
[12] J. d'Incan, C. Effantin, A. Bernard, J. Vergès, and R. F. Barrow, J. Phys. B **24**, L71 (1991).
[13] S. Fredin, D. Gauyacq, M. Horani, Ch. Jungen, and G. Lefevre, Mol. Phys. **60**, 825 (1987).
[14] A. J. Kotlar, R. W. Field, J. I. Steinfeld, and J. A. Coxon, J. Mol. Spectrosc. **80**, 86 (1980).

Appendix 2

Rydberg States of Calcium Fluoride

N. A. Harris[a] and Ch. Jungen

Laboratoire Aimé-Cotton du Centre National de la Recherche Scientifique, Université de Paris-Sud, 91405 Orsay, France

We derive the entire singly excited electronic level spectrum of a *dipolar molecule* (CaF) from *atomic properties alone* (the quantum defects of Ca^+). In the approach presented here the motion of the lone electron is treated as a double scattering process involving the closed-shell Ca^{++} and F^- centers with F^- treated as a point charge. The energies of all known electronic states of CaF are well reproduced by the theory. Refinements of the model such as inclusion of the finite volume of F^- or of polarization effects are deferred as are extensions of the model to account for spin-orbit and other fine structure effects.

Two years ago Murphy *et al.* [1] used optical-optical double resonance fluorescence spectroscopy to study excited states of the calcium fluoride molecule. They uncovered an extended system of previously unknown states, showing that CaF belongs to a novel class of Rydberg molecules (not encompassed by Herzberg's earlier definition [2]). This is one in which the outer electron is bound to a core with total electric charge +1, but where the core itself is subdivided into two distinct entities, a closed-shell calcium ion carrying two positive charges and a closed-shell fluorine atom carrying a single negative charge.

A few years prior to this, Rice, Martin, and Field [3] had already shown that the electronic structure of the lowest states then known of CaF, as well as of several related alkaline earth halides, could be calculated successfully on the simple assumption that these states result from the interaction between a free Ca^+ ion, in various of its lowest states, perturbed and distorted by the field of a negative point charge placed at the position of the fluorine atom. While this "ligand field model" accounts nicely for the lowest states of several alkaline earth halides it cannot be readily extended to the newly observed higher states. This is because with increasing energy the electron cloud of the lone electron on Ca^{++} gradually grows around the F^- ligand until *both* ions are completely surrounded by it, a situation which is not easily handled by the perturbation approach of Ref. [3].

We have here an interesting prototype system. If the F^- indeed acts as a negative point charge it should then be possible to derive the full system of electronic states of CaF from the properties of the Ca^+ ion alone. Specifically, the *three nonzero quantum defects of* Ca^+, μ_s =0.802, μ_p =0.432, μ_d =0.615, should tell us all that is required to predict the molecular electronic structure of CaF, including the evolution between the limiting situations of an "electron on Ca^{++}" and an "electron on $Ca^{++}F^-$." This is therefore a novel application of the concept of "atoms in molecules," and it is one of the simplest ways to turn an atom into a strongly dipolar molecule.

The theoretical development presented below treats the electron core interaction in terms of scattering theory; it is an application of the so-called "generalized quantum defect theory" [4], and it is closely related to the molecular multiple scattering method (MSM) put forward a number of years ago by Dill and Dehmer [5]. We make use of the fact that the Schrödinger equation is *locally separable* in two regions of space (cf. Fig. 1 for reference), namely, outside an appropriately chosen ellipsoid $\xi=\xi_0$ surrounding the two ions (region I), as well as near the surface of the Ca^{++} ion (region III). The main task of the calculation then consists in bridging the gap between those two regions; it is here in the reaction zone II, that the lone electron evolves from an *atomic* into a *molecular* electron or vice versa. We discuss regions I, III, and II in turn.

In region I the lone electron experiences only the electrostatic field $-Z_1/r_1 - Z_2/r_2$, where r_1 and r_2 are the distances from the calcium ($Z_1 = +2$) and the fluorine ($Z_2 = -1$) ions, respectively. The quantum description of its motion is therefore separable in elliptical coordinates $\xi=(r_1+r_2)/R$ $(1 \leq \xi \leq \infty)$ and $\eta=(r_1-r_2)/R$ $(-1 \leq \eta \leq +1)$. Any particular solution ψ_β of the
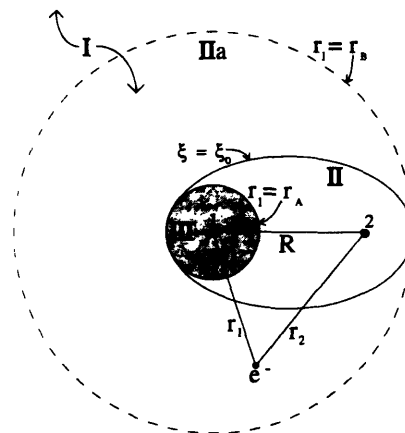
FIG. 1. Various zones relevant to the description of an electron interacting with an atomic core and a point charge.

2549

molecular electronic Schrödinger equation can therefore be written as a superposition of products of elliptical radial channel functions $\tilde{f}_{\tilde{l}}(\epsilon,\xi)$ and $\tilde{g}_{\tilde{l}}(\epsilon,\xi)$ (regular and irregular at the origin, respectively) with elliptical angular factors $\tilde{Y}_{\tilde{l}\lambda}(\eta,\phi)$,

$$\psi_\beta(\epsilon,\xi,\eta,\phi) = \sum_{\tilde{l}} \tilde{Y}_{\tilde{l}\lambda}(\epsilon,\eta,\phi) \frac{1}{(\xi^2-1)^{1/2}}$$

$$\times [\tilde{f}_{\tilde{l}}(\epsilon,\xi)I_{\tilde{l}\beta}(\epsilon) - \tilde{g}_{\tilde{l}}(\epsilon,\xi)J_{\tilde{l}\beta}(\epsilon)] . \quad (1)$$

Here ϵ is the electron energy which may be positive (electronic continuum) or negative (bound state spectrum). λ is the electron orbital angular momentum component with respect to the axis joining atoms 1 and 2. It is a good quantum number as long as the nuclei are kept fixed. The tildes on $\tilde{f}$, $\tilde{g}$, and $\tilde{Y}$ (and on other quantities later in the text) serve to distinguish these functions from their spherical analogs. The differential equations which yield the elliptical functions $\tilde{f}_{\tilde{l}}$, $\tilde{g}_{\tilde{l}}$, and $\tilde{Y}_{\tilde{l}\lambda}$ depend on Z_1, Z_2, R, and ϵ; they are well known [6] and will not be repeated here. The calculation of the energy-normalized channel basis functions $\tilde{f}_{\tilde{l}}$ and $\tilde{g}_{\tilde{l}}$ for arbitrary positive ϵ is straightforward and may be performed by any standard numerical propagation scheme. For negative energy it is the main task of generalized quantum defect theory [4,7].

We wish to determine the coefficients $I_{\tilde{l}\beta}$ and $J_{\tilde{l}\beta}$ in Eq. (1) in terms of an adequate set of independent eigensolutions ψ_β. The reactance matrix $K_{\tilde{l}\tilde{l}'}$, or the equivalent quantum defect matrix $\mu_{\tilde{l}\tilde{l}'}$, is then given by

$$K_{\tilde{l}\tilde{l}'}(\epsilon,R) \equiv \tan\pi\mu_{\tilde{l}\tilde{l}'}(\epsilon,R) = \sum_\beta J_{\tilde{l}\beta}I_{\beta\tilde{l}'}^{-1} . \quad (2)$$

The matrices I, J, K, and μ depend on what happens to the lone electron inside the reaction zone II. If both ions were simple point charges, then J, and consequently K and μ, would be zero. Once the quantum defect matrix μ is known, the electronic bound state spectrum emerges from the requirement that the wave function vanish for $\xi \to \infty$. In the framework of generalized quantum defect

theory this leads to the condition that

$$\sum_{\tilde{l}'} [\tan\pi\mu_{\tilde{l}\tilde{l}'}(\epsilon,R) + \tan\beta_{\tilde{l}}(\epsilon,R)\delta_{\tilde{l}\tilde{l}'}]Z_{\tilde{l}'} = 0 \quad (3)$$

for each elliptical partial wave $\tilde{l}$. The parameter $\beta_{\tilde{l}}$ in Eq. (3) is the so-called accumulated phase at the given energy $\epsilon \leq 0$, which, on division by π, simply gives the number of half oscillations carried out by the regular function $\tilde{f}_{\tilde{l}}(\epsilon,\xi)$ of arbitrary ϵ before it diverges as $\xi \to \infty$. $\beta_{\tilde{l}}/\pi$ is just the generalization of the familiar effective principal quantum number for a Coulomb field, $\beta_{\tilde{l}}^{(\text{Coul})}/\pi = \nu^{\text{Coul}} - l = Z(-2\epsilon)^{-1/2} - l$, with the difference that in the general case the relationship between the accumulated phase and the energy is no longer given by the Rydberg equation but must be evaluated numerically. The reader who is not familiar with quantum defect theory may easily convince himself that for a single channel Eq. (3) reduces to the condition $\mu + \beta/\pi = n$ (n integer). In other words, the contributions to the total accumulated phase of the bound state radial wave function arising inside ($\pi\mu$) and outside (β) the reaction zone must add up to a multiple of π.

We next consider the wave function near each of the scattering centers Ca^{++} and F$^-$, respectively, and, in the spirit of the MSM, we consider each center separately. The $e^- $-F$^-$ interaction is repulsive and hence the corresponding scattering phase shifts must be small. We actually set them to zero, thus replacing the fluorine ion by a negative point charge as is done in ligand field theory. By contrast, the scattering off the strongly attractive calcium ion depends sensitively on the internal structure of the latter. Near the doubly charged core the potential term $-Z_1/r_1$ dominates so that the electronic Schrödinger equation becomes *locally separable* in terms of the spherical coordinates r_1,θ_1,ϕ centered on the nucleus 1. Therefore we obtain the constraint on each eigensolution ψ_β in region II that it must reduce to a superposition of *spherical atomic* partial waves on the boundary of the atomic region III, $r_1 = r_A$,

$$\psi_l(\epsilon,r_1,\theta_1,\phi) = Y_{l\lambda}(\theta_1,\phi)\frac{1}{r_1}[f_l(\epsilon,r_1)\cos\pi\mu_l - g_l(\epsilon,r_1)\sin\pi\mu_l] , \quad (4)$$

where the $Y_{l\lambda}$ are now ordinary spherical harmonics and f_l and g_l are energy-normalized regular and irregular Coulomb functions, respectively. Each component $r_1\psi_l(r_1)$ is characterized by a *constant* logarithmic derivative on the ion surface $r_1 = r_A$,

$$b_l(r_1) = -\frac{\partial(r_1\psi_l)/\partial r_1}{(r_1\psi_l)}$$

$$= -\frac{f_l'(r_1)\cos\pi\mu_l - g_l'(r_1)\sin\pi\mu_l}{f_l(r_1)\cos\pi\mu_l - g_l(r_1)\sin\pi\mu_l} . \quad (5)$$

The coefficients μ_l in Eqs. (4) and (5) are simply the known atomic quantum defects of the Ca$^+$ ion. Equation (5) expresses the fact that the knowledge of these quantum defects is tantamount to the knowledge of a corresponding set of radial boundary conditions b_l on a suit-

ably chosen spherical surface near the Ca^{++} nucleus.

We now turn to the problem of constructing a set of eigensolutions ψ_β valid throughout the reaction zone II, which have the correct logarithmic derivatives on the III/II boundary as required by Eq. (5) and which may be matched to the asymptotic form Eq. (1) at the II/I boundary. We introduce at this point the auxiliary region IIa which is the region between the two spherical surfaces $r_1 = r_A$ and $r_1 = r_B$ centered on the metal nucleus 1 and enclosing the ellipsoid $\xi = \xi_0$ (see Fig. 1), and the smaller atomic core surface $r_1 = r_A$. The advantage of using region IIa is that it may be spanned by a set of spherical free-particle eigenfunctions defined for positive as well as negative energy that have well defined boundary condi-

268

tions on the edge of region III. These are

$$\psi_{m l \lambda}(r_1,\theta_1,\phi) = Y_{l \lambda}(\theta_1,\phi)\frac{1}{r_1}[c_{ml}\sin(k_{ml}r_1)+d_{ml}\cos(k_{ml}r_1)] \quad (\epsilon_{ml} = \tfrac{1}{2}k_{ml}^2 \geq 0), \tag{6a}$$

$$\psi_{m l \lambda}(r_1,\theta_1,\phi) = Y_{l \lambda}(\theta_1,\phi)\frac{1}{r_1}[c_{ml}e^{\kappa_{ml}r_1}+d_{ml}e^{-\kappa_{ml}r_1}] \quad (\epsilon_{ml} = -\tfrac{1}{2}\kappa_{ml}^2 \leq 0). \tag{6b}$$

The coefficients c and d in Eqs. (6) are determined for each function by the appropriate atomic boundary condition $b_l(r_1=r_A)$ [Eq. (5)] on the one hand, and by an additional condition $b_l(r_1=r_B)$ at the outer boundary of region IIa on the other hand. This second condition is regarded as a free parameter at this stage and is chosen to be the same for all partial components l, $b_l(r_1=r_B) \equiv b(r_B)$. The set of functions $\psi_{m l \lambda}(b_B)$ defined by Eq. (6) is *orthonormal* and *discrete* as indicated by the radial quantum number m.

The Hamiltonian in region IIa for $r_A \leq r_1 \leq r_B$, is simply the electrostatic interaction between the lone electron and the two charges Z_1 and Z_2. The matrix representation of the potential energy for each value of λ is given by the integrals

$$H^{(\lambda)}_{ml,m'l'}(b(r_B)) = \iiint \psi^*_{m l \lambda}(r_1,\theta_1,\phi)\left[-\frac{Z_1}{r_1}+\frac{l(l+1)}{2r_1^2}-\frac{Z_2}{(r_1^2-2r_1 R\cos\theta_1+R^2)^{1/2}}\right]\psi_{m'l'\lambda}(r_1,\theta_1,\phi)r_1^2\sin\theta_1 dr_1 d\theta_1 d\phi. \tag{7}$$

All matrix elements depend parametrically on the boundary condition $b(r_B)$ and are of course diagonal in the quantum number λ.

Diagonalization of the Hamiltonian matrix Eq. (7) yields a set of eigenenergies $\epsilon_\beta^{(\lambda)}(b(r_B))$ and eigenfunctions $\psi_\beta^{(\lambda)}(b(r_B))$ valid everywhere in region IIa and thus also in the enclosed region II. Since we wish to match the eigenfunctions ψ_β to the asymptotic form of Eq. (1) at a *preselected energy* ϵ, the parameter $b(r_B)$ must be varied until one of the eigenvalues ϵ_β coincides with ϵ. This is the iterative eigenchannel R-matrix procedure of Fano and Lee [8], with the difference that here boundary conditions are imposed on an *inner* as well as on an *outer* boundary. There will be as many distinct eigenvalues $b_\beta(r_B)$ as there are partial waves l in the basis set Eq. (6). Their inverses are just the eigenvalues of the conventional R matrix [9]. Rather than varying $b(r_B)$ explicitly we have used the equivalent noniterative variant [10] of the eigenchannel R-matrix method which yields the eigenvalues b_β directly as the solutions of a generalized eigenvalue problem.

Once the set of eigenfunctions ψ_β spanning region IIa has been evaluated for the desired energy ϵ, the values $\psi_\beta(\xi_0)$ and derivatives $\psi'_\beta(\xi_0)$ with respect to ξ on the surface of the reaction zone II are also known. The matrices I and J are then calculated through matching by means of Eq. (1) and its derivative. The result is

$$I_{l\beta} = \pi(\bar{g}'_l u_{l\beta} - \bar{g}_l u'_{l\beta}), \quad J_{l\beta} = \pi(\bar{f}'_l u_{l\beta} - \bar{f}_l u'_{l\beta}), \tag{8a}$$

where primes refer to differentiation with respect to ξ and where we have made use of the fact that the Wronskian $W(\bar{f}_l,\bar{g}_l)$ equals $1/\pi$. The coefficients u result from expanding ψ_β on the reaction surface in terms of the orthonormal "surface harmonics" $\bar{Y}_{l\lambda}(\eta)$:

$$u_{l\beta}(\xi) = \iint \bar{Y}^*_{l\lambda}(\eta,\phi)[(\xi^2-1)^{1/2}\psi_\beta^{(\lambda)}(\xi,\eta,\phi)]d\eta d\phi. \tag{8b}$$

The right-hand side of Eq. (8) is evaluated for $\xi = \xi_0$; the

resulting matrices I and J are independent of ξ_0. Use of Eq. (2) then completes the calculation of the elliptical quantum defect matrix $\bar{\mu}_{\bar{l}\bar{l}'}$.

In a typical calculation we have taken the values $r_A = 0.8$ a.u., $r_B = 6.5$ a.u., $\xi_0 = 2.7$, and $\epsilon = -0.01$ a.u. corresponding to $\nu^{(\text{Coul})} \sim 7$. $R = 3.54$ a.u. is the equilibrium internuclear distance of CaF$^+$. The Ca$^+$ quantum defects for $l = 0\text{-}2$ used are those quoted at the beginning of this Letter. For $l \geq 3$ we set $\mu_l = 0$. We have found that ten radial components m and five angular components l in the basis Eq. (6) yielded converged results. The Rydberg energies $\epsilon_{n\lambda}(R)$ are then calculated from the $\bar{\mu}$ matrices by means of the generalized Rydberg equation (3).

The results are conveniently displayed with reference to the effective principal quantum number

$$\nu_{n\lambda}^{(\text{Coul})} = \frac{Z_1+Z_2}{(-2\epsilon_{n\lambda})^{1/2}}, \quad n=1,2,\ldots, \tag{9}$$

referring to the Coulomb system with total charge $Z_1+Z_2 = +1$. The effective quantum numbers thus evaluated combine contributions due to the core dipole field and higher multipole components as well as penetration into the Ca^{++} core. Figures 2(a) and 2(b) are plots of $\nu_{n\lambda}^{(\text{Coul})}$(modulo 1) vs $\nu_{n\lambda}^{(\text{Coul})}$ and compare the experimental values from various sources [1,11,12] (dots) with the theoretical results (lines). It can be seen that the agreement is satisfying. An important point to note is that the theory predicts correctly the lowest state of each of the six known Rydberg series; the successful calculation of the ground state at $\nu^{(\text{Coul})} = 1.541$ (observed 1.528) is particularly gratifying and shows that even the ground state of CaF can be viewed as a Rydberg state in the generalized sense employed here. In terms of energy, the lowest states are reproduced to within 0.1–0.2 eV, with a smaller mean error than in all previous calculations [3,13,14]. The agreement is about 10 times better for the higher states.
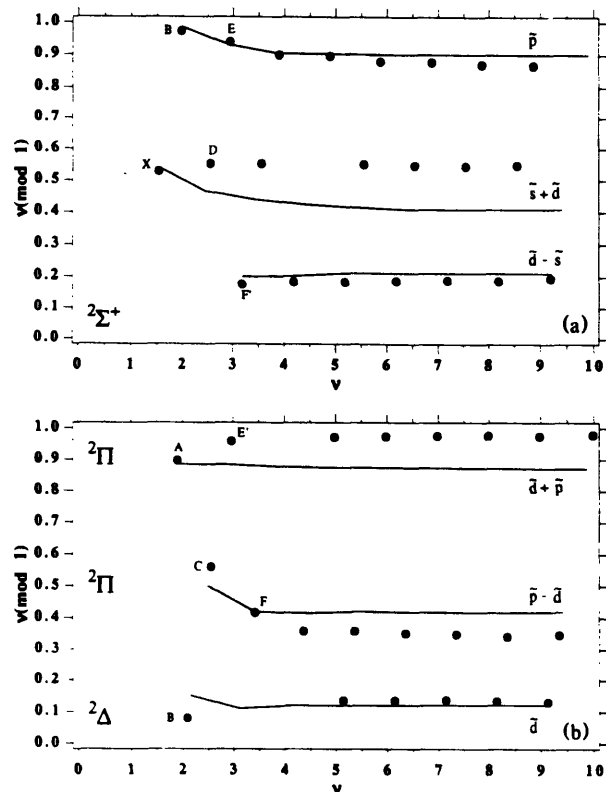
FIG. 2. Effective principal quantum numbers (modulo 1) of CaF plotted vs their absolute values. (a) $^2\Sigma^+$ states; (b) $^2\Pi$ and $^2\Delta$ states. Dots, observed values; lines, calculated values. All presently known electronic states of CaF are included. The labels at the right indicate for each Rydberg series the dominant elliptical angular momentum components $\bar{l}$ including their phases.

The theoretical method presented here opens up a range of avenues to be pursued in the future. First of all, it should be possible to predict several finer features of the CaF states such as the spin-orbital coupling, which is a probe of the wave function near the Ca nucleus [15]. The evolution of the effective principal quantum numbers $\nu_{n\lambda}^{(Coul)}$ as functions of the internuclear distance R may be calculated, giving in effect the electronic potential energy curves which are the goal of standard quantum-chemical calculations. In addition the R dependence of the quantum defect matrix elements $\bar{\mu}_{ll'}$ will allow the coupling between vibrational and electronic degrees of freedom to be calculated, i.e., the breakdown of the Born-Oppenheimer separation. Experimental information on all of these effects exists already [16].

Second, the method outlined here should allow us to deal with dipolar systems in general. Obvious candidates are the alkaline earth halides other than CaF, such as BaF for which s,p,d as well as f states are core penetrating and the corresponding more extended system of states ($\bar{l}=0-3$) has indeed been found [17]. The rare gas hydrides constitute another class of dipolar systems which have recently been studied [18] extensively, and where a comprehensive interpretation of the electronic structure is still lacking.

Finally, the present work should lead to a considerable extension of the multiple scattering method for calculating e^--molecule scattering processes [5]. This will involve representing the second center (here F^-) by an atomic core region with associated quantum defects as has been done here for center 1. Our diagonalization procedure then removes a major drawback of the MSM, namely, the need to have a constant potential between the centers. Charged constituent atoms can thus be treated as well as neutral ones, and polarization terms are incorporated readily.

(a)Permanent address: Department of Chemistry, Massachusetts Institute of Technology, Cambridge, MA 02138.

[1] J. E. Murphy, J. M. Berg, A. J. Merer, Nicole A. Harris, and R. W. Field, Phys. Rev. Lett. 65, 1861 (1990).

[2] G. Herzberg, Annu. Rev. Phys. Chem. 38, 27 (1987).

[3] S. Rice, H. Martin, and R. W. Field, J. Chem. Phys. 82, 5023 (1985).

[4] C. H. Greene, A. R. P. Rau, and U. Fano, Phys. Rev. A 26, 2441 (1982); F. Mies, J. Chem. Phys. 80, 2514 (1984).

[5] D. Dill and J. L. Dehmer, J. Chem. Phys. 61, 692 (1974).

[6] See, e.g., R. A. Buckingham, in Quantum Theory I. Elements, edited by D. R. Bates (Academic, New York, 1961), pp. 121–132.

[7] B. Yoo and C. H. Greene, Phys. Rev. A 34, 1635 (1986); Ch. Jungen (to be published).

[8] U. Fano and C. M. Lee, Phys. Rev. Lett. 31, 1573 (1973).

[9] U. Fano and A. R. P. Rau, Atomic Collisions and Spectra (Academic, New York, 1986).

[10] H. Le Rouzo and G. Raseev, Phys. Rev. A 29, 1214 (1984); Chris H. Greene, Phys. Rev. A 28, 2209 (1983).

[11] J. D'Incan, C. Effantin, A. Bernard, J. Vergès, and R. F. Barrow, J. Phys. B 24, L71 (1991).

[12] N. A. Harris and R. W. Field, J. Chem. Phys. (to be published).

[13] T. Törring, W. E. Ernst, and J. Kändler, J. Chem. Phys. 90, 4927 (1989).

[14] P. Bündgen, B. Engels, and S. D. Peyerimhoff, Chem. Phys. Lett. 176, 407 (1991).

[15] J. M. Berg, J. E. Murphy, N. A. Harris, and R. W. Field (to be published).

[16] J. E. Murphy, Ph.D. thesis, Massachusetts Institute of Technology, 1992.

[17] Z. Jakubek (private communication).

[18] I. Dabrowski, G. Herzberg, B. P. Hurley, R. H. Lipson, M. Vervloet, and D.-C. Wang, Mol. Phys. 63, 289 (1988).